UC San Diego

UC San Diego Electronic Theses and Dissertations

Title

Towards an artificial formate dehydrogenase : : mechanistic studies of formate oxidation and CO_2 reduction by metal P_2N_2 complexes

Permalink

https://escholarship.org/uc/item/3wd2q0d5

Author

Seu, Candace Sachi Wai Mei

Publication Date

2013

Peer reviewed|Thesis/dissertation

eScholarship.org Powered by the California Digital Library
University of California

UNIVERSITY OF CALIFORNIA, SAN DIEGO

Towards an artificial formate dehydrogenase: mechanistic studies of formate oxidation and CO_2 reduction by metal P_2N_2 complexes

A dissertation submitted in partial satisfaction of the
requirements for the degree of Doctor of Philosophy

in

Chemistry

by

Candace Sachi Wai Mei Seu

Committee in charge:

Professor Clifford P. Kubiak, Chair
Professor Joshua S. Figueroa
Professor Melvin Y. Okamura
Professor Arnold L. Rheingold
Professor Michael J. Tauber

2013

Copyright

Candace Sachi Wai Mei Seu, 2013

All rights reserved

The dissertation of Candace Sachi Wai Mei Seu is approved, and it is acceptable in quality and form for publication on microfilm and electronically:

_____

_____

_____

_____

_____

Chair

University of California, San Diego

2013

DEDICATION

This thesis is dedicated to my family,

to Mr. Shaun Lee,

and Ms. MOMO Tomato

EPIGRAPH

I can't keep stressin' on it

I keep movin' on

wherever I'm going.

—The Hue and Kissey Asplund

TABLE OF CONTENTS

LIST OF FIGURES

LIST OF SCHEMES

LIST OF TABLES

ACKNOWLEDGEMENTS

Emerson writes that one should be grateful for all things. It would be easiest and shortest to leave it at that, but it is rather fun to look back at the people who have filled my life and supported or encouraged me for the past 30 years. This PhD would not have been possible without them, and there are so many that I must apologize for the people I've inevitably forgotten.

First and foremost among all these people are my parents, Michael and Claire. In reading to me every night when I was young, enduring my endless questions and chattering, and being willing to let me break (and subsequently fix) every computer we had, they encouraged me to take interest in the world and to be fascinated with the way things work. They pushed me hard, but were wise enough to respect the times I pushed back. They are kind people and firm believers in thank-you letters. My parents are Asian, but they have always seen education as a means of self-improvement and gainful employment more than anything else, and have always been reluctant to brag about us. For this, I will be forever grateful. My siblings Lauren and Mark were much appreciated playmates and have always impressed me with their superior work ethics.

I have had many excellent teachers in my lifetime, but I would single out Mr. Kloetzel as the man who first introduced me to chemistry and Mrs. Chong as the woman who taught me to take writing seriously. Mrs. Shindo and Mr. Masuhara both let me play—with books and with electronics, respectively—and it is probably in their classrooms that I discovered that I enjoyed making things with my hands. Dr. Marc Baum was the first to instill in me a sense that I could really become a research scientist, and remains a trusted mentor to this day. I count myself lucky that my committee members, Arnie, Josh, Mike, and Melvin, have always been willing to guide, challenge, and encourage me as necessary. Dr.

Christina Lambert at CAPS was never formally my professor, but she taught me a lot about how to listen and be kind to both others and myself.

In my application to graduate school, I wrote that I would love to return to a learning environment in which I could act as a student. What I hoped for was for someone to teach me exactly how to do chemistry. In the end, I got that partially from observing my colleagues and mostly from hours and hours of reading papers, failing at the bench, barely succeeding, failing, writing, and failing some more. What I learned from others during my time in school did include some chemistry how-to, but more than that it was the about the nebulous and squishy business of being a person and a scientist.

I did not intend to join the Kubiak lab when I came to UCSD, but I would count this as one of the best decisions I've made in my life. Cliff Kubiak gives his students an unprecedented amount of freedom to struggle or thrive, which was at times frustrating and occasionally terrifying, but in the end I think I would have learned less and been equally frustrated had he always been looking over my shoulder. He has been extremely generous and forward-looking in his willingness to involve us in conferences, grants, and collaborations, emotionally supportive when I most needed it, and always willing to give people a second chance. I have been extremely fortunate to have had him as my guide in the essential tasks of being a scientist, particularly in choosing problems and impressing their relevance upon funding and paper reviewers. He has excellent taste not only in research topics, but also in words, cocktails, and bowties. I respect him as much for his scientific instinct and ability to come up with new ideas on the fly as for his openness to sticky rice and chicken feet.

Jim Collins writes that one of the hallmarks of a successful leader is that he chooses the right people to "get on the bus". The Kubiak lab is the noisiest bus I've ever ridden, and I wouldn't have had it any other way. Starla’s friendliness is probably the reason why I initially joined the Kubiak lab, and I think that there were many days where her joyfulness was the

one thing that kept the lab together. I cannot say that Goeltz was normally as joyful, but his candor was equally encouraging and I have always admired his clear-sightedness. I am very fond of the way that Smeej treats everything with care, and hope to someday be as assertive as he is. Eric's do-it-yourself ethic and his passion for building the lab have inspired me to try to do the same. Bhupi is the only person to have treated me like a younger sister and lived to tell the tale, and I am grateful for the simple advice and encouragement he gave me at every critical moment in my grad school career.

One of the things I wish for most in life is to be able to spend my time with people who inspire me to become a better person, and my labmates have all done so in their different ways. Gabe has been the source of a thousand much-needed reminders that science should be fun and that life should be enjoyed. Kyle's passion for the lab and his dedication to encouraging and helping everyone in the group inspired us and changed our culture for the better, and is something that I hope I'll be able to give when I am a postdoc as well. Although I can't claim to be very good at it yet, Tram has taught me to be gentler with myself and with others. Mark L has been the extrovert to my introvert and the voice for so many of the things worth feeling and remembering about graduate school. I enjoy Jane for her outspoken honesty and for her focus on living with gratitude, a skill which has been invaluable for getting me through the past few months. Steven is easily the most dedicated and diplomatic person I've ever known. I will miss Alissa's quiet optimism coupled with thoughtfulness, occasional sassyness, and cake. I already miss the quiet chats I used to have with Alyssia when she was my hard-working desk neighbor. My good memories of lab would not be complete without Julia, Sayak, Ricky, Aaron, Roger, Charles, Michelle, Jerry, Jesse, Mark R, Matt, Melissa, and Jason. I will deeply miss the pirate metal, the contagious laughter, the daily chats, pubsketball jokes, and labbit playdates.

Two of my labmates deserve special mention. Michael Doud was my first collaborator when I inherited the Ni P_2N_2 project from Julia, and I am so grateful that I can look back at where we started (as two confused graduate students) and see how much we've both grown as chemists. He has probably seen me at my very worst in the lab, and yet he has always been forgiving, warm, and patient. There is no good reason for this except that he is just really good at being a person. His positive outlook, his caring about other people, and his willingness to let loose and have fun have gotten me through some of the darkest times I experienced in the second half of graduate school. I will miss making tamales with him. David Ung worked on the water-soluble Ni and Pd projects with me during my last year of grad school. When he first walked into our lab looking very nervous (I later learned that he'd heard some scary stories about me), I had no idea that we'd get along so well or that I'd eventually learn so many things from working with him: how to structure a research experience (it's difficult), how to skin a gerbil (not a real gerbil), and how to bike to delicious blueberry donuts (take PCH to VG's in Cardiff). He is a good listener and a supportive friend, and I will miss our chats about chemistry and life.

Dr. Aaron Appel is not a member of the Kubiak lab, but he would have been a most welcome addition! Aaron was my main contact at PNNL, and I do not think that our collaboration (or my graduate career) would have lasted without his openness and patience. Simply put, Aaron is a damned good scientist and a wonderful person, and I am extremely grateful that I had the chance to work with him and observe him in action. As a scientist he is open-minded but rigorous, and his constant challenges to go back and look at the data were an important part of my training. As a person and as a mentor, his gentle way of approaching disagreements, his quietly positive attitude, and his patience with many of my anxieties and mistakes are all qualities (among many others!) that nurtured and encouraged me to stay in

science. When I think about the kind of scientist I hope to someday become, I will imagine him sitting in the dark in his office.

I cannot forget Dr. Brandon Galan, Dr. John Linehan, and Dr. Dan DuBois, also at PNNL, for their contributions to our collaboration and for their kindness to me on my research visit. Dr. Curtis Moore, Dr. Andrew Mrse, and Dr. Yongxuan Su were all amazingly helpful and friendly to me on the many days that I needed to use their facilities. I am grateful to Mr. Millard, Treff, Liezel, Stephen, RHolland, Yuchen, Maria, and Annette for lending me reagents, walking me through computations, giving me a fresh perspective on our chemistries, and making me laugh. Grad school felt better knowing that they were down the hall.

Over the last five years I have been lucky to spend some of my time outside of the lab with a diverse but supportive group of friends. James, Jason, Tomomi, Alex, Daisy, Megan, Satoko, Tad, Mike W, Karen, Hao, MT, Traci, Rick F, Nikki, Holli, Lawrence, Ben, and Phyllis all made San Diego a little more fun at various times. Maria H, AK, Sarah, Maryam, Sangeeta, Joe, and Jessica E often encouraged me from afar, and I am particularly grateful to Jason, Sangeeta, and Jessica for constantly reminding me that I would eventually make it through. Mr. and Mrs. Lee and Mrs. Ung never said so much in words, but showed it in buckets of 水煮魚 and curry.

Last, Mr. Shaun Lee has been with me for a crazy long time and been the best friend and partner that I could have ever imagined. Although I could imagine life without him, I don't want to, and I hope we'll have many more adventures together.

Chapter 2: Some of the material in the introduction to this chapter was adapted from a manuscript entitled "Electrocatalytic Oxidation of Formate by $[Ni(P^{R}_{2}N^{R'}_{2})_2(CH_3CN)]^{2+}$ Complexes," by Brandon R. Galan, Julia Schöffel, John C. Linehan, Candace Seu, Aaron M. Appel, John A. S. Roberts, Monte L. Helm, Uriah J. Kilgore, Jenny Y. Yang, Daniel L. DuBois, and Clifford P. Kubiak, published in *J. Am. Chem. Soc*., **2011**, *133* (32), 12767-12779. The dissertation author is a contributing author to this manuscript.

The majority of the material for this chapter comes directly from a manuscript entitled "Formate oxidation via β-deprotonation in $[Ni(P^{R}_{2}N^{R'}_{2})_2(CH_3CN)]^{2+}$ complexes, " by Candace S Seu, Aaron M. Appel, Michael D. Doud, Daniel L. DuBois, and Clifford P. Kubiak, published in *Energy Environ. Sci.*, **2012**, *5,* 6480-6490. The dissertation author is the primary author of this manuscript.

Chapter 5: Much of the material in this chapter has been derived from a manuscript entitled "Synthesis, structural, and electrocatalytic reduction studies of $[Pd(P_2N_2)_2]^{2+}$ complexes," by Candace S. Seu, David Ung, Michael D. Doud, Curtis E. Moore, Arnold L. Rheingold, and Clifford P. Kubiak. This manuscript is currently in preparation.

VITA

2005	Bachelor of Science, California Institute of Technology
2009	Master of Science, University of California, San Diego
2013	Doctor of Philosophy, University of California, San Diego

PUBLICATIONS

Seu, C.S., Ung, D., Doud, M.D., Moore, C.E., Rheingold, A.L., Kubiak, C.P. "Synthesis, structural, and electrocatalytic reduction studies of $[Pd(P_2N_2)_2]^{2+}$ complexes." Submitted to *Organometallics*, May **2013**.

Seu, C.S., Appel, A.M., Doud, M.D., DuBois, D.L., Kubiak, C.P. "Formate oxidation via β-deprotonation in $[Ni(P^R_2N^{R'}_2)_2(CH_3CN)]^{2+}$ complexes." *Energy Environ. Sci.*, **2012**, *5,* 6480-6490.

Doud, M.D., Grice, K.A., Lilio, A.M., **Seu, C.S.**, Kubiak, C.P. "A Versatile Synthesis of $P^R_2N^{R'}_2$ Ligands for Molecular Electrocatalysts with Pendant Bases in the Second Coordination Sphere." *Organometallics*, **2012**, *31* (3), 779-782.

Smieja, J.M., Benson, E.E., Kumar, B., Grice, K.A., **Seu, C.S.**, Miller, A.J.M., Mayer, J.M.; Kubiak, C.P. "Artificial photosynthesis of CO: Kinetic and structural studies, origins of selectivity, and importance of interfacial charge transfer." *Proc. Natl. Acad. Sci*, **2012**, *109* (39), 15646-15650.

Galan, B.R., Schöffel, J., Linehan, J.C., **Seu, C**., Appel, A.M., Roberts, J.A.S., Helm, M.L., Kilgore, U.J., Yang, J.Y., DuBois, D.L., Kubiak, C.P. "Electrocatalytic Oxidation of Formate by $[Ni(P^R_2N^{R'}_2)_2(CH_3CN)]^{2+}$ Complexes." *J. Am. Chem. So*c., **2011**, *133* (32), 12767-12779.

Graët, A., Sinault, L., Fusaro, M.B., Vallet, A., **Seu, C.,** Kilgore, J.L. and Baum, M.M. "Reactivity of the Nickel(0)−CO_2−Imine System: New Pathway to Vicinal Diamines." *Organometallics*, **2010**, *29* (9), 1997–2000.

Seu, C. and Chen, Y. "Identification of SUMO-Binding Motifs by NMR." *Methods Mol. Biol.,* **2008**, *497*, 121-138.

Cai, S., **Seu, C.,** Kovacs, Z., Sherry, A.D., Chen, Y. "Sensitivity Enhancement of Multidimensional NMR Experiments by Paramagnetic Relaxation Effects." *J. Am. Chem. Soc*., **2006**, *128* (41), 13474-13478.

ABSTRACT OF THE DISSERTATION

Towards an artificial formate dehydrogenase: mechanistic studies of formate oxidation and CO_2 reduction by metal P_2N_2 complexes

by

Candace Sachi Wai Mei Seu

Doctor of Philosophy in Chemistry

University of California, San Diego, 2013

Professor Clifford P. Kubiak, Chair

The efficient electrochemical production and use of CO_2-based solar fuels is a problem of precisely coordinating the associated proton and electron transfers. One strategy for controlling these proton-coupled electron transfers is to use catalysts that contain proton relays in their secondary coordination spheres. The work described in this thesis explores the function of 1,5-diaza-3,7-diphosphacyclooctane (P_2N_2) ligands in molecular electrocatalysts for HCOOH/CO_2 conversion. By focusing on a mechanistic understanding of the catalysis that occurs with these ligands, we seek to develop the chemistry of these systems and to guide the design of better CO_2 catalysts.

A variety of NMR and electrochemical experiments were used to explore the likelihoods of several different proton or hydride transfer pathways for the oxidation of formate by $[Ni(P_2N_2)_2]^{2+}$ complexes. The experiments suggest that oxidation occurs via a rate-determining proton transfer from the Ni–O_2CH β-H to the pendant base, coupled with a $2e^-$ transfer to Ni(II). The measurement of electrocatalytic k_H/k_D KIEs between 3–7 suggests that this unexpected non-hydride process may be an unusual example of multi-site concerted proton-coupled electron transfer, which has been rarely observed in well-defined catalyst systems.

We attempted to develop a catalyst for the reduction of CO_2 to formic acid by using metals with increased electron donating ability, as predicted by their hydride donating ability (hydricity). $[Co(P_2N_2)_2]^{1-}$ complexes react with CO_2 even in the absence of extra protons, but are unstable under the high potentials necessary to generate these species. $[Pd(P_2N_2)_2]^{2+}$ complexes crystallize in square planar or minimally tetrahedrally distorted geometries and exhibit a single quasi-reversible $2e^-$ Pd(II/0) redox couple in voltammetric studies. $[Pd(P^{Ph}{}_2N^{Bn}{}_2)_2]^{2+}$ and $[Pd(P^{Me}{}_2N^{Ph}{}_2)_2]^{2+}$ were tested for electrochemical CO_2 reduction in the presence of excess protons and found to preferentially produce H_2. Comparative analysis of the intermediates involved in proton reduction by analogous $[Pd(P_2N_2)_2]^{2+}$ and $[Ni(P_2N_2)_2]^{2+}$ complexes suggests that large reorganizational energy barriers render the Pd catalysts much less efficient than their Ni counterparts. The ability of the Ni-P_2N_2 metal-ligand combination to access multiple redox and protonation states with a minimum of reorganization appears to be essential to both proton reduction and formate oxidation.

Chapter 1

On solar fuels, electron transfer, and mechanistic electrochemistry.

1.1 Introduction

It has been said by many members of the Kubiak lab that nothing is more fundamental to chemistry than the study of electron transfer,[1–3] and this continues to hold true when it comes to the redox reactions of solar fuels. The reduction of CO_2 to generate carbon monoxide, methanol, or higher carbon liquids and the controlled oxidation of these molecules are reactions that have the power to drastically change the way we fuel our lives. Learning to enable and direct these transformations through the use of electrocatalysts is an important theme in our lab and in the solar fuels community. Like their traditional thermal cousins, electrocatalysts are used to open up kinetically favorable bond-breaking and -making pathways in normally slow reactions, but they are additionally able to decouple the movement of electrons from their associated bonding atoms under the influence of an

externally applied potential. In this way, electrocatalysts act as a conduit by which chemical and electrical energy can be directly interconverted and stored within or harvested from a molecular substrate.

The concept of electrocatalysis was first coined by Kobosev and Monblanowa as early as 1936[4] and explored to a small extent by the fuel cell community in the late 1960s.[5] Interest in the topic was renewed in the early 1990s and has exploded in recent years, driven by increasing scientific and public awareness about peak oil and anthropogenic climate change. While the majority of research in energy-related electrocatalysis has focused primarily on heterogenous materials for use in oxidative fuel cells,[6] the scope of the field has recently expanded to encompass reductive catalysts for use in the "artificial photosynthesis" of solar fuels, as well as homogenous molecular catalysts, which may be more amenable to mechanistic studies and cost considerations than their solid-state counterparts.

This thesis describes our efforts to develop molecular electrocatalysts for the two proton, one electron interconversion of CO_2 and formate ($HCOO^-$) using a ligand framework that places pendant bases in the second coordination sphere of the catalyst. These have been previously shown to accelerate proton and electron movement in nickel-based hydrogenases,[7,8] and we found that they continued to do the same when presented with formate. Through a variety of mechanistic electrochemical and spectroscopic studies, we discovered that formate oxidation occurred via a completely unexpected proton transfer mechanism. Using this knowledge, we attempted to extend the chemistry of this ligand on various metals for the reaction's microscopic reverse, or reduction of CO_2 to formate. While many of these studies did not result in useful catalysts, they often revealed or reiterated several crucial CO_2 reduction catalyst design principles. We hope that future researchers in this area will consider them carefully and find their thought-lines fruitful.

The first chapter of this thesis introduces the multiple chemical research threads—among them CO_2 hydrogenation, electrocatalysis, and proton relays—that inform the research projects undertaken in this thesis. Chapter Two describes our efforts to understand the mechanism of formate oxidation by the $[Ni(P^R_2N^{R'}_2)_2]^{2+}$ system, while Chapter Three discusses our attempts to extend catalysis to the oxidation of carbon monoxide. Chapters Four and Five deal with our work on catalysis of the reduction reaction using the same ligand system attached to cobalt and palladium, respectively. Finally, Chapter Six summarizes our recommendations for future development of catalysts in both directions.

1.2 A short history of HCOOH/CO_2 thermal catalysis

The reduction of CO_2 to formic acid or formate can be easily envisioned as a C=O bond hydrogenation. Breaking the hydrogenation reaction down further into one that is not necessarily concerted, one can think about the reduction as a hydride transfer to the carbon, accompanied by transfer of a proton or other cation that neutralizes the resulting negative charge on the oxygen atoms. As such, much of the current work on electrocatalytic CO_2 reduction has been informed by early studies on the migratory insertion of CO_2 into a metal hydride bond. This elementary organometallic reaction was studied most famously by Darensbourg *et al*., who demonstrated the reversible insertion of CO_2 into Group 6 (M = Cr, Mo, W) metal–hydride bonds.[9–11] Other early studies on this topic include those by Trogler,[12] Musco,[13] and Meyer,[14] who observed CO_2 insertion into the metal–hydride bonds of Pt–H and Re(bpy)$(CO)_3$H complexes. None of these reactions, however, were demonstrated to participate in catalytic cycles.

The first studies on *catalytic* CO_2 to HCOOH reduction using H_2 as a hydride and proton source were pioneered by the Jessop and Noyori groups, who generated the highly stable Ru bis-diphosphine catalysts[15–17] that remain the benchmarks for this class of reaction.

The most promising catalysts to have been developed since then are also notable for the bifunctional nature of their ligands. Himeda and coworkers have modified the Ru(bpy) half-sandwich complexes first introduced by Ziessel[18] so that they contain OH groups in the 4 and 4' positions, which are used to modulate the solubility and hence activity of the catalyst according to pH.[19,20] This aids in catalyst separation and recovery, and more importantly prevents catalysis of the often highly favorable back-reaction that occurs once hydrogen pressure is released. In a completely different vein, the PXP (X = C, N) pincer-type ligands recently explored by Nozaki[21,22] and others[23,24] based on older studies showing CO_2 insertion into PCP–rhodium hydride complexes[25,26] do not appear to exhibit any apparent bifunctionality. However, mechanistic studies have suggested that (depending on the type of N) either the coordinated N itself[24] or an aromatically conjugated carbon[22] can donate a proton that stabilizes the CO_2 insertion reaction or provides a faster hydride regeneration pathway, respectively.

The oxidation of HCOOH to CO_2 has been less frequently studied, although it should be noted that many of the thermal catalysts catalyze the reaction in both directions. Meyer studied the catalytic decarboxylation of $HCOO^-$ by $[Ru(bpy)_2(py)_2(OH)]^{2+}$ and $[Ru(bpy)_2(py)_2(O)]^{2+}$ to give CO_2 and H_2O, in part to explore the possibility of using Ru–OH to reduce CO_2.[27] He noted that the disappointing kinetics of the oxidative reaction suggested that reduction was unlikely. Casey and coworkers have shown that the Shvo transfer hydrogenation catalyst can reversibly decarboxylate formate.[28] More recent publications by Beller, Himeda, and others have brought up the possibility of using formic acid as a liquid hydrogen carrier.[28–30] The Beller catalysts are particularly notable for their use of first-row Fe and Co, as the majority of HCOOH oxidation electrocatalysts (discussed later) are based on noble metals.

Over the past few years the solar fuels catalysis community has become more interested in electrochemistry, and one idea currently in rapid circulation is that of transforming traditional thermal hydrogenation catalysts into electrocatalysts. By having reducing equivalents delivered as protons and electrons rather than as pressurized H_2 gas, these systems should be more able to overcome the H_2 activation and $HCOO^-$ elimination bottlenecks that often slow down their thermal analogues. Deronzier and coworkers explored a similar idea in 1997, taking a known H_2 production catalyst and showing that the reducing equivalents could be directed to an organic substrate, albeit at low efficiencies.[31,32] Brookhart and Meyer were the first to demonstrate the feasibility of adapting a transfer hydrogenation catalyst, showing in 2012 that derivatives of the Ir PCP pincer system described above could selectively electrochemically reduce CO_2 to HCOOH at lower TONs but significantly higher TOFs than their thermal counterparts.[33] This report was quickly followed by a paper by Norton and co-workers on the reactions of electrochemically generated Ir and Ru half-sandwich hydride complexes (although they conspicuously neglected to discuss any reactions with CO_2).[34] Others are certain to follow, and with that we turn to a short primer on electrocatalysis.

1.3 The basics of molecular electrocatalysis

Electrochemistry is challenging enough on its own (**Figure 1-1**), which makes electrocatalysis all the more so. The following tutorial attempts to introduce the practical basics of molecular electrocatalysis from the perspective of a onetime potentiostat-shy organometallic chemist, since this is a common background for an increasing number of students. Interested readers are encouraged to consult one or more of several introductory[35] and encyclopedic references,[36] preferably long before they start writing a thesis based heavily on these concepts.

Figure 1-1. You'd think things would be better by the time you get through grad school, but in fact they get worse.

1.3.1 What's happening in electrocatalysis?

In an electrochemical half-reaction, electrons are produced or consumed such that there is a change in the overall formal oxidation state of a species of interest. Two half-reactions are coupled so that electrons produced on one end pass through a load and then are consumed by the other. In the reduction of CO_2 to HCOOH in a laboratory electrochemical cell setup, the half reaction of interest reduces the carbon from C(IV) to C(II) at the working electrode, and is coupled with a half reaction in which an unknown species (likely solvent or electrolyte) is oxidized by two electrons at the counter electrode. In a practical fuel cell, CO_2 reduction would most likely be coupled with water oxidation in a membrane-separated compartment.

Whereas electron flow occurs spontaneously in a discharging battery, electron flow in a solar fuel production or fuel cell setup requires the application of an appropriate electrical potential. This is due to the involvement of bond-breaking and -making chemical reactions that require energy input to overcome activation barriers. Electrocatalysts thus play a key role in enabling fast, lower energy pathways for these reactions and the associated electron transfers. What sets electrocatalysts apart from thermal catalysts is that they necessarily act as conduits for charge transfer (envisioned as either holes or electrons) between the substrate and the electrode, rather than just within the substrate. That is, they must be designed to facilitate and manage the separated movement of atoms and electrons in both spatial and temporal coordinates. This latter aspect is often described in terms of a combination of Es and

Cs, referring in turn to electron transfer and chemical steps. Thus, an ECE metal–hydride formation mechanism would describe a three-step process in which the metal is reduced by one electron (E), is subsequently protonated (C), and then rapidly gains another electron (E). This formalism does not specify the relative speeds of each step, and in some cases two steps may occur so quickly that they may be considered to occur simultaneously.

Experimentally, the easiest way to observe molecular electrocatalysis is via cyclic voltammetry. The standard practice in this case is to observe the voltage-dependent electrochemical behavior of the redox-active catalyst in the absence of, then the presence of the substrate. If catalysis of the substrate is occurring, it will be often be seen as a new, irreversible reduction (or oxidation) event with a current that exceeds that of the peak current observed in the non-catalyzed situation (**Figure 1-2**). The increase in current, referred to as "catalytic current" or i_{cat}, occurs because an increased number of electrons is being shuttled through the catalyst as it goes through multiple substrate cycles. The amplitude of the catalytic current reflects the efficiency of the catalyst; faster catalysts will go through a larger number of cycles and move more electrons in a given time, yielding higher currents.

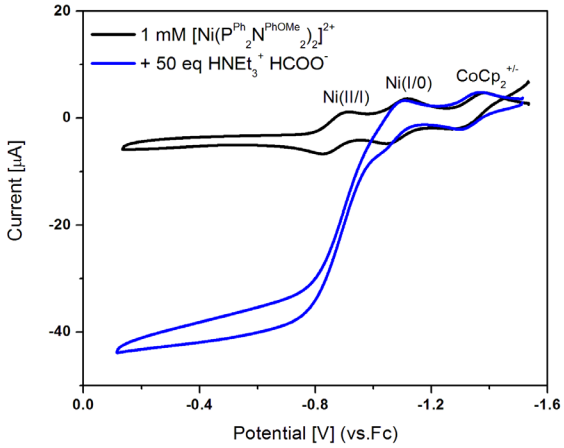

Figure 1-2. Cyclic voltammograms of the $[Ni(P^{Ph}_2N^{PhOMe}_2)]^{2+}$ formate oxidation catalyst alone (black trace) and in the presence of its formate substrate (blue trace). When formate is present and the catalyst is held at a potential more positive than ~0.85 V, the previously reversible Ni(II/I) couple becomes irreversible and an increase in oxidative catalytic current is observed. Conditions: Glassy carbon working and counter electrodes, AgCl reference electrode, 0.2 M NBu_4OTf electrolyte in PhCN, scan rate 50 mV/s.

1.3.2 Evaluating the activity of an electrocatalyst

The robustness and efficiency of an electrocatalyzed reaction can be partially characterized in terms of *turnover number* and *frequency* (TON and TOF) in accordance with the convention used for thermal catalyzed reactions. The TOF is a pseudo-first order rate constant, but rate constants of other orders are occasionally reported. Alternatively, the speed of an electrocatalyst is frequently cited in terms of current density (amperes/area), which focuses on the rate of electron flux through the electrode, instead of substrate turnover. The choice of convention is often dictated by the availability and quality of data for the system; for example, calculating the rate constant from the expression for the catalytic current i_{cat} requires knowledge of the diffusion constant, D.[37,38] Such considerations will be discussed further in chapter two.

A full evaluation of electrocatalyst efficiency requires consideration of another parameter known as the *overpotential*. The overpotential is the difference between the standard redox potential and the actual potential required to run the reaction. This amount

can be visualized on a reaction coordinate as the difference between $\Delta G^{\ddagger}$ and $\Delta G°$; in effect, it is a measure of the height of the activation barrier (**Figure 1-3**). An ideal electrocatalyst provides a lowered barrier that minimizes this difference as much as possible.

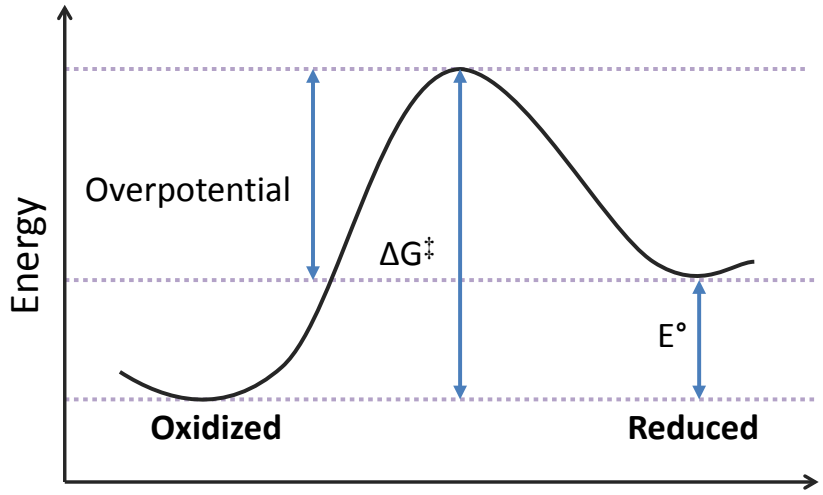

Figure 1-3. Relationship between standard reduction potential, overpotential, and activation energy as depicted on a reaction coordinate.

Although the Arrhenius equation $k = Ae^{-Ea/RT}$ describes the relationship between reaction rate, activation barrier, and energy input in thermal reactions, it is useful to consider how it might be analogous to an expression describing the collision rate of electrons instead of molecules. According to such an equation, faster reaction rates should be correlated with lower activation barriers, as well as greater energy inputs. As such, further increasing the energy input by way of the applied potential can be expected to increase the reaction rate. The Butler-Volmer equation is in fact the analogous expression that describes the relationship between current (the rate of electron flow in amperes/second) and potential (energy input past the activation barrier), and is given by:[35,36]

$$i = nFAk_0\left([\mathrm{Ox}]\exp\left[-\frac{anF}{RT}(E-E_0)\right] - [\mathrm{Red}]\exp\left[\frac{(1-a)nF}{RT}(E-E_0)\right]\right) \quad \textbf{(1)}$$

The first term corresponds to [oxidizing] current and the second corresponds to [reducing] current; in the absence of an external potential ($E = E_o$), the two currents cancel each other out and the net electron flux is zero. As E diverges from E_o, one term increases and the other approaches zero, resulting in net current flow. Applying a higher overpotential should result in an even higher net current. Since the speed of the electron transfer reaction depends on the potential, current densities and turnover frequencies should always be considered in the context of the overpotential at which they are measured.

The selectivity of a catalyst is often reported in terms of *Faradaic efficiency*, which describes the percentage of electrons that participated in the reaction of interest out of the total number of transferred electrons. This can be calculated by quantifying the amount of product(s), converting to the number of electrons necessary to achieve this yield, and comparing this to the total number of electrons passed through the solution. Gaseous products are often conveniently measured via gas chromatography;[39,40] non-volatile products are often measured by quantitative NMR.[41]

1.3.3 Always polish your electrode, and other practical advice

Always polish your electrode. This cannot be stressed enough. You never know when spurious peaks or irreversibility may be simply due to sluggish electron transfer through a dirty electrode. Other helpful suggestions I have received over the years include: always start with as many controls as possible (blank electrolyte, catalyst only, substrate only, catalyst with internal standard, etc.) to make troubleshooting easier. Take multiple scans of the same sample to see if your signal remains constant, as a decrease could indicate catalyst degradation, electrode surface modification, or any number of things that would change the way the data can be interpreted. Take time to recrystallize your electrolyte even if you've just opened a fresh bottle. If you experience problems, try systematically changing and testing

every component of your experiment, and don't overlook things like your internal standard, possible contaminants in the environment, and the way you source or prepare your samples or substrate. But above all, polish your electrode first, every time.

1.4 An introduction to CO_2 electrocatalysis

The reduction potentials for various electrochemical half-reactions of CO_2 are given in **Table 1-1**. The thermodynamic and kinetic stability of CO_2 is reflected in the highly negative reduction potentials in the table, particularly that for the one electron reduction. It is unsurprising that it takes a substantial amount of energy to insert an electron into the high-lying C–O π^* anti-bonding LUMO and to overcome the stable conjugation of the co-linear C=O double bonds (this can also be described as reorganizational energy).[42,43] It is notable, however, that the reduction potentials become less negative when protons are involved in the equation. In fact, contrary to expectation that it should be more difficult to add a greater number of electrons, the reduction potentials continue to decrease *as long as the electrons are matched with an equal number of protons*. These protons neutralize and prevent the buildup of highly localized negative charges, and also participate in bonding interactions that impart some stability to the resulting product state.

Table 1-1. Reduction potentials for electrochemical half-reactions of CO_2 at pH = 7 vs. NHE in aqueous solution. Reproduced from Benson *et al*.[42]

CO_2		$+ e^- \rightarrow$	$CO_2^{\bullet -}$	$E^\circ = -1.90$ V
CO_2	$+ 2H^+$	$+ 2e^- \rightarrow$	$CO + H_2O$	$E^\circ = -0.53$ V
CO_2	$+ 2H^+$	$+ 2e^- \rightarrow$	$HCOOH$	$E^\circ = -0.61$ V
CO_2	$+ 4H^+$	$+ 4e^- \rightarrow$	$HCHO + H_2O$	$E^\circ = -0.48$ V
CO_2	$+ 6H^+$	$+ 6e^- \rightarrow$	$CH_3OH + H_2O$	$E^\circ = -0.38$ V
CO_2	$+ 8H^+$	$+ 8e^- \rightarrow$	$CH_4 + 2\ H_2O$	$E^\circ = -0.24$ V

It can be seen that CO and HCOOH are both possible two electron reduction products, and the production of one versus the other appears to be related to the way that CO_2 interacts initially with the catalyst. For example, CO_2 may bind to a catalyst to yield a metallocarboxylate that is protonated at the O^- to yield OH^- and bound CO. With another catalyst, the active species may be a metal hydride into which CO_2 inserts to yield bound $HCOO^-$. In a study of CO_2 reduction at bare metal electrodes, Hori *et al*. found that most metals were highly selective for one product and could be divided into "CO formation" and "$HCOO^-$ formation" categories.[44] Many molecular electrocatalysts are similarly selective although it should be noted that proton reduction to H_2 is a common competing reaction, particularly when metal hydrides are involved.

The majority of known homogenous two-electron CO_2 reduction catalysts produce CO. Exceptions include the Pd pyridine complexes studied by Ogura and coworkers,[45,46] the Rh(diphosphine)Cl complexes studied by Slater and Wagenknecht,[47] various Rh and Ir-based bipyridine systems explored by Meyer, Tanaka, and Deronzier,[32,48,49] the Fe, Co, and Ni polypyridine films studied by Abruna,[50] the Fe_4 clusters developed by Berben,[51] and the earlier-mentioned Ir–PCP catalysts adapted by Meyer.[33] The last of these is by far the best catalyst in terms of both kinetic efficiency and selectivity, with side production of H_2 being attributed to non-specific reduction of H_2O at the electrode.

The oxidative reverse of this reaction has been studied more often by surface and materials chemists than by synthetic chemists, due to its relevance to direct formic acid fuel cell (DFAFC) applications. In this case, a different selectivity rule favoring oxidation of formic acid to CO_2 rather than surface-poisoning CO is ideal.[52–54] The heterogeneous catalysts used in these systems are largely based on noble metals such as Rh, Pt, and Au, with nanostructured Pd-based anodes being the most commercially viable thus far.[55–61] To our knowledge, the Ni complexes studied in this thesis are currently the only synthetic

homogenous formate oxidation electrocatalysts available, and we briefly discuss our attempts to apply this chemistry to aqueous fuel cells in Chapter Six.

Finally, in keeping with the many efforts in the solar fuels community to achieve biology-inspired "artificial photosynthesis", it is worth discussing the $HCOO^-/CO_2$ interconversion enzyme that serves as the benchmark for our work on "artificial formate dehydrogenases". Formate dehydrogenase (FDH) enzymes are typically found in anaerobic bacteria that use formic acid as an electron (energy) source and are thus most efficient for the oxidative reaction; however, a few of these are able to catalyze the reaction in both directions. The active site of the enzyme is typically a Mo or W atom coordinated by two pterins, which can assume a variety of oxidation states and are often modeled as non-innocent dithiolenes. In 2008, Reda and Hirst demonstrated that the *S. fumaroxidans*-derived W-FDH1 enzyme could be attached to an electrode surface to drive both formate oxidation and CO_2 reduction at very high rates and low overpotentials.[62] In other words, the transition state in this enzyme has been optimized to an extreme such that the activation energy in both directions is as low as possible. Unfortunately, the oxygen sensitivity and low expression levels of this enzyme prevent it from being used in practical applications. Several groups are targeting structural models of this enzyme class in hopes of emulating its activity;[63–65] functional models based on the little-understood mechanism[66–68] are farther behind.

1.5 Proton relays in CO_2 reduction

The application of "nature-inspired" principles to artificial catalysis, and in particular, the prevalence of proton-containing amino acid functional groups in the active site of many enzymes, has inspired many researchers to focus on incorporating similar moieties in the second coordination sphere of their molecules. This strategy for controlling (or at least accelerating) the transfer of protons in catalysis has been applied to a very wide range of

systems, a full review of which is beyond the scope of this thesis. However, we will briefly discuss the use of proton relays in electrocatalysts for solar fuel production.

The rate-enhancing effect of proton relays on catalysts for CO_2 reduction has been recently demonstrated to great effect by Savéant and coworkers for the electrochemical reduction of CO_2 to CO by an Fe porphyrin.[69] In this report, the inclusion of 2,5-bis-hydroxyphenyl groups around the periphery of the porphyrin resulted in a 10 to 100-fold increase in TOF, as well as a 0.5 V decrease in overpotential. A report by Himeda and collaborators focused instead on the thermal reduction of CO_2 to HCOOH by a H_2-generated Ir hydride complex.[70] In this complex, inclusion of hydroxyl groups in the 2 and 2' positions of the bipyridine ligand resulted in CO_2 activation at ambient temperature and pressure, and a 16-fold increase in TOF despite the much gentler conditions. To our knowledge, these are the only CO_2 reduction catalysts that have been enhanced by the addition of proton relays. This may be partially because proton transfer is not rate-determining in many catalysts. The utility of proton relays in electrocatalysis has been explored more extensively for the reduction of protons to hydrogen gas, and the abundance of work in this field led us to explore the possibility of adapting hydrogenase electrocatalysts to CO_2 hydrogenation. A full review of this work is again beyond the scope of this thesis, and we will focus on the $Ni(P_2N_2)_2$ and related systems developed by DuBois and coworkers.[7,8,40,71,72]

1.6 The DuBois P_2N_2 system

When it comes to functional models of biological catalysts, few have been as successful as the $Ni(P_2N_2)_2$ system developed by Daniel DuBois (**Figure 1-4**).[7,8] This class of electrocatalysts mimics the H_2 splitting and H^+ reducing activity of hydrogenase enzymes[73] using the d^8/d^{10} Ni(II/0) couple as the relevant electron acceptor/donor. The azadithiolate ligand in the hydrogenase enzyme is replaced by cyclic diphosphines that bind to the Ni via

the phosphorus atoms, leaving the amine groups free to act as "pendant bases" that can shuttle protons between the catalyst active site and the bulk solution. This proton-concentrating activity enables some of the highest known turnover frequencies for proton reduction and H_2 oxidation by an artificial catalyst.[74–76]

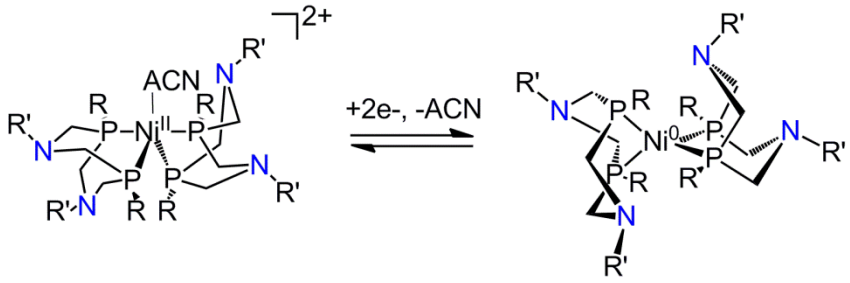

Figure 1-4. $Ni(P^{R}_{2}N^{R'}_{2})_2$ catalyst in the Ni(II) and Ni(0) oxidation states.

The determining factor in whether these complexes are able to oxidize hydrogen or reduce protons is the thermodynamic parameter known as "hydricity". Hydricity is a measure of hydride donor ability, analogous to how acidity is a measure of proton donor ability (**Scheme 1-1**). When the hydricity of the Ni complex is more negative than that of H_2, it is more favorable for Ni–H to donate the hydride to a proton to release H_2, and proton reduction occurs. When the hydricity of H_2 is more negative than that of the Ni complex, the reverse reaction (H_2 oxidation to form Ni–H and H^+) occurs instead.

Hydricity (ΔG_{H^-}): M–H $\rightleftharpoons$ $M^+ + H^-$

Acidity (pK_a): M–H $\rightleftharpoons$ $M^- + H^+$

Scheme 1-1. Chemical equations illustrating the hydride and proton donor ability, respectively, of a generic metal hydride.

The hydricities of these $Ni(P_2N_2)_2$ complexes can tuned most dramatically by changing the phosphine substituents, and to a lesser extent by changing the amine substituent. In general, more donating ligands (those with electron-donating substituents) and ligands that overlap better with the d_{x2-y2} orbital (those with smaller dihedral angles and bite angles) result in more hydridic Ni compounds.[77–82] This can be understood from a molecular orbital perspective in the sense that the energies of the Ni d orbitals should be destabilized (via mixing with increasingly anti-bonding M–L orbitals), resulting in a destabilized Ni(d_{z2}) –H (1s) interaction and hence an increased hydride donor ability (**Figure 1-5**). This can also be understood from a hand-waving perspective in that a greater electron donating ability in the ligands is passed on as a greater electron donating ability in the hydride.

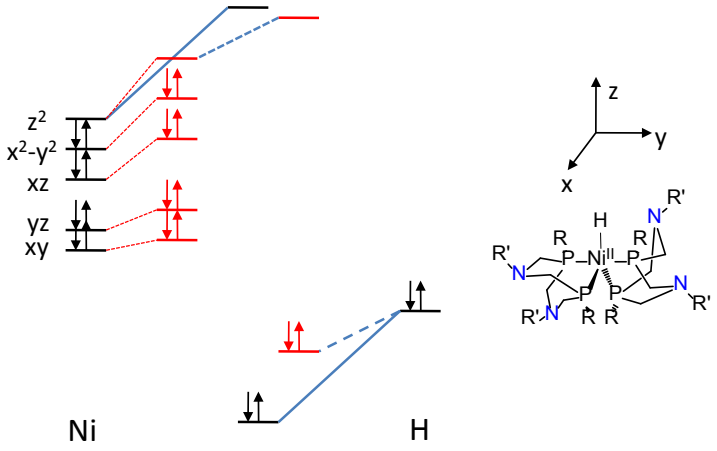

Figure 1-5. MO diagram showing the interaction between a Ni^{2+}-ligand fragment and a hydride. An increase in the overlap between the Ni and its phosphine ligands results in destabilization of the Ni d orbitals and the Ni-H bonding orbital (red lines).

Our initial idea in working with the $Ni(P_2N_2)_2$ catalysts was to extend their proton reduction activity to the reduction of CO_2. The demonstrated ability of these compounds to hold a hydride and a proton in close proximity suggested that the active site of these catalysts might also be suitable for hydrogenation of the C=O double bound. Upon reading the

literature, however, we realized that the hydricities of the Ni complexes (+55–65 kcal/mol) were unsuitable for CO_2 reduction ($HCOO^-$ hydricity = +43 kcal/mol).[83] Accordingly, we were unable to observe any CO_2 reduction activity. The thermodynamics did suggest that the reverse reaction (hydride donation from formate to the Ni) would be favorable, and our studies of this oxidative process are the subject of the next chapter.

1.7 References

1. Lear, B. J. The effects of electronic delocalization in highly coupled mixed valence systems, University of California, San Diego, 2007.

2. Glover, S. D. Dynamics of Electron Transfer at the Localized-to-Delocalized Transition of Mixed Valency, University of California, San Diego, 2011.

3. Goeltz, J. C. Mixed Valency and Electronic Structure in Self-Assembled Monolayers, Self-Exchange, and Hydrogen Bonded Assemblies, University of California, San Diego, 2011.

4. Kobosev, N. I.; Monblanowa, W. W. *Acta Physicochemica U.R.S.S.*, **1936**, *4*, 395–408.

5. Grubb, W. T. *Nature*, **1963**, *198*, 883–884.

6. Marković, N.; Ross, P. *Surf. Sci. Rep.*, **2002**, *45*, 117–229.

7. DuBois, M. R.; DuBois, D. L. *C. R. Chim.*, **2008**, *11*, 805–817.

8. DuBois, M. R.; DuBois, D. L. *Acc. Chem. Res.*, **2009**, *42*, 1974–1982.

9. Darensbourg, D. J.; Rokicki, A. *J. Am. Chem. Soc.*, **1982**, *104*, 349–350.

10. Darensbourg, D. J.; Rokicki, A.; Darensbourg, M. Y. *J. Am. Chem. Soc.*, **1981**, *103*, 3223–3224.

11. Darensbourg, D. J.; Rokicki, A. *Organometallics*, **1982**, *1*, 1685–1693.

12. Paonessa, R.; Trogler, W. C. *J. Am. Chem. Soc.*, **1982**, *3529*, 3529–3530.

13. Immirzi, A.; Musco, A. *Inorg. Chim. Acta*, **1977**, *22*, 35–36.

14. Sullivan, B.; Meyer, T. J. *J. Chem. Soc., Chem. Commun.*, **1984**, 1244–1245.

15. Jessop, P. G.; Ikariya, T.; Noyori, R. *Chem. Rev.*, **1995**, *95*, 259–272.

16. Jessop, P. G.; Joo, F.; Tai, C.-C. *Coord. Chem. Rev.*, **2004**, *248*, 2425–2442.

17. Tai, C.-C.; Pitts, J.; Linehan, J. C.; Main, D.; Munshi, P.; Jessop, P. G. *Inorg. Chem.*, **2002**, *41*, 1606–1614.

18. Ziessel, R. *J. Am. Chem. Soc.*, **1993**, *115*, 118–127.

19. Himeda, Y. *Eur. J. Inorg. Chem.*, **2007**, 3927–3941.

20. Himeda, Y.; Miyazawa, S.; Hirose, T. *ChemSusChem*, **2011**, *4*, 487–493.

21. Tanaka, R.; Yamashita, M.; Nozaki, K. *J. Am. Chem. Soc.*, **2009**, *131*, 14168–14169.

22. Tanaka, R.; Yamashita, M.; Chung, L. W.; Morokuma, K.; Nozaki, K. *Organometallics*, **2011**, *30*, 6742–6750.

23. Langer, R.; Diskin-Posner, Y.; Leitus, G.; Shimon, L. J. W.; Ben-David, Y.; Milstein, D. *Angew. Chem., Int. Ed.*, **2011**, 9948 –9952.

24. Schmeier, T. J.; Dobereiner, G. E.; Crabtree, R. H.; Hazari, N. *J. Am. Chem. Soc.*, **2011**, *133*, 9274–9277.

25. Vigalok, A.; Ben-David, Y.; Milstein, D. *Organometallics*, **1996**, *15*, 1839–1844.

26. Kaska, W.; Nemeh, S.; Shirazi, A.; Potuznik, S. *Organometallics*, **1988**, *7*, 13–15.

27. Roecker, L.; Meyer, T. J. *J. Am. Chem. Soc.*, **1986**, *108*, 4066–4073.

28. Casey, C. P.; Singer, S. W.; Powell, D. R. *Can. J. Chem.*, **2001**, *79*, 1002–1011.

29. Himeda, Y. *Green Chem.*, **2009**, *11*, 2018–2022.

30. Boddien, A.; Mellmann, D.; Gartner, F.; Jackstell, R.; Junge, H.; Dyson, P. J.; Laurenczy, G.; Ludwig, R.; Beller, M. *Science*, **2011**, *333*, 1733–1736.

31. Enthaler, S.; Von Langermann, J.; Schmidt, T. *Energy Environ. Sci.*, **2010**, *3*, 1207–1217.

32. Caix, C.; Chardon-Noblat, S.; Deronzier, A.; Moutet, J.-C.; Tingry, S. *J. Organomet. Chem.*, **1997**, *540*, 105–111.

33. Caix, C.; Chardon-Noblat, S.; Deronzier, A. *J. Electroanal. Chem.*, **1997**, *434*, 163–170.

34. Kang, P.; Cheng, C.; Chen, Z.; Schauer, C.; Meyer, T. J.; Brookhart, M. *J. Am. Chem. Soc.*, **2012**, *134*, 5000–5003.

35. Hu, Y.; Li, L.; Shaw, A. P.; Norton, J. R.; Sattler, W.; Rong, Y. *Organometallics*, **2012**, *31*, 5058–5064.

36. Wang, J. *Analytical Electrochemistry*; Wang, J., Ed.; John Wiley and Sons: Hoboken, NJ, 2006; Vol. 3, p. 250.

37. Bard, A. J.; Faulkner, L. R. *Electrochemical Methods: Fundamentals and Applications*; John Wiley and Sons: Hoboken, NJ, 2000; p. 856.

38. Savéant, J.-M.; Vianello, E. *Electrochim. Acta*, **1962**, *8*, 905–923.

39. DuBois, D. L.; Miedaner, A.; Haltiwanger, R. C. *J. Am. Chem. Soc.*, **1991**, *113*, 8153–8164.

40. Smieja, J. M.; Kubiak, C. P. *Inorg. Chem.*, **2010**, *49*, 449.

41. Wilson, A. D.; Newell, R.; McNevin, M. J.; Muckerman, J. T.; DuBois, M. R.; DuBois, D. L. *J. Am. Chem. Soc.*, **2006**, *128*, 358–366.

42. Bocarsly, A. B.; Gibson, Q. D.; Morris, A. J.; L'Esperance, R. P.; Detweiler, Z. M.; Lakkaraju, P. S.; Zeitler, E. L.; Shaw, T. W. *ACS Catal.*, **2012**, *2*, 1684–1692.

43. Benson, E. E.; Kubiak, C. P.; Sathrum, A. J.; Smieja, J. M. *Chem. Soc. Rev.*, **2009**, *38*, 89–99.

44. Sutin, N.; Creutz, C.; Fujita, E. *Comments Inorg. Chem.*, **1997**, *19*, 67–92.

45. Hori, Y.; Wakebe, H.; Tsukamoto, T.; Koga, O. *Electrochim. Acta*, **1994**, *39*, 1833–1839.

46. Hossain, A. G. M. M.; Nagaoka, T.; Ogura, K. *Electrochim. Acta*, **1997**, *42*, 2577–2585.

47. Hossain, A. G. M. M.; Nagaoka, T.; Ogura, K. *Electrochim. Acta*, **1996**, *41*, 2773–2780.

48. Slater, S.; Wagenknecht, J. *J. Am. Chem. Soc.*, **1984**, 5367–5368.

49. Bolinger, C.; Story, N.; Sullivan, B.; Meyer, T. J. *Inorg. Chem.*, **1988**, *27*, 4582–4587.

50. Ishida, H.; Tanaka, H.; Tanaka, K.; Tanaka, T. *J. Chem. Soc., Chem. Commun.*, **1987**, 131–132.

51. Arana, C.; Yan, S.; Keshavarz-K, M.; Potts, K.; Abruna, H. *Inorg. Chem.*, **1992**, *31*, 3680–3682.

52. Rail, M. D.; Berben, L. A. *J. Am. Chem. Soc.*, **2011**, *133*, 18577–18579.

53. Chen, Y.-X.; Heinen, M.; Jusys, Z.; Behm, R. J. *Langmuir*, **2006**, *22*, 10399–10408.

54. Yu, Y.; Wang, X.; Lim, K. H. *Catal. Lett.*, **2011**, *141*, 1872–1882.

55. Cuesta, A.; Escudero, M.; Lanova, B.; Baltruschat, H. *Langmuir*, **2009**, *25*, 6500–6507.

56. Zhu, Y.; Khan, Z.; Masel, R. I. *J. Power Sources*, **2005**, *139*, 15–20.

57. Morgan, R. D.; Salehi-Khojin, A.; Masel, R. I. *J. Phys. Chem. C*, **2011**, *115*, 19413–19418.

58. Haan, J.; Masel, R. I. *ECS Trans.*, **2008**, *16*, 627–638.

59. Yu, X.; Pickup, P. G. *J. Power Sources*, **2008**, *182*, 124–132.

60. Jiang, J.; Kucernak, A. *J. Electroanal. Chem.*, **2009**, *630*, 10–18.

61. Sathe, B. R.; Balan, B. K.; Pillai, V. K. *Energy Environ. Sci.*, **2011**, *4*, 1029–1036.

62. Wang, S.; Wang, X.; Jiang, S. P. *Phys. Chem. Chem. Phys.*, **2011**, *13*, 6883–6891.

63. Reda, T.; Plugge, C. M.; Abram, N. J.; Hirst, J. *Proc. Natl. Acad. Sci. U. S. A.*, **2008**, *105*, 10654–10658.

64. Jiang, J.; Holm, R. H. *Inorg. Chem.*, **2004**, *43*, 1302–1310.

65. Sung, K.-M.; Holm, R. H. *Inorg. Chem.*, **2001**, *40*, 4518–4525.

66. Enemark, J. H.; Cooney, J. J. A.; Wang, J.-J.; Holm, R. H. *Chem. Rev.*, **2004**, *104*, 1175–1200.

67. Raaijmakers, H. C. A.; Romão, M. J. *J. Biol. Inorg. Chem.*, **2006**, *11*, 849–854.

68. Leopoldini, M.; Chiodo, S. G.; Toscano, M.; Russo, N. *Chemistry*, **2008**, *14*, 8674–8681.

69. Axley, M. J.; Böck, A.; Stadtman, T. C. *Proc. Natl. Acad. Sci. U. S. A.*, **1991**, *88*, 8450–8454.

70. Costentin, C.; Drouet, S.; Robert, M.; Savéant, J.-M. *Science*, **2012**, *338*, 90–94.

71. Hull, J. F.; Himeda, Y.; Wang, W.-H.; Hashiguchi, B.; Periana, R.; Szalda, D. J.; Muckerman, J. T.; Fujita, E. *Nature Chem.*, **2012**, *4*, 383–388.

72. Curtis, C. J.; Miedaner, A.; Ciancanelli, R.; Ellis, W. W.; Noll, B. C.; DuBois, M. R.; DuBois, D. L. *Inorg. Chem.*, **2003**, *42*, 216–227.

73. Helm, M. L.; Stewart, M. P.; Bullock, R. M.; DuBois, M. R.; DuBois, D. L. *Science*, **2011**, *333*, 863–866.

74. Frey, M. *Chembiochem*, **2002**, *3*, 153–160.

75. Wilson, A. D.; Newell, R.; McNevin, M. J.; Muckerman, J. T.; DuBois, M. R.; DuBois, D. L. *J. Am. Chem. Soc.*, **2006**, *128*, 358–366.

76. Wiese, S.; Kilgore, U. J.; DuBois, D. L.; Bullock, R. M. *ACS Catal.*, **2012**, *2*, 720–727.

77. Yang, J. Y.; Chen, S.; Dougherty, W. G.; Kassel, W. S.; Bullock, R. M.; DuBois, D. L.; Raugei, S.; Rousseau, R. J.; Dupuis, M.; DuBois, M. R. *Chem. Commun.*, **2010**, *46*, 8618–8620.

78. Chen, S.; Rousseau, R.; Raugei, S.; Dupuis, M.; DuBois, D. L.; Bullock, R. M. *Organometallics*, **2011**, *30*, 6108–6118.

79. Curtis, C. J.; Miedaner, A.; Raebiger, J. W.; DuBois, D. L. *Organometallics*, **2004**, *23*, 511–516.

80. Berning, D. E.; Noll, B. C.; DuBois, D. L. *J. Am. Chem. Soc.*, **1999**, *121*, 11432–11447.

81. Miedaner, A.; Haltiwanger, R. C.; DuBois, D. L. *Inorg. Chem.*, **1991**, *30*, 417–427.

82. Raebiger, J. W.; Miedaner, A.; Curtis, C. J.; Miller, S. M.; Anderson, O. P.; DuBois, D. L. *J. Am. Chem. Soc.*, **2004**, *126*, 5502–5514.

83. Nimlos, M. R.; Chang, C. H.; Curtis, C. J.; Miedaner, A.; Pilath, H. M.; DuBois, D. L. *Organometallics*, **2008**, *27*, 2715–2722.

84. DuBois, D. L.; Berning, D. E. *Appl. Organomet. Chem.*, **2000**, *14*, 860–862.

Chapter 2

The mechanism of electrocatalytic formate oxidation by $[Ni(P_2N_2)_2]^{2+}$ complexes

2.1 Introduction

At the end of her year-long postdoctoral appointment in the Kubiak lab, Dr. Julia Schöffel left behind four important things as her legacy: a recorded announcement for lunch on the porch, group familiarity with "the mysterious Knödel", knowledge that the $[Ni(P_2N_2)_2]^{2+}$ complexes that she had made in the lab were formate oxidation electrocatalysts, and a new collaboration with Dr. Dan DuBois's group at PNNL. "Now it is your job to make the mechanism," she said, then laughed as she rode away on her bicycle. This chapter discusses our collaborative efforts with Drs. John Linehan, Brandon Galan, and Aaron Appel to elucidate the mechanism of formate oxidation in hopes of developing better catalysts.

Dr. Linehan is the NMR expert in the PNNL group, and on Dr. Schoffel's visit they measured the hydricities of the new Ni complexes by observing the equilibrium between H_2

gas and nickel hydrides using high-pressure NMR. This equilibrium value can be combined with others obtained from electrochemical measurements to yield both the hydricity (**Scheme 1**) and pK_a (**Scheme 2**) of the Ni-H complex. Using his high pressure NMR setup, they also confirmed that the complexes did not reduce CO_2 even when CO_2 and H_2 were held at high pressures.

	ΔG° (kcal/mol)	
$[HNi(P_2N_2)_2]^+ + HB^+ \rightleftharpoons H_2 + [Ni(P_2N_2)_2]^{2+} + B$	$-RT \ln K_{eq}$	(1)
$B + H^+ \rightleftharpoons HB^+$	$-1.364\ pK_a$	(2)
$H_2 \rightleftharpoons H^+ + H^-$	76.0 kcal/mol	(3)
$[HNi(P_2N_2)_2]^+ \rightleftharpoons [Ni(P_2N_2)_2]^{2+} + H^-$	$-RT \ln K_{eq} - 1.364\ pK_a + 76.0$	(4)

Scheme 2-1. Thermodynamic scheme for calculation of hydricity ($\Delta G°_{H-}$).

	ΔG° (kcal/mol)	
$[HNi(P_2N_2)_2]^+ \rightleftharpoons [Ni(P_2N_2)_2]^{2+} + H^-$	$\Delta G°_{H-}$	(5)
$[Ni(P_2N_2)_2]^{2+} + 2e^- \rightleftharpoons [Ni(P_2N_2)_2]$	$-F\{E(Ni_{II/I}) + E(Ni_{I/0})\}$	(6)
$H^- \rightleftharpoons H^+ + 2e^-$	−79.6 kcal/mol	(7)
$[HNi(P_2N_2)_2]^+ \rightleftharpoons [Ni(P_2N_2)_2] + H^+$	$\Delta G°_{H-} - F\{E(Ni_{II/I}) + E(Ni_{I/0})\} - 79.6$ kcal/mol	(8)
	$pK_a = \Delta G°_{H+}/(2.303RT)$	

Scheme 2-2. Thermodynamic scheme for calculation of pK_a.

Dr. Appel and Dr. Galan planned and executed the majority of the early electrochemical work on this project, including measurements of the redox potentials of all the complexes. The cyclic voltammetry of the new compounds was very similar to other Ni compounds, and showed two reversible one-electron waves corresponding to the Ni(II/I) and Ni(I/0) redox couples (**Figure 2-1**, black trace). From there, Dr. Galan collected other several important pieces of data. First, he showed that there was an increase in oxidative catalytic

current when formate was added to the catalyst solution (**Figure 2-1**, all traces). By varying the concentration of formate and catalyst and observing the effect on the reaction rate, he determined that the reaction was first order in [catalyst] and first order in [formate] at lower concentrations, then [formate]-independent at higher concentrations. Next, he compared the activity of the $[Ni(P_2N_2)_2]^{2+}$ catalysts to that of $[Ni(dppe)_2]^{2+}$, which does not contain a pendant base, and found that this latter compound did not act as a catalyst. Finally, he compared the formate oxidation rates of a large range of $[Ni(P_2N_2)_2]^{2+}$ catalysts under identical conditions.

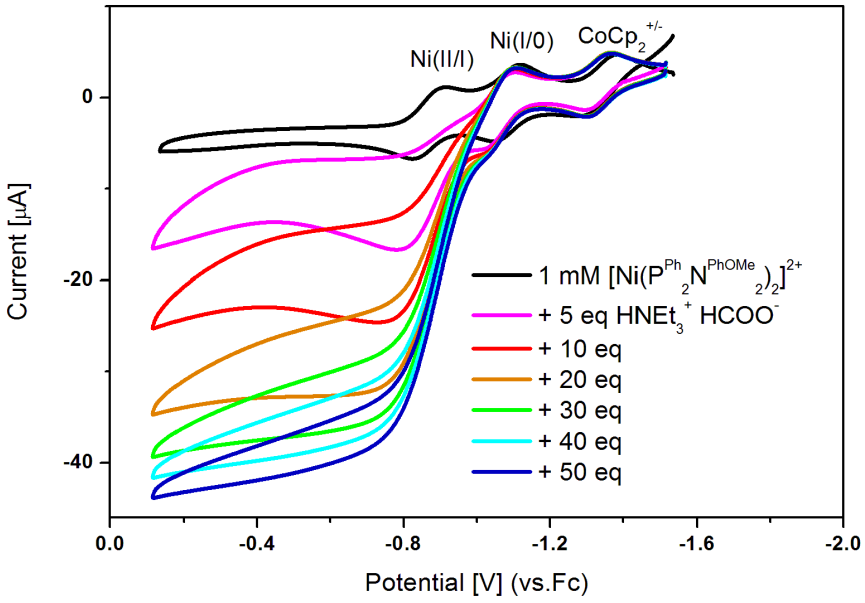

Figure 2-1. Cyclic voltammograms of $[Ni(P^{Ph}_2N^{PhOMe}_2)_2]^{2+}$ in solution alone (black trace) and in the presence of increasing amounts of $HNEt_3^+$ $HCOO^-$. Conditions: Glassy carbon working electrode, Pt counter electrode, AgCl reference electrode, 0.2 M NBu_4OTf electrolyte in ACN, scan rate 50 mV/s.

The results of the hydricity, pK_a, and electrochemical measurements are summarized in **Table 2-1**. In agreement with previous studies, there was a strong linear correlation between hydricity and the Ni(II/I) potential, and between the Ni–H pK_a and the Ni(I/0) potential.[1] Working in parallel, Dr. Appel and I noticed several other interesting trends. First,

there was a general (although not linear) inverse correlation between hydride acceptor ability and formate oxidation rate. In the context of Darensbourg's studies on metal hydride insertion[2–4] and the DuBois group's studies on hydrogen oxidation with these complexes,[5–8] we anticipated that formate oxidation would similarly proceed as a hydride transfer between formate and the metal; thus, the better hydride acceptors would also be the fastest catalysts. Our observation of exactly the opposite was our first indication that unraveling this story would not be easy.

Table 2-1. Thermodynamic, electrochemical, and catalytic rate data for various $[Ni(P_2N_2)_2]^{2+}$ compounds tested as formate oxidation electrocatalysts, listed in order of increasing donor acceptor ability. Rate data collected in benzonitrile; all other data collected in acetonitrile. Adapted from Galan, B.R. *et al*.[9]

$[Ni(P_2N_2)_2]^{2+}$ Ligands	$E_{1/2}(Ni^{II/I})$ (V *vs*. $Fc^{+/0}$)	$E_{1/2}(Ni^{I/0})$ (V *vs*. $Fc^{+/0}$)	ΔG^{o}_{H-} (kcal/mol)	Ni–H pK_a	TOF (s^{-1})
$P^{Ph}_2N^{Me}_2$	–0.98	–1.14	56.4	18.5	15.8
$P^{Ph}_2N^{Bn}_2$	–0.94	–1.19	57.1	19.4	12.5
$P^{Ph}_2N^{PhOMe}_2$	–0.87	–1.07	58.6	17.4	8.7
$P^{Ph}_2N^{Ph}_2$	–0.84	–1.02	59.0	16.3	7.4
$P^{Cy}_2N^{Bn}_2$	–0.80	–1.28	60.7	21.2	9.6
$P^{Ph}_2N^{PhCF3}_2$	–0.74	–0.89	61.4	13.8	3.4
$P^{Cy}_2N^{Ph}_2$	–0.62	–1.09	63.7	17.3	<1.1

Next, there appeared to be no relationship between Ni–H pK_a and TOF. We then began looking at the pK_as of the pendant bases on the ligands, as a correlation here would support our premise that the bifunctional ligand would assist catalysis. Here, we saw a general correlation between stronger bases and faster catalysis, which suggested that the rate-determining step of catalysis involved a proton transfer to the ligand (**Table 2-2**).

Table 2-2. pK_a and rate data for various $[Ni(P_2N_2)_2]^{2+}$ compounds tested as formate oxidation electrocatalysts, listed in order of fastest to slowest. Adapted from Galan, B.R. *et al*.[9]

$[Ni(P_2N_2)_2]^{2+}$ Ligands	Ni–H pK_a	$N^{R'}H_3^+$ pK_a	ΔpK_a	TOF (s^{-1})
$P^{Ph}{}_2N^{Me}{}_2$	18.5	18.4	0.1	15.8
$P^{Ph}{}_2N^{Bn}{}_2$	19.4	16.9	2.5	12.5
$P^{Cy}{}_2N^{Bn}{}_2$	21.2	16.9	4.3	9.6
$P^{Ph}{}_2N^{PhOMe}{}_2$	17.4	11.9	5.5	8.7
$P^{Ph}{}_2N^{Ph}{}_2$	16.3	10.6	5.7	7.4
$P^{Ph}{}_2N^{PhCF3}{}_2$	13.8	8.0	5.8	3.4
$P^{Cy}{}_2N^{Ph}{}_2$	17.3	10.6	6.7	<1.1

The exact nature of this proton transfer, however, was unclear. Again, the correlation between ligand pK_a and rate was not linear (**Figure 2-2a**). In particular, it appeared that the catalysts bearing cyclohexylphosphine substituents were much slower than their phenylphosphine counterparts. We then considered the fact that a proton transfer involves a donor, and working under the hypothesis that the donor was a Ni–H, calculated the pK_a differences between each metal hydride and its respective ligand. This yielded a correlation between ΔpK_a and rate that increased monotonically, and gratifyingly so—except for the fact that the correlation was also not linear, but followed a polynomial curve (**Figure 2-2b**).

Dr. Appel pointed out that treating the $P^{Ph}{}_2N^{R'}{}_2$ and $P^{Cy}{}_2N^{R'}{}_2$ catalysts as two separate groups would yield two distinct, linear correlations between ligand pK_a and TOF. The two-point P^{Cy} trend was of course not very reliable, but we could add more data points to test it further. Regardless of the outcome, the question of how exactly to "make the mechanism" would still be wide open, and we resolved to go through the possibilities as systematically as we could.

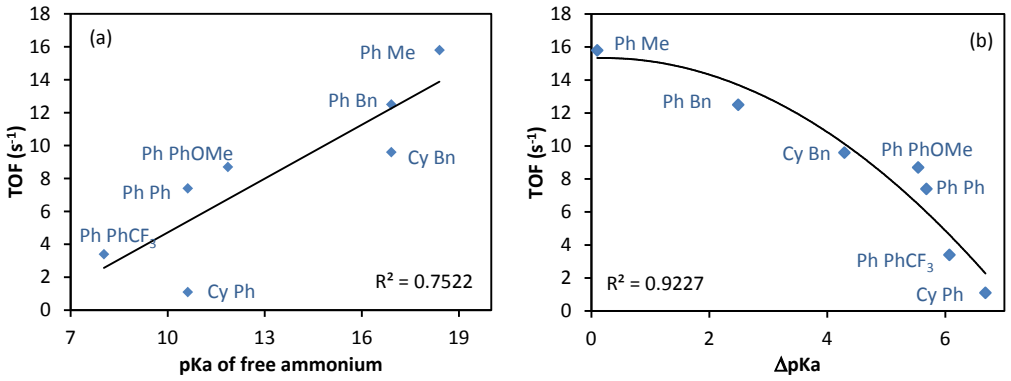

Figure 2-2. (a) Correlation between ligand pK_a and TOF, (b) correlation between ΔpK_a and TOF for various $[Ni(P_2N_2)_2]^{2+}$ compounds tested as formate oxidation electrocatalysts.

2.2 Possible Mechanisms

The reverse of formate oxidation is the two electron, one proton reduction of CO_2 which, on the basis of extensive work on metal hydricities[1,10–12] and many examples of CO_2 insertion into a metal-hydride bond,[13–22] is often envisioned as occurring through a hydride transfer reaction to the central carbon. Therefore, we thought it essential to carefully consider formate oxidation mechanisms in which the oxidation proceeds through a direct hydride transfer from formate to the metal center. There are two common and generally accepted pathways for hydride transfer to a metal center. β-hydride elimination requires pre-coordination of a hydride donor reagent to the metal center; the hydride is transferred to an empty coordination site and the remaining atoms in the donor are released in a double-bonded oxidized form, such as an olefin in the case of alkyl β-hydride elimination. Alternatively, direct hydride transfer does not require pre-association of the hydride donor, and the hydride is thought to transfer to the metal in a linear, outer-sphere transition state (**Figure 2-3**).

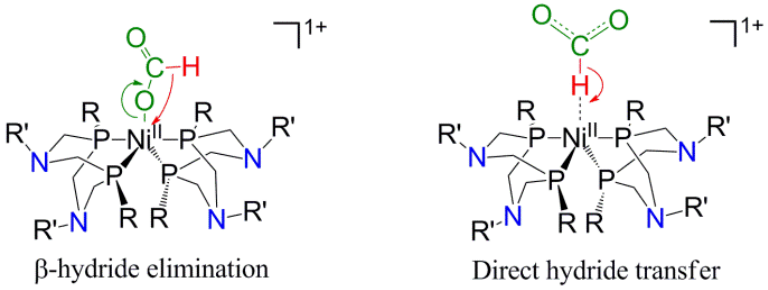

Figure 2-3. Pathways for formation of a metal hydride species.

However, the lack of a correlation between electrocatalytic TOF and driving force for hydride donation to the metal center suggested to us that if hydride formation did occur, it was not the rate-limiting step. We also agreed it was more likely that the electrode would oxidize a Ni(0) species back to Ni(II) to regenerate the starting complex, rather than oxidizing a Ni(II) hydride species to a highly acidic Ni(III) hydride that would subsequently lose a proton and second electron to return to Ni(II). This was based on evidence that catalytic current enhancement appears at the Ni(II/I) oxidation potential, which is 0.4 V more negative than that required to oxidize Ni(II)–H.[9]

Reasoning that the catalytic cycle had to start with formate binding to the Ni center and would involve generation of a Ni(0) NH^+ species, we came up with two possible pathways, both with several variations regarding the rate-determining step (**Scheme 2-3**). These included:

1. β-hydride elimination involving a rate-determining phosphine ligand dissociation necessary to create a 16-electron complex with an empty coordination site
2. β-hydride elimination or direct hydride transfer, followed by rate-determining intramolecular deprotonation of the nickel hydride
3. Rate-determining β-deprotonation of bound formate

The last of these seemed to be an unlikely shot in the dark with very little precedent, a suggestion better suited to biologists and other non-chemists. However, as we will see, the

most important thing I learned during my first foray into mechanistic chemistry was this: never discount any possibility until you have data to warrant it.

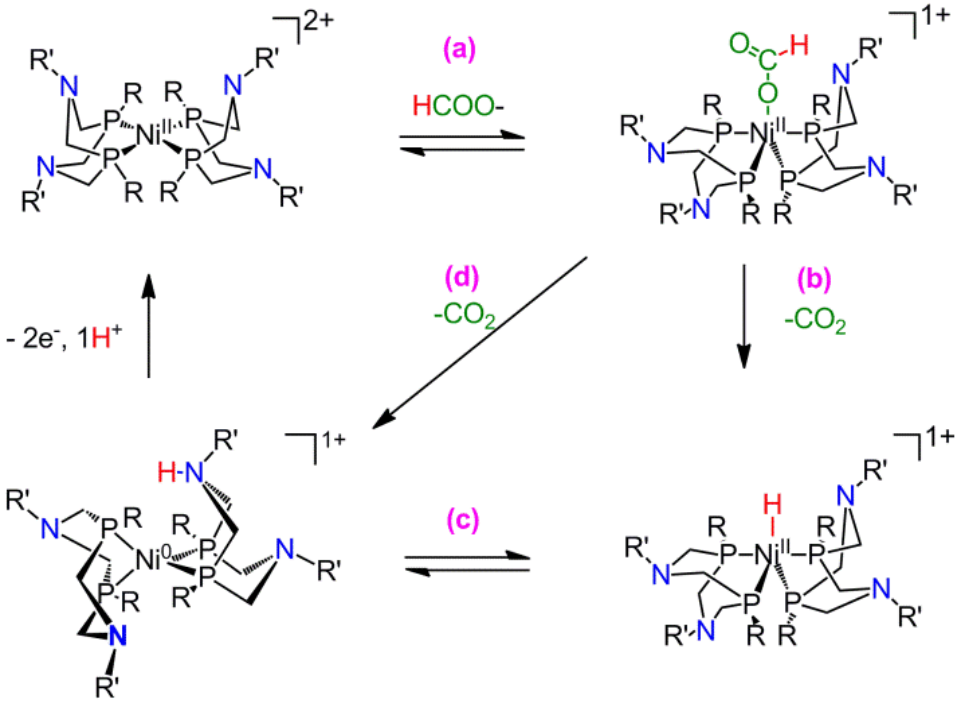

Scheme 2-3. Possible rate-determining steps and pathways for formate oxidation.

2.3 Experimental

General procedures

All chemicals were purchased from commercial sources and used as received unless otherwise specified. All manipulations were carried out using standard Schlenk and glove box techniques under an atmosphere of nitrogen. Acetonitrile, tetrahydrofuran (THF), pentane, and diethyl ether (Et_2O) were sparged with argon and dried over basic alumina in a custom dry solvent system. Liquid aniline reagents were generally dried over CaH_2 and distilled under vacuum or nitrogen to yield clear, air-free reagents. Solid aniline reagents were purified by recrystallization from H_2O/Et_2O and dried under vacuum overnight.

Tetrabutylammonium trifluoromethanesulfonate (NBu_4OTf) and tetrabutylammonium hexafluorophosphate (NBu_4PF_6) were recrystallized from MeOH before use in electrochemical experiments. $NBu_4HCO_2{\bullet}HCO_2H$ was prepared according to a modification of a previously published procedure, in which the ratio of formic acid to tetrabutylammonium hydroxide (NBu_4OH) used was 2:1 and the aqueous layer of the extraction was saturated with NaHCOO.[9] $NBu_4DCO_2{\bullet}HCO_2D$ was prepared by the analogous reaction of NBu_4OH and d_2-formic acid. ^1H, ^{31}P, and $^{31}P\{1H\}$ NMR spectra were recorded on a Varian 300 or a Jeol ECA-500 spectrometer. ^1H NMR spectra are referenced to residual resonances of the protonated solvent, and ^{31}P NMR shifts are referenced to H_3PO_4. Elemental analysis was performed by Midwest MicroLab, LLC, Indianapolis, IN and Numega Resonance Labs, San Diego, CA.

Electrochemical experiments

All electrochemical experiments were carried out under an atmosphere of nitrogen in a 0.2 M NBu_4OTf or NBu_4PF_6 solution in benzonitrile using a BAS Epsilon or Gamry Reference 600 series three electrode potentiostat. The working electrode was a glassy carbon disk (1 or 3 mm diameter), the counter electrode was a glassy carbon rod, and a silver wire in electrolyte solution separated from the working compartment by porous Vycor (4 mm, BAS) was used as a pseudo-reference electrode. All potentials were measured using $CoCp_2^{+/0}$ (–1.33 V) as an internal reference, with all potentials reported vs. the $FeCp_2^{+/0}$ couple.

CV titrations of the catalysts were generally carried out using 1 mL volumes of 1 mM catalyst solutions in electrolyte solution. 1 M solutions of the appropriate titrant were prepared using the same electrolyte solution, such that adding 1 μL of titrant solution to the 1 mL catalyst solution resulted in introduction of 1 equivalent of titrant. CVs were taken after addition and hand mixing of 5-10 equivalents at a time. In some cases 10 mL solutions of the

catalyst were titrated and the volume of titrant was increased accordingly by a factor of 10 as well.

Formate and acetate competition

1 M solutions of $(HNEt_3)O_2CH$ and $(HNEt_3)OAc$ were prepared by mixing equal amounts of triethylamine (0.697 mL, 0.005 mol) and either 88% formic (0.261 g) or glacial acetic acid (0.285 mL), and diluting with the electrolyte solution (0.2 M NBu_4PF_6 in PhCN) up to 5 mL in a volumetric flask. A 1 M solution of NBu_4Br was prepared using the same electrolyte solution. The solutions were transferred to Schlenk flasks and sparged with N_2 for 10 minutes before use. Solutions of 1 mM $[Ni(P^{Ph}{}_2N^{PhOMe}{}_2)_2(CH_3CN)](BF_4)_2$ were then titrated and followed via CV using the general procedure.

Scan rate dependence study

A 1 mM solution of $[Ni(P^{Ph}{}_2N^{PhOMe}{}_2)_2(CH_3CN)](BF_4)_2$ in 0.2 M NBu_4PF_6/PhCN was titrated with the 1 M solution of $(HNEt_3)O_2CH$ described above, using the same general titration procedure. Data was collected at various formate concentrations and multiple scan rates ranging between 50 mV/s – 50 V/s using a Gamry Reference 600 potentiostat with CI-IR compensation. Electrolyte blanks were taken and subtracted from all data sets to partially correct for the charging current.

$Na[B(OMe)_3H]$ titration

A 1 M solution of $Na[HB(OMe)_3]$ (0.640 g, 0.005 mol) was prepared in 5 mL of a 0.2 M NBu_4OTf solution of THF. 100 μL aliquots of this solution were titrated into 10 mL of a 1 mM solution of $[Ni(P^{Ph}{}_2N^{PhOMe}{}_2)_2(CH_3CN)](BF_4)_2$ in 0.2 M NBu_4OTf/PhCN using the same general procedure.

Kinetic isotope effect

NBu_4HCO_2•HCO_2H and NBu_4DCO_2•DCO_2D were prepared by mixing two equivalents of formic acid or deuterated formic acid with one equivalent of NBu_4OH. The solution was stirred overnight and subsequently extracted with 3x15 mL EtOAc. The organic layer was dried over $MgSO_4$, gravity filtered, and evaporated under high vacuum to yield on oil, which solidified into white crystals upon addition and evaporation of Et_2O. The solid was purified by recrystallization in THF layered with pentane, rinsed with pentane, and dried under vacuum overnight. Catalyst solutions were titrated and TOFs were calculated for both variants using the exact same setup and parameters in the previous paper,[9] and k_H/k_Ds were calculated from the ratio of TOFs.

Arrhenius and Eyring parameters

Titrations of $[Ni(P^{Ph}{}_2N^{PhOMe}{}_2)_2(CH_3CN)](BF_4)_2$ with NBu_4HCO_2•HCO_2H in 0.2 M NBu_4OTf/PhCN were carried out using the standard procedure at temperatures between 5-34°C (intervals of approximately 5 °C). Heating and cooling of the sample was accomplished by placing the sample in an acetonitrile bath wrapped in copper piping attached to a circulating chiller/heater, and the temperature of the bath was monitored throughout the titration to ensure that it remained stable.

Crystallography

Crystals of $[Ni(P^{Cy}{}_2N^{PhOMe}{}_2)_2(CH_3CN)](BF_4)_2$ suitable for X-ray structural determinations were mounted in polybutene oil on a glass fiber and transferred on the goniometer head to the precooled instrument. Crystallographic measurements were carried out on a Bruker P4 diffractometer using Mo Kα radiation (λ = 0.71073 Å) in conjunction with a Bruker APEX detector. All structures were solved by direct methods using OLEX2 and refined with full-matrix least-squares procedures using SHELXL-97. All non-hydrogen atoms are anisotropically refined unless otherwise reported; the hydrogen atoms were included in

calculated positions as riding models in the refinement. Crystallographic data collection and refinement information can be found in the Appendix.

Synthesis of $P^{Cy}{}_2N^{PhOMe}{}_2$

Cyclohexylphosphine (1.00 mL, 7.5 mmol) was placed in a Schlenk flask and cannula transferred into a flask containing paraformaldehyde (0.45 g, 15.0 mmol) in EtOH (15 mL). The reaction was stirred under reflux for 2 h and the white suspension became clear. 4-methoxyaniline (0.92 g, 7.5 mmol) was added via syringe and the reaction was further refluxed for 3 h, then cooled. A white precipitate began forming within 30 minutes of the 2nd reflux, and after cooling, the solid was collected by cannula filtration, rinsed twice with ethanol, and dried under vacuum to yield 1.74 g (3.37 mmol, 90%) of $P^{Cy}{}_2N^{PhOMe}{}_2$ ligand, used without further purification. ^{1}H NMR ($CDCl_3$, 300 MHz, $CHCl_3$) [ppm]: δH 6.8 (4H, d, J_{23}= 9Hz, Ar 2,6-H), 6.6 (4H, d, J_{32} = 9Hz, Ar 3,5-H), 4.2-3.4 (8H, m, PCH2N), 3.76 (3H, s, OMe), 3.71 (3H, s, OMe), 1.9-1.2 (22H, m, Cy). $^{31}P\{^1H\}$NMR ($CDCl_3$, 121 MHz, H_3PO_4) [ppm]: δP –39.9 (s).

Synthesis of $[Ni(P^{Cy}{}_2N^{PhOMe}{}_2)_2(CH_3CN)](BF_4)_2$

$P^{Cy}{}_2N^{PhOMe}{}_2$ (340 mg, 0.66 mmol) was added to a blue solution of $[Ni(CH_3CN)_6](BF_4)_2$ (144 mg, 0.30 mmol) in acetonitrile (15 mL). The initially cloudy red suspension was stirred at room temperature overnight until the ligand dissolved. The dark red solution was cannula filtered to remove unreacted ligand, reduced to 10 mL under vacuum, and layered with diethyl ether to induce crystallization. Yield = 337 mg (0.25 mmol, 86%). Single crystals suitable for x-ray diffraction were obtained via vapor diffusion of diethyl ether into a concentrated acetonitrile solution of the complex at room temperature. ^{1}H NMR ($CDCl_3$, 300 MHz, $CHCl_3$) [ppm]: δH 7.1 (4H, d, J_{23}= 9Hz, Ar 2,6-H), 6.7 (4H, d, J_{32} = 9Hz, Ar 3,5-H), 3.8-3.4 (8H, m, PCH_2N), 3.78 (6H, s, OMe), 1.9-1.2 (22H, m, Cy). $^{31}P\{^1H\}$ NMR

($CDCl_3$, 121 MHz, H_3PO_4) [ppm]: δP 7.31 (s). Elemental analysis calculated for $C_{62}H_{91}B_2F_8N_5NiO_4P_4$: C, 56.1; H, 6.9; N, 5.3. Found: C, 56.6; H, 7.3; N, 5.6.

Synthesis of $P^{Cy}{}_2N^{PhCF3}{}_2$

Cyclohexylphosphine (0.53 mL, 4.0 mmol) was placed in a Schlenk flask and cannula transferred into a flask containing paraformaldehyde (0.24 g, 8.0 mmol) in 1-butanol 12 (mL). The reaction was stirred under reflux for 2 h and the white suspension became clear. 4-trifluoromethylaniline (0.50 mL, 4.0 mmol) was added via syringe and the reaction was further refluxed for 3 h, then cooled. A white precipitate began forming within 30 minutes of the 2nd reflux, and after cooling, the solid was collected by cannula filtration, rinsed twice with ethanol, and dried under vacuum to yield 0.85 g (1.4 mmol, 71%) of $P^{Cy}{}_2N^{PhCF3}{}_2$ ligand. ^1H NMR ($CDCl_3$, 300 MHz, $CHCl_3$) δH[ppm]: 7.4 (4H, d, J_{23} = 9 Hz, Ar 2,6-H), 6.6 (4H, d, J_{32} = 9Hz, Ar 3,5-H), 4.4-3.7 (8H, m, PCH_2N), 2.0-1.3 (22H, m, Cy). $^{31}P\{^1H\}$ NMR ($CDCl_3$, 121 MHz, H_3PO_4) δP[ppm]: –36.1 (s, major), –28.2 (s, minor), 10:1 intensities. Elemental analysis calculated for $C_{30}H_{38}F_6P_2N_2$: C, 59.8; H, 6.4; N, 4.65. Found: C, 59.6; H, 6.3; N, 4.5.

Synthesis of $[Ni(P^{Cy}{}_2N^{PhCF3}{}_2)_2(CH_3CN)](BF_4)_2$

$P^{Cy}{}_2N^{PhCF3}{}_2$ (360 mg, 0.60 mmol) was added to a blue solution of $[Ni(CH_3CN)_6](BF_4)_2$ (140 g, 0.30 mmol) in acetonitrile (12 mL). The initially cloudy red suspension was stirred at room temperature overnight until the ligand dissolved. The dark red solution was cannula filtered to remove unreacted ligand and dried under vacuum. The metal-ligand complex is rather unstable and tends to dissociate to mono-ligand complexes at room temperature in the presence of non-polar solvents and high concentrations of anions. This dissociation is signaled by a color change to yellow, corresponding to formation of square-planar Ni(II) complexes. Yield = 250 mg (0.17 mmol, 56%). Attempts to purify the complex by crystallization and to obtain crystals via liquid and vapor diffusion of diethyl ether into a concentrated acetonitrile solution of the red homoleptic Ni(II) complex at various

temperatures yielded highly disordered crystals of the above-mentioned square-planar complexes. ^{1}H NMR ($CDCl_3$, 300 MHz, $CHCl_3$) [ppm]: δH 7.8-7.6 (2H, d, J_{23} = 8.7 Hz, J_{25} = 39Hz, Ar 2,6-H), 6.6 (4H, d, J_{32} = 9Hz, Ar 3,5-H), 4.4-3.7 (8H, m, PCH_2N), 2.0-1.3 (22H, m, Cy). $^{31}P\{^{1}H\}$ NMR ($CDCl_3$, 121 MHz, H_3PO_4) [ppm]: δP 7.28 (s).

General procedure for $[HNi(P^{Ph}_2N^{PhOMe}_2)_2(CH_3CN)]^+$ disproportionation by NMR

A 1:4 mixture of CD_3CN and PhCN was used as the NMR solvent in order to avoid precipitation of the Ni(0) product. 0.4 mL of a 14 mM solution of $[Ni(P^{Ph}_2N^{PhOMe}_2)_2(CH_3CN)](BF_4)_2$ was placed in an NMR tube, which was then sealed with a septum. A solution of NBu_4HCO_2•HCO_2H was prepared separately in the same mixed solvent system at an appropriate concentration such that a 100 µL aliquot would deliver 1 or 20 equivalents of formate, relative to the Ni.

For the study of $[Ni(P^{Ph}_2N^{PhOMe}_2)_2(CH_3CN)]^{2+}$ with one equivalent of formate, the 0.4 mL $[Ni(P^{Ph}_2N^{PhOMe}_2)_2(CH_3CN)](BF_4)_2$ solution was heated to 50 °C in the spectrometer and a baseline spectrum was taken to confirm the stability of the complex. The pw90 and T_1 were measured via the inverse recovery method to be 15.4 µs and 0.6 s, respectively, and d_1 was set to 3 s. The sample was ejected, and 100 µL of titrant (56 mM, 1 equivalent formate) was added via syringe. The sample was shaken and replaced in the spectrometer. A 2D data set array consisting of 1D ^{31}P spectra taken at 1 hr intervals was collected using the standard spectrometer software.

For the study of $[Ni(P^{Ph}_2N^{PhOMe}_2)_2(CH_3CN)]^{2+}$ with excess formate, the same procedure was used except the formate concentration of the titrant was 112 mM (20 eq), the sample temperature was 22 °C, and pw90 and T_1 were measured to be 14.5 µs and 0.5 s. The first ^{31}P NMR was taken 4 minutes after mixing and showed that conversion was already complete.

2.4 Results and Discussion

2.4.1 NMR studies of intramolecular proton transfer

At the very beginning of our study, prior to our collaboration with Dr. Appel, we decided to start by looking at the proton transfer equilibrium between the metal and the pendant base. Julia had previously demonstrated that a Ni–H signal could be observed in the ^{31}P and ^{1}H NMR when $[Ni(P_2N_2)(CH_3CN)]^{2+}$ complexes were mixed with $HCOO^-$, and based on this, we hypothesized a very simple model for the oxidation and subsequent equilibrium:

$$[Ni(P_2N_2)_2]^{2+} + HCOO^- \rightleftharpoons [HNi(P_2N_2)_2]^+ \quad (1)$$

$$[HNi(P_2N_2)_2]^+ + :NR \rightleftharpoons [Ni(P_2N_2)_2] + HNR^+ \quad (2)$$

Scheme 2-4. Proposed $HCOO^-$ oxidation and proton transfer equilibrium. The :NR group depicted in (2) corresponds to the pendant base of the P_2N_2 ligand; the proton transfer is intramolecular.

We assumed that (1) would be fast enough to be completed in a few seconds, whereas (2) would reach equilibrium on a timescale of minutes to hours, and the kinetics of this step would thus be amenable to NMR observation. The signals corresponding to various Ni species are well separated in the ^{31}P NMR spectrum, and we thought that it would be convenient to follow the disappearance of the Ni(II)–H doublet and the appearance of the Ni(0) singlet. In this way, we could study how the identity of the pendant base affected the rate of proton transfer and the final equilibrium.

Focusing our initial efforts on the $[Ni(P^{Ph}{}_2N^{PhOMe}{}_2)_2(CH_3CN)](BF_4)_2$ complex, we mixed this catalyst with an equal amount of $NBu_4HCO_2{\bullet}HCO_2H$ and saw complete, immediate conversion of the Ni(II) species into a Ni–H species. Noting that the disappearance of the hydride under these conditions was extremely slow, we raised the temperature to 50 °C and found that the signal decreased at a rate compatible with overnight

or weekend NMR experiments (**Figure 2-4**). However, we were confused and troubled by the absence of any corresponding new signals. Hypothesizing that the lack of a Ni(0) signal might be due to precipitation of this species, we tested a variety of solvents and eventually settled on a mixture of CD_3CN and PhCN. We again received a similar result.

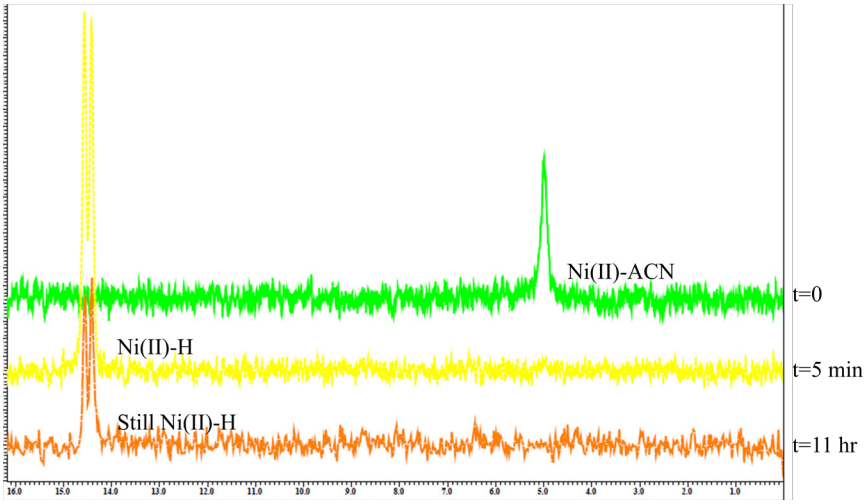

Figure 2-4. Series of NMR spectra showing 14 mM $[Ni(P^{Ph}_2N^{PhOMe}_2)_2]^{2+}$ before (green), 5 minutes after the addition of 1 equivalent of $NBu_4HCO_2{\bullet}HCO_2H$ (yellow), and 11 hours after mixing (orange). Conditions: 10% CD_3CN/90% PhCN, 50° C.

Recalling that Julia had earlier reported that solutions of Ni(II)–H decomposed slowly to release H_2 gas, we realized that this reaction, a disproportionation of Ni(II)–H, was likely happening in our NMR samples as well. It would thus be impossible to observe the intramolecular proton transfer in isolation from the subsequent intermolecular proton transfer that would evolve H_2. However, this explanation still left the question of why we did not observe signals for the Ni(II) and Ni(0) species that would be produced in this reaction. After sitting at my desk and staring into space for a little while, working on a hunch that production of a paramagnetic species was the reason for lack of signal, I realized that the equilibrium constant for the comproportionation of Ni(II) and Ni(0) to make Ni(I) could be calculated from their redox potentials, and was furthermore quite favorable (**Scheme 2-5**). Based on

this, we reasoned that an additional equivalent of formate might trap the half equivalent of Ni(II) before it could comproportionate with the half equivalent of Ni(0). This portion of Ni hydride would again disproportionate and the Ni(II) half would again be trapped, eventually resulting in complete conversion of Ni(II) into Ni(0) à la the convergent summation $\sum \frac{1}{2n}$. Subsequent NMR experiments with 2 or more equivalents of added formate bore out this prediction (**Figure 2-5**).

Scheme 2-5. Equilibrium constant calculation for the comproportionation of Ni(II) and Ni(0). Redox potentials measured in 0.1 M NBu_4OTf PhCN on glassy carbon vs. SHE.

$Ni^{2+} + 1\ e^- \rightleftharpoons Ni^+$	$E° = -0.26$ V
$Ni^0 \rightleftharpoons Ni^+ + 1\ e^-$	$E° = 0.46$ V
$Ni^{2+} + Ni^0 \rightleftharpoons 2\ Ni^+$	$E° = +0.20$ V
$E = RT/nF \ln(K) = 0.059\ V * \log(K)/2$	$K = 6.0 \times 10^6$

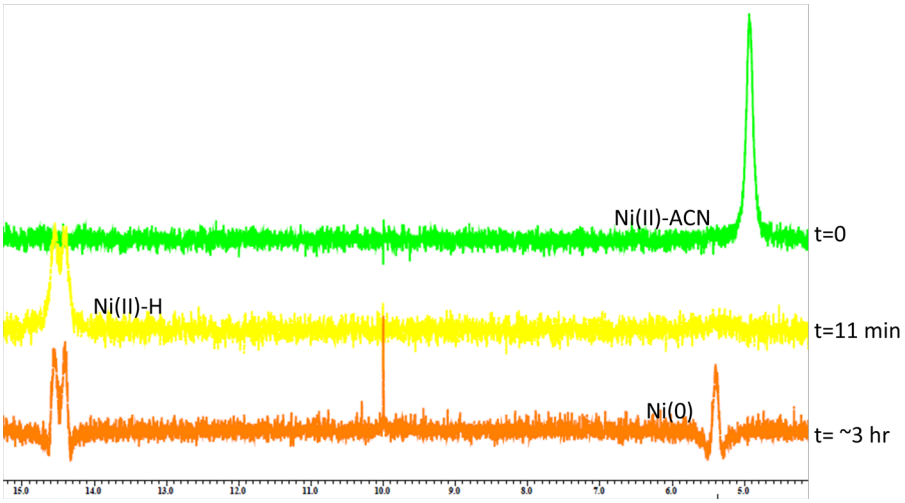

Figure 2-5. Series of NMR spectra showing 14 mM $[Ni(P^{Ph}_2N^{PhOMe}_2)_2]^{2+}$ before (green), 5 minutes after the addition of 1 equivalent of $NBu_4HCO_2•HCO_2H$ (yellow), and 11 hours after mixing (orange). Conditions: 20% CD_3CN/80% PhCN, 50 °C.

The results of our NMR experiments and our subsequent proposed thermal mechanism are summarized in **Scheme 2-6**. The intramolecular proton transfer step of

interest cannot be separated from the fast following reactions. Furthermore, it was not clear to us that these following reactions, while facile on the NMR timescale, would necessarily be relevant under electrochemical conditions. The link between structural geometry and Ni(II)/Ni(0) comproportionation rates would become the topic of an early EPR study by my colleague, Michael Doud, but for the purposes of the mechanistic project we decided to move on towards focusing on electrochemical experiments.

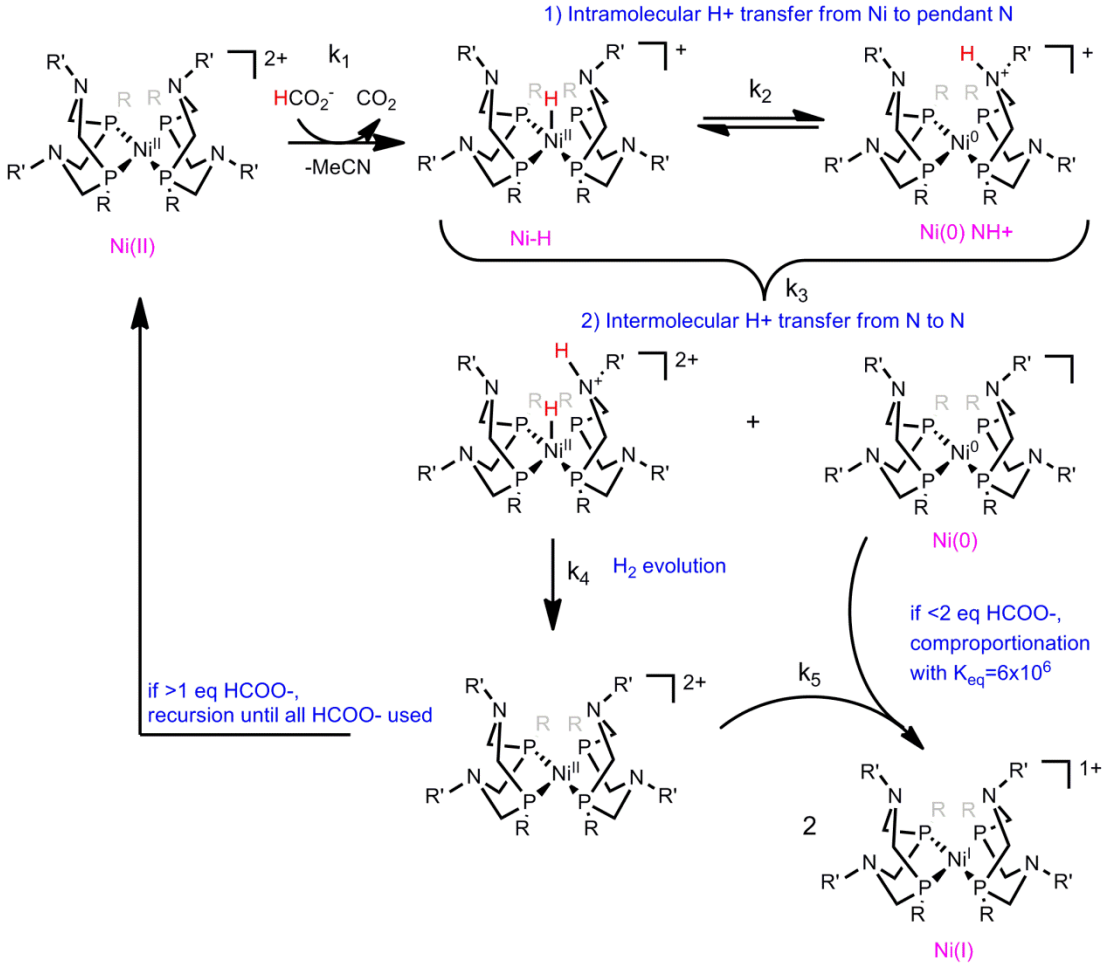

Scheme 2-6. Proposed mechanistic scheme for the thermal reaction of $[Ni(P^{Ph}_2N^{PhOMe}_2)_2]^{2+}$ with formate and associated comproportionation in solution.

2.4.2 Synthesis and characterization of new $[Ni(P^{Cy}_2N^{R'}_2)_2]^{2+}$catalysts

In order to test the validity of two separate pK_a-rate trends for the $P^{Ph}_2N^{R'}_2$ and $P^{Cy}_2N^{R'}_2$ catalysts, we attempted to synthesize two new $[Ni(P^{Cy}_2N^{R'}_2)_2]^{2+}$ complexes so that a larger number of direct analogues could be compared. The $P^{Cy}_2N^{PhOMe}_2$ and $P^{Cy}_2N^{PhCF3}_2$ ligands were synthesized using slight modifications of previously published methods,[7,9] and were obtained as fluffy white crystals. For $P^{Cy}_2N^{PhCF3}_2$, this required changing the solvent from ethanol to 1-butanol (b.p. = 118 °C) to thermally enhance the rate of nucleophilic attack by the poorly basic amine on $P^{Cy}(CH_2OH)_2$. The corresponding $[Ni(P^{Cy}_2N^{R'}_2)_2(CH_3CN)](BF_4)_2$ complexes were then obtained via reaction of the ligands with $[Ni(CH_3CN)_6](BF_4)_2$, yielding dark red products.

Crystals of $[Ni(P^{Cy}_2N^{PhOMe}_2)_2(CH_3CN)](BF_4)_2$ suitable for x-ray diffraction were obtained by liquid diffusion of diethyl ether into concentrated acetonitrile solutions of the complexes at –35 °C. Attempts to crystallize $[Ni(P^{Cy}_2N^{PhCF3}_2)_2(CH_3CN)](BF_4)_2$, however, were unsuccessful because solutions of the bis-homoleptic complex were unstable in the presence of non-polar solvents such as diethyl ether, which are able to dissolve the ligand and hence drive the dissociation of the complex through precipitation of the resulting ionic species. Furthermore, the $P^{Cy}_2N^{PhCF3}_2$ ligand appeared to exchange rapidly with coordinating anions such as ^-OTf and ^-O_2CH, precluding electrochemical characterization and use as an active catalyst.

The redox potentials for $[Ni(P^{Cy}_2N^{PhOMe}_2)_2(CH_3CN)](BF_4)_2$ were measured to be $E_{1/2}(Ni^{II/I})$ = –0.646 V and $E_{1/2}(Ni^{I/0})$ = –1.172 V. The electrocatalytic rate of formate oxidation was measured to be 3.4 s^{-1}, and is summarized along with previous results in **Figure 2-6**. When the collective rate data were plotted versus the pK_a values of the conjugate acids of the free amines used to synthesize the complex, the P^{Cy} (green) and P^{Ph} (blue)

complexes clearly followed two separate linear trends, suggesting that the two groups would be best treated separately.

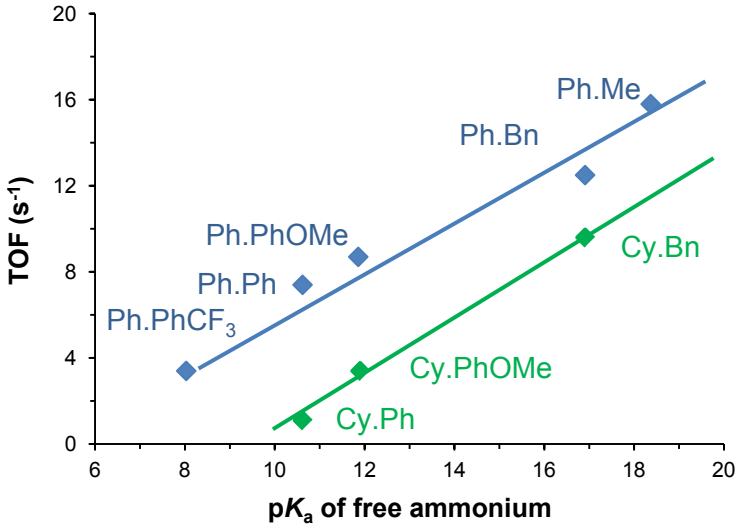

Figure 2-6. Electrocatalytic TOF for formate oxidation vs. the pK_a of the free primary ammonium (RNH_3^+) used to synthesize the $P^R{}_2N^{R'}{}_2$ ligands for each nickel complex. Data point labels in the figure refer to the R and R' substituents, respectively.

2.4.3 Competitive Ni(II) binding experiments with formate and acetate

One strategy for designing experiments to explore a mechanism involves looking at individual steps in the catalytic cycle and systematically perturbing their equilibria. This was not directly possible in the case of Ni(II) binding to formate, since this step is immediately followed by the irreversible decomposition of the Ni-formate complex to generate the Ni(II) hydride and CO_2. We thus explored the use of acetate as a formate analogue that is expected to bind Ni(II) in a manner similar to formate, but preclude the following decomposition reaction due to its lack of a β-hydrogen.

Overlays of multiple cyclic voltammograms taken after the titration of a $[Ni(P^{Ph}{}_2N^{PhOMe}{}_2)_2(CH_3CN)]^{2+}$ solution with 1-10 equivalents of $(HNEt_3)OAc$ are shown in **Figure 2-7a**. As the concentration of acetate increases and the binding equilibrium is shifted

towards Ni–OAc formation, the Ni(II/I) oxidation and reduction peaks both shift to more negative potentials. The reduction peak broadens as it shifts, and eventually becomes a shoulder overlapping with the Ni(I/0) reduction peak. The peaks do not change appreciably after 5 equivalents of acetate, suggesting complete conversion to the nickel-acetate complex.

When 10 equivalents of $(HNEt_3)O_2CH$ are added to a solution containing 1 equivalent of $[Ni(P^{Ph}{}_2N^{PhOMe}{}_2)_2(CH_3CN)]^{2+}$ and 10 eq. of $(HNEt_3)OAc$, the CV immediately changes (**Figure 2-7b**). An increase in catalytic current can be seen at the potential for the Ni(II/I) oxidation, suggesting that electrocatalytic formate oxidation is occurring even in the presence of excess acetate. In contrast, when 1 equivalent of NBu_4Br is subsequently added to this solution, the CV changes to a voltammogram characteristic of a Ni-halide complex, and no catalytic current enhancement can be seen at any formate concentration (**Figure 2-5c**).

Taken together, the data suggest that formate and acetate are both highly labile ligands for $[Ni(P^R{}_2N^{R'}{}_2)_2]^{2+}$ complexes, whereas halides are not (k_{dissoc} for $^-OAc \approx {}^-O_2CH >> {}^-X$). Furthermore, since formate oxidation occurs in the presence of pre-formed Ni–OAc complex at just slightly lower rates than without acetate, it is likely that ^-OAc does not bind more strongly than ^-O_2CH. Formate oxidation does not appear to compete with halide binding, consistent with a much lower association constant for both the formate and acetate than for halides (K_A for $^-OAc \approx {}^-O_2CH << {}^-X$). The K_A of ^-OAc can thus be treated as an approximation for the K_A of ^-O_2CH, and any experiments using acetate as a model for formate should take this binding behavior into account. Additionally, the irreversible inhibition of these catalysts by bromide underscores a need to avoid halide contamination in substrate sources and solvents.

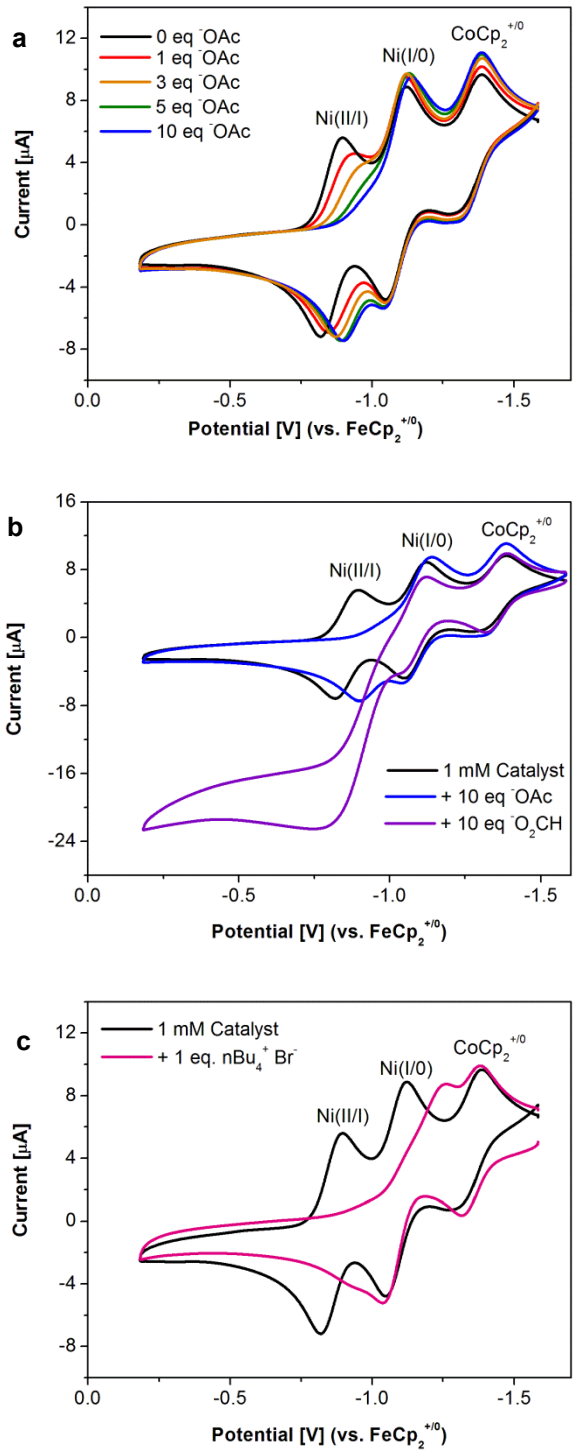

Figure 2-7. (a) Cyclic voltammograms of 1 mM $[Ni(P^{Ph}{}_2N^{PhOMe}{}_2)_2(CH_3CN)]^{2+}$ titrated with 10 equivalents acetate, (b) with 10 eq. formate, and (c) with 1 eq. bromide. Conditions: 1 mM catalyst in benzonitrile, 0.2 M NBu_4PF_6 as supporting electrolyte, glassy carbon working electrode, scan rate 50 mV/s.

2.4.4 Electrochemical scan rate dependence study of formate binding

Kinetic information about the chemical components of an electrochemical reaction can be gained by studying the dependence of the current response upon the scan rate of the potential sweep. Reactions that follow an electron transfer can, in some cases, be avoided by sweeping through the potential for the electron transfer and back (to a resting potential) before the subsequent reaction can occur, resulting in a simple, reversible CV. This technique can thus be used to bracket and estimate the rate of a reaction, and to thereby distinguish faster reaction steps from slower ones in an electrocatalytic cycle.

Cyclic voltammograms of $[Ni(P^{Ph}_2N^{PhOMe}_2)_2(CH_3CN)]^{2+}$ in the presence of excess $(HNEt_3)O_2CH$ were taken at variable scan rates between 0.05–50 V/s. At a catalytic TOF of ~9 s^{-1}, or ~0.1 s per turnover, and a potential sweep that is reversed ~0.27 V past the catalytic potential (and therefore a total traversed potential of ~0.5 V), the scan rate needed to prevent catalytic current enhancement is expected to be ~5 V/s. Between 50–500 mV/s, the CVs look essentially the same in that they contain the same features (**Figure 2-8a, b**). The increases in capacitive current and peak separation at higher scan rates are artifacts of the technique and do not reflect any fundamental change in reactivity.[23] While catalytic current is scan rate independent,[23] the peak current for non-catalytic waves is proportional to the square root of the scan rate, and therefore the height of the catalytic wave should appear to be smaller relative to the non-catalytic waves as the scan rate increases. In the presence of formate at 5 V/s, current enhancement from catalysis is essentially absent (**Figure 2-8c**). The overall shape of the CV with formate at this scan rate is reminiscent of that seen for Ni–acetate binding experiments (**Figure 2-7b**). These results suggest that the rate of formate association is much faster than the overall rate of catalysis, and therefore, formate association is not the rate determining step.

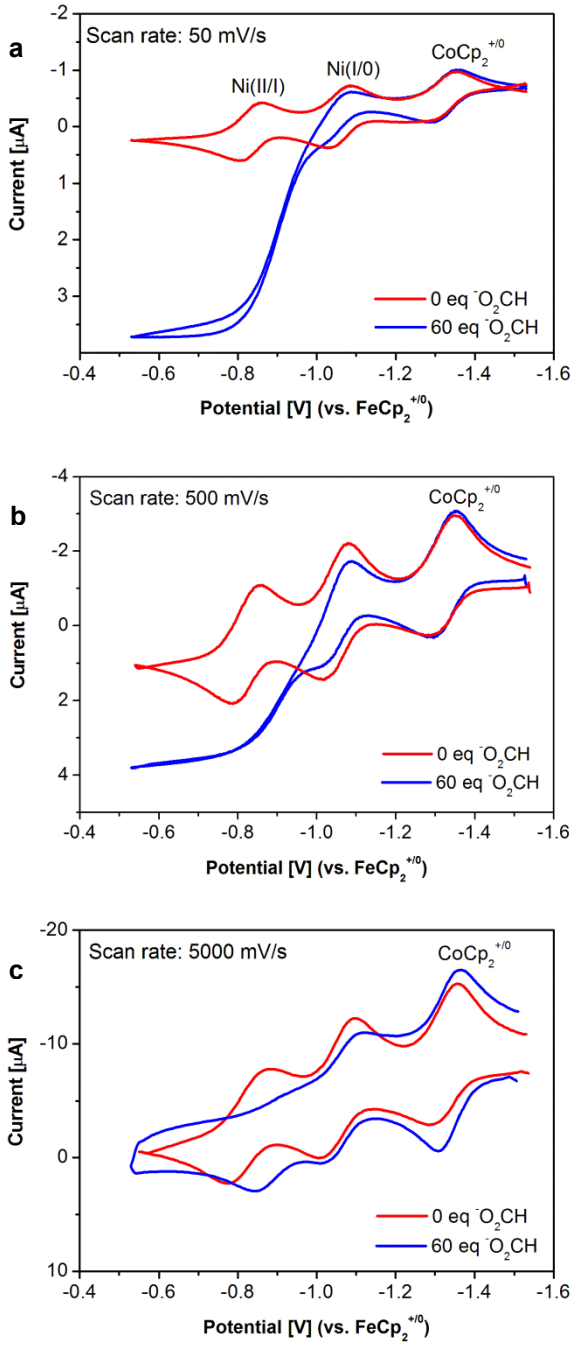

Figure 2-8. (a) CVs of catalyst in the presence of formate at scan rates of 50 mV/s, (b) 500 mV/s, (c) and 5000 mV/s. Conditions: 1 mM $[Ni(P^{Ph}_2N^{PhOMe}_2)_2(CH_3CN)]^{2+}$ in benzonitrile, 0.2 M NBu_4OTf as supporting electrolyte, glassy carbon working electrode.

2.4.5 Electrocatalysis with a hydride transfer reagent

Previous cyclic voltammetry studies showed that oxidation of Ni(II)–H occurs approximately 0.4 V positive of the observed electrocatalytic formate oxidation wave, inconsistent with a catalytic cycle that proceeds through oxidation of Ni(II)–H and deprotonation of the oxidized species. A key hypothesis in one subsequently proposed catalytic mechanism is that electrocatalysis proceeds through a β-proton abstraction pathway that avoids the direct formation of a nickel hydride species. We therefore sought to compare the reaction of Ni and formate with the reaction of Ni and an alternate, non-acidic hydride transfer reagent that would definitely form an observable Ni–H. $Na[HB(OMe)_3]$ was chosen since it fulfilled the requirement of being non-acidic, and was already known to react with the Ni(II) complexes to make either Ni(II)–H (1 eq) or Ni(0) (≥2 eq) without degradation of the metal complex.

Cyclic voltammograms of $[Ni(P^{Ph}{}_2N^{PhOMe}{}_2)_2(CH_3CN)]^{2+}$ taken after multiple $Na[HB(OMe)_3]$ additions are shown in **Figure 2-9**. As previously observed[9] and illustrated in **Figure 2-7b**, the CVs of the Ni complex in the presence of formate show the greatest increase in oxidative catalytic current at the Ni(II/I) potential, with a smooth plateau that continues out to more positive potentials. In contrast, the CVs in **Figure 2-9** show a smaller increase in catalytic current at the Ni(II/I) potential at all concentrations of substrate, relative to formate (i_{cat}/i_p = 0.7, 0.7 at 10 and 60 equivalents for $Na[HB(OMe)_3]$, vs. i_{cat}/i_p = 3.2, 9.4 for formate, respectively). Additionally, a diffusion-controlled peak appeared near –0.4 V at 10 eq of $Na[HB(OMe)_3]$ that seemed to shift more positive at higher concentrations. The positive oxidative peak indicates Ni–H formation in the presence of $Na[HB(OMe)_3]$, in agreement with previous data[9] that showed an oxidation peak in the CV of $[HNi(P^{Ph}{}_2N^{PhOMe}{}_2)_2]^+$ at –0.5 V vs. $FeCp_2^{+/0}$ in acetonitrile. The general lack of such a feature

in CVs of the catalysts with formate again suggests that a Ni(0) species, not Ni(II)–H, is being oxidized at the electrode under catalytic conditions.

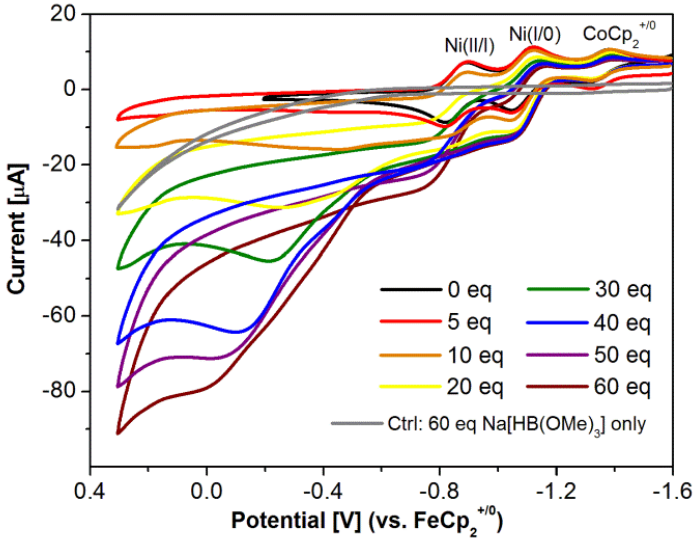

Figure 2-9. Electrochemical titration of $[Ni(P^{Ph}_2N^{PhOMe}_2)_2(CH_3CN)]^{2+}$ with $Na[HB(OMe)_3]$. Conditions: 1 mM catalyst in benzonitrile, 0.2 M NBu_4OTf as supporting electrolyte, glassy carbon working electrode, scan rate 50 mV/s.

A pertinent question in the formate case is whether the Ni(0) species being oxidized at the Ni(II/I) potential spontaneously forms via β-deprotonation of bound formate, or is accessed via hydride transfer to the metal and fast subsequent deprotonation of the Ni(II) hydride, either by the pendant base or by excess formate. The latter possibility would suggest that the lack of catalytic current enhancement in the trimethoxyborohydride case could arise from the absence of a suitable base to deprotonate the hydride. Trimethoxyborohydride should be able to fulfill both roles, as it is capable of acting as a hydride donor to a metal center or to a protic species to generate H_2 (thereby acting as a base), as previously exploited for preparations of Ni(0) complexes.[9] As an additional control, however, the experiment was repeated in the presence of an equal amount of NEt_3 as a substitute for formate acting as an external base. In this case, an increase in catalytic current was still not observed at the Ni(II/I)

couple. Therefore, β-deprotonation of formate and deprotonation of the hydride by the pendant base were compared as possible rate determining steps.

The apparent persistence of the hydride peak in the trimethoxyborohydride titration suggested that Ni–H is more stable than its Ni(0)–NH^+ isomer, and that the equilibrium between the two species lies towards the hydride. This is consistent with our previous results, in which $[HNi(P^{Ph}_2N^{PhOMe}_2)_2]^+$ formed upon reaction with 1 equivalent of formate was stable enough to be isolable and electrochemically characterized. Although the pendant base notably decreases the potential required for hydride oxidation, it does not appear to spontaneously deprotonate the hydride, such that a Ni(0) species is oxidized instead.[9] Thus, the fact that Ni(II)-H is not the main oxidative feature and does not appear to build up in reactions of $Ni(P^{Ph}_2N^{PhOMe}_2)_2]^{2+}$ with formate under electrocatalytic conditions is consistent with a mechanism in which a Ni(II)–H is not directly formed.

2.4.6 Kinetic isotope effect measurements

The presence of a primary kinetic isotope effect would imply a rate-determining X–H bond breaking step and possibly aid in its identification, so we decided to use H/D isotope studies as a method to further distinguish between several possibilities. Nickel complexes were titrated with NBu_4HCO_2•HCO_2H and NBu_4DCO_2•DCO_2D in parallel, which differ in H/D in both the oxygen-bound and carbon-bound positions. Kinetic isotope effects ranging from 3–7 were observed for all nickel compounds tested, and furthermore appeared to correlate with both the Ni(I/0) redox potential and the pK_a of the corresponding Ni(II)–H compound (**Table 2-3** and **Figure 2-10**). Again, it should be noted that Ni(I/0) redox potentials and Ni(II)–H pK_a values are inherently correlated.[1,9] The KIEs for all of the complexes together did not correlate with catalyst turnover frequencies or other thermodynamic properties, including Ni(II/I) redox potentials, amine pK_a values, hydricities,

and the differences between the Ni–H and NH^+ pK_a. However, when the phenylphosphine complexes were considered separately from the cyclohexylphosphine complex, the observed KIE values appear to correlate with the TOFs, redox potentials, and amine pK_a values.

Table 2-3. Primary KIEs of selected $[Ni(P^R_2N^{R'}_2)_2]^{2+}$ formate oxidation catalysts.

Catalyst ($P^R_2.N^{R'}_2$)	KIE	Ni–H pK_a	Ni(I/0) (V *vs*. $FeCp_2^{+/0}$)
Ph.Ph	6.7	16.3	–1.02
Ph.PhOMe	5.8	17.4	–1.07
Cy.PhOMe	4.0	18.9	–1.17
Ph.Bn	3.1	19.4	–1.19

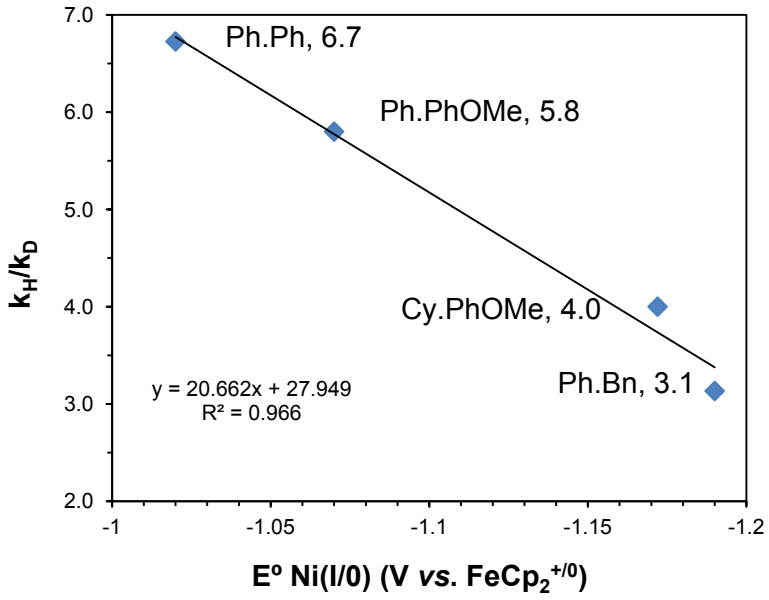

Figure 2-10. Ni(I/0) reduction potentials *vs*. magnitude of H/D KIE for selected catalysts.

The measured KIE values were compared to those from known inorganic and organometallic systems for formate oxidation (**Table 2-4**). Of these, the most well known is probably the Group 6 $[M(CO)_5O_2CH]^{-1}$ system studied by Darensbourg and coworkers, which had a measured k_H/k_D value of 1.1 for the Cr derivative. The KIEs of other systems

appear to cluster by mechanism, with multi-site electron-proton transfer mechanisms correlating with intermediate KIEs and direct hydride transfers correlating with even higher values. The large difference in KIE between a β-hydride elimination mechanism and a direct hydride transfer mechanism is likely due to a difference in the geometry of the transition state, with direct hydride transfer being more linear and hence involving a higher frequency vibrational mode with a larger difference between H and D zero-point energies at the transition state.[24]

Table 2-4. Primary KIEs and proposed mechanisms for formate oxidation systems in the literature.

Catalyst	KIE	Proposed mechanism	Reference
$[Cr(CO)_5O_2CH]^{-1}$	1.1	β-hydride elimination	Darensbourg[3]
$(\eta_5\text{-}C_5H_5)Re(NO)(PPh_3)(O_2CH)$	1.6	β-hydride elimination	Gladysz[25]
$[(bpy)_2(py)Ru^{III}(OH)]^{2+}$	3	ET, PT	Meyer[26]
Hg_2^{2+}, Hg^{+}, Tl^{3+}	3.4-3.9	ET, PT	Halpern[27,28]
MnO_4^-	7	Direct hydride transfer	Halpern[28]
$[(bpy)_2(py)Ru(O)]^{2+}$	19	Direct hydride transfer	Meyer[26]

The KIE data were also compared to data from the more numerous examples of metal alkene elimination and metal alkoxide oxidation in the literature. These values tended to range from 1–3, and in most cases were interpreted as being characteristic of β-hydride elimination mechanisms.[29–35] One relevant exception was that of the $[Pd(IiPr)(OAc)_2(H_2O)]$ system (IiPr = 1,3-bis(2,6-diisopropylphenyl)imidazol-2-ylidene) studied by Mueller, *et al.*,[35] in which the notably larger KIE value of 5.5 initially seen as support for an unusual late transition state β-hydride elimination mechanism has been computationally argued by

Nielson and Goddard to be indicative of a "reductive β- hydride elimination" mechanism, in which bound acetate acts as an intramolecular base and deprotonates the alcohol at the β-carbon.[36]

Based on the literature, we believe that the magnitudes of the KIEs measured in this study are most consistent with a β-deprotonation mechanism rather than a direct hydride transfer. However, great care should be taken when interpreting KIE magnitudes in organometallic systems due to the complications stemming from a multistep mechanism in which more than one H+/•/– transfer may occur. The one clear conclusion that can be drawn from this observed KIE is that the rate-determining step involves formate C–H bond cleavage or a subsequent transfer. This is consistent with the results of the acetate/formate binding studies, above, which suggest that formate binding is not rate limiting.

2.4.7 Determination of Arrhenius and Eyring parameters

The temperature dependence of electrocatalytic turnover frequencies, analyzed via Arrhenius and Eyring plots to determine activation parameters, was studied to determine the energetics of the rate-determining transition state. Electrochemical titrations of $[Ni(P^{Ph}_2N^{PhOMe}_2)_2(CH_3CN)]^{2+}$ with $NBu_4HCO_2{\bullet}HCO_2H$ were thus carried out over a temperature range of +5 to +34 °C, and the resulting turnover frequencies were used to generate both the Eyring and Arrhenius plots (**Figure 2-11**).

The calculated activation parameters from the linear fits of the plots are $\Delta H^{\ddagger} = 15.4 \pm 1.7$ kcal/mol, $\Delta S^{\ddagger} = -2.7 \pm 5.7$ cal/mol, $E_A = 16.0 \pm 1.7$ kcal/mol, and logA = 12.6 ± 1.2, characteristic of a moderate activation barrier. Notably, the closeness of the activation entropy to zero signals that very little intramolecular or solvent reorganization is required to form the transition state, consistent with a first order mechanism in which a proton transfer

occurs within the active site of the complex. This highlights the favorable positioning of the P_2N_2 ligand for proton movement around the active site.[6–8,37]

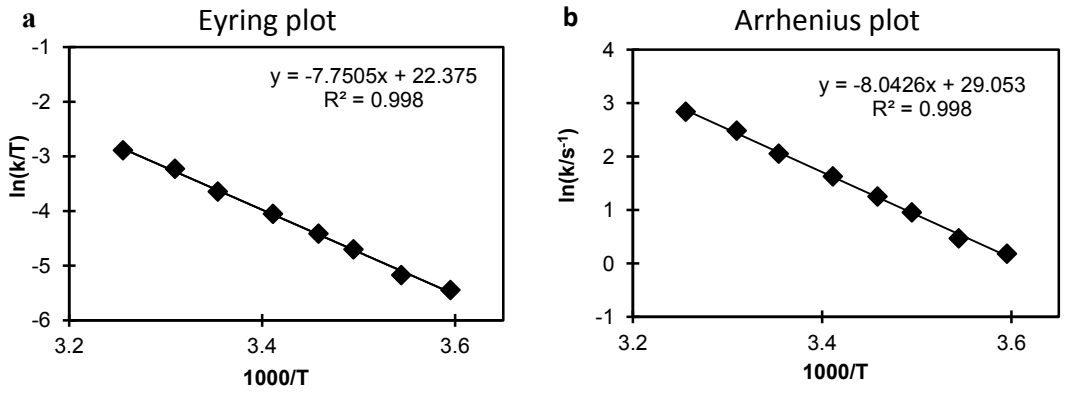

Figure 2-11. (a) Eyring and (b) Arrhenius plots for formate oxidation by $[Ni(P^{Ph}{}_2N^{PhOMe}{}_2)_2]^{2+}$, calculated from temperature-dependent TOFs.

2.4.8 Comparison of possible mechanisms

With multiple pieces of data in hand, we compared our possible mechanisms. Case **a**, rate-determining formate association, could be ruled out on the basis of the activation parameters, the KIE for H vs. D, and the electrochemical experiments investigating the binding of formate/acetate, which taken together suggest that the rate determining step is unimolecular and follows the binding of formate to the Ni(II) complex. Case **b**, β-hydride elimination requiring ligand dissociation, likewise could be ruled out by the H vs. D KIE and the slight decrease in entropy at the transition state, as well as the empirical observation that $P^{Cy}{}_2N^{R'}{}_2$ ligands appear to be much more prone to dissociation than their $P^{Ph}{}_2N^{R}{}_2$ counterparts, and yet are slower electrocatalysts for the oxidation of formate. Case **c**, rate-determining intramolecular deprotonation, was more compelling, as it was consistent with the observation that more basic pendant amines correlate with faster catalysis. Furthermore, the observation that larger kinetic isotope effects correlate with more acidic Ni–H pK_as could reflect some consequence of having to break a Ni–H bond. However, many of these

thermodynamic parameters are intrinsically inter-related, and we were wary of adventitious correlations.

In case **d** bound formate is intramolecularly deprotonated at the β-position by the pendant amine, bypassing formation of a Ni(II)–H. The next proposed step is that the ligand then loses a proton to excess formate in solution, and the Ni(0) center is re-oxidized at the electrode to Ni(II). The deprotonating role of formate in this last proposed step was supported by NMR experiments, which showed that a solution of $[HNi(P^{Ph}_2N^{PhOMe}_2)_2]^+$ formed by reacting Ni(II) and formate in a 1:1 ratio then disproportionates and releases H_2 over the course of several hours at elevated temperatures. In the presence of excess formate, however, $[HNi(P^{Ph}_2N^{PhOMe}_2)_2]^+$ undergoes complete H^+ loss and conversion to Ni(0) within a few minutes at room temperature.

This mechanism is consistent with the correlation of the ligand pK_a and the catalytic rate, as well as the observation of a KIE. Furthermore, we argued that this mechanism is more likely to be operative than cases **b** and **c** based on the following lines of reasoning:

1. The magnitudes of the observed KIEs in this system (3–7) were larger than those generally observed for β-hydride mechanisms (1–3) and smaller than those observed for direct hydride transfer mechanisms (7+).
2. There is no evidence that Ni–H species are being oxidized in CVs of the catalysts under formate concentration independent conditions. If Ni–H deprotonation were the rate-determining step (case **c**), such hydrides would be expected to build up quickly, yielding a correspondingly larger oxidative peak.

In the context of traditional organometallic chemistry, particularly for work relating to metal hydrides and β-hydride elimination, the proposed mechanism was highly unusual. However, we felt that the combined data supported this mechanism more strongly than it supported any of the traditional mechanisms. The electrocatalytic behavior of this system

suggests that base-assisted, non-canonical hydride mechanisms warrant further consideration, both as an acceptable model for catalysis in enzymatic systems and as a design choice in artificial catalysis.[38,39]

2.4.9 Steady state analysis: effect of phosphorus substituent on catalytic rates.

In our attempts to understand the origin of the systematic difference in catalytic rates between complexes with the same pendant base, but different phosphorus substituents, we considered two possibilities: (a) that the cyclohexyl complexes have a lower affinity for formate such that the decreased rates derive from a change in the binding pre-equilibrium, or (b) that some aspect of the cyclohexyl ligands results in decreased kinetics for the formate decomposition step. The similarities in the form of our proposed mechanism and rate vs. [substrate] curves[9] to the mechanism and curves invoked in Michaelis-Menten kinetics prompted us to analyze our data via the steady-state approximation normally applied to enzymes:

$$\mathrm{Ni} + \mathrm{O_2CH} \underset{k_{-1}}{\overset{k_1}{\rightleftharpoons}} \mathrm{Ni\text{-}O_2CH} \xrightarrow{k_2} \mathrm{Ni(0)\ NH^+} \longrightarrow \mathrm{Ni(II)} + 2e^-, 1H^+ \qquad (9)$$

$$\mathrm{E} + \mathrm{S} \underset{k_{-1}}{\overset{k_1}{\rightleftharpoons}} \mathrm{E{\bullet}S} \xrightarrow{k_2} \mathrm{E{\bullet}P} \longrightarrow \mathrm{E} + \mathrm{P} \qquad (10)$$

in which k_1, $k_{-1} >> k_2$, and the shapes of the rate-[substrate] saturation curves can be described by the following parameters:[40]

$$V_o = \frac{V_{max}[S]}{[S]+K_M}\ ,\ V_{max} = k_2[S] \qquad (11, 12)$$

$$K_M = \frac{(k_{-1} + k_2)}{k_1} \qquad (13)$$

In these equations, V_{max} refers to the maximum reaction velocity and K_M is the Michaelis-Menten constant, which describes the speed of kinetic saturation and can be interpreted as the [S] for which the reaction velocity is half-maximum. A lower K_M reflects a steeper saturation curve.

If a change in the pre-equilibrium is the determining factor in the rate differences, i.e. if P^{Cy} causes the catalyst to have a smaller k_1 or larger k_{-1} relative to P^{Ph}, it will exhibit a larger K_M. In contrast, if P^{Cy} causes the catalyst to have a smaller deprotonation k_2 relative to P^{Ph}, it will exhibit a smaller K_M. Graphical inspection of the saturation curves for pairs of $[Ni(P^{Cy}_2N^{R'}_2)_2(CH_3CN)]^{2+}$, $[Ni(P^{Ph}_2N^{R'}_2)_2(CH_3CN)]^{2+}$, catalysts showed the latter case to be operative (**Figure 2-12**). The effect was weaker for pairs with a stronger base, again highlighting the relative importance of the pK_a of the pendant amine in determining the overall rate of reaction.

The exact reason for the effect of the phosphorus substituent on the deprotonation step was unclear, with "sterics" being a possible, but somewhat vague answer. The phosphorus substituent could affect the rate of formate decomposition by changing the angle or distance between the proton donor and acceptor sites as a result of increased distortion by the larger P^{Cy} substituent. Alternatively, the electron accepting properties of the metal center could be affected due to both the larger bulk as well as the increased electron donating properties of the cyclohexyl substituent.[41] The influence of these subtle structural changes upon catalytic activity is not only important for the present catalysts but is also an important aspect of proton transfer and regulation that appears to have been optimized in biological systems, and it is hoped, will someday be understood and optimized in artificial systems as well.

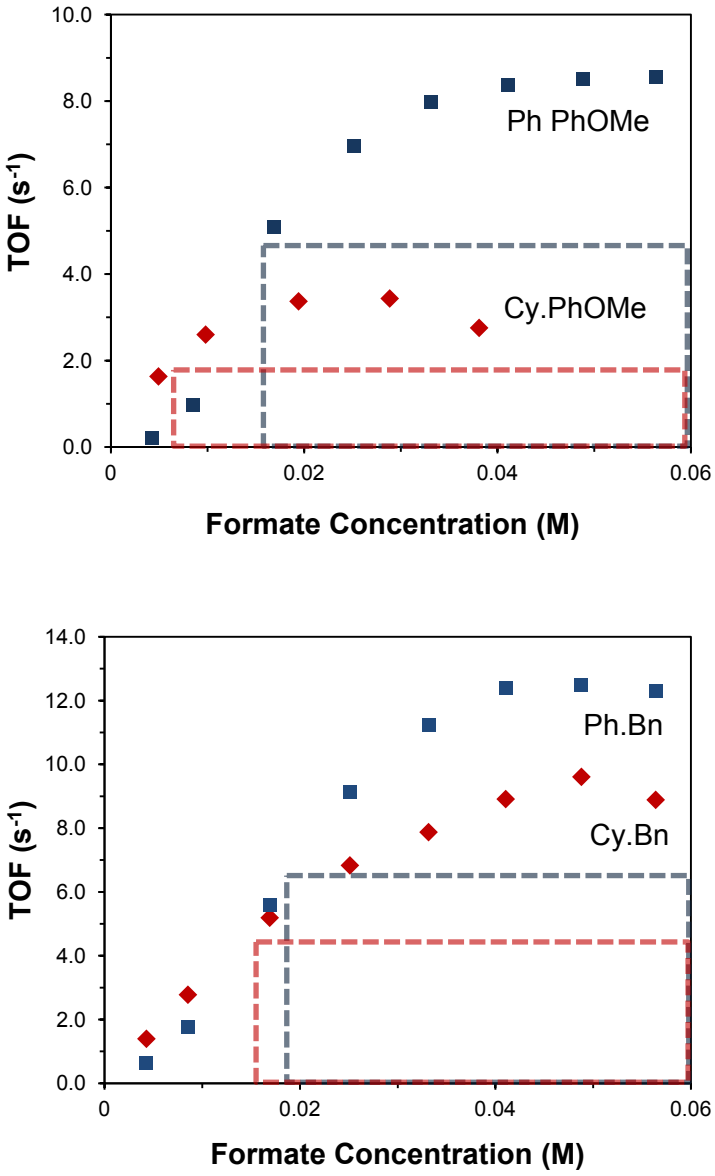

Figure 2-12. Rate-[substrate] saturation curves for pairs of P^{Cy} and P^{Ph} catalysts.

2.4.10 Possible role of concerted PCET in catalysis

The β-deprotonation depicted in **Scheme 2-3** describes a mechanism in which a proton is transferred to the pendant amine and two electrons are transferred to the metal center. The magnitude of the KIEs and the fact that a Ni–OCO_2^- intermediate left behind at the metal center upon deprotonation would be thermodynamically very unfavorable are

consistent with the occurrence of concerted multi-site proton-coupled electron transfer (MS-PCET) in the rate-determining step of this reaction.[42,43] In other words, the normally hydridic β-hydrogen of formate can only become acidic if there is a significant loss of electron density at the carbon due to delocalization or electron transfer. If so, this would be a rare example of an organometallic C-H bond breaking reaction identified as involving non-hydride concerted PCET, the understanding of which could aid the development of efficient catalysts for CO_2 reduction and fuel utilization.

PCET processes are known to play important roles in photosynthesis, fuel cells, and many other energy conversion processes, and it is noteworthy that the bifunctional ligands in this system that were initially designed to mimic the second coordination sphere of a protein may enable PCET for formate oxidation according to the same principles. Additionally, the proposed PCET mechanism involves movement of a proton to one site and two electrons to a separate site, which is more typical of enzymatic reactions. Structural[39,44,45] and biochemical[46] studies of formate dehydrogenase enzymes and their mutants indeed suggest that catalysis is highly dependent on the presence and specific identities of amino acids that can act as proton acceptors from formate. These results suggest that the extremely low overpotentials for both formate oxidation and CO_2 reduction exhibited by *S. fumaroxidans* W FDH1 may be partially enabled by the involvement of a concerted PCET process.[47,48] Our ideas and attempts to study the physical parameters that determine the rates of this PCET reaction are briefly addressed in Chapter 6.

2.5 Summary and Conclusions

The mechanism of formate oxidation by $[Ni(P^{R}_{2}N^{R'}_{2})_2(CH_3CN)]^{2+}$ electrocatalysts was studied by electrochemical and spectroscopic methods. The reaction is thought to proceed through intramolecular deprotonation of bound formate by the pendant amine and a

concomitant two-electron reduction of the metal. KIE, activation parameters, and formate/acetate binding studies suggest that this rate-determining step may be a concerted proton-coupled electron transfer reaction, further highlighting possible roles and the importance of bifunctional catalysts in the interconversion of energy and fuels.

2.6 References

1. Berning, D. E.; Miedaner, A.; Curtis, C. J.; Noll, B. C.; DuBois, M. R.; DuBois, D. L. *Organometallics*, **2001**, *20*, 1832–1839.

2. Darensbourg, D. J.; Rokicki, A. *Organometallics*, **1982**, *1*, 1685–1693.

3. Darensbourg, D. J.; Wiegreffe, H. P.; Wiegreffe, P. *J. Am. Chem. Soc.*, **1990**, *112*, 9252–9257.

4. Darensbourg, D. J.; Rokicki, A.; Darensbourg, M. Y. *J. Am. Chem. Soc.*, **1981**, *103*, 3223–3224.

5. Yang, J. Y.; Chen, S.; Dougherty, W. G.; Kassel, W. S.; Bullock, R. M.; DuBois, D. L.; Raugei, S.; Rousseau, R. J.; Dupuis, M.; DuBois, M. R. *Chem. Commun.*, **2010**, *46*, 8618–8620.

6. Wilson, A. D.; Shoemaker, R. K.; Miedaner, A.; Muckerman, J. T.; DuBois, D. L.; DuBois, M. R. *Proc. Natl. Acad. Sci. U. S. A.*, **2007**, *104*, 6951–6956.

7. Wilson, A. D.; Newell, R.; McNevin, M. J.; Muckerman, J. T.; DuBois, M. R.; DuBois, D. L. *J. Am. Chem. Soc.*, **2006**, *128*, 358–366.

8. Yang, J. Y.; Bullock, R. M.; Shaw, W. J.; Twamley, B.; Fraze, K.; DuBois, M. R.; DuBois, D. L. *J. Am. Chem. Soc.*, **2009**, *131*, 5935–5945.

9. Galan, B. R.; Schöffel, J.; Linehan, J. C.; Seu, C. S.; Appel, A. M.; Roberts, J. A. S.; Helm, M. L.; Kilgore, U. J.; Yang, J. Y.; DuBois, D. L.; Kubiak, C. P. *J. Am. Chem. Soc.*, **2011**, *133*, 12767–12779.

10. DuBois, D. L.; Berning, D. E. *Appl. Organomet. Chem.*, **2000**, *14*, 860–862.

11. Price, A. J.; Ciancanelli, R.; Noll, B. C.; Curtis, C. J.; DuBois, D. L.; DuBois, M. R. *Organometallics*, **2002**, *21*, 4833–4839.

12. Creutz, C.; Chou, M. H. *J. Am. Chem. Soc.*, **2009**, 2794–2795.

13. Himeda, Y.; Miyazawa, S.; Hirose, T. *ChemSusChem*, **2011**, *4*, 487–493.

14. Darensbourg, D. J.; Wiegreffe, H. P. *Inorg. Chem.*, **1990**, *29*, 592–597.

15. Sakaki, S.; Ohkubo, K. *Inorg. Chem.*, **1989**, *28*, 2583–2590.

16. Koike, T.; Ikariya, T. *Adv. Synth. Catal.*, **2004**, *346*, 37–41.

17. Chakraborty, S.; Zhang, J.; Krause, J.; Guan, H. *J. Am. Chem. Soc.*, **2010**, *132*, 8872–8873.

18. Chen, J.; Szalda, D. J.; Fujita, E.; Creutz, C. *Inorg. Chem.*, **2010**, *49*, 9380–9391.

19. Sattler, W.; Parkin, G. *J. Am. Chem. Soc.*, **2011**, *133*, 9708–9711.

20. Schmeier, T. J.; Dobereiner, G. E.; Crabtree, R. H.; Hazari, N. *J. Am. Chem. Soc.*, **2011**, *133*, 9274–9277.

21. Darensbourg, D. J.; Wiegreffe, P.; Riordan, C. G. *J. Am. Chem. Soc.*, **1990**, *112*, 5759–5762.

22. Tanaka, R.; Yamashita, M.; Chung, L. W.; Morokuma, K.; Nozaki, K. *Organometallics*, **2011**, *30*, 6742–6750.

23. Bard, A. J.; Faulkner, L. R. *Electrochemical Methods: Fundamentals and Applications*; John Wiley and Sons: Hoboken, NJ, 2000; p. 856.

24. Anslyn, E. V; Dougherty, D. A. *Modern Physical Organic Chemistry*; 3rd ed.; University Science: Sausalito, CA, 2005.

25. Merrifield, J. H.; Gladysz, J. A. *Organometallics*, **1983**, *2*, 782–784.

26. Roecker, L.; Meyer, T. J. *J. Am. Chem. Soc.*, **1986**, *108*, 4066–4073.

27. Halpern, J.; Taylor, S. M. *Discuss. Faraday Soc.*, **1960**, *29*, 174–181.

28. Taylor, S. M.; Halpern, J. *J. Am. Chem. Soc.*, **1959**, *81*, 2933–2937.

29. Ozawa, F.; Ito, T.; Yamamoto, A. *J. Am. Chem. Soc.*, **1980**, *102*, 6457–6463.

30. Romeo, R.; Alibrandi, G.; Scolaro, L. M. *Inorg. Chem.*, **1993**, *32*, 4688–4694.

31. Saura-Llamas, I.; Gladysz, J. A. *J. Am. Chem. Soc.*, **1992**, *114*, 2136–2144.

32. Goj, L. A.; Widenhoefer, R. A. *J. Am. Chem. Soc.*, **2001**, *123*, 11133–11147.

33. Zhao, J.; Hesslink, H.; Hartwig, J. F. *J. Am. Chem. Soc.*, **2001**, *123*, 7220–7227.

34. Steinhoff, B. A.; Stahl, S. S. *Org. Lett.*, **2002**, *4*, 4179–4181.

35. Mueller, J. A.; Goller, C. P.; Sigman, M. S. *J. Am. Chem. Soc.*, **2004**, *126*, 9724–9734.

36. Nielsen, R. J.; Goddard, W. A. *J. Am. Chem. Soc.*, **2006**, *128*, 9651–9660.

37. Yang, J. Y.; Bullock, R. M.; Dougherty, W. G.; Kassel, W. S.; Twamley, B.; DuBois, D. L.; DuBois, M. R. *Dalton Trans.*, **2010**, *39*, 3001–3010.

38. Boyington, J. C. *Science*, **1997**, *275*, 1305–1308.

39. Raaijmakers, H. C. A.; Romão, M. J. *J. Biol. Inorg. Chem.*, **2006**, *11*, 849–854.

40. Johnson, K. A.; Goody, R. S. *Biochemistry*, **2011**, *50*, 8264–8269.

41. Fraze, K.; Wilson, A. D.; Appel, A. M.; DuBois, M. R.; DuBois, D. L. *Organometallics*, **2007**, *26*, 3918–3924.

42. Soudackov, A. V; Hammes-Schiffer, S. *Chem. Phys.*, **2000**, *113*, 2385–2396.

43. Hammes-Schiffer, S. *Acc. Chem. Res.*, **2009**, *42*, 1881–1889.

44. George, G. N.; Colangelo, C. M.; Dong, J.; Scott, R. A.; Khangulov, S. V.; Gladyshev, V. N.; Stadtman, T. C. *J. Am. Chem. Soc.*, **1998**, *120*, 1267–1273.

45. Khangulov, S. V.; Gladyshev, V. N.; Dismukes, G. C.; Stadtman, T. C. *Biochemistry*, **1998**, *37*, 3518–3528.

46. Axley, M. J.; Böck, A.; Stadtman, T. C. *Proc. Natl. Acad. Sci. U. S. A.*, **1991**, *88*, 8450–8454.

47. Armstrong, F. A.; Hirst, J. *Proc. Natl. Acad. Sci. U. S. A.*, **2011**, *108*, 14049–14054.

48. Reda, T.; Plugge, C. M.; Abram, N. J.; Hirst, J. *Proc. Natl. Acad. Sci. U. S. A.*, **2008**, *105*, 10654–10658.

2.7 Appendix

2.7.1 Crystal data for $[Ni(P^{Cy}_2N^{PhOMe}_2)_2(CH_3CN)](BF_4)_2$

Crystals of $Ni(P^{Cy}_2N^{PhOMe}_2)_2(CH_3CN)](BF_4)_2$ were found to have crystallized on space group $C_{2/c}$ such that the Ni–acetonitrile vector was located on the C_2 axis of symmetry. As a result, the phenyl and cyclohexyl substituents off N and P, respectively, appeared disordered due to slight conformational variations between the two halves of the molecule. These rings were modeled simultaneously by setting analogous atoms in different

conformations to partial occupancy. It should be noted that this disorder is the root cause of several false checkCIF alerts regarding short intramolecular H–H contacts and missing hydrogen bond acceptors. Despite these alerts and extensive disorder, the crystal data was modeled satisfactorily to 4.19% (using 2Θ). Attempts to model the structure in a space group of lower symmetry did not converge.

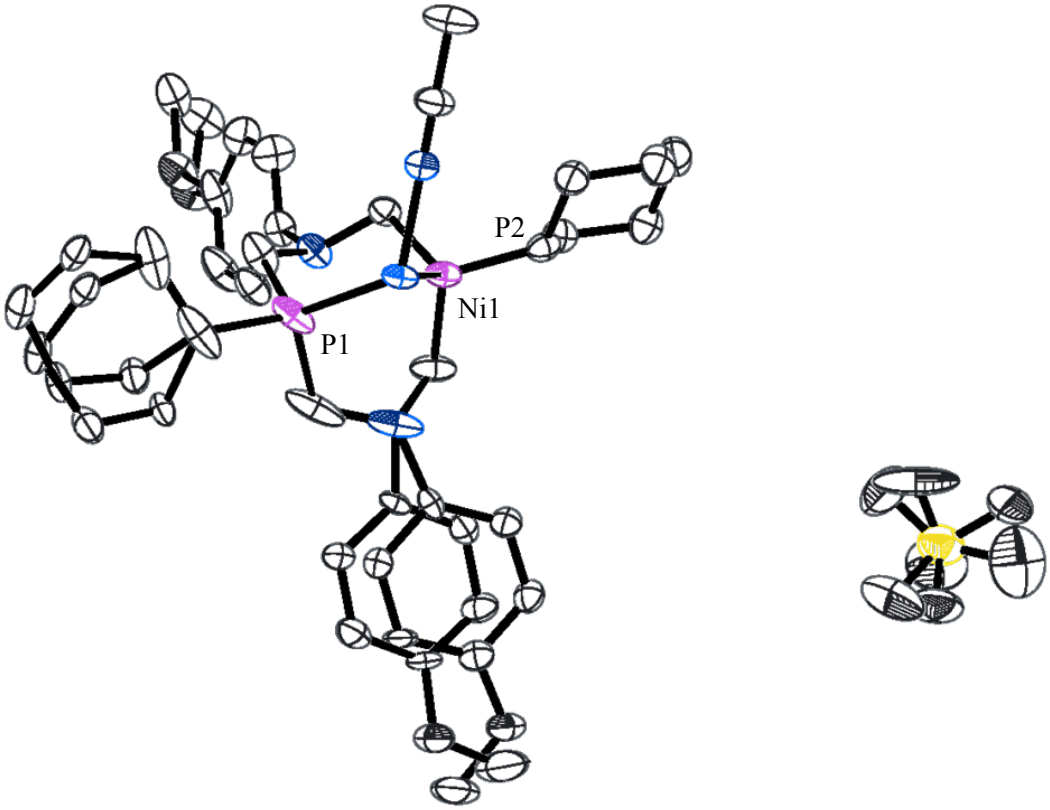

Figure 2-13. Thermal ellipsoid plot of $Ni(P^{Cy}{}_2N^{PhOMe}{}_2)_2(CH_3CN)](BF_4)_2$ asymmetric unit, showing ligand disorder (note that only half of the complex is contained in each asymmetric unit). Hydrogen atoms have been omitted for clarity.

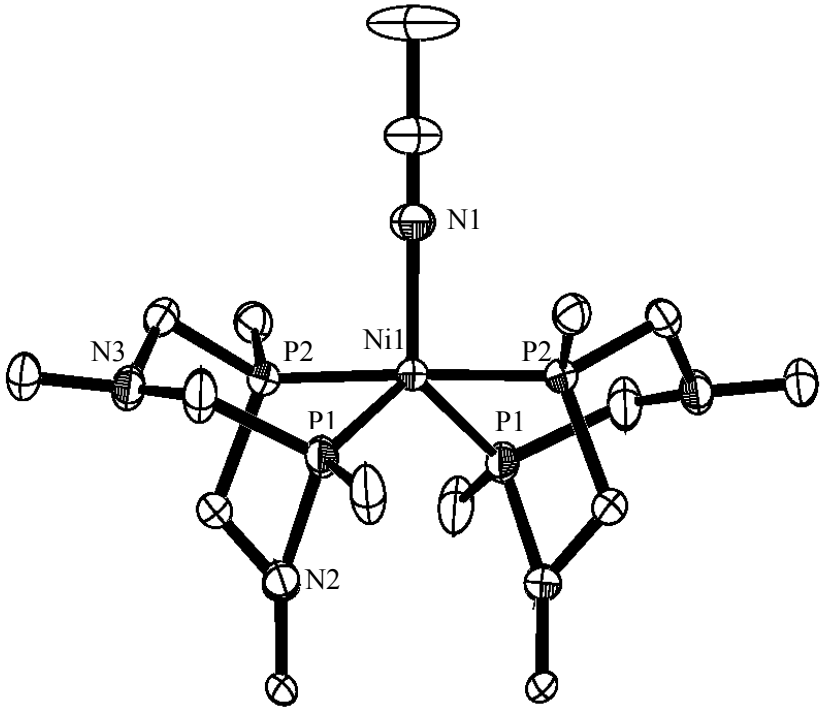

Figure 2-14. Thermal ellipsoid plot of $Ni(P^{Cy}{}_2N^{PhOMe}{}_2)_2(CH_3CN)](BF_4)_2$ showing ligand conformation around Ni core. Hydrogen atoms and counter ions have been omitted for clarity.

Table 2-5. Crystal data and structure refinement for $Ni(P^{Cy}{}_2N^{PhOMe}{}_2)_2(CH_3CN)](BF_4)_2$.

Identification code	cseu624_0m	
Empirical formula	C62 H91 B2 F8 N5 Ni O4 P4	
Formula weight	1326.61	
Temperature	296.15 K	
Wavelength	0.71073 Å	
Crystal system	Monoclinic	
Space group	C 1 2/c 1	
Unit cell dimensions	a = 19.9269(10) Å	α= 90°.
	b = 15.0019(8) Å	β= 102.6428(7)°.
	c = 21.7450(11) Å	γ = 90°.
Volume	6342.9(6) $Å^3$	
Z	4	
Density (calculated)	1.389 Mg/m^3	
Absorption coefficient	0.481 mm^{-1}	
F(000)	2800	
Crystal size	0.12 x 0.1 x 0.08 mm^3	
Theta range for data collection	1.71 to 25.36°.	
Index ranges	-14<=h<=24, -17<=k<=18, -25<=l<=26	
Reflections collected	17445	
Independent reflections	5803 [R(int) = 0.0288]	
Completeness to theta = 25.36°	99.9 %	
Absorption correction	SADABS	
Max. and min. transmission	0.9625 and 0.9445	
Refinement method	Full-matrix least-squares on F^2	
Data / restraints / parameters	5803 / 0 / 548	
Goodness-of-fit on F^2	1.031	
Final R indices [I>2sigma(I)]	R1 = 0.0408, wR2 = 0.1028	
R indices (all data)	R1 = 0.0523, wR2 = 0.1115	
Largest diff. peak and hole	0.454 and -0.424 $e.Å^{-3}$	

Table 2-6. Bond lengths [Å] and angles for $Ni(P^{Cy}{}_2N^{PhOMe}{}_2)_2(CH_3CN)](BF_4)_2$.

C(1)-C(2)	1.471(5)	C(1)-N(1)	1.137(4)
C(1A)-C(15)	1.370(4)	C(1A)-C(16)	1.401(3)
C(1B)-N(2)	1.455(4)	C(1B)-P(1)	1.850(3)
C(3)-C(4)	1.536(5)	C(3)-C(8)	1.644(6)
C(3)-C(8B)	1.532(6)	C(3)-P(1)	1.864(3)
C(4)-C(5)	1.504(7)	C(4)-C(5B)	1.638(7)
C(5)-C(6)	1.509(12)	C(5B)-C(6B)	1.505(10)
C(6)-C(7)	1.545(9)	C(6B)-C(7B)	1.518(10)
C(7)-C(8)	1.531(8)	C(7B)-C(8B)	1.536(10)
C(9)-N(3)	1.447(3)	C(9)-P(1)	1.851(2)
C(11)-C(12)	1.382(3)	C(11)-C(13)	1.385(3)
C(12)-C(15)	1.389(4)	C(13)-C(16)	1.375(3)
C(13)-N(3)	1.446(3)	C(14)-O(1)	1.418(17)
C(14B)-O(1B)	1.453(18)	C(15)-O(1)	1.369(15)
C(15)-O(1B)	1.414(14)	C(17)-N(3)	1.456(3)
C(17)-P(2)	1.849(2)	C(18)-C(19)	1.539(3)
C(18)-C(23)	1.535(3)	C(18)-P(2)	1.848(2)
C(19)-C(20)	1.525(3)	C(20)-C(21)	1.517(4)
C(21)-C(22)	1.523(4)	C(22)-C(23)	1.538(4)
C(24)-N(2)	1.460(3)	C(24)-P(2)	1.855(2)
C(25)-C(26)	1.387(9)	C(25)-C(31)	1.399(9)
C(25)-N(2)	1.563(9)	C(25B)-C(26B)	1.396(8)
C(25B)-C(31B)	1.382(8)	C(25B)-N(2)	1.384(7)
C(26)-C(27)	1.382(9)	C(26B)-C(27B)	1.374(8)
C(27)-C(28)	1.387(10)	C(27B)-C(28B)	1.396(10)
C(28)-C(30)	1.392(8)	C(28)-O(2)	1.362(8)
C(28B)-C(30B)	1.383(11)	C(28B)-O(2B)	1.368(8)
C(29)-O(2)	1.420(8)	C(29B)-O(2B)	1.375(10)
C(30)-C(31)	1.366(8)	C(30B)-C(31B)	1.417(10)
N(1)-Ni(1)	1.993(3)	P(1)-Ni(1)	2.2333(6)
P(2)-Ni(1)	2.2293(6)	Ni(1)-P(1)#1	2.2333(6)
Ni(1)-P(2)#1	2.2293(6)	B(1)-F(1)	1.389(4)
B(1)-F(2)	1.388(7)	B(1)-F(2B)	1.432(6)
B(1)-F(3)	1.224(9)	B(1)-F(3B)	1.388(9)
B(1)-F(4)	1.461(9)	B(1)-F(4B)	1.303(8)

Table 2-6. (cont'd)

N(1)-C(1)-C(2)	180.000(1)	C(15)-C(1A)-C(16)	119.8(2)
N(2)-C(1B)-P(1)	116.21(18)	C(4)-C(3)-C(8)	121.1(3)
C(4)-C(3)-P(1)	111.57(19)	C(8)-C(3)-P(1)	106.9(3)
C(8B)-C(3)-C(4)	93.4(3)	C(8B)-C(3)-C(8)	27.7(2)
C(8B)-C(3)-P(1)	122.7(3)	C(3)-C(4)-C(5B)	121.8(3)
C(5)-C(4)-C(3)	98.5(3)	C(5)-C(4)-C(5B)	24.9(2)
C(4)-C(5)-C(6)	118.9(6)	C(6B)-C(5B)-C(4)	103.9(5)
C(5)-C(6)-C(7)	109.9(8)	C(5B)-C(6B)-C(7B)	110.1(7)
C(8)-C(7)-C(6)	112.5(7)	C(6B)-C(7B)-C(8B)	114.5(8)
C(7)-C(8)-C(3)	105.8(4)	C(3)-C(8B)-C(7B)	116.6(6)
N(3)-C(9)-P(1)	113.11(18)	C(12)-C(11)-C(13)	120.3(2)
C(11)-C(12)-C(15)	120.2(2)	C(11)-C(13)-N(3)	117.4(2)
C(16)-C(13)-C(11)	119.4(2)	C(16)-C(13)-N(3)	123.2(2)
C(1A)-C(15)-C(12)	119.8(2)	C(1A)-C(15)-O(1B)	131.7(6)
C(12)-C(15)-O(1B)	108.0(5)	O(1)-C(15)-C(1A)	116.7(5)
O(1)-C(15)-C(12)	122.9(6)	O(1)-C(15)-O(1B)	20.3(6)
C(13)-C(16)-C(1A)	120.5(2)	N(3)-C(17)-P(2)	108.71(14)
C(19)-C(18)-P(2)	112.96(15)	C(23)-C(18)-C(19)	110.6(2)
C(23)-C(18)-P(2)	114.68(17)	C(20)-C(19)-C(18)	109.64(19)
C(21)-C(20)-C(19)	110.9(2)	C(20)-C(21)-C(22)	110.7(2)
C(21)-C(22)-C(23)	111.6(2)	C(18)-C(23)-C(22)	110.2(2)
N(2)-C(24)-P(2)	111.38(16)	C(26)-C(25)-C(31)	117.3(7)
C(26)-C(25)-N(2)	113.7(6)	C(31)-C(25)-N(2)	128.9(5)
C(31B)-C(25B)-C(26B)	118.3(6)	C(31B)-C(25B)-N(2)	111.4(5)
N(2)-C(25B)-C(26B)	130.1(6)	C(27)-C(26)-C(25)	121.7(6)
C(27B)-C(26B)-C(25B)	121.8(6)	C(26)-C(27)-C(28)	120.1(7)
C(26B)-C(27B)-C(28B)	120.5(6)	C(27)-C(28)-C(30)	118.7(6)
O(2)-C(28)-C(27)	126.5(7)	O(2)-C(28)-C(30)	114.8(5)
C(30B)-C(28B)-C(27B)	118.2(7)	O(2B)-C(28B)-C(27B)	115.6(6)
O(2B)-C(28B)-C(30B)	126.1(8)	C(31)-C(30)-C(28)	120.6(6)
C(28B)-C(30B)-C(31B)	121.2(7)	C(30)-C(31)-C(25)	121.5(6)
C(25B)-C(31B)-C(30B)	119.7(7)	C(1)-N(1)-Ni(1)	180.0
C(1B)-N(2)-C(24)	114.6(2)	C(1B)-N(2)-C(25)	126.4(3)
C(24)-N(2)-C(25)	106.3(3)	C(25B)-N(2)-C(1B)	102.1(3)
C(25B)-N(2)-C(24)	126.3(4)	C(25B)-N(2)-C(25)	24.6(2)

Table 2-6. (cont'd)

C(9)-N(3)-C(17)	113.19(18)	C(13)-N(3)-C(9)	113.23(18)
C(13)-N(3)-C(17)	115.54(17)	C(15)-O(1)-C(14)	124.3(10)
C(15)-O(1B)-C(14B)	109.7(9)	C(28)-O(2)-C(29)	117.5(5)
C(28B)-O(2B)-C(29B)	115.4(6)	C(1B)-P(1)-C(3)	103.20(15)
C(1B)-P(1)-Ni(1)	107.23(11)	C(3)-P(1)-Ni(1)	125.94(8)
C(9)-P(1)-C(1B)	103.43(13)	C(9)-P(1)-C(3)	98.73(13)
C(9)-P(1)-Ni(1)	115.73(8)	C(17)-P(2)-C(24)	102.33(10)
C(17)-P(2)-Ni(1)	111.42(8)	C(18)-P(2)-C(17)	105.18(10)
C(18)-P(2)-C(24)	103.80(12)	C(18)-P(2)-Ni(1)	119.83(7)
C(24)-P(2)-Ni(1)	112.54(8)	N(1)-Ni(1)-P(1)	120.05(2)
N(1)-Ni(1)-P(1)#1	120.05(2)	N(1)-Ni(1)-P(2)#1	90.960(17)
N(1)-Ni(1)-P(2)	90.960(17)	P(1)#1-Ni(1)-P(1)	119.91(4)
P(2)#1-Ni(1)-P(1)	97.14(2)	P(2)-Ni(1)-P(1)	81.89(2)
P(2)#1-Ni(1)-P(1)#1	81.89(2)	P(2)-Ni(1)-P(1)#1	97.14(2)
P(2)#1-Ni(1)-P(2)	178.08(3)	F(1)-B(1)-F(2B)	112.7(4)
F(1)-B(1)-F(4)	107.3(5)	F(2)-B(1)-F(1)	99.2(4)
F(2)-B(1)-F(2B)	42.3(3)	F(2)-B(1)-F(4)	109.3(5)
F(2B)-B(1)-F(4)	133.3(5)	F(3)-B(1)-F(1)	115.6(7)
F(3)-B(1)-F(2)	119.5(7)	F(3)-B(1)-F(2B)	78.0(6)
F(3)-B(1)-F(3B)	25.1(7)	F(3)-B(1)-F(4)	105.5(7)
F(3)-B(1)-F(4B)	125.7(8)	F(3B)-B(1)-F(1)	106.2(6)
F(3B)-B(1)-F(2)	143.9(6)	F(3B)-B(1)-F(2B)	103.1(5)
F(3B)-B(1)-F(4)	87.4(6)	F(4B)-B(1)-F(1)	110.0(5)
F(4B)-B(1)-F(2)	78.7(4)	F(4B)-B(1)-F(2B)	110.0(4)
F(4B)-B(1)-F(3B)	114.8(7)	F(4B)-B(1)-F(4)	30.7(3)

Symmetry transformations used to generate equivalent atoms:
#1 –X, Y, 1/2-Z

2.7.2 Copyright note

Some of the material in the introduction to this chapter was adapted from a manuscript entitled "Electrocatalytic Oxidation of Formate by $[Ni(P^{R}_2N^{R'}_2)_2(CH_3CN)]^{2+}$ Complexes," by Brandon R. Galan, Julia Schöffel, John C. Linehan, Candace Seu, Aaron M. Appel, John A. S. Roberts, Monte L. Helm, Uriah J. Kilgore, Jenny Y. Yang, Daniel L.

DuBois, and Clifford P. Kubiak, published in *J. Am. Chem. Soc*., **2011**, *133* (32), 12767-12779. The dissertation author is a contributing author to this manuscript.

The majority of the material for this chapter comes directly from a manuscript entitled "Formate oxidation via β-deprotonation in $[Ni(P^{R}_{2}N^{R'}_{2})_{2}(CH_{3}CN)]^{2+}$ complexes, " by Candace S Seu, Aaron M. Appel, Michael D. Doud, Daniel L. DuBois, and Clifford P. Kubiak, published in *Energy Environ. Sci.*, **2012**, *5*, 6480-6490. The dissertation author is the primary author of this manuscript.

Chapter 3

CO binding and oxidation by $[Ni(P_2N_2)_2]^{2+}$ catalysts

3.1 Introduction

CO, like formic acid, is a $2H^+$, $2e^-$ reduced form of CO_2. Both are valuable chemical commodities, and both can be used as fuel feedstocks. CO, however, must be chemically converted into hydrocarbons via the Fischer-Tropsch process for this to be true; in the context of a fuel cell it is more often seen as a pollutant. Whereas formic acid is the preferred fuel in a direct formic acid fuel cell (DFAFC), CO is an inhibitor that stably binds to the surface of the fuel cell electrode, reducing the number of active sites and decreasing the fuel cell efficiency.[1,2] CO is produced as an intermediate in the so-called "indirect pathway" of formic acid oxidation at Pt surfaces, and much DFAFC research is focused on developing electrode materials that either avoid this pathway[3] or favor CO oxidation.[4,5]

The success of the $[Ni(P^{R}_{2}N^{R'}_{2})_2]^{2+}$ system in catalyzing the oxidation of formate prompted us to explore the possibility that it would also be effective at catalyzing the base-assisted oxidation of CO. We hypothesized this could proceed via the mechanism shown in **Figure 3-1**, in which Ni-bound CO is attacked at the carbon by hydroxide and subsequently deprotonated by the pendant base to yield CO_2. This is very similar to the microscopic reverse of how the reduction of CO_2 to CO is thought to occur, although it is run under basic conditions and thus avoids the extra initial step of water deprotonation to yield hydroxide. Studies by Darensbourg and coworkers on nucleophilic reactions of metal carbonyls followed by CO_2 extrusion set an additional precedent for this idea.[6] The oxidation of CO at Pt surfaces is also thought to proceed by a similar mechanism, although pre-absorption of CO and $^{-}$OH converts the final oxidation step into a 1-electron process.[7]

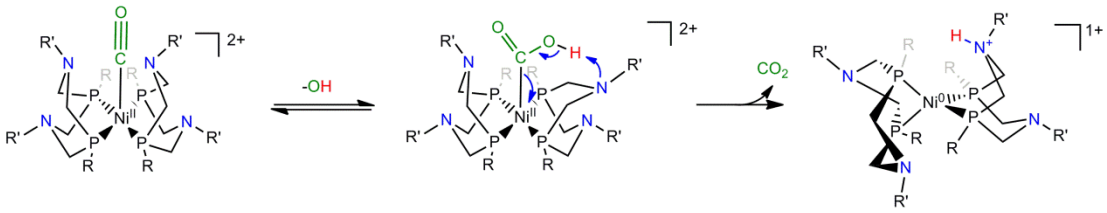

Figure 3-1. Mechanism for the proposed $[Ni(P^{R}_{2}N^{R'}_{2})_2]^{2+}$-mediated oxidation of CO to CO_2.

In the proposed mechanism, two electrons would be transferred from CO to the nickel center. For the overall electrochemical reaction to be thermodynamically favorable, the reduction of Ni(II) to Ni(0) must be more positive than the CO_2/CO reduction potential. In general, the redox potentials of the Ni catalysts range from –0.6 to –0.9 V for Ni(II/I) and –0.9 to –1.5 V for Ni(I/0). The standard redox potential for the $2H^{+}/2e^{-}$ interconversion of CO_2 and CO is –1.16 V *vs*. $FeCp_2^{+/0}$ at pH = 7. The addition of hydroxide would change the pH of the organic solution and hence the redox potential by an unknown amount. However, if we assume that the pH effects in organic and aqueous solution are similar, then we would expect a pH of approximately 12-13 after the addition of 10–50 equivalents (10–50 mM)

hydroxide. The redox potential of a two electron transformation should shift +0.03 V more positive for each pK_a unit, and we can estimate the redox potential to be between –1.01 to –0.98 V under working conditions. Thermodynamic calculations taking this shift into account show that the redox reaction should be energetically favorable for some of the derivatives (**Scheme 3-1**).

$CO + H_2O \rightleftharpoons CO_2 + 2e^- + 2H^+$	E° = +1.01 V
$Ni(I) + 1e^- \rightleftharpoons Ni(0)$	E° = –0.60 V
$Ni(II) + 1e^- \rightleftharpoons Ni(I)$	E° = –1.24 V
$CO + H_2O + Ni(II) \rightleftharpoons CO_2 + 2H^+ + Ni(0)$	Σ –nFE = +0.18 V

Scheme 3-1. Thermodynamic calculation for the feasibility of $[Ni(P_2N_2)_2]^{2+}$ or $[Ni(PNP)_2]^{2+}$-mediated oxidation of CO to CO_2, using $[Ni(P^{Et2}N^{Me}P)_2]^{2+}$ at 10 mM $^-$OH as an example.

In choosing which catalysts to target, we also considered the electronic structure of the Ni(II)–CO complex that would necessarily be formed as an intermediate. Nucleophilic attack of $^-$OH at the bound C atom would be disfavored by M–L backbonding due to the increased electron density at the C atom. Therefore, the best catalysts should contain a high-lying d_{z2} LUMO separated from lower energy occupied d_{xz} and d_{yz} orbitals, such that the resulting metal–CO bond in the five-coordinate Ni(II) complex is of primarily σ and minimal π character. Such a configuration would be favored by more donating ligands and a geometry distortion from square planar towards tetrahedral, as would be expected for $P^{Cy}{}_2N^{R'}{}_2$ ligands.

The DuBois group has explored the possibility of using their Ni catalysts in PEM fuel cell applications, and has thus looked at the hydrogen oxidation activity of various Ni complexes in the presence of CO-contaminated H_2.[8] Most of these complexes were inert in the presence of CO. $[Ni(P^{Cy}{}_2N^{Bn}{}_2)_2(CH_3CN)][BF_4]_2$ reversibly formed a Ni–CO complex that appeared to be stabilized by the interaction of the pendant bases with the "partial positive charge of the carbonyl carbon", while $Ni(P^{Et2}N^{Me}P)_2(CH_3CN)[BF_4]_2$ appeared to react

irreversibly over the course of 24 hours to form what they suggested was a Ni(0) species. They did not explore this reaction further or attempt any CO oxidation studies.

Based on the DuBois group's results and our ideas about the chemical requirements for CO oxidation, we decided to test these and three other Ni bis-diphosphine catalysts for CO binding and oxidation activity (**Table 3-1**). Despite the unfavorable thermodynamics for oxidation by the $P^{Cy}_2N^{tBu}_2$ complex at higher pH, we retained it in the study so as to be able to compare the series of P^{Cy} complexes at the various $^-$OH concentrations. We included $P^{Ph}_2N^{PhCF3}_2$ because it was the least donating P^{Ph} complex available, and had the largest driving force for oxidation of all possible catalysts. Lastly, we targeted $P^{Et2}N^{Me}P$ in hopes of following up on the report of possible substrate oxidation.

Table 3-1. Reduction potentials of $[Ni(P_2N_2)_2]^{2+}$ and $[Ni(PNP)_2]^{2+}$ complexes tested for CO binding and oxidation activity, reported *vs*. $FeCp_2^{+/0}$ in PhCN.

Complex (ligand)	$E°_{II/I}$ (V)	$E°_{I/0}$ (V)	Σ–nFE at pH = 7	pH = 12
$P^{Cy}_2N^{tBu}_2$	–0.81	–1.45	+0.06 V	–0.24 V
$P^{Cy}_2N^{Bn}_2$	–0.70	–1.33	+0.29 V	–0.01 V
$P^{Cy}_2N^{PhOMe}_2$	–0.62	–1.16	+0.54 V	+0.24 V
$P^{Ph}_2N^{PhCF3}_2$	–0.71	–0.90	+0.71 V	+0.41 V
$P^{Et2}N^{Me}P$	–0.60	–1.24	+0.48 V	+0.18 V

3.2 Experimental

General procedures

All chemicals were purchased from commercial sources and used as received unless otherwise specified. All manipulations were carried out using standard Schlenk and glove box techniques under an atmosphere of nitrogen. Acetonitrile, tetrahydrofuran (THF), pentane, and diethyl ether (Et_2O) were sparged with argon and dried over basic alumina in a custom dry solvent system. $Ni(P^{Cy}_2N^{tBu}_2)_2(CH_3CN)[BF_4]_2$, $Ni(P^{Cy}_2N^{Bn}_2)_2(CH_3CN)[BF_4]_2$,

$Ni(P^{Cy}_2N^{PhOMe}_2)_2(CH_3CN)[BF_4]_2$, $Ni(P^{Ph}_2N^{PhCF3}_2)_2(CH_3CN)[BF_4]_2$, and $Ni(P^{Et2}N^{Me}P)_2(CH_3CN)[BF_4]_2$ were synthesized according to previously published procedures.[9–13]

Electrochemical experiments

All electrochemical experiments were carried out under an atmosphere of nitrogen in a 0.1 M tetrabutylammonium hexafluorophosphate (NBu_4PF_6) solution in benzonitrile using a BAS Epsilon or CV-50 three electrode potentiostat. The working electrode was a 1 mm diameter glassy carbon disk, the counter electrode was a glassy carbon rod, and a silver wire in electrolyte solution separated from the working compartment by porous Vycor (4mm, BAS) was used as a pseudo-reference electrode. All potentials are reported *vs*. the $FeCp_2^{+/0}$ couple, and in some cases were corrected by less than 20 mV to be consistent with previously published redox potentials.

CV titrations of the catalysts were carried out using 1 mL volumes of 1 mM catalyst solutions in electrolyte solution. 1 M solutions of NBu_4OH were prepared by dilution of 55% NBu_4OH in H_2O with the same electrolyte solution, such that adding 1 μL of titrant solution to the 1 mL catalyst solution resulted in introduction of 1 equivalent of titrant. CVs were taken after sparging with N_2 or CO as well as after addition and hand mixing of 5–10 equivalents at a time.

3.3 Discussion and Results

3.3.1 Cyclic voltammetry of $[Ni(P_2N_2)_2(CH_3CN)][BF_4]_2$ complexes

Cyclic voltammograms were taken to confirm the purity of the five tested complexes and serve as baselines prior to reaction with CO (**Figure 3-2**). As expected, in the series consisting of the three P^{Cy} catalysts, the Ni(II/I) and Ni(I/0) redox potentials shift negative with more basic amine groups.[12] The redox potentials of the $P^{Et2}N^{Me}P$ catalyst are shifted more positive relative to the P^{Cy} catalysts due to the reduced number of amines and larger

cone angle of the phosphine ligand.[14] The potentials of the $P^{Ph}_2N^{PhCF3}_2$ complex are at the positive end of the range observed for $P^{Ph}_2N^{R'}_2$ catalysts due to the reduced basicity of the amine. It has been generally observed that the Ni(II/I) potentials are more negative for P^{Ph} catalysts than their P^{Cy} counterparts, which is counterintuitive to the expectation that P^{Ph} should be less donating. This inverse trend can be explained as being more strongly dependent on the geometry of the ligands around the metal; Ni(II) P^{Cy} complexes tend to be more strongly distorted towards trigonal bipyramidal, which results in a lower LUMO.[15,16]

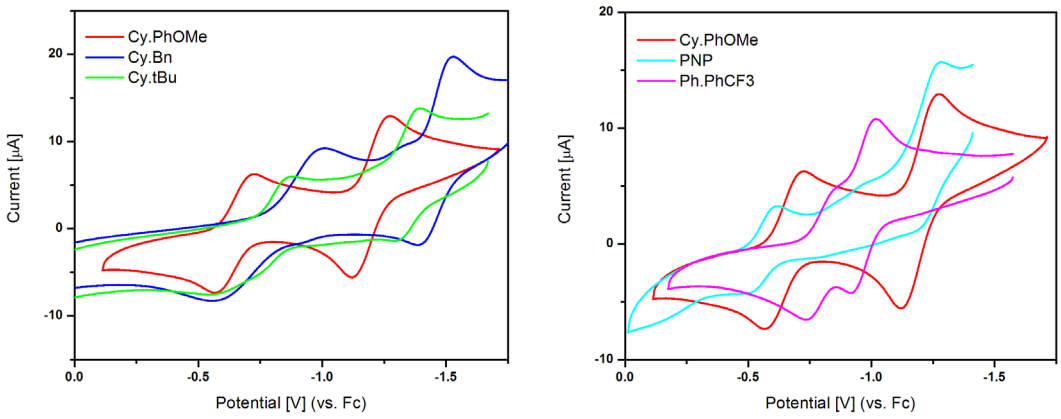

Figure 3-2. Cyclic voltammograms of Ni complexes prior to reaction with CO and $^{-}$OH. Conditions: Glassy carbon working and counter electrodes, AgCl reference electrode, 0.2 M NBu_4PF_6 electrolyte in PhCN, scan rate 100 mV/s.

3.3.2 Reactions of $[Ni(P_2N_2)_2(CH_3CN)][BF_4]_2$ complexes with CO and NBu_4OH

The samples were subsequently sparged with CO for 1 minute, and CVs were taken to test for any reaction or complex formation. No reactions or changes were observed for $[Ni(P^{Cy}_2N^{PhOMe}_2)_2]^{2+}$ or $[Ni(P^{Ph}_2N^{PhCF3}_2)_2]^{2+}$. The CVs of $[Ni(P^{Cy}_2N^{tBu}_2)_2]^{2+}$ and $[Ni(P^{Cy}_2N^{Bn}_2)_2]^{2+}$ showed a negative shift in the peak corresponding to reduction of Ni(II) to Ni(I), but were otherwise unchanged(**Figure 3-3a, b**). This was interpreted to be consistent with the DuBois group's previous isolation of the stable $[Ni(P^{Cy}_2N^{Bn}_2)_2(CO)]^{2+}$ complex. Binding of apical CO to Ni(II) would shift the Ni(II/I) reduction potential more negative due

to the resulting slight anti-bonding character of the d_{z2} LUMO. The 1 e^- reduction would result in CO loss, and subsequent reductions and oxidation would be unchanged from the original $[Ni(P^{Cy}_2N^{R'}_2)_2]^{2+}$ CVs. The lack of a shift on the return Ni(II/I) oxidation suggests that CO binding is relatively slow on the electrochemical timescale. No new oxidations were observed when the CVs were scanned up to approximately +0.4 V, which suggests that neither catalyst is able to oxidize CO at this pH.

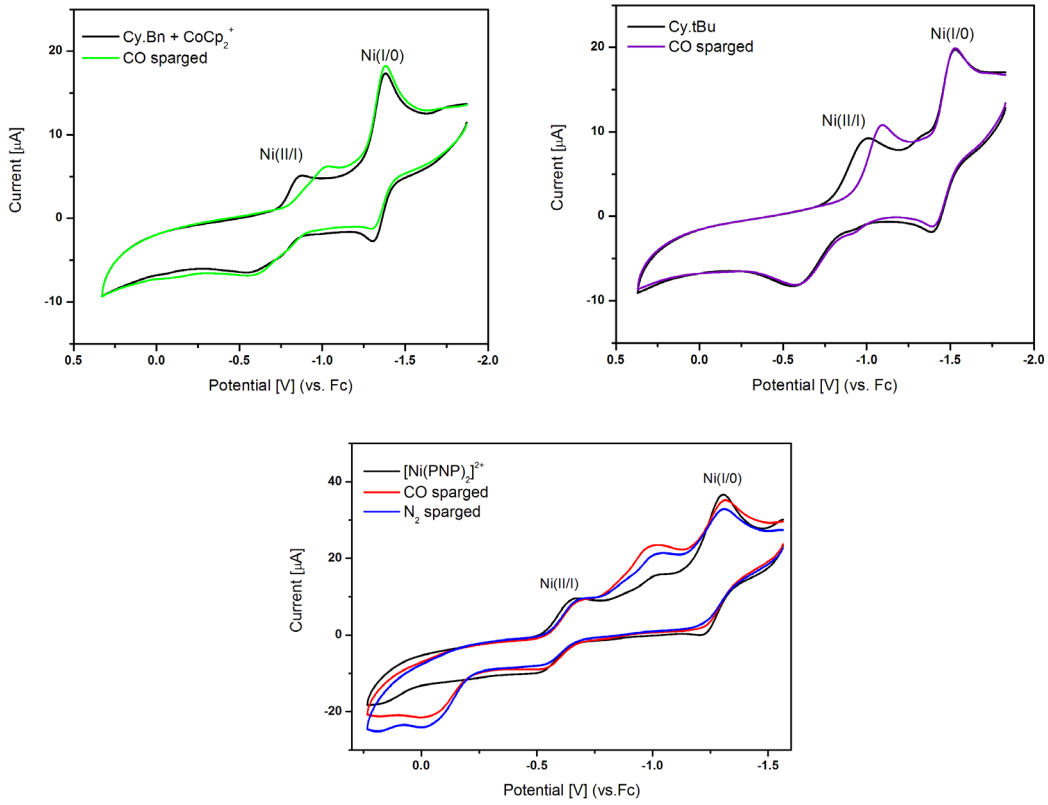

Figure 3-3. Cyclic voltammograms under N_2 and CO of (a) $[Ni(P^{Cy}_2N^{tBu}_2)_2]^{2+}$, (b) $[Ni(P^{Cy}_2N^{Bn}_2)_2]^{2+}$, (c) $[Ni(P^{Et2}N^{Me}P)_2]^{2+}$. Conditions: Glassy carbon working and counter electrodes, AgCl reference electrode, 0.2 M NBu_4PF_6 electrolyte in PhCN, scan rate 100 mV/s.

The Ni(II/I) reduction potential of $[Ni(P^{Et2}N^{Me}P)_2]^{2+}$ shifts much more subtly. An additional reduction peak was seen at –0.97 V, close to or possibly augmenting a previously existing peak in the baseline (black) scan (**Figure 3-3c**). This peak was absent in the blank

solvent and did not disappear after extensive sparging with either CO or N_2, which suggests that it is a Ni-based side product. We suspect that it may be a mono-P_2N_2 complex; however, we did not pursue this further. A new oxidation peak at +0.05 V is similar to that observed by DuBois's group in a CV of the CO reaction product after 24 hours, and may correspond to oxidation of a Ni–CO complex.[8] Sparging of the solution with N_2 resulted only in a small decrease of the new peaks, suggesting that the reverse CO reaction is very slow.

The three Ni complexes suspected to react with CO were titrated with NBu_4OH. In all cases, the solution turned yellow and oxidative catalytic current was observed near 0 V (**Figure 3-4**). This initially seemed promising since it recalled the reaction of red Ni(II) solutions with formate to produce yellow Ni(0). However, phosphine ligand displacement by anionic ligands can also produce yellow Ni(II) complexes. The fact that the current increase did not correspond to any existing peak and was furthermore extremely positive of the Ni(II/I) redox potential gave us additional cause for concern. Lastly, the decrease in size of the original Ni redox potentials with increasing amounts of hydroxide led us to wonder whether hydroxide was degrading the complexes and actually being oxidized at the electrode.

A set of control CVs in which blank electrolyte was titrated using the same electrode setup appeared to confirm this hypothesis (**Figure 3-5**). The same increase in oxidative current near 0 V can be clearly attributed to ^{-}OH oxidation at the glassy carbon electrode surface, as there is no catalyst in solution to mediate the electron transfer. It is thus extremely likely that the addition of ^{-}OH to $Ni(P_2N_2)_2$ solutions results in ligand exchange to form catalytically inactive $Ni(OH)_2$, precluding the use of $[Ni(P_2N_2)_2]^{2+}$ complexes as CO oxidation catalysts. A similar degradation process was also hypothesized to occur in the presence of high concentrations of formate;[11] the reaction of the complexes at much lower $^{-}$OH concentrations is possibly due to the increased electrostatic attraction between Ni(II) and

the inorganic ligand, resulting in stronger charge transfer upon binding. It is also possible that $^{-}$OH oxidizes the phosphine ligands, resulting in inactive phosphine oxide complexes.[17]

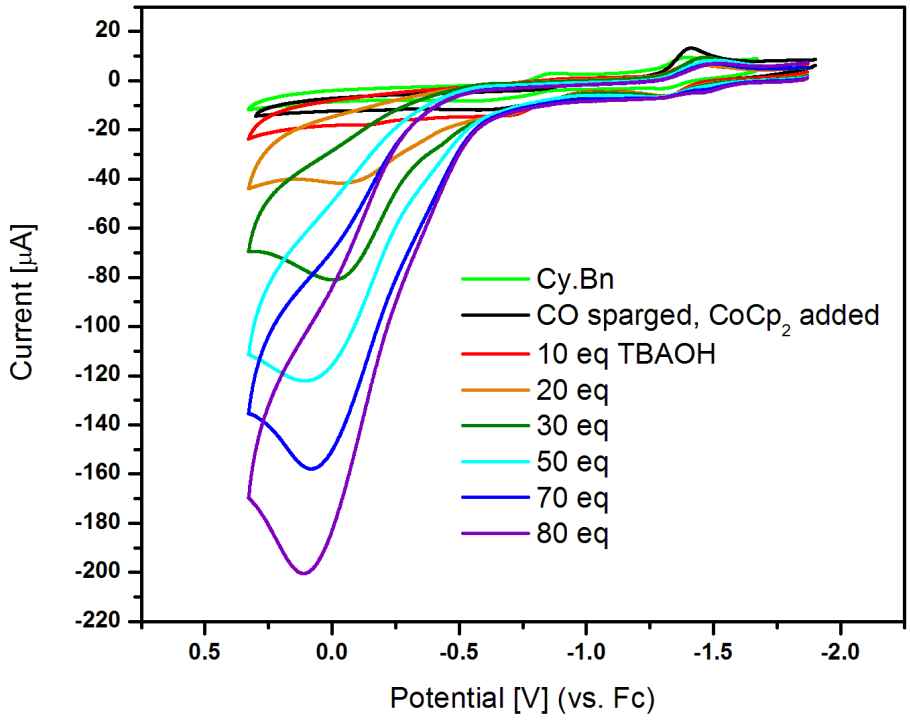

Figure 3-4. Cyclic voltammograms of $[Ni(P^{Cy}_2N^{Bn}_2)_2]^{2+}$ under a CO atmosphere titrated with increasing amounts of NBu_4OH. Conditions: Glassy carbon working and counter electrodes, AgCl reference electrode, 0.2 M NBu_4PF_6 electrolyte in PhCN, scan rate 100 mV/s.

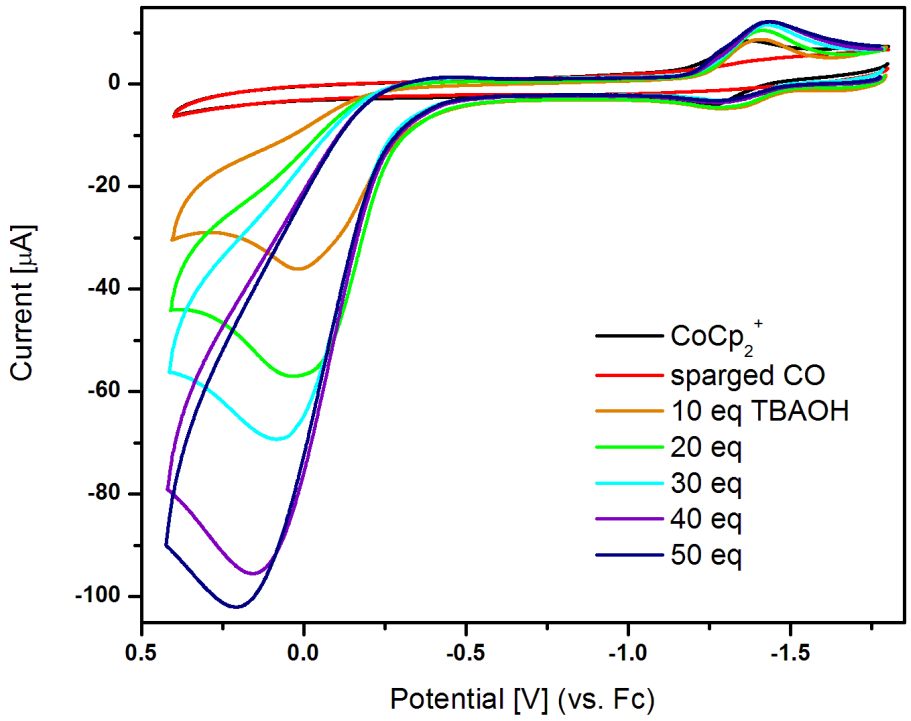

Figure 3-5. Cyclic voltammograms of 0.2 M NBu_4PF_6 electrolyte in PhCN under a CO atmosphere titrated with increasing amounts of NBu_4OH. Conditions: Glassy carbon working and counter electrodes, AgCl reference electrode, scan rate 100 mV/s.

Although this lack of catalytic activity is disappointing, the data collected in this study on the series of $P^{Cy}N^{R'}$ complexes allow us to add to the discussion posed in the DuBois paper regarding the factors that enable certain Ni catalysts to stably bind CO.[8] Wilson *et al.* argue that stabilization of the CO complexes is enabled by two electrostatic interactions between the lone pairs of the nitrogens and the positively charged carbon atom. The three complexes that are thought to interact with CO have ligands composed of basic alkyl amines, the pK_as of which are augmented by the presence of basic alkyl phosphines. The complexes that did not bind CO lacked one or both of these features, and we suggest that the stabilizing electrostatic interactions are stronger with more negative and donating amines.

3.4 Conclusions

A series of $[Ni(P_2N_2)_2]^{2+}$ and $[Ni(PNP)_2]^{2+}$ complexes were tested for CO oxidation activity in the presence of NBu_4OH, but found to be unstable under these conditions. The susceptibility of the catalysts to ^{-}OH degradation should be taken into account when attempting to adapt these catalysts to different applications.

3.5 References

1. Yu, X.; Pickup, P. G. *J. Power Sources*, **2008**, *182*, 124–132.

2. Gottesfeld, S. *J Electrochem. Soc.*, **1988**, 135, 2651–2652.

3. Arenz, M.; Stamenkovic, V.; Schmidt, T. J.; Wandelt, K.; Ross, P. N.; Markovic, N. M. *Phys. Chem. Chem. Phys.*, **2003**, *5*, 4242–4251.

4. Oh, S.; Sinkevitch, R. *J. Catal.*, **1993**, *142*, 254–262.

5. Manasilp, A.; Gulari, E. *Appl. Catal., B*, **2002**, *37*, 17–25.

6. Darensbourg, D. J.; Baldwin, B. J.; Froelich, J. A. *J. Am. Chem. Soc.*, **1980**, *102*, 4688–4694.

7. Marković, N.; Ross, P. *Surf. Sci. Rep.*, **2002**, *45*, 117–229.

8. Wilson, A. D.; Fraze, K.; Twamley, B.; Miller, S. M.; DuBois, D. L.; DuBois, M. R. *J. Am. Chem. Soc.*, **2008**, *130*, 1061–1068.

9. Yang, J. Y.; Chen, S.; Dougherty, W. G.; Kassel, W. S.; Bullock, R. M.; DuBois, D. L.; Raugei, S.; Rousseau, R. J.; Dupuis, M.; DuBois, M. R. *Chem. Commun.*, **2010**, *46*, 8618–8620.

10. Wilson, A. D.; Newell, R.; McNevin, M. J.; Muckerman, J. T.; DuBois, M. R.; DuBois, D. L. *J. Am. Chem. Soc.*, **2006**, *128*, 358–366.

11. Galan, B. R.; Schöffel, J.; Linehan, J. C.; Seu, C. S.; Appel, A. M.; Roberts, J. A. S.; Helm, M. L.; Kilgore, U. J.; Yang, J. Y.; DuBois, D. L.; Kubiak, C. P. *J. Am. Chem. Soc.*, **2011**, *133*, 12767–12779.

12. Kilgore, U. J.; Roberts, J. A. S.; Pool, D. H.; Appel, A. M.; Stewart, M. P.; DuBois, M. R.; Dougherty, W. G.; Kassel, W. S.; Bullock, R. M.; DuBois, D. L. *J. Am. Chem. Soc.*, **2011**, *133*, 5861–5872.

13. Curtis, C. J.; Miedaner, A.; Ciancanelli, R.; Ellis, W. W.; Noll, B. C.; DuBois, M. R.; DuBois, D. L. *Inorg. Chem.*, **2003**, *42*, 216–227.

14. Wilson, A. D.; Miller, A. J. M.; DuBois, D. L.; Labinger, J. A.; Bercaw, J. E. *Inorg. Chem.*, **2010**, *49*, 3918–3926.

15. Fraze, K.; Wilson, A. D.; Appel, A. M.; DuBois, M. R.; DuBois, D. L. *Organometallics*, **2007**, *26*, 3918–3924.

16. Miedaner, A.; Noll, B. C.; DuBois, D. L. *Organometallics*, **1997**, *16*, 5779–5791.

17. Yang, J. Y.; Bullock, R. M.; Dougherty, W. G.; Kassel, W. S.; Twamley, B.; DuBois, D. L.; DuBois, M. R. *Dalton Trans.*, **2010**, *39*, 3001–3010.

Chapter 4

Harnessing trends in hydricity: CO_2 reduction by $[Co(P_2N_2)_2]^{-1}$ catalysts

4.1 Introduction

In Chapters 1 and 2, we discussed the concept of hydricity and established that the hydricities of the $[HNi(P_2N_2)_2]^+$ complexes we studied were insufficient to reduce CO_2 to HCOOH. At that time, the range of available $P^R{}_2N^{R'}{}_2$ ligands was largely limited to P^{Ph} and P^{Cy} derivatives due to the limited availability and hazardous nature of the primary phosphines used in the synthetic procedure.[1] Michael Doud and Dr. Kyle Grice's subsequent development of a new synthetic method for alkyl phosphine ligands opened up many catalytic possibilities, and was in part motivated by the idea that more donating ligands should support more hydridic catalysts.[2] The DuBois group measured the hydricity of the newly synthesized $[HNi(P^{Me}{}_2N^{Ph}{}_2)_2]^+$ complex to be 54 kcal/mol, which was indeed at the higher end of the range but is still insufficient to reduce CO_2 (43 kcal/mol in ACN).[3]

The concept of hydricity as a guiding concept in catalyst development and its calculation through the use of thermodynamic cycles was an early focus of the DuBois group,[4–14] following up on work done by Tilset and Parker[15,16] on metal hydride bond dissociation energies (BDE). Experimental measurement of M–H hydricities has been achieved for a few classes of compounds, including the Group 9 and 10 bis-diphosphines measured by DuBois's group, Group 8 Cp and terpy bipyridines measured by the Creutz and Norton groups,[17–19] and Group 5 and 6 Cp half-sandwich complexes measured by Sarker and Bruno.[20,21] The data set collected by the DuBois group is the most comprehensive by far, and is summarized in **Figure 4-1.**

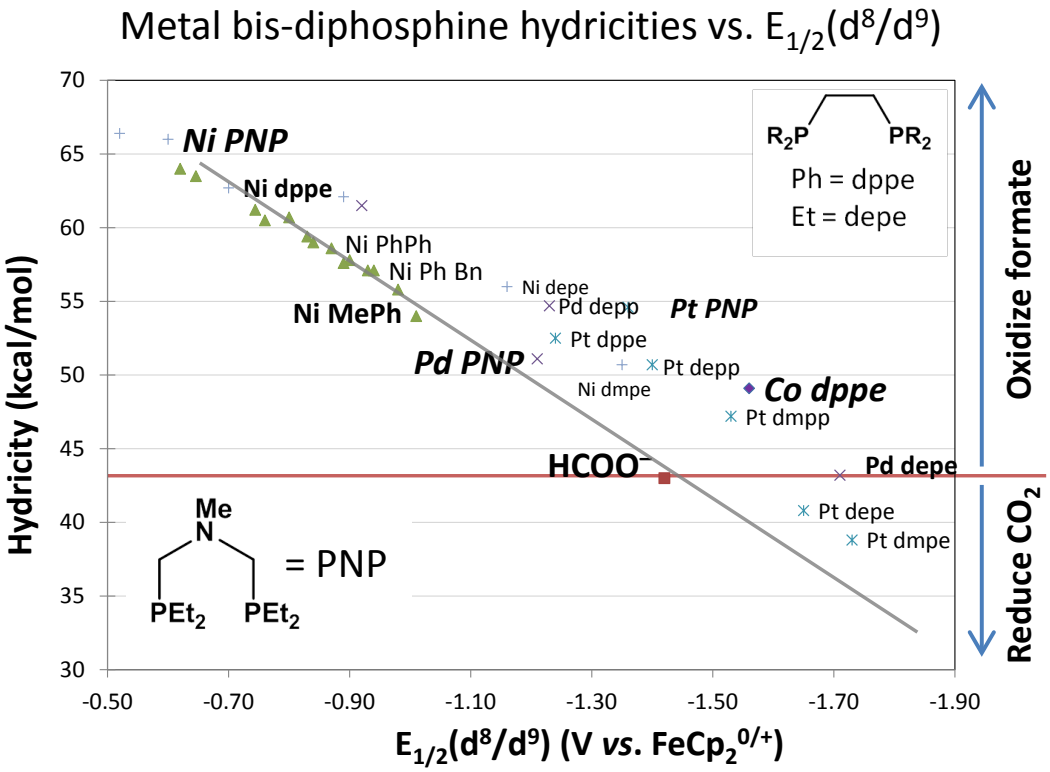

Figure 4-1. Experimentally determined hydricities vs M d^8/d^9 reduction potential for various Group 9 and 10 bis(diphosphine complexes), showing the strongly linear relationship between these two thermodynamic parameters. Only selected data point labels have been included on the plot to enhance clarity. Refer to references for ligand abbreviations and numerical values.[3–5,7,8,12,13,22,23]

The plot clearly illustrates the linear free energy relationship between hydricity and the d^8/d^9 reduction potential of the metal center, which corresponds to $E_{II/I}$ for Ni, Pd, and Pt, and $E_{I/0}$ for Co and Rh.[8] This relationship between the energy of a hydride and the energy of the metal HOMO electrons suggests that hydricity can still serve as a predictive parameter of metal reactivity in the case that CO_2 reduction occurs by means of a concerted two-electron, single proton transfer as the microscopic reverse of the mechanism in Chapter 2. Hess's law can be used to calculate the standard reduction potential for CO_2 to formate in neutral acetonitrile:

	$\Delta G°$ (kcal/mol)	
$CO_2 + H^- \rightleftharpoons HCOO^-$	–43	(1)
$H^+ + 2e^- \rightleftharpoons H^-$	+79.6	(2)
$CO_2 + H^+ + 2e^- \rightleftharpoons HCOO^-$	+36.6	(3)
$\Delta G = -nFE$	$= -0.79$ V vs NHE	
	$= -1.42$ V (vs $FeCp_2^{+/0}$)[24]	

which is marked as the red point in **Figure 4-1**, and is consistent with this hydricity-potential trend. Complexes that fall to the right of this point or below this line should be thermodynamically able to reduce CO_2.

Comparisons between complexes containing different metals and the same ligand set, such as $[Ni(dppe)_2]^{2+}$ *vs*. $[Co(dppe)_2]^{+1}$ and $[Ni(depe)_2]^{2+}$ *vs*. $[Pd(depe)_2]^{2+}$, suggest that P_2N_2 complexes of these earlier or heavier transition metals should be sufficiently hydridic or energetic enough to reduce CO_2. Similar predictions have been published in computational studies.[25–27] The increase in hydricity and negative reduction potential as you move down or left on the periodic table is consistent with the destabilization of d orbital energies arising from a decrease in Z_{eff}, and a resulting destabilization of the M–H bonding orbital (similar to the situation depicted in **Figure 1-5**).

We decided to first explore the possibility of reducing CO_2 with $[Co(P_2N_2)_2]^-$ complexes due to the abundance and cost advantage of this first-row transition metal. Additionally, an earlier paper by the DuBois group on $Co(P^{Ph}_2N^{Ph}_2)_2$ assured us that these catalysts could be successfully synthesized, and set a precedent for enhancement of catalysis by the pendant base.[28] However, it should be noted that the active catalyst in this paper was found to be $[Co(P^{Ph}_2N^{Ph}_2)(CH_3CN)_3]^+$, generated by trifluoroacetic acid-induced ligand loss. The Co(I/–I) couple of this mono-P_2N_2 complex would be expected to be extremely negative; meanwhile, the Co(0) species active in H_2 production would not be hydridic enough to reduce CO_2. The instability of the bis-P_2N_2 complex constrained our synthetic targets and experimental conditions, and was eventually found to limit the utility of these complexes.

4.2 Experimental

General procedures

All chemicals were purchased from commercial sources and used as received unless otherwise specified. All manipulations were carried out using standard Schlenk and glove box techniques under an atmosphere of nitrogen. Acetonitrile, tetrahydrofuran (THF), pentane, and diethyl ether (Et_2O) were sparged with argon and dried over basic alumina in a custom dry solvent system. $P^{Ph}_2N^{Ph}_2$, $P^{Ph}_2N^{PhOMe}_2$, $P^{Ph}_2N^{Bn}_2$, $[Co(P^{Ph}_2N^{Ph}_2)_2(CH_3CN)][BF_4]_2$, and $[Co(dmpe)_2(CH_3CN)_2](BF_4)_2$ were synthesized according to previously published procedures.[1,9,23,29]

Electrochemical experiments

All electrochemical experiments were carried out under an atmosphere of nitrogen in a 0.1 tetrabutylammonium hexafluorophosphate (NBu_4PF_6) solution in acetonitrile using a BAS Epsilon of CV-50 three electrode potentiostat. The working electrode was a 1 mm diameter glassy carbon disk, the counter electrode was a glassy carbon rod, and a silver wire

in electrolyte solution separated from the working compartment by porous Vycor (4mm, BAS) was used as a pseudo-reference electrode. All potentials are reported *vs*. the $FeCp_2^{+/0}$ couple.

CV titrations of the catalysts were carried out using 1 mL volumes of 1 mM catalyst solutions in electrolyte solution. In some cases the solutions were sparged with CO_2 prior to acid addition. 1 M solutions of the various acids were prepared in the same electrolyte solution, such that adding 1 μL of titrant acid to the 1 mL catalyst solution resulted in introduction of 1 equivalent of titrant. CVs were taken after addition and hand mixing of 5-10 equivalents at a time.

Crystallography

Crystals of $[Co(P^{Ph}_2N^{Bn}_2)_2(CH_3CN)](BF_4)_2$ and $[Co(P^{Ph}_2N^{PhOMe}_2)_2Cl](BF_4)$ suitable for X-ray structural determinations were mounted in polybutene oil on a glass fiber and transferred on the goniometer head to the precooled instrument. Crystallographic measurements were carried out on a Bruker P4 diffractometer using Mo Kα radiation (λ = 0.71073 Å) in conjunction with a Bruker APEX detector. All structures were solved by direct methods using OLEX2 and refined with full-matrix least-squares procedures using SHELXL-97. All non-hydrogen atoms are anisotropically refined unless otherwise reported; the hydrogen atoms were included in calculated positions as riding models in the refinement. Crystallographic data collection and refinement information can be found in the Appendix.

Synthesis of $[Co(P^{Ph}_2N^{Ph}_2)_2(CH_3CN)](BF_4)_2$

$P^{Ph}_2N^{Ph}_2$ (136 mg, 0.3 mmol) was added to a pink solution of $[Co(CH_3CN)_6](BF_4)_2$ (72 mg, 0.15 mmol) in acetonitrile (10 mL). The initially cloudy brown suspension was stirred at room temperature overnight until the ligand dissolved. The dark brown solution was cannula filtered to remove unreacted ligand, reduced to 10 mL under vacuum, and

layered with diethyl ether to induce crystallization. The dark red crystals were cannula filtered and dried under vacuum. Yield = 47 mg (0.04 mmol, 28%). ESI^+ MS: $[Co(P^{Ph}{}_2N^{Ph}{}_2)_2]^+ = 967$.

Synthesis of $[Co(P^{Ph}{}_2N^{PhOMe}{}_2)_2(CH_3CN)](BF_4)_2$

$P^{Ph}{}_2N^{PhOMe}{}_2$ (206 mg, 0.4 mmol) was added to a pink solution of $[Co(CH_3CN)_6](BF_4)_2$ (96 mg, 0.2 mmol) in acetonitrile (10 mL). The initially cloudy brown suspension was stirred at room temperature overnight until the ligand dissolved. The dark brown solution was cannula filtered to remove unreacted ligand, reduced to 3 mL under vacuum, and layered with diethyl ether to induce crystallization. The dark red crystals were cannula filtered and dried under vacuum. Yield = 158 mg (0.127 mmol, 63.7%). ESI^+ MS: $[Co(P^{Ph}{}_2N^{PhOMe}{}_2)_2]^+ = 1087$.

Synthesis of $[Co(P^{Ph}{}_2N^{Bn}{}_2)_2(CH_3CN)](BF_4)_2$

$P^{Ph}{}_2N^{Bn}{}_2$ (193 mg, 0.4 mmol) was added to a pink solution of $[Co(CH_3CN)_6](BF_4)_2$ (96 mg, 0.2 mmol) in acetonitrile (10 mL). The initially cloudy brown suspension was stirred at room temperature overnight until the ligand dissolved. The dark brown solution was cannula filtered to remove unreacted ligand, reduced to 2 mL under vacuum, and layered with diethyl ether to induce crystallization. The dark red crystals were cannula filtered and dried under vacuum. Yield = 148 mg (0.119 mmol, 59.7%). ESI^+ MS: $[Co(P^{Ph}{}_2N^{Bn}{}_2)_2]^+ = 1023$.

4.3 Results and discussion

4.3.1 Synthesis

During our previous work with Ni-P_2N_2 complexes, we noticed that the $P^{Cy}{}_2N^{R'}{}_2$ ligands tended to bind less strongly than their $P^{Ph}{}_2N^{R'}{}_2$ counterparts. This is counterintuitive given the stronger donating strength of the P^{Cy} substituents, and may be related to trans-ligand effects or steric clashing. Regardless, we discovered that the $P^{Cy}{}_2N^{R'}{}_2$ ligands bound even more weakly to Co and were labile in the presence of any amount of ether, precluding

their isolation as pure material. As such, we decided to focus on synthesizing the more stable $P^{Ph}{}_2N^{R'}{}_2$ complexes. $[Co(P^{Ph}{}_2N^{Ph}{}_2)_2(CH_3CN)][BF_4]_2$, $[Co(P^{Ph}{}_2N^{PhOMe}{}_2)_2(CH_3CN)][BF_4]_2$, and $[Co(P^{Ph}{}_2N^{Bn}{}_2)_2(CH_3CN)][BF_4]_2$ were synthesized by mixing 2:1 solutions of ligand and $[Co(CH_3CN)_6][BF_4]_2$ in a manner analogous to that used for the Ni complexes. The brown complexes were crystallized and isolated by layering of the acetonitrile solutions with ether. Since Co^{2+} is paramagnetic, we were unable to use NMR to characterize these products. However, the synthesis of the products was confirmed by the observation of $[Co(P_2N_2)_2]^+$ parent ions using ESI mass spectrometry. Furthermore, clean CVs of the complexes suggested that the isolated products were pure.

4.3.2 X-ray diffraction studies

Diffractometer-quality crystals were obtained from the $[Co(P^{Ph}{}_2N^{Bn}{}_2)_2]^{2+}$ and $[Co(P^{Ph}{}_2N^{PhOMe}{}_2)_2]^{2+}$ reactions. However, the latter was obtained as a $[Co(P^{Ph}{}_2N^{PhOMe}{}_2)_2Cl]^+$ adduct (**Figure 4-2, 4-3**). It is unknown how or when the complex was exposed to a chloride source; however, the similarity of the CV to those of the other complexes, combined with the fact that the electrochemistry of the analogous Ni complex changed dramatically upon Cl^- binding, suggests that this particular adduct was adventitious and is not representative of the entire sample.

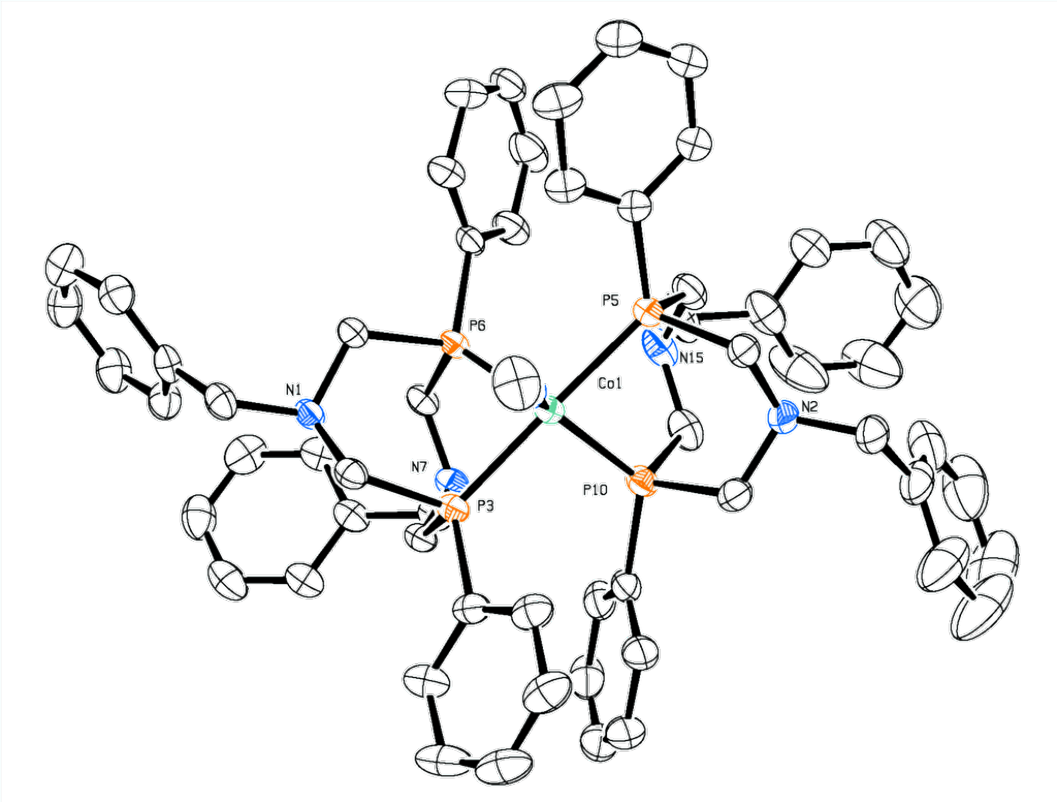

Figure 4-2. Crystal structure of $[Co(P^{Ph}_2N^{Bn}_2)_2(CH_3CN)](BF_4)_2 \bullet 14(CH_3CN)$. Counter ions and additional molecule (Z'=2) have been omitted for clarity.

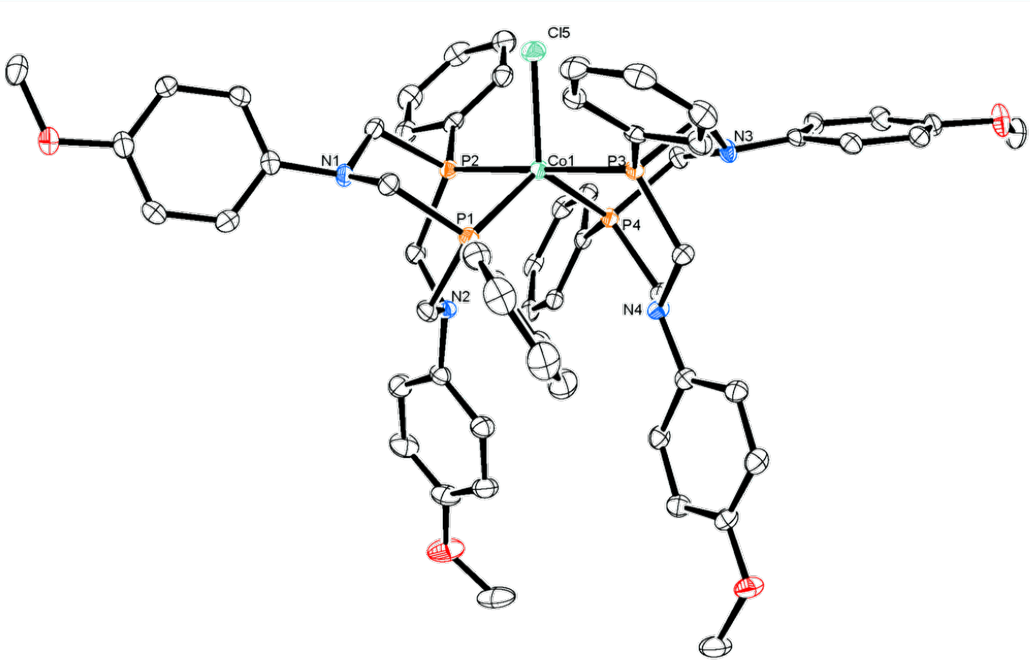

Figure 4-3. Crystal structure of $[Co(P^{Ph}_2N^{PhOMe}_2)_2Cl](BF_4) \bullet 3(CH_3CN)$.

4.3.3 Electrochemical studies

The cyclic voltammograms of all three complexes are very similar, and show a reversible wave near –0.6 V that corresponds to the Co(II/I) couple (**Figure 4-4**). The irreversible reduction near –2.25 V corresponds to the two-electron Co(I/–I) couple, and the subsequent oxidation is separated into two waves on the return scan. The DuBois group has suggested that the irreversibility of this reduction may arise from formation of dimeric bridged complexes to reduce ligand strain associated with the change to a tetrahedral geometry.[28] However, neither of our groups has pursued evidence to support this. As expected, the redox couples generally shift more negative as N^R becomes more basic (**Table 4-1**). The peak separation of the Co(I/–I) reduction and first oxidation also decreases as N^R becomes more basic. The reason for this is unclear, but may be related to the predisposition of the more strongly donating ligands towards an energy-lowering tetrahedral geometry, as

seen in the dihedral angles of the two crystal structures. (62° and 67° for $[Co(P^{Ph}{}_2N^{Bn}{}_2)_2(CH_3CN)]^{2+}$ *vs*. 55° for $[Co(P^{Ph}{}_2N^{PhOMe}{}_2)_2Cl]^{+}$.

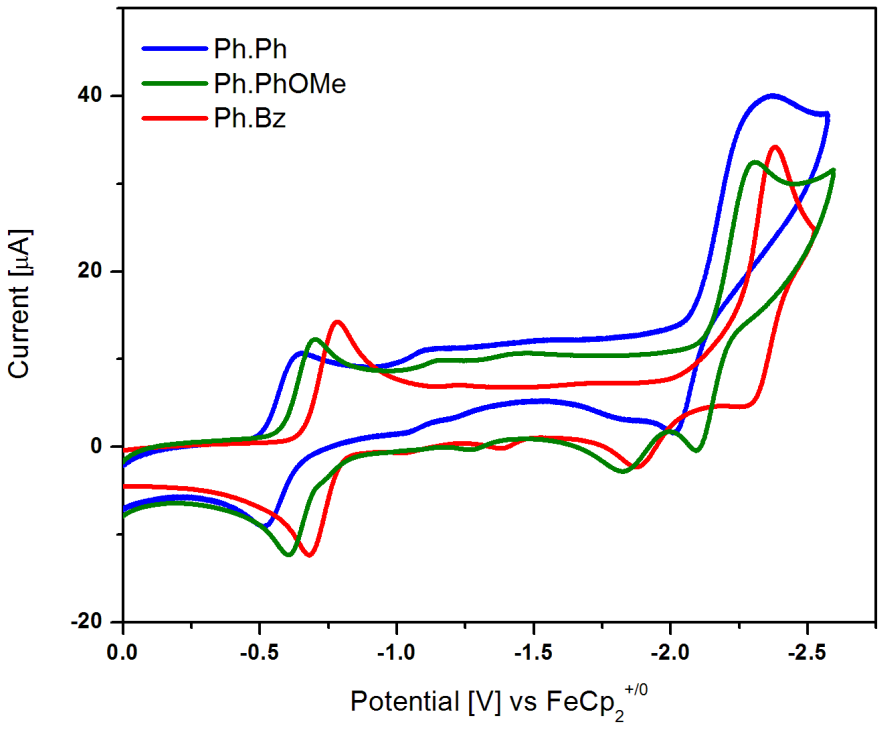

Figure 4-4. Cyclic voltammograms of $[Co(P_2N_2)_2]^{2+}$ complexes in ACN. Potentials are reported *vs*. $FeCp_2^{+/0}$. Conditions: Glassy carbon working and counter electrodes, AgCl reference electrode, 0.2 M NBu_4PF_6 electrolyte, scan rate 100 mV/s.

Table 4-1. Redox potentials of $[Co(P_2N_2)_2]^{2+}$ complexes in ACN, reported as V vs. $FeCp_2^{+/0}$.

Complex	$Co_{II/I}$	$Co_{I/-I}$	1st ox	2nd ox	ΔV
$P^{Ph}{}_2N^{Ph}{}_2$	–0.58	–2.35	–2.01	–1.82	0.34
$P^{Ph}{}_2N^{PhOMe}{}_2$	–0.65	–2.30	–2.09	–1.84	0.21
$P^{Ph}{}_2N^{Bn}{}_2$	–0.75	–2.48	–2.28	–1.90	0.20

4.3.4 Electrocatalytic studies with formate, formic acid, and protons

Our first catalysis experiment was to see if $[Co(P_2N_2)_2]^{2+}$ complexes still retained the ability to oxidize formate despite their significantly higher metal hydride pK_as. Titration of $[Co(P^{Ph}_2N^{PhOMe}_2)_2]^{2+}$ with $NBu_4HCO_2{\bullet}HCO_2H$ resulted in a very small increase in oxidative current at the Co(II/I) couple (**Figure 4-5**). Instead, the major feature of these CVs is an increase in reductive current at –2.2 V, or the Co(I/–I) couple, which is much more negative than the potential required for proton reduction in the DuBois paper.[28] It is unclear whether the current at 20 eq and above is due to reduction by the catalyst or is the result of a narrowed solvent window; however, the plateau shape of the 5 and 10 equivalent CVs are more clearly due to the former and should be reliable. The new reduction peak at –1.1 V may correspond to the formation of $[Co(P_2N_2)(CH_3CN)_3]^+$ or a $[Co(P_2N_2)_2(O_2CH)]^+$ adduct, but this appears to be limited.

Given the predicted hydride donating ability of these compounds, we considered the possibility that the catalyst is reducing the carbonyl of formate or formic acid to produce formaldehyde. To probe this further, we titrated the catalyst with a solution of formic acid (pK_a = 3.7) rather than the mixture afforded by $NBu_4HCO_2{\bullet}HCO_2H$ (**Figure 4-6**). Under these conditions, the catalytic current was instead seen at an onset potential of approximately –1.4 V. This is relatively close to the onset potential seen in the DuBois paper for proton reduction by $[Co(P^{Ph}_2N^{Ph}_2)(CH_3CN)_3]^+$, and suggests that the current seen here is the result of proton reduction by $[Co(P^{Ph}_2N^{PhOMe}_2)(CH_3CN)_3]^+$. The slight negative shift here is expected, given the more basic amines. It should be noted that the current/potential curve in that experiment has an S-shape, whereas these waves do not plateau. These differences may be related to the use of different acid titrants in the different studies, but we did not explore this further.

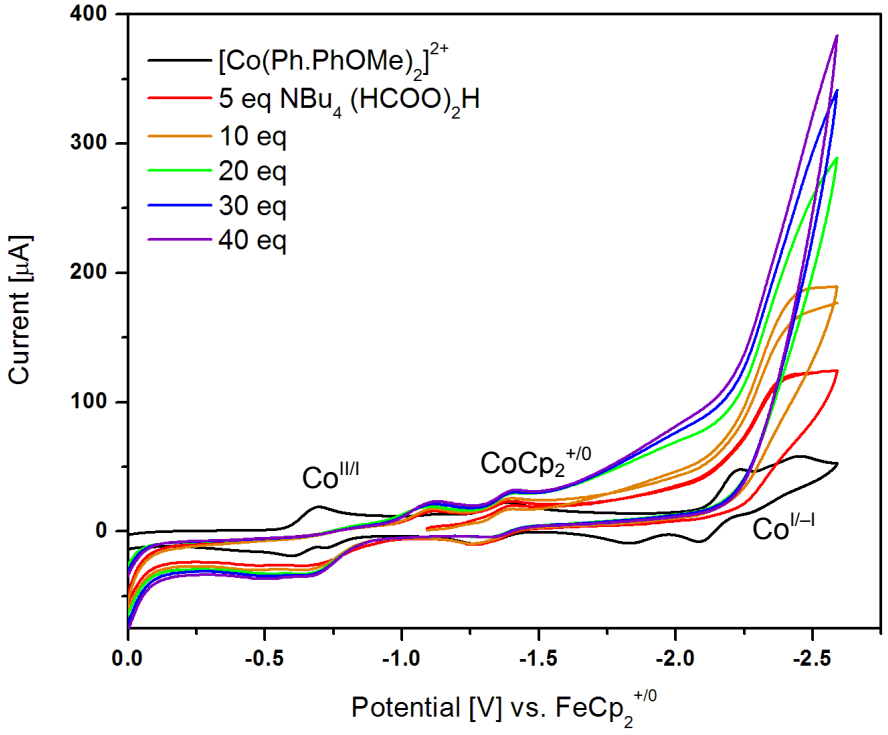

Figure 4-5. Cyclic voltammograms of $[Co(P^{Ph}_2N^{PhOMe}_2)_2(CH_3CN)](BF_4)_2$ upon titration with $NBu_4HCO_2{\bullet}HCO_2H$ in ACN. Potentials are reported *vs*. $FeCp_2^{+/0}$ using $CoCp_2^{+/0}$ as an internal reference. Conditions: Glassy carbon working and counter electrodes, AgCl reference electrode, 0.2 M NBu_4PF_6 electrolyte, scan rate 100 mV/s.

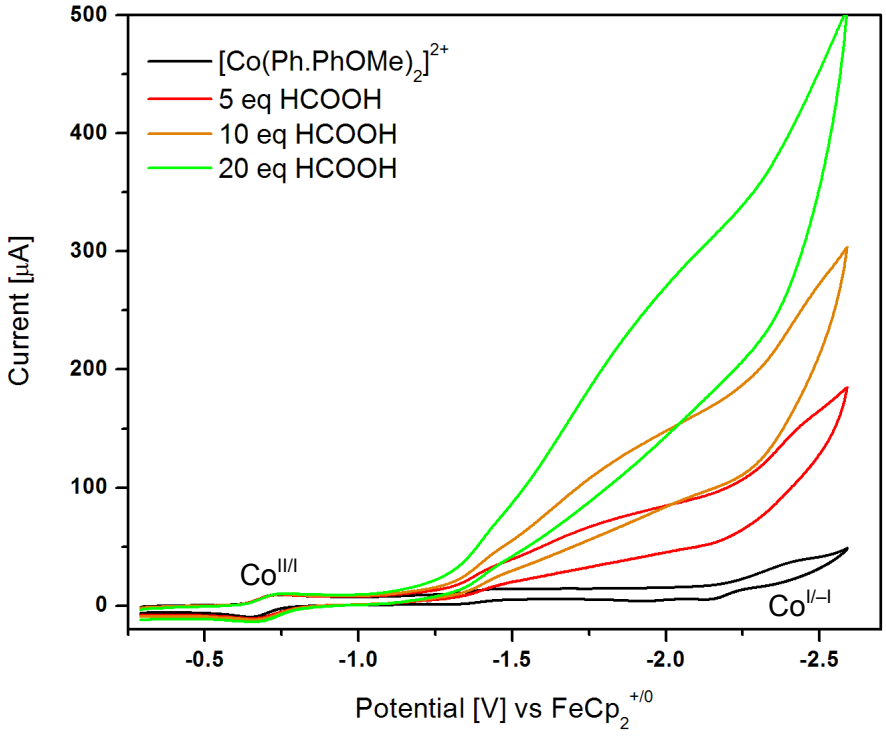

Figure 4-6. Cyclic voltammograms of $[Co(P^{Ph}_2N^{PhOMe}_2)_2(CH_3CN)](BF_4)_2$ upon titration with HCOOH in ACN. Conditions: Glassy carbon working and counter electrodes, AgCl reference electrode, 0.2 M NBu_4PF_6 electrolyte, scan rate 100 mV/s.

Hypothesizing that the difference in activity between NBu_4HCO_2•HCO_2H and HCOOH might be related to differences in pK_a rather than the presence of formate, we carried out a titration with 2,2,2-trifluoroethanol (TFE, pK_a = 12.5), which does not have a carbonyl. In this experiment, any reductive current should be the result of proton reduction. **Figure 6-7** shows that proton reduction occurs at the Co(I/–I) couple in this case.

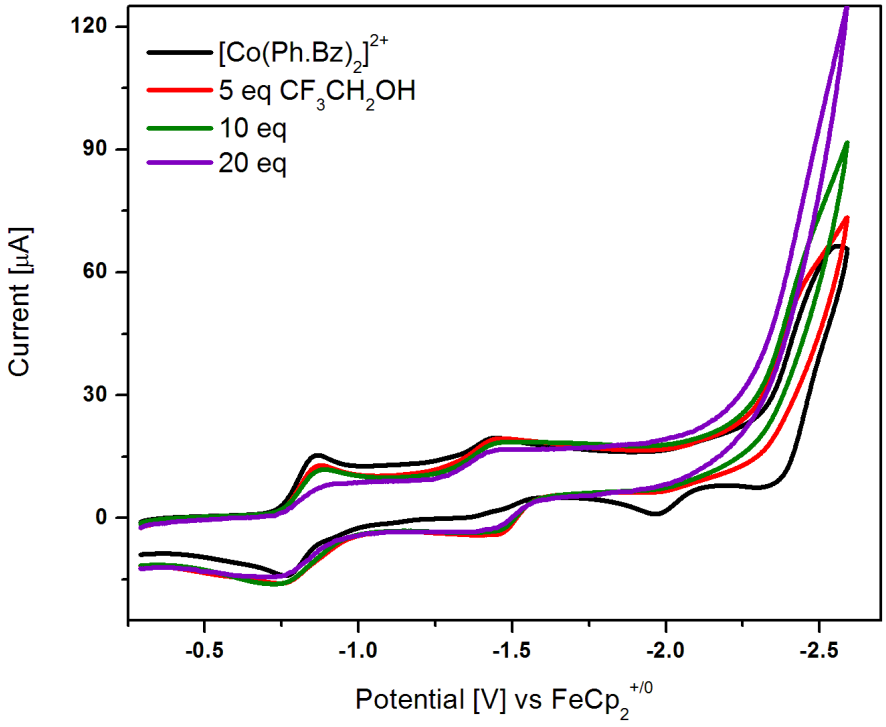

Figure 4-7. Cyclic voltammograms of $[Co(P^{Ph}_2N^{Bn}_2)_2(CH_3CN)](BF_4)_2$ upon titration with 2,2,2-trifluoroethanol in ACN. Conditions: Glassy carbon working and counter electrodes, AgCl reference electrode, 0.2 M NBu_4PF_6 electrolyte, scan rate 100 mV/s.

Taken together, these three experiments suggest that the current increase seen in the NBu_4HCO_2•HCO_2H titration can be attributed to proton reduction by the bis-P_2N_2 Co catalyst. The stability of these complexes in TFE and NBu_4HCO_2•HCO_2H but not HCOOH or 1,1,1-trifluoroacetic acid (TFA) can be explained by the significantly higher $\{H^+\}$ of the latter two. Protonation of the ligand at the amine inductively reduces its donating strength at the phosphine, making ligand loss kinetically favorable. This reaction appears to predominate in the HCOOH and TFA cases. The relative unavailability of the proton in NBu_4HCO_2•HCO_2H is due to hyperconjugation, which can be physically observed in the crystal structure as the sharing of the proton between two formate anions.[23]

4.3.5 Electrocatalytic studies with CO_2

Having ruled out $HCOO^-$ oxidation, we moved on to experiments on CO_2 reduction. All three complexes register a change in their CVs upon sparging with CO_2, suggesting binding or another reaction. **Figure 4-8** shows a representative CV of $[Co(P^{Ph}{}_2N^{Bn}{}_2)_2(CH_3CN)](BF_4)_2$, in which the Co(I/–I) reduction peak becomes taller and more irreversible.

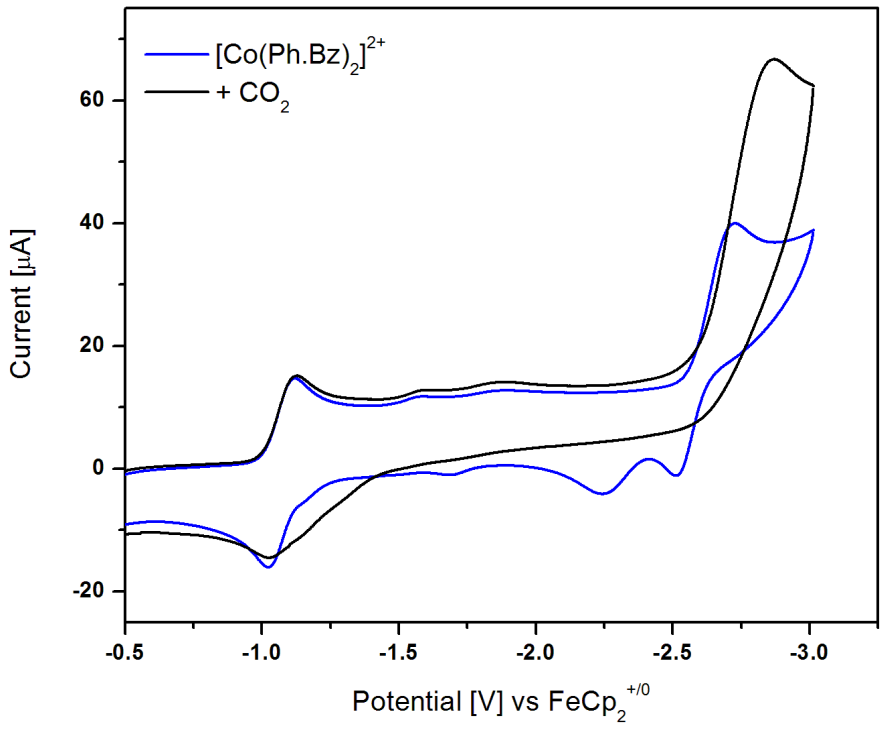

Figure 4-8. Cyclic voltammograms of $[Co(P^{Ph}{}_2N^{Bn}{}_2)_2(CH_3CN)](BF_4)_2$ under N_2 and upon sparging with CO_2 in ACN. The peak in the black trace at –1.2 V is likely oxygen. Conditions: Glassy carbon working and counter electrodes, AgCl reference electrode, 0.2 M NBu_4PF_6 electrolyte, scan rate 100 mV/s.

Since CO_2 reduction is a proton-coupled process, we wanted to see if catalysis would be enhanced in the presence of added protons. Given the tendency of these compounds to form mono-P_2N_2 complexes in the presence of strong acids, we decided to use TFE as our

proton source. A solution of $[Co(P^{Ph}_2N^{Bn}_2)_2(CH_3CN)](BF_4)_2$ was sparged with CO_2 and subsequently titrated with TFE (**Figure 4-9**). The reductive catalytic current increased slightly upon addition of the first equivalent, then decreased upon further acid addition, suggesting catalyst degradation or inhibition by a side reaction.

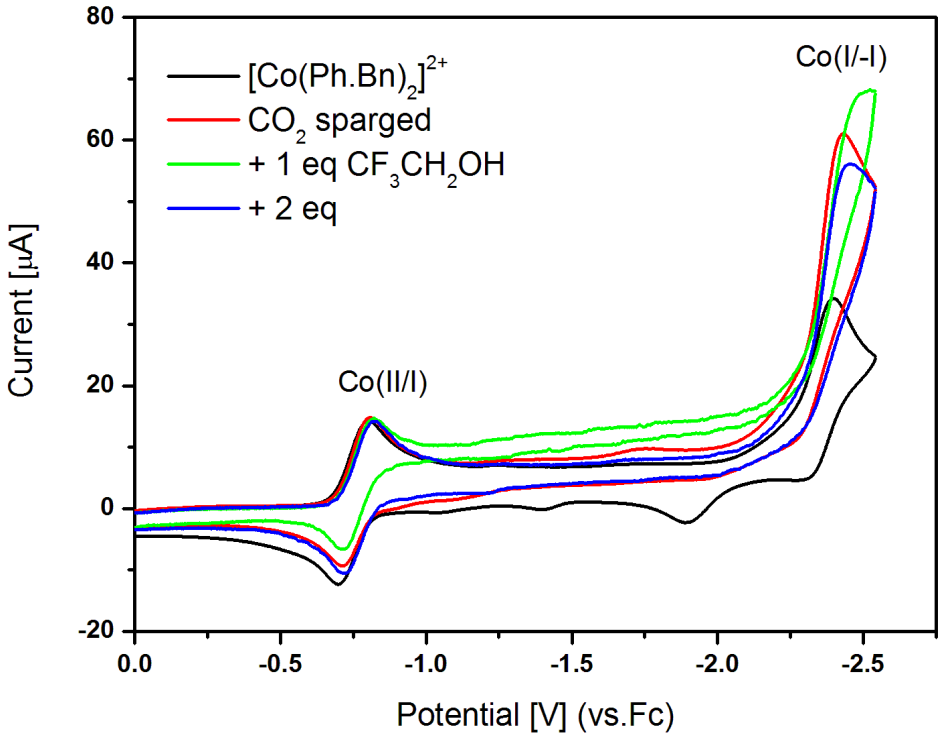

Figure 4-9. Cyclic voltammograms of $[Co(P^{Ph}_2N^{Bn}_2)_2(CH_3CN)](BF_4)_2$ upon sparging with CO_2 and addition of TFE in ACN. Potentials are reported vs. $FeCp_2^{+/0}$. Conditions: Glassy carbon working and counter electrodes, AgCl reference electrode, 0.2 M NBu_4PF_6 electrolyte, scan rate 100 mV/s.

Attempts to use bulk electrolysis to identify any products from the reaction of $[Co(P^{Ph}_2N^{Bn}_2)_2(CH_3CN)](BF_4)_2$ with CO_2 in the absence of acid failed due to the rapid decrease in current within the first 10 minutes of the electrolysis. This suggested to us that the catalyst was degrading under CO_2. Indeed, CVs taken at one minute intervals demonstrated that the catalyst was degrading over time (**Figure 4-10**). The crossover feature at –1.8 V and

the shiny blue film that was apparent on the electrode after this experiment further suggest that the degradation process involves ligand loss and subsequent cobalt electroplating. The experiment was subsequently redone under an N_2 atmosphere and showed a similar result; we thus conclude that reducing the Co complex to the Co(–I) state unfortunately results in ligand loss and electrode fouling. $[Co(P^{Ph}{}_2N^{PhOMe}{}_2)_2(CH_3CN)](BF_4)_2$ was also found to degrade similarly despite its slightly lower reduction potentials.

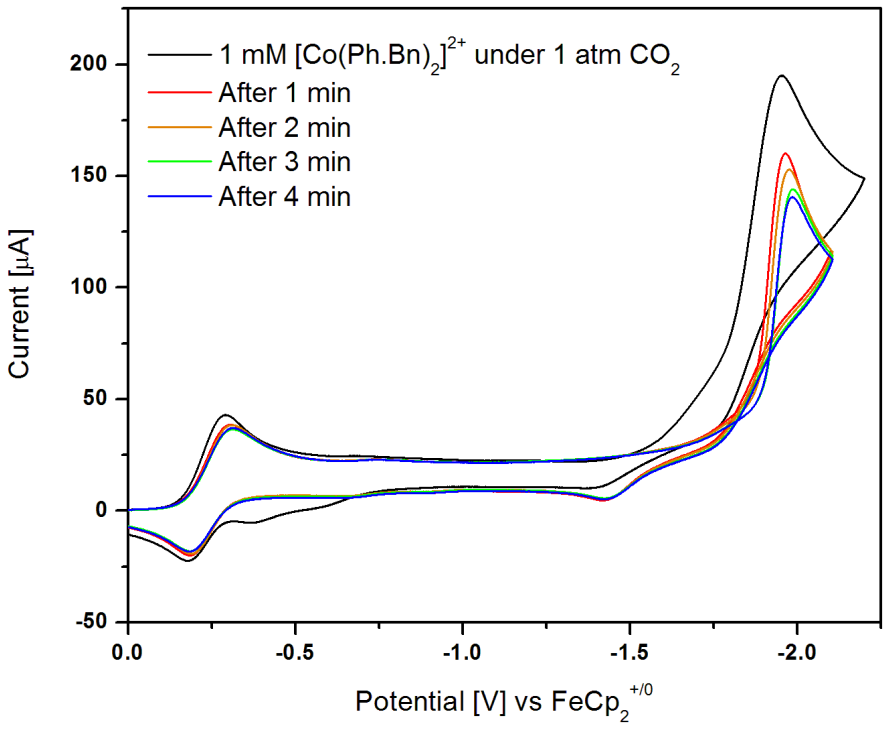

Figure 4-10. Cyclic voltammograms of $[Co(P^{Ph}{}_2N^{Bn}{}_2)_2(CH_3CN)](BF_4)_2$ upon sparging with CO_2, taken after 1 minute intervals. Potentials are reported vs. $FeCp_2^{+/0}$. Conditions: Glassy carbon working and counter electrodes, AgCl reference electrode, 0.2 M NBu_4PF_6 electrolyte, scan rate 100 mV/s.

As a last control, we studied the reactivity of the $[Co(dmpe)_2]^{2+}$ complex. This Co bis-diphosphine compound has a hydricity of 36 kcal/mol and does not contain a pendant base. The electrochemistry of this complex is similar to that of the P_2N_2 complexes.

Furthermore, $[Co(dmpe)_2]^{2+}$ is able to react with CO_2 in the presence and absence of acid despite its lack of a pendant base (**Figure 4-11**). The scale of the peak current increase (66% vs 100% for $[Co(P^{Ph}_2N^{Bn}_2)_2]^{2+}$) is slightly smaller, but the fact remains that there is not a large reactivity difference. Moreover, it is impossible to tell without further studies whether the reactivity difference is due to the change in the speed of a proton transfer step, or to some other factor such as a difference in hydricity. Given the instability of the more negative P_2N_2 complexes, we opted to move on to our next target on the periodic table, discussed in Chapter 5.

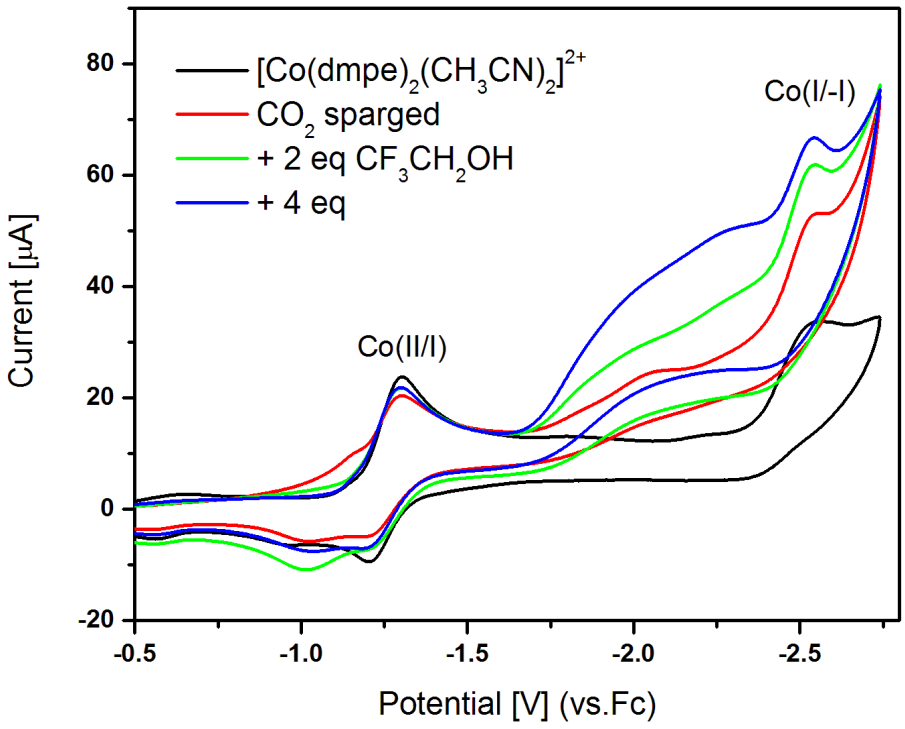

Figure 4-11. Cyclic voltammograms of $[Co(dmpe)_2(CH_3CN)_2](BF_4)_2$ upon sparging with CO_2 and addition of TFE in ACN. Potentials are reported vs. $FeCp_2^{+/0}$. Conditions: Glassy carbon working and counter electrodes, AgCl reference electrode, 0.2 M NBu_4PF_6 electrolyte, scan rate 100 mV/s.

4.4 Conclusions

A series of $[Co(P_2N_2)_2(CH_3CN)]^{2+}$ complexes were synthesized and tested for their ability to electrochemically reduce CO_2 to HCOOH. CV experiments suggested that the Co(–I) species are sufficiently energetic to react with CO_2. However, their marked instability to ligand loss precluded further study and use. Comparative studies of proton reduction with different acids demonstrated the importance of carefully controlling the proton source and concentration, a lesson that proved increasingly important in our later work.

4.5 References

1. Markl, V. G.; Jin, G. Y.; Schoerner, C. *Tetrahedron Lett.*, **1982**, *21*, 1409–1412.

2. Doud, M. D.; Grice, K.; Lilio, A.; Seu, C. S.; Kubiak, C. P. *Organometallics*, **2012**, *31*, 779–782.

3. Wiese, S.; Kilgore, U. J.; DuBois, D. L.; Bullock, R. M. *ACS Catal.*, **2012**, *2*, 720–727.

4. Price, A. J.; Ciancanelli, R.; Noll, B. C.; Curtis, C. J.; DuBois, D. L.; DuBois, M. R. *Organometallics*, **2002**, *21*, 4833–4839.

5. Curtis, C. J.; Miedaner, A.; Raebiger, J. W.; DuBois, D. L. *Organometallics*, **2004**, *23*, 511–516.

6. Nimlos, M. R.; Chang, C. H.; Curtis, C. J.; Miedaner, A.; Pilath, H. M.; DuBois, D. L. *Organometallics*, **2008**, *27*, 2715–2722.

7. Berning, D. E.; Noll, B. C.; DuBois, D. L. *J. Am. Chem. Soc.*, **1999**, *121*, 11432–11447.

8. Berning, D. E.; Miedaner, A.; Curtis, C. J.; Noll, B. C.; DuBois, M. R.; DuBois, D. L. *Organometallics*, **2001**, *20*, 1832–1839.

9. Fraze, K.; Wilson, A. D.; Appel, A. M.; DuBois, M. R.; DuBois, D. L. *Organometallics*, **2007**, *26*, 3918–3924.

10. Miedaner, A.; Haltiwanger, R. C.; DuBois, D. L. *Inorg. Chem.*, **1991**, *30*, 417–427.

11. Raebiger, J. W.; Miedaner, A.; Curtis, C. J.; Miller, S. M.; Anderson, O. P.; DuBois, D. L. *J. Am. Chem. Soc.*, **2004**, *126*, 5502–5514.

12. Raebiger, J. W.; DuBois, D. L. *Organometallics*, **2005**, *24*, 110–118.

13. Ellis, W. W.; Miedaner, A.; Curtis, C. J.; Gibson, D. H.; DuBois, D. L. *J. Am. Chem. Soc.*, **2002**, *124*, 1926–1932.

14. DuBois, D. L.; Berning, D. E. *Appl. Organomet. Chem.*, **2000**, *14*, 860–862.

15. Tilset, M.; Parker, V. D. *J. Am. Chem. Soc.*, **1989**, *111*, 6711–6717.

16. Tilset, M.; Parker, V. D.; Cowburn, D. *J. Am. Chem. Soc.*, **1990**, *112*, 2843.

17. Matsubara, Y.; Fujita, E.; Doherty, M. D.; Muckerman, J. T.; Creutz, C. *J. Am. Chem. Soc.*, **2012**, *134*, 15743–15757.

18. Creutz, C.; Chou, M. H. *J. Am. Chem. Soc.*, **2009**, 2794–2795.

19. Estes, D. P.; Vannucci, A. K.; Hall, A. R.; Lichtenberger, D. L.; Norton, J. R. *Organometallics*, **2011**, 3444–3447.

20. Sarker, N.; Bruno, J. *J. Am. Chem. Soc.*, **1999**, *979*, 2174–2180.

21. Sarker, N.; Bruno, J. *Organometallics*, **2001**, *20*, 55–61.

22. Ciancanelli, R.; Noll, B. C.; DuBois, D. L.; DuBois, M. R. *J. Am. Chem. Soc.*, **2002**, *124*, 2984–2992.

23. Galan, B. R.; Schöffel, J.; Linehan, J. C.; Seu, C. S.; Appel, A. M.; Roberts, J. A. S.; Helm, M. L.; Kilgore, U. J.; Yang, J. Y.; DuBois, D. L.; Kubiak, C. P. *J. Am. Chem. Soc.*, **2011**, *133*, 12767–12779.

24. Pavlishchuk, V. V; Addison, A. W. *Inorg. Chim. Acta*, **2000**, *298*, 97–102.

25. Qi, X.-J.; Fu, Y.; Liu, L.; Guo, Q.-X. *Organometallics*, **2007**, *26*, 4197–4203.

26. Kovács, G.; Pápai, I. *Organometallics*, **2006**, *25*, 820–825.

27. Chen, S.; Rousseau, R.; Raugei, S.; Dupuis, M.; DuBois, D. L.; Bullock, R. M. *Organometallics*, **2011**, *30*, 6108–6118.

28. Jacobsen, G. M.; Yang, J. Y.; Twamley, B.; Wilson, A. D.; Bullock, R. M.; DuBois, M. R.; DuBois, D. L. *Energy Environ. Sci.*, **2008**, *1*, 167–174.

29. Mock, M. T.; Potter, R. G.; O'Hagan, M. J.; Camaioni, D. M.; Dougherty, W. G.; Kassel, W. S.; DuBois, D. L. *Inorg. Chem.*, **2011**, *50*, 11914–11928.

4.6 Appendix

4.6.1 Crystal data for $[Co(P^{Ph}_2N^{Bn}_2)_2(CH_3CN)](BF_4)_2 \bullet 14(CH_3CN)$

Crystals of $[Co(P^{Ph}_2N^{Bn}_2)_2(CH_3CN)](BF_4)_2 \bullet 14(CH_3CN)$ were found to have crystallized in space group P–1 with two molecules per asymmetric unit (Z'=2). Both cations were observed in the chair-boat/chair-boat configuration, which refers to the conformations of the four M–P–C–N–C–P– rings formed by the ligands, with the rings adjacent to the acetonitrile given first. The crystal data was modeled to 6.1% (using 2Θ). Positional disorder arising from slight rotations of the floppy benzyl substituents can be observed as elongated ADPs; attempts to model this discretely were wildly unsuccessful. The unit cell also contains two voids (1282 $Å^3$ total) containing 14 molecules of acetonitrile that were modeled using SQUEEZE.

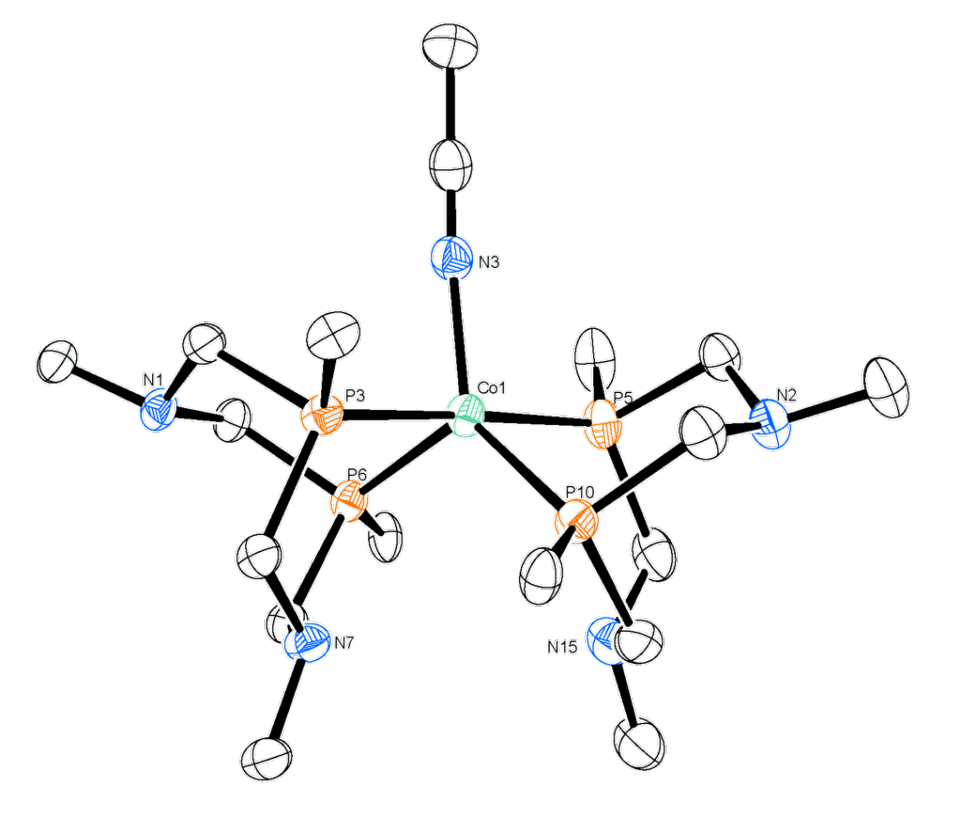

Figure 4-12. Crystal structure of $[Co(P^{Ph}_2N^{Bn}_2)_2(CH_3CN)]^{2+}$ core.

Table 4-2. Crystal data and structure refinement for $[Co(P^{Ph}{}_2N^{Bn}{}_2)_2(CH_3CN)](BF_4)_2 \bullet 14(CH_3CN)$.

Identification code	cseu_6_98_0m	
Empirical formula	C76 H88 B2 Co F8 N12 P4	
Formula weight	1526.01	
Temperature	296.15 K	
Wavelength	0.71073 Å	
Crystal system	Triclinic	
Space group	P-1	
Unit cell dimensions	a = 14.7328(11) Å	α= 102.5501(9)°.
	b = 19.6282(14) Å	β= 92.0867(9)°.
	c = 24.1902(18) Å	γ = 91.2048(9)°.
Volume	6820.6(9) $Å^3$	
Z	4	
Density (calculated)	1.486 Mg/m^3	
Absorption coefficient	0.425 mm^{-1}	
F(000)	3188	
Crystal size	0.6 x 0.12 x 0.11 mm^3	
Theta range for data collection	1.38 to 26.54°.	
Index ranges	-18<=h<=18, -24<=k<=24, -30<=l<=30	
Reflections collected	87872	
Independent reflections	28270 [R(int) = 0.0457]	
Completeness to theta = 25.00°	99.9 %	
Absorption correction	Semi-empirical from equivalents	
Max. and min. transmission	0.9548 and 0.7848	
Refinement method	Full-matrix least-squares on F^2	
Data / restraints / parameters	28270 / 0 / 1479	
Goodness-of-fit on F^2	1.090	
Final R indices [I>2sigma(I)]	R1 = 0.0604, wR2 = 0.1677	
R indices (all data)	R1 = 0.0824, wR2 = 0.1809	
Largest diff. peak and hole	2.245 and -0.744 $e.Å^{-3}$	

Table 4-3. Bond lengths [Å] and angles [°] for $[Co(P^{Ph}{}_2N^{Bn}{}_2)_2(CH_3CN)](BF_4)_2 \bullet 14(CH_3CN)$.

Co(1)-P(3)	2.1966(8)	Co(1)-P(5)	2.2209(9)
Co(1)-P(6)	2.2316(9)	Co(1)-P(10)	2.2268(9)
Co(1)-N(3)	1.959(3)	P(3)-C(21)	1.852(3)
P(3)-C(22)	1.835(3)	P(3)-C(36)	1.827(3)
P(5)-C(26)	1.843(3)	P(5)-C(42)	1.846(4)
P(5)-C(67)	1.820(4)	P(6)-C(16)	1.820(3)
P(6)-C(18)	1.847(3)	P(6)-C(19)	1.853(3)
P(10)-C(28)	1.832(3)	P(10)-C(32)	1.847(3)
P(10)-C(84)	1.849(3)	N(1)-C(19)	1.474(4)
N(1)-C(22)	1.450(4)	N(1)-C(50)	1.474(4)
N(2)-C(26)	1.460(4)	N(2)-C(32)	1.456(4)
N(2)-C(78)	1.480(4)	N(3)-C(45)	1.145(4)
N(7)-C(18)	1.464(4)	N(7)-C(21)	1.468(4)
N(7)-C(69)	1.494(4)	N(15)-C(42)	1.460(4)
N(15)-C(84)	1.457(5)	N(15)-C(115)	1.495(4)
C(16)-C(58)	1.406(5)	C(16)-C(60)	1.395(5)
C(18)-H(18A)	0.9700	C(18)-H(18B)	0.9700
C(19)-H(19A)	0.9700	C(19)-H(19B)	0.9700
C(21)-H(21A)	0.9700	C(21)-H(21B)	0.9700
C(22)-H(22A)	0.9700	C(22)-H(22B)	0.9700
C(26)-H(26A)	0.9700	C(26)-H(26B)	0.9700
C(28)-C(52)	1.396(5)	C(28)-C(72)	1.392(5)
C(31)-H(31)	0.9300	C(31)-C(51)	1.391(4)
C(31)-C(92)	1.389(5)	C(32)-H(32A)	0.9700
C(32)-H(32B)	0.9700	C(36)-C(48)	1.391(5)
C(36)-C(64)	1.386(5)	C(38)-H(38)	0.9300
C(38)-C(39)	1.402(5)	C(38)-C(87)	1.386(5)
C(39)-C(44)	1.394(5)	C(39)-C(50)	1.504(4)
C(42)-H(42A)	0.9700	C(42)-H(42B)	0.9700
C(44)-H(44)	0.9300	C(44)-C(80)	1.389(5)
C(45)-C(126)	1.462(5)	C(48)-H(48)	0.9300
C(48)-C(110)	1.394(5)	C(50)-H(50A)	0.9700
C(50)-H(50B)	0.9700	C(51)-C(68)	1.388(5)
C(51)-C(69)	1.509(4)	C(52)-H(52)	0.9300
C(52)-C(109)	1.391(5)	C(58)-H(58)	0.9300

Table 4-3. (cont'd)

C(58)-C(118)	1.388(5)	C(60)-H(60)	0.9300
C(60)-C(98)	1.386(5)	C(64)-H(64)	0.9300
C(64)-C(112)	1.395(5)	C(67)-C(97)	1.391(6)
C(67)-C(106)	1.397(5)	C(68)-H(68)	0.9300
C(68)-C(79)	1.383(5)	C(69)-H(69A)	0.9700
C(69)-H(69B)	0.9700	C(72)-H(72)	0.9300
C(72)-C(93)	1.387(5)	C(77)-H(77)	0.9300
C(77)-C(98)	1.379(6)	C(77)-C(118)	1.363(6)
C(78)-H(78A)	0.9700	C(78)-H(78B)	0.9700
C(78)-C(105)	1.512(5)	C(79)-H(79)	0.9300
C(79)-C(96)	1.390(6)	C(80)-H(80)	0.9300
C(80)-C(116)	1.396(5)	C(84)-H(84A)	0.9700
C(84)-H(84B)	0.9700	C(87)-H(87)	0.9300
C(87)-C(116)	1.388(5)	C(92)-H(92)	0.9300
C(92)-C(96)	1.380(6)	C(93)-H(93)	0.9300
C(93)-C(103)	1.385(6)	C(96)-H(96)	0.9300
C(97)-H(97)	0.9300	C(97)-C(164)	1.377(6)
C(98)-H(98)	0.9300	C(102)-H(102)	0.9300
C(102)-C(110)	1.362(6)	C(102)-C(112)	1.377(6)
C(103)-H(103)	0.9300	C(103)-C(109)	1.377(6)
C(105)-C(137)	1.377(6)	C(105)-C(146)	1.381(6)
C(106)-H(106)	0.9300	C(106)-C(140)	1.375(6)
C(109)-H(109)	0.9300	C(110)-H(110)	0.9300
C(112)-H(112)	0.9300	C(115)-H(11A)	0.9700
C(115)-H(11B)	0.9700	C(115)-C(124)	1.511(5)
C(116)-H(116)	0.9300	C(118)-H(118)	0.9300
C(123)-H(123)	0.9300	C(123)-C(140)	1.385(8)
C(123)-C(164)	1.371(7)	C(124)-C(132)	1.355(6)
C(124)-C(141)	1.382(5)	C(126)-H(12A)	0.9600
C(126)-H(12B)	0.9600	C(126)-H(12C)	0.9600
C(130)-H(130)	0.9300	C(130)-C(138)	1.362(7)
C(130)-C(141)	1.381(6)	C(132)-H(132)	0.9300
C(132)-C(174)	1.365(7)	C(137)-H(137)	0.9300
C(137)-C(181)	1.397(6)	C(138)-H(138)	0.9300
C(138)-C(174)	1.374(7)	C(140)-H(140)	0.9300

Table 4-3. (cont'd)

C(141)-H(141)	0.9300	C(146)-H(146)	0.9300
C(146)-C(152)	1.408(7)	C(152)-H(152)	0.9300
C(152)-C(169)	1.368(10)	C(164)-H(164)	0.9300
C(169)-H(169)	0.9300	C(169)-C(181)	1.419(10)
C(174)-H(174)	0.9300	C(181)-H(181)	0.9300
Co(2)-P(4)	2.2307(9)	Co(2)-P(7)	2.2252(9)
Co(2)-P(8)	2.2306(9)	Co(2)-P(9)	2.2120(9)
Co(2)-N(8)	1.952(3)	P(4)-C(14)	1.820(3)
P(4)-C(27)	1.839(3)	P(4)-C(40)	1.848(3)
P(7)-C(30)	1.843(3)	P(7)-C(33)	1.822(3)
P(7)-C(41)	1.849(3)	P(8)-C(23)	1.853(3)
P(8)-C(47)	1.847(3)	P(8)-C(57)	1.828(3)
P(9)-C(29)	1.858(3)	P(9)-C(43)	1.816(3)
P(9)-C(54)	1.851(3)	N(4)-C(40)	1.462(4)
N(4)-C(47)	1.458(4)	N(4)-C(95)	1.486(4)
N(5)-C(41)	1.462(4)	N(5)-C(54)	1.456(4)
N(5)-C(88)	1.477(4)	N(6)-C(23)	1.470(4)
N(6)-C(27)	1.453(4)	N(6)-C(56)	1.499(4)
N(8)-C(24)	1.144(4)	N(9)-C(29)	1.459(4)
N(9)-C(30)	1.472(4)	N(9)-C(82)	1.482(4)
F(11)-B(111)	1.388(5)	C(13)-H(13)	0.9300
C(13)-C(33)	1.391(4)	C(13)-C(34)	1.386(5)
C(14)-C(49)	1.400(4)	C(14)-C(59)	1.400(4)
F(17)-B(111)	1.383(5)	C(23)-H(23A)	0.9700
C(23)-H(23B)	0.9700	C(24)-C(74)	1.445(5)
C(27)-H(27A)	0.9700	C(27)-H(27B)	0.9700
C(29)-H(29A)	0.9700	C(29)-H(29B)	0.9700
C(30)-H(30A)	0.9700	C(30)-H(30B)	0.9700
C(33)-C(91)	1.406(5)	C(34)-H(34)	0.9300
C(34)-C(70)	1.386(5)	C(37)-C(46)	1.406(5)
C(37)-C(56)	1.514(5)	C(37)-C(66)	1.397(5)
C(40)-H(40A)	0.9700	C(40)-H(40B)	0.9700
C(41)-H(41A)	0.9700	C(41)-H(41B)	0.9700
C(43)-C(61)	1.385(5)	C(43)-C(71)	1.410(5)
C(46)-H(46)	0.9300	C(46)-C(101)	1.388(5)

Table 4-3. (cont'd)

C(47)-H(47A)	0.9700	C(47)-H(47B)	0.9700
C(49)-H(49)	0.9300	C(49)-C(94)	1.374(5)
C(53)-H(53)	0.9300	C(53)-C(70)	1.381(5)
C(53)-C(91)	1.382(5)	C(54)-H(54A)	0.9700
C(54)-H(54B)	0.9700	C(56)-H(56A)	0.9700
C(56)-H(56B)	0.9700	C(57)-C(65)	1.397(5)
C(57)-C(89)	1.383(5)	C(59)-H(59)	0.9300
C(59)-C(86)	1.376(5)	C(61)-H(61)	0.9300
C(61)-C(90)	1.399(5)	F(62)-B(111)	1.369(5)
F(63)-B(111)	1.340(5)	C(65)-H(65)	0.9300
C(65)-C(121)	1.396(5)	C(66)-H(66)	0.9300
C(66)-C(83)	1.388(5)	C(70)-H(70)	0.9300
C(71)-H(71)	0.9300	C(71)-C(100)	1.374(5)
C(74)-H(74A)	0.9600	C(74)-H(74B)	0.9600
C(74)-H(74C)	0.9600	C(75)-H(75)	0.9300
C(75)-C(83)	1.369(5)	C(75)-C(101)	1.380(5)
C(76)-C(88)	1.519(5)	C(76)-C(107)	1.391(5)
C(76)-C(108)	1.399(5)	C(82)-H(82A)	0.9700
C(82)-H(82B)	0.9700	C(82)-C(114)	1.510(5)
C(83)-H(83)	0.9300	C(85)-H(85)	0.9300
C(85)-C(86)	1.385(5)	C(85)-C(94)	1.367(5)
C(86)-H(86)	0.9300	C(88)-H(88A)	0.9700
C(88)-H(88B)	0.9700	C(89)-H(89)	0.9300
C(89)-C(128)	1.394(5)	C(90)-H(90)	0.9300
C(90)-C(117)	1.373(6)	C(91)-H(91)	0.9300
C(94)-H(94)	0.9300	C(95)-H(95A)	0.9700
C(95)-H(95B)	0.9700	C(95)-C(122)	1.498(6)
C(100)-H(100)	0.9300	C(100)-C(117)	1.391(6)
C(101)-H(101)	0.9300	C(104)-H(104)	0.9300
C(104)-C(121)	1.379(5)	C(104)-C(128)	1.378(5)
C(107)-H(107)	0.9300	C(107)-C(120)	1.383(6)
C(108)-H(108)	0.9300	C(108)-C(113)	1.375(5)
C(113)-H(113)	0.9300	C(113)-C(131)	1.387(6)
C(114)-C(119)	1.384(6)	C(114)-C(143)	1.394(6)
C(117)-H(117)	0.9300	C(119)-H(119)	0.9300

Table 4-3. (cont'd)

C(119)-C(125)	1.391(6)	C(120)-H(120)	0.9300
C(120)-C(131)	1.373(6)	C(121)-H(121)	0.9300
C(122)-C(134)	1.344(8)	C(122)-C(6)	1.392(8)
C(125)-H(125)	0.9300	C(125)-C(190)	1.331(7)
C(128)-H(128)	0.9300	C(131)-H(131)	0.9300
C(134)-H(134)	0.9300	C(134)-C(20)	1.594(11)
C(143)-H(143)	0.9300	C(143)-C(157)	1.423(8)
C(148)-H(148)	0.9300	C(148)-C(151)	1.284(11)
C(148)-C(20)	1.409(11)	C(151)-H(151)	0.9300
C(151)-C(6)	1.312(10)	C(157)-H(157)	0.9300
C(157)-C(190)	1.353(8)	C(190)-H(190)	0.9300
F(10)-B(142)	1.400(5)	F(55)-B(142)	1.380(5)
F(73)-B(142)	1.353(6)	F(81)-B(142)	1.368(5)
F(12)-B(154)	1.420(6)	F(20)-B(154)	1.392(6)
F(25)-B(154)	1.321(5)	F(35)-B(154)	1.381(6)
F(99)-B(147)	1.488(7)	F(133)-B(147)	1.325(6)
F(135)-B(147)	1.288(6)	F(144)-B(147)	1.294(6)
C(6)-H(6)	0.9300	C(20)-H(20)	0.9300
P(3)-Co(1)-P(5)	177.15(4)	P(3)-Co(1)-P(6)	81.36(3)
P(3)-Co(1)-P(10)	95.20(3)	P(5)-Co(1)-P(6)	98.34(3)
P(5)-Co(1)-P(10)	82.37(3)	P(10)-Co(1)-P(6)	116.25(3)
N(3)-Co(1)-P(3)	90.63(8)	N(3)-Co(1)-P(5)	92.12(8)
N(3)-Co(1)-P(6)	110.55(8)	N(3)-Co(1)-P(10)	133.19(8)
C(21)-P(3)-Co(1)	116.05(9)	C(22)-P(3)-Co(1)	111.45(10)
C(22)-P(3)-C(21)	101.09(14)	C(36)-P(3)-Co(1)	118.02(11)
C(36)-P(3)-C(21)	106.49(14)	C(36)-P(3)-C(22)	101.51(14)
C(26)-P(5)-Co(1)	108.01(11)	C(26)-P(5)-C(42)	102.19(15)
C(42)-P(5)-Co(1)	116.84(11)	C(67)-P(5)-Co(1)	121.20(12)
C(67)-P(5)-C(26)	101.50(15)	C(67)-P(5)-C(42)	104.48(18)
C(16)-P(6)-Co(1)	121.17(10)	C(16)-P(6)-C(18)	105.11(14)
C(16)-P(6)-C(19)	101.02(14)	C(18)-P(6)-Co(1)	114.61(10)
C(18)-P(6)-C(19)	100.86(14)	C(19)-P(6)-Co(1)	111.43(10)
C(28)-P(10)-Co(1)	123.46(10)	C(28)-P(10)-C(32)	100.66(15)
C(28)-P(10)-C(84)	104.52(16)	C(32)-P(10)-Co(1)	105.50(11)

Table 4-3. (cont'd)

C(32)-P(10)-C(84)	102.05(16)	C(84)-P(10)-Co(1)	117.32(12)
C(22)-N(1)-C(19)	112.9(2)	C(22)-N(1)-C(50)	109.8(2)
C(50)-N(1)-C(19)	109.8(2)	C(26)-N(2)-C(78)	111.8(2)
C(32)-N(2)-C(26)	113.8(2)	C(32)-N(2)-C(78)	110.6(2)
C(45)-N(3)-Co(1)	172.4(3)	C(18)-N(7)-C(21)	114.4(2)
C(18)-N(7)-C(69)	109.9(2)	C(21)-N(7)-C(69)	110.5(2)
C(42)-N(15)-C(115)	110.3(3)	C(84)-N(15)-C(42)	114.3(3)
C(84)-N(15)-C(115)	111.0(3)	C(58)-C(16)-P(6)	119.5(3)
C(60)-C(16)-P(6)	121.1(3)	C(60)-C(16)-C(58)	119.2(3)
P(6)-C(18)-H(18A)	108.7	P(6)-C(18)-H(18B)	108.7
N(7)-C(18)-P(6)	114.0(2)	N(7)-C(18)-H(18A)	108.7
N(7)-C(18)-H(18B)	108.7	H(18A)-C(18)-H(18B)	107.6
P(6)-C(19)-H(19A)	109.4	P(6)-C(19)-H(19B)	109.4
N(1)-C(19)-P(6)	111.3(2)	N(1)-C(19)-H(19A)	109.4
N(1)-C(19)-H(19B)	109.4	H(19A)-C(19)-H(19B)	108.0
P(3)-C(21)-H(21A)	109.0	P(3)-C(21)-H(21B)	109.0
N(7)-C(21)-P(3)	112.76(19)	N(7)-C(21)-H(21A)	109.0
N(7)-C(21)-H(21B)	109.0	H(21A)-C(21)-H(21B)	107.8
P(3)-C(22)-H(22A)	109.1	P(3)-C(22)-H(22B)	109.1
N(1)-C(22)-P(3)	112.53(19)	N(1)-C(22)-H(22A)	109.1
N(1)-C(22)-H(22B)	109.1	H(22A)-C(22)-H(22B)	107.8
P(5)-C(26)-H(26A)	109.6	P(5)-C(26)-H(26B)	109.6
N(2)-C(26)-P(5)	110.2(2)	N(2)-C(26)-H(26A)	109.6
N(2)-C(26)-H(26B)	109.6	H(26A)-C(26)-H(26B)	108.1
C(52)-C(28)-P(10)	119.0(3)	C(72)-C(28)-P(10)	121.4(3)
C(72)-C(28)-C(52)	119.6(3)	C(51)-C(31)-H(31)	119.7
C(92)-C(31)-H(31)	119.7	C(92)-C(31)-C(51)	120.5(3)
P(10)-C(32)-H(32A)	109.3	P(10)-C(32)-H(32B)	109.3
N(2)-C(32)-P(10)	111.6(2)	N(2)-C(32)-H(32A)	109.3
N(2)-C(32)-H(32B)	109.3	H(32A)-C(32)-H(32B)	108.0
C(48)-C(36)-P(3)	119.5(2)	C(64)-C(36)-P(3)	120.5(3)
C(64)-C(36)-C(48)	120.0(3)	C(39)-C(38)-H(38)	119.9
C(87)-C(38)-H(38)	119.9	C(87)-C(38)-C(39)	120.2(3)
C(38)-C(39)-C(50)	120.9(3)	C(44)-C(39)-C(38)	118.7(3)
C(44)-C(39)-C(50)	120.2(3)	P(5)-C(42)-H(42A)	108.8

Table 4-3. (cont'd)

P(5)-C(42)-H(42B)	108.8	N(15)-C(42)-P(5)	113.7(2)
N(15)-C(42)-H(42A)	108.8	N(15)-C(42)-H(42B)	108.8
H(42A)-C(42)-H(42B)	107.7	C(39)-C(44)-H(44)	119.4
C(80)-C(44)-C(39)	121.1(3)	C(80)-C(44)-H(44)	119.4
N(3)-C(45)-C(126)	179.2(4)	C(36)-C(48)-H(48)	120.2
C(36)-C(48)-C(110)	119.6(3)	C(110)-C(48)-H(48)	120.2
N(1)-C(50)-C(39)	114.3(2)	N(1)-C(50)-H(50A)	108.7
N(1)-C(50)-H(50B)	108.7	C(39)-C(50)-H(50A)	108.7
C(39)-C(50)-H(50B)	108.7	H(50A)-C(50)-H(50B)	107.6
C(31)-C(51)-C(69)	120.9(3)	C(68)-C(51)-C(31)	118.5(3)
C(68)-C(51)-C(69)	120.7(3)	C(28)-C(52)-H(52)	120.1
C(109)-C(52)-C(28)	119.9(4)	C(109)-C(52)-H(52)	120.1
C(16)-C(58)-H(58)	120.3	C(118)-C(58)-C(16)	119.5(4)
C(118)-C(58)-H(58)	120.3	C(16)-C(60)-H(60)	120.2
C(98)-C(60)-C(16)	119.5(3)	C(98)-C(60)-H(60)	120.2
C(36)-C(64)-H(64)	120.5	C(36)-C(64)-C(112)	119.0(3)
C(112)-C(64)-H(64)	120.5	C(97)-C(67)-P(5)	122.4(3)
C(97)-C(67)-C(106)	119.0(4)	C(106)-C(67)-P(5)	118.7(3)
C(51)-C(68)-H(68)	119.4	C(79)-C(68)-C(51)	121.2(3)
C(79)-C(68)-H(68)	119.4	N(7)-C(69)-C(51)	115.6(3)
N(7)-C(69)-H(69A)	108.4	N(7)-C(69)-H(69B)	108.4
C(51)-C(69)-H(69A)	108.4	C(51)-C(69)-H(69B)	108.4
H(69A)-C(69)-H(69B)	107.4	C(28)-C(72)-H(72)	119.9
C(93)-C(72)-C(28)	120.2(4)	C(93)-C(72)-H(72)	119.9
C(98)-C(77)-H(77)	120.1	C(118)-C(77)-H(77)	120.1
C(118)-C(77)-C(98)	119.9(3)	N(2)-C(78)-H(78A)	109.4
N(2)-C(78)-H(78B)	109.4	N(2)-C(78)-C(105)	111.1(3)
H(78A)-C(78)-H(78B)	108.0	C(105)-C(78)-H(78A)	109.4
C(105)-C(78)-H(78B)	109.4	C(68)-C(79)-H(79)	120.1
C(68)-C(79)-C(96)	119.9(3)	C(96)-C(79)-H(79)	120.1
C(44)-C(80)-H(80)	120.2	C(44)-C(80)-C(116)	119.5(3)
C(116)-C(80)-H(80)	120.2	P(10)-C(84)-H(84A)	109.0
P(10)-C(84)-H(84B)	109.0	N(15)-C(84)-P(10)	113.0(2)
N(15)-C(84)-H(84A)	109.0	N(15)-C(84)-H(84B)	109.0
H(84A)-C(84)-H(84B)	107.8	C(38)-C(87)-H(87)	119.7

Table 4-3. (cont'd)

C(38)-C(87)-C(116)	120.6(3)	C(116)-C(87)-H(87)	119.7
C(31)-C(92)-H(92)	119.8	C(96)-C(92)-C(31)	120.4(3)
C(96)-C(92)-H(92)	119.8	C(72)-C(93)-H(93)	120.1
C(103)-C(93)-C(72)	119.7(4)	C(103)-C(93)-H(93)	120.1
C(79)-C(96)-H(96)	120.2	C(92)-C(96)-C(79)	119.5(3)
C(92)-C(96)-H(96)	120.2	C(67)-C(97)-H(97)	120.0
C(164)-C(97)-C(67)	120.0(4)	C(164)-C(97)-H(97)	120.0
C(60)-C(98)-H(98)	119.5	C(77)-C(98)-C(60)	120.9(4)
C(77)-C(98)-H(98)	119.5	C(110)-C(102)-H(102)	120.0
C(110)-C(102)-C(112)	119.9(3)	C(112)-C(102)-H(102)	120.0
C(93)-C(103)-H(103)	119.6	C(109)-C(103)-C(93)	120.7(4)
C(109)-C(103)-H(103)	119.6	C(137)-C(105)-C(78)	120.0(4)
C(137)-C(105)-C(146)	120.2(4)	C(146)-C(105)-C(78)	119.7(4)
C(67)-C(106)-H(106)	119.7	C(140)-C(106)-C(67)	120.5(4)
C(140)-C(106)-H(106)	119.7	C(52)-C(109)-H(109)	120.1
C(103)-C(109)-C(52)	119.9(4)	C(103)-C(109)-H(109)	120.0
C(48)-C(110)-H(110)	119.7	C(102)-C(110)-C(48)	120.6(4)
C(102)-C(110)-H(110)	119.7	C(64)-C(112)-H(112)	119.6
C(102)-C(112)-C(64)	120.9(4)	C(102)-C(112)-H(112)	119.6
N(15)-C(115)-H(11A)	107.9	N(15)-C(115)-H(11B)	107.9
N(15)-C(115)-C(124)	117.6(3)	H(11A)-C(115)-H(11B)	107.2
C(124)-C(115)-H(11A)	107.9	C(124)-C(115)-H(11B)	107.9
C(80)-C(116)-H(116)	120.1	C(87)-C(116)-C(80)	119.8(3)
C(87)-C(116)-H(116)	120.1	C(58)-C(118)-H(118)	119.5
C(77)-C(118)-C(58)	121.0(4)	C(77)-C(118)-H(118)	119.5
C(140)-C(123)-H(123)	119.8	C(164)-C(123)-H(123)	119.8
C(164)-C(123)-C(140)	120.3(4)	C(132)-C(124)-C(115)	121.2(4)
C(132)-C(124)-C(141)	116.5(4)	C(141)-C(124)-C(115)	122.2(4)
C(45)-C(126)-H(12A)	109.5	C(45)-C(126)-H(12B)	109.5
C(45)-C(126)-H(12C)	109.5	H(12A)-C(126)-H(12B)	109.5
H(12A)-C(126)-H(12C)	109.5	H(12B)-C(126)-H(12C)	109.5
C(138)-C(130)-H(130)	120.0	C(138)-C(130)-C(141)	120.0(4)
C(141)-C(130)-H(130)	120.0	C(124)-C(132)-H(132)	118.8
C(124)-C(132)-C(174)	122.4(5)	C(174)-C(132)-H(132)	118.8
C(105)-C(137)-H(137)	119.4	C(105)-C(137)-C(181)	121.2(5)

Table 4-3. (cont'd)

C(181)-C(137)-H(137)	119.4	C(130)-C(138)-H(138)	120.9
C(130)-C(138)-C(174)	118.3(5)	C(174)-C(138)-H(138)	120.9
C(106)-C(140)-C(123)	119.6(4)	C(106)-C(140)-H(140)	120.2
C(123)-C(140)-H(140)	120.2	C(124)-C(141)-H(141)	119.0
C(130)-C(141)-C(124)	121.9(4)	C(130)-C(141)-H(141)	119.0
C(105)-C(146)-H(146)	120.0	C(105)-C(146)-C(152)	120.0(6)
C(152)-C(146)-H(146)	120.0	C(146)-C(152)-H(152)	120.2
C(169)-C(152)-C(146)	119.7(6)	C(169)-C(152)-H(152)	120.2
C(97)-C(164)-H(164)	119.7	C(123)-C(164)-C(97)	120.5(5)
C(123)-C(164)-H(164)	119.7	C(152)-C(169)-H(169)	119.5
C(152)-C(169)-C(181)	120.9(5)	C(181)-C(169)-H(169)	119.5
C(132)-C(174)-C(138)	120.8(5)	C(132)-C(174)-H(174)	119.6
C(138)-C(174)-H(174)	119.6	C(137)-C(181)-C(169)	117.9(6)
C(137)-C(181)-H(181)	121.0	C(169)-C(181)-H(181)	121.0
P(7)-Co(2)-P(4)	113.69(3)	P(7)-Co(2)-P(8)	96.09(3)
P(8)-Co(2)-P(4)	81.47(3)	P(9)-Co(2)-P(4)	95.52(3)
P(9)-Co(2)-P(7)	81.09(3)	P(9)-Co(2)-P(8)	174.72(4)
N(8)-Co(2)-P(4)	134.65(8)	N(8)-Co(2)-P(7)	111.64(8)
N(8)-Co(2)-P(8)	95.12(8)	N(8)-Co(2)-P(9)	90.08(8)
C(14)-P(4)-Co(2)	124.26(10)	C(14)-P(4)-C(27)	104.40(14)
C(14)-P(4)-C(40)	98.74(14)	C(27)-P(4)-Co(2)	116.21(11)
C(27)-P(4)-C(40)	102.52(15)	C(40)-P(4)-Co(2)	107.32(11)
C(30)-P(7)-Co(2)	112.83(11)	C(30)-P(7)-C(41)	102.22(15)
C(33)-P(7)-Co(2)	120.53(10)	C(33)-P(7)-C(30)	107.29(14)
C(33)-P(7)-C(41)	98.79(14)	C(41)-P(7)-Co(2)	112.88(11)
C(23)-P(8)-Co(2)	116.58(10)	C(47)-P(8)-Co(2)	108.71(11)
C(47)-P(8)-C(23)	102.53(15)	C(57)-P(8)-Co(2)	122.31(11)
C(57)-P(8)-C(23)	103.45(16)	C(57)-P(8)-C(47)	100.48(15)
C(29)-P(9)-Co(2)	113.84(11)	C(43)-P(9)-Co(2)	119.83(11)
C(43)-P(9)-C(29)	107.03(15)	C(43)-P(9)-C(54)	99.38(15)
C(54)-P(9)-Co(2)	112.56(11)	C(54)-P(9)-C(29)	101.88(15)
C(40)-N(4)-C(95)	110.9(3)	C(47)-N(4)-C(40)	113.4(3)
C(47)-N(4)-C(95)	109.7(2)	C(41)-N(5)-C(88)	109.5(3)
C(54)-N(5)-C(41)	111.8(2)	C(54)-N(5)-C(88)	109.3(2)
C(23)-N(6)-C(56)	108.4(2)	C(27)-N(6)-C(23)	112.6(2)

Table 4-3. (cont'd)

C(27)-N(6)-C(56)	108.8(2)	C(24)-N(8)-Co(2)	170.1(3)
C(29)-N(9)-C(30)	114.5(3)	C(29)-N(9)-C(82)	111.1(3)
C(30)-N(9)-C(82)	110.0(3)	C(33)-C(13)-H(13)	120.0
C(34)-C(13)-H(13)	120.0	C(34)-C(13)-C(33)	120.1(3)
C(49)-C(14)-P(4)	118.5(2)	C(49)-C(14)-C(59)	117.9(3)
C(59)-C(14)-P(4)	123.6(2)	P(8)-C(23)-H(23A)	108.7
P(8)-C(23)-H(23B)	108.7	N(6)-C(23)-P(8)	114.0(2)
N(6)-C(23)-H(23A)	108.7	N(6)-C(23)-H(23B)	108.7
H(23A)-C(23)-H(23B)	107.6	N(8)-C(24)-C(74)	179.2(4)
P(4)-C(27)-H(27A)	108.5	P(4)-C(27)-H(27B)	108.5
N(6)-C(27)-P(4)	115.2(2)	N(6)-C(27)-H(27A)	108.5
N(6)-C(27)-H(27B)	108.5	H(27A)-C(27)-H(27B)	107.5
P(9)-C(29)-H(29A)	109.2	P(9)-C(29)-H(29B)	109.2
N(9)-C(29)-P(9)	112.2(2)	N(9)-C(29)-H(29A)	109.2
N(9)-C(29)-H(29B)	109.2	H(29A)-C(29)-H(29B)	107.9
P(7)-C(30)-H(30A)	108.9	P(7)-C(30)-H(30B)	108.9
N(9)-C(30)-P(7)	113.4(2)	N(9)-C(30)-H(30A)	108.9
N(9)-C(30)-H(30B)	108.9	H(30A)-C(30)-H(30B)	107.7
C(13)-C(33)-P(7)	122.7(2)	C(13)-C(33)-C(91)	119.0(3)
C(91)-C(33)-P(7)	118.2(2)	C(13)-C(34)-H(34)	119.7
C(70)-C(34)-C(13)	120.7(3)	C(70)-C(34)-H(34)	119.7
C(46)-C(37)-C(56)	122.4(3)	C(66)-C(37)-C(46)	118.1(3)
C(66)-C(37)-C(56)	119.4(3)	P(4)-C(40)-H(40A)	109.0
P(4)-C(40)-H(40B)	109.0	N(4)-C(40)-P(4)	112.8(2)
N(4)-C(40)-H(40A)	109.0	N(4)-C(40)-H(40B)	109.0
H(40A)-C(40)-H(40B)	107.8	P(7)-C(41)-H(41A)	109.0
P(7)-C(41)-H(41B)	109.0	N(5)-C(41)-P(7)	113.0(2)
N(5)-C(41)-H(41A)	109.0	N(5)-C(41)-H(41B)	109.0
H(41A)-C(41)-H(41B)	107.8	C(61)-C(43)-P(9)	120.8(3)
C(61)-C(43)-C(71)	119.2(3)	C(71)-C(43)-P(9)	119.9(3)
C(37)-C(46)-H(46)	119.9	C(101)-C(46)-C(37)	120.2(3)
C(101)-C(46)-H(46)	119.9	P(8)-C(47)-H(47A)	109.4
P(8)-C(47)-H(47B)	109.4	N(4)-C(47)-P(8)	111.3(2)
N(4)-C(47)-H(47A)	109.4	N(4)-C(47)-H(47B)	109.4
H(47A)-C(47)-H(47B)	108.0	C(14)-C(49)-H(49)	119.5

Table 4-3. (cont'd)

C(94)-C(49)-C(14)	120.9(3)	C(94)-C(49)-H(49)	119.5
C(70)-C(53)-H(53)	119.7	C(70)-C(53)-C(91)	120.7(3)
C(91)-C(53)-H(53)	119.7	P(9)-C(54)-H(54A)	109.1
P(9)-C(54)-H(54B)	109.1	N(5)-C(54)-P(9)	112.5(2)
N(5)-C(54)-H(54A)	109.1	N(5)-C(54)-H(54B)	109.1
H(54A)-C(54)-H(54B)	107.8	N(6)-C(56)-C(37)	113.0(3)
N(6)-C(56)-H(56A)	109.0	N(6)-C(56)-H(56B)	109.0
C(37)-C(56)-H(56A)	109.0	C(37)-C(56)-H(56B)	109.0
H(56A)-C(56)-H(56B)	107.8	C(65)-C(57)-P(8)	120.7(3)
C(89)-C(57)-P(8)	119.6(3)	C(89)-C(57)-C(65)	119.6(3)
C(14)-C(59)-H(59)	119.9	C(86)-C(59)-C(14)	120.2(3)
C(86)-C(59)-H(59)	119.9	C(43)-C(61)-H(61)	120.0
C(43)-C(61)-C(90)	119.9(3)	C(90)-C(61)-H(61)	120.0
C(57)-C(65)-H(65)	120.3	C(121)-C(65)-C(57)	119.3(3)
C(121)-C(65)-H(65)	120.3	C(37)-C(66)-H(66)	119.6
C(83)-C(66)-C(37)	120.7(3)	C(83)-C(66)-H(66)	119.6
C(34)-C(70)-H(70)	120.3	C(53)-C(70)-C(34)	119.5(3)
C(53)-C(70)-H(70)	120.3	C(43)-C(71)-H(71)	120.0
C(100)-C(71)-C(43)	120.1(3)	C(100)-C(71)-H(71)	120.0
C(24)-C(74)-H(74A)	109.5	C(24)-C(74)-H(74B)	109.5
C(24)-C(74)-H(74C)	109.5	H(74A)-C(74)-H(74B)	109.5
H(74A)-C(74)-H(74C)	109.5	H(74B)-C(74)-H(74C)	109.5
C(83)-C(75)-H(75)	119.8	C(83)-C(75)-C(101)	120.3(3)
C(101)-C(75)-H(75)	119.8	C(107)-C(76)-C(88)	120.8(3)
C(107)-C(76)-C(108)	118.6(3)	C(108)-C(76)-C(88)	120.4(3)
N(9)-C(82)-H(82A)	108.1	N(9)-C(82)-H(82B)	108.1
N(9)-C(82)-C(114)	116.8(3)	H(82A)-C(82)-H(82B)	107.3
C(114)-C(82)-H(82A)	108.1	C(114)-C(82)-H(82B)	108.1
C(66)-C(83)-H(83)	119.9	C(75)-C(83)-C(66)	120.2(3)
C(75)-C(83)-H(83)	119.9	C(86)-C(85)-H(85)	120.2
C(94)-C(85)-H(85)	120.2	C(94)-C(85)-C(86)	119.5(3)
C(59)-C(86)-C(85)	120.8(3)	C(59)-C(86)-H(86)	119.6
C(85)-C(86)-H(86)	119.6	N(5)-C(88)-C(76)	112.6(3)
N(5)-C(88)-H(88A)	109.1	N(5)-C(88)-H(88B)	109.1
C(76)-C(88)-H(88A)	109.1	C(76)-C(88)-H(88B)	109.1

Table 4-3. (cont'd)

H(88A)-C(88)-H(88B)	107.8	C(57)-C(89)-H(89)	119.8
C(57)-C(89)-C(128)	120.5(3)	C(128)-C(89)-H(89)	119.8
C(61)-C(90)-H(90)	119.8	C(117)-C(90)-C(61)	120.5(4)
C(117)-C(90)-H(90)	119.8	C(33)-C(91)-H(91)	120.0
C(53)-C(91)-C(33)	120.1(3)	C(53)-C(91)-H(91)	120.0
C(49)-C(94)-H(94)	119.7	C(85)-C(94)-C(49)	120.6(3)
C(85)-C(94)-H(94)	119.7	N(4)-C(95)-H(95A)	109.4
N(4)-C(95)-H(95B)	109.4	N(4)-C(95)-C(122)	111.2(3)
H(95A)-C(95)-H(95B)	108.0	C(122)-C(95)-H(95A)	109.4
C(122)-C(95)-H(95B)	109.4	C(71)-C(100)-H(100)	119.7
C(71)-C(100)-C(117)	120.5(4)	C(117)-C(100)-H(100)	119.7
C(46)-C(101)-H(101)	119.9	C(75)-C(101)-C(46)	120.2(3)
C(75)-C(101)-H(101)	119.9	C(121)-C(104)-H(104)	119.9
C(128)-C(104)-H(104)	119.9	C(128)-C(104)-C(121)	120.2(4)
C(76)-C(107)-H(107)	119.8	C(120)-C(107)-C(76)	120.5(4)
C(120)-C(107)-H(107)	119.8	C(76)-C(108)-H(108)	119.8
C(113)-C(108)-C(76)	120.5(4)	C(113)-C(108)-H(108)	119.8
F(17)-B(111)-F(11)	111.1(3)	F(62)-B(111)-F(11)	108.1(3)
F(62)-B(111)-F(17)	106.9(3)	F(63)-B(111)-F(11)	109.1(3)
F(63)-B(111)-F(17)	109.0(4)	F(63)-B(111)-F(62)	112.8(4)
C(108)-C(113)-H(113)	119.9	C(108)-C(113)-C(131)	120.3(4)
C(131)-C(113)-H(113)	119.9	C(119)-C(114)-C(82)	120.4(3)
C(119)-C(114)-C(143)	116.2(4)	C(143)-C(114)-C(82)	123.3(4)
C(90)-C(117)-C(100)	119.8(4)	C(90)-C(117)-H(117)	120.1
C(100)-C(117)-H(117)	120.1	C(114)-C(119)-H(119)	119.1
C(114)-C(119)-C(125)	121.9(4)	C(125)-C(119)-H(119)	119.1
C(107)-C(120)-H(120)	119.8	C(131)-C(120)-C(107)	120.4(4)
C(131)-C(120)-H(120)	119.8	C(65)-C(121)-H(121)	119.7
C(104)-C(121)-C(65)	120.5(4)	C(104)-C(121)-H(121)	119.7
C(134)-C(122)-C(95)	120.6(5)	C(134)-C(122)-C(6)	121.0(6)
C(6)-C(122)-C(95)	118.5(6)	C(119)-C(125)-H(125)	119.4
C(190)-C(125)-C(119)	121.3(5)	C(190)-C(125)-H(125)	119.4
C(89)-C(128)-H(128)	120.1	C(104)-C(128)-C(89)	119.8(4)
C(104)-C(128)-H(128)	120.1	C(113)-C(131)-H(131)	120.1
C(120)-C(131)-C(113)	119.8(4)	C(120)-C(131)-H(131)	120.1

Table 4-3. (cont'd)

C(122)-C(134)-H(134)	123.2	C(122)-C(134)-C(20)	113.5(7)
C(20)-C(134)-H(134)	123.2	C(114)-C(143)-H(143)	119.8
C(114)-C(143)-C(157)	120.4(5)	C(157)-C(143)-H(143)	119.8
C(151)-C(148)-H(148)	112.4	C(151)-C(148)-C(20)	135.2(8)
C(20)-C(148)-H(148)	112.4	C(148)-C(151)-H(151)	126.0
C(148)-C(151)-C(6)	108.1(9)	C(6)-C(151)-H(151)	126.0
C(143)-C(157)-H(157)	119.8	C(190)-C(157)-C(143)	120.4(5)
C(190)-C(157)-H(157)	119.8	C(125)-C(190)-C(157)	119.7(5)
C(125)-C(190)-H(190)	120.1	C(157)-C(190)-H(190)	120.1
F(55)-B(142)-F(10)	110.3(4)	F(73)-B(142)-F(10)	109.8(4)
F(73)-B(142)-F(55)	110.0(4)	F(73)-B(142)-F(81)	110.5(4)
F(81)-B(142)-F(10)	108.4(3)	F(81)-B(142)-F(55)	107.8(4)
F(20)-B(154)-F(12)	106.6(3)	F(25)-B(154)-F(12)	111.7(4)
F(25)-B(154)-F(20)	109.2(5)	F(25)-B(154)-F(35)	113.5(4)
F(35)-B(154)-F(12)	107.3(4)	F(35)-B(154)-F(20)	108.3(4)
F(133)-B(147)-F(99)	100.0(5)	F(135)-B(147)-F(99)	99.9(5)
F(135)-B(147)-F(133)	110.1(5)	F(135)-B(147)-F(144)	115.6(6)
F(144)-B(147)-F(99)	98.8(4)	F(144)-B(147)-F(133)	126.1(6)
C(122)-C(6)-H(6)	114.6	C(151)-C(6)-C(122)	130.7(9)
C(151)-C(6)-H(6)	114.6	C(134)-C(20)-H(20)	124.6
C(148)-C(20)-C(134)	110.7(7)	C(148)-C(20)-H(20)	124.6

4.6.2 Crystal data for $[Co(P^{Ph}_2N^{PhOMe}_2)_2Cl](BF_4)\bullet 3(CH_3CN)$

Crystals of $[Co(P^{Ph}_2N^{PhOMe}_2)_2Cl](BF_4)\bullet 3(CH_3CN)$ were found to have crystallized in space group P–1. Both cations were observed in the chair-boat/chair-boat configuration, which refers to the conformations of the four M–P–C–N–C–P– rings formed by the ligands, with the rings adjacent to the acetonitrile given first. The crystal data was modeled to 4.0% (using 2Θ). The unit cell contains one void (240 $Å^3$) containing 3 molecules of disordered acetonitrile that were modeled using SQUEEZE.

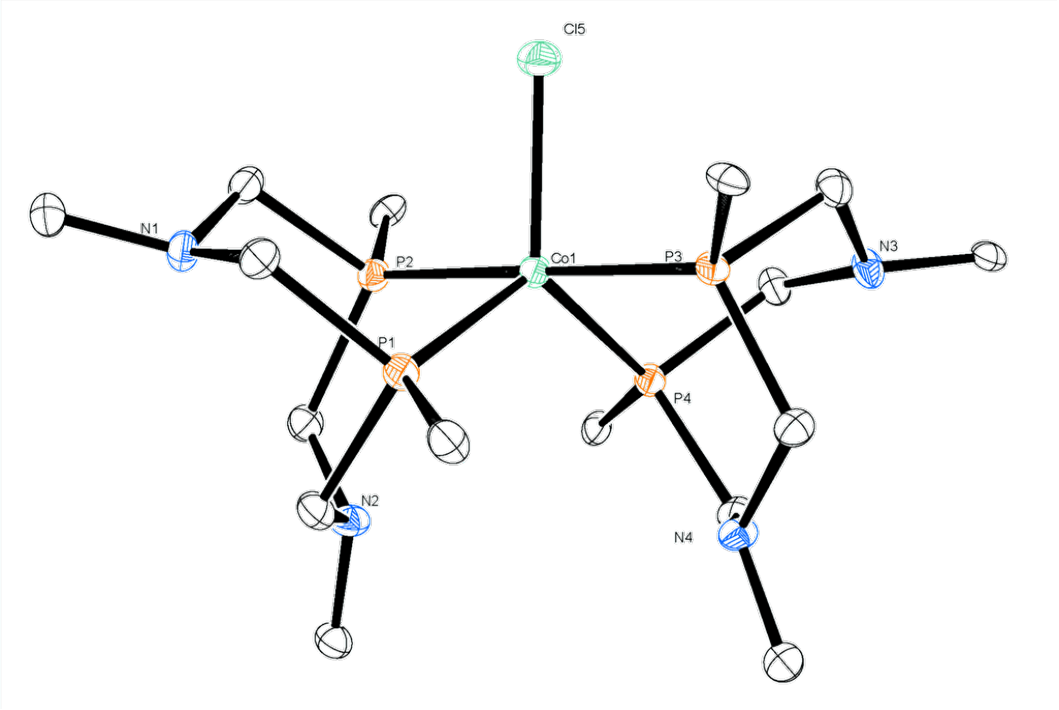

Figure 4-13. Crystal structure of $[Co(P^{Ph}_2N^{PhOMe}_2)_2Cl]^+$ core.

Table 4-4. Crystal data and structure refinement for $[Co(P^{Ph}{}_2N^{PhOMe}{}_2)_2Cl](BF_4)\bullet 3(CH_3CN)$.

Identification code	cseu_6_110_0m	
Empirical formula	C66 H73 B Cl Co F4 N7 O4 P4	
Formula weight	1333.43	
Temperature	293(2) K	
Wavelength	0.71073 Å	
Crystal system	Triclinic	
Space group	P-1	
Unit cell dimensions	a = 13.4984(6) Å	α= 80.412(2)°.
	b = 13.5548(6) Å	β= 84.269(2)°.
	c = 18.2694(8) Å	γ = 63.7340(10)°.
Volume	2954.4(2) $Å^3$	
Z	2	
Density (calculated)	1.499 Mg/m^3	
Absorption coefficient	0.515 mm^{-1}	
F(000)	1390	
Crystal size	0.11 x 0.08 x 0.07 mm^3	
Theta range for data collection	1.69 to 29.25°.	
Index ranges	-18<=h<=13, -17<=k<=17, -24<=l<=23	
Reflections collected	42035	
Independent reflections	12934 [R(int) = 0.0372]	
Completeness to theta = 25.00°	97.0 %	
Absorption correction	Semi-empirical from equivalents	
Max. and min. transmission	0.9648 and 0.9455	
Refinement method	Full-matrix least-squares on F^2	
Data / restraints / parameters	12934 / 0 / 716	
Goodness-of-fit on F^2	1.040	
Final R indices [I>2sigma(I)]	R1 = 0.0411, wR2 = 0.0910	
R indices (all data)	R1 = 0.0662, wR2 = 0.0973	
Largest diff. peak and hole	0.582 and -0.323 $e.Å^{-3}$	

Table 4-5. Bond lengths [Å] and angles [°] for $[Co(P^{Ph}{}_2N^{PhOMe}{}_2)_2Cl](BF_4)\bullet 3(CH_3CN)$.

C(1)-N(3)	1.463(3)	C(1)-P(3)	1.846(2)
C(2)-C(3)	1.398(3)	C(2)-C(7)	1.389(3)
C(2)-P(3)	1.823(2)	C(3)-C(4)	1.381(3)
C(4)-C(5)	1.381(3)	C(5)-C(6)	1.381(3)
C(6)-C(7)	1.391(3)	C(8)-N(4)	1.461(2)
C(8)-P(3)	1.845(2)	C(9)-C(10)	1.396(3)
C(9)-C(14)	1.394(3)	C(9)-N(4)	1.440(3)
C(10)-C(11)	1.381(3)	C(11)-C(12)	1.383(3)
C(12)-C(13)	1.387(3)	C(12)-O(4)	1.378(2)
C(13)-C(14)	1.385(3)	C(15)-O(4)	1.426(3)
C(16)-N(4)	1.462(3)	C(16)-P(4)	1.853(2)
C(17)-C(18)	1.398(3)	C(17)-C(22)	1.394(3)
C(17)-P(4)	1.828(2)	C(18)-C(19)	1.385(3)
C(19)-C(20)	1.381(3)	C(20)-C(21)	1.383(3)
C(21)-C(22)	1.391(3)	C(23)-N(3)	1.442(3)
C(23)-P(4)	1.862(2)	C(24)-C(25)	1.401(3)
C(24)-C(29)	1.391(3)	C(24)-N(3)	1.431(3)
C(25)-C(26)	1.376(3)	C(26)-C(27)	1.393(3)
C(27)-C(28)	1.372(3)	C(27)-O(3)	1.382(2)
C(28)-C(29)	1.395(3)	C(30)-O(3)	1.421(3)
C(31)-N(1)	1.461(3)	C(31)-P(2)	1.840(2)
C(32)-C(33)	1.398(3)	C(32)-C(37)	1.389(3)
C(32)-P(2)	1.818(2)	C(33)-C(34)	1.383(3)
C(34)-C(35)	1.380(3)	C(35)-C(36)	1.382(3)
C(36)-C(37)	1.390(3)	C(38)-N(2)	1.456(3)
C(38)-P(2)	1.862(2)	C(39)-C(40)	1.388(3)
C(39)-C(44)	1.388(3)	C(39)-N(2)	1.444(3)
C(40)-C(41)	1.383(3)	C(41)-C(42)	1.377(3)
C(42)-C(43)	1.381(3)	C(42)-O(2)	1.385(3)
C(43)-C(44)	1.391(3)	C(45)-O(2)	1.426(3)
C(46)-N(2)	1.467(3)	C(46)-P(1)	1.851(2)
C(47)-C(48)	1.389(3)	C(47)-C(52)	1.394(3)
C(47)-P(1)	1.822(2)	C(48)-C(49)	1.380(3)
C(49)-C(50)	1.376(4)	C(50)-C(51)	1.372(4)
C(51)-C(52)	1.388(3)	C(53)-N(1)	1.467(3)

Table 4-5. (cont'd)

C(53)-P(1)	1.857(2)	C(54)-C(55)	1.388(3)
C(54)-C(59)	1.377(3)	C(54)-N(1)	1.441(3)
C(55)-C(56)	1.378(3)	C(56)-C(57)	1.378(3)
C(57)-C(58)	1.378(3)	C(57)-O(1)	1.376(3)
C(58)-C(59)	1.393(3)	C(60)-O(1)	1.424(3)
P(1)-Co(1)	2.2343(6)	P(2)-Co(1)	2.1949(6)
P(3)-Co(1)	2.1876(6)	P(4)-Co(1)	2.2296(6)
Co(1)-Cl(5)	2.2712(6)	B(1)-F(1)	1.392(3)
B(1)-F(2)	1.379(3)	B(1)-F(3)	1.395(3)
B(1)-F(4)	1.399(3)		
N(3)-C(1)-P(3)	110.79(13)	C(3)-C(2)-P(3)	119.31(16)
C(7)-C(2)-C(3)	119.37(19)	C(7)-C(2)-P(3)	121.32(16)
C(4)-C(3)-C(2)	119.9(2)	C(5)-C(4)-C(3)	120.6(2)
C(4)-C(5)-C(6)	120.0(2)	C(5)-C(6)-C(7)	120.0(2)
C(2)-C(7)-C(6)	120.2(2)	N(4)-C(8)-P(3)	115.08(13)
C(10)-C(9)-N(4)	122.12(18)	C(14)-C(9)-C(10)	117.09(19)
C(14)-C(9)-N(4)	120.63(18)	C(11)-C(10)-C(9)	121.0(2)
C(10)-C(11)-C(12)	120.7(2)	C(11)-C(12)-C(13)	119.58(19)
O(4)-C(12)-C(11)	115.70(18)	O(4)-C(12)-C(13)	124.72(19)
C(14)-C(13)-C(12)	119.13(19)	C(13)-C(14)-C(9)	122.36(19)
N(4)-C(16)-P(4)	114.66(13)	C(18)-C(17)-P(4)	120.60(16)
C(22)-C(17)-C(18)	118.62(19)	C(22)-C(17)-P(4)	120.65(16)
C(19)-C(18)-C(17)	120.3(2)	C(20)-C(19)-C(18)	120.4(2)
C(19)-C(20)-C(21)	120.2(2)	C(20)-C(21)-C(22)	119.6(2)
C(21)-C(22)-C(17)	120.8(2)	N(3)-C(23)-P(4)	111.38(14)
C(25)-C(24)-N(3)	119.44(18)	C(29)-C(24)-C(25)	118.03(19)
C(29)-C(24)-N(3)	122.38(19)	C(26)-C(25)-C(24)	121.2(2)
C(25)-C(26)-C(27)	119.9(2)	C(28)-C(27)-C(26)	120.0(2)
C(28)-C(27)-O(3)	124.4(2)	O(3)-C(27)-C(26)	115.59(19)
C(27)-C(28)-C(29)	120.1(2)	C(24)-C(29)-C(28)	120.8(2)
N(1)-C(31)-P(2)	110.57(13)	C(33)-C(32)-P(2)	119.84(16)
C(37)-C(32)-C(33)	119.1(2)	C(37)-C(32)-P(2)	121.02(16)
C(34)-C(33)-C(32)	119.9(2)	C(35)-C(34)-C(33)	120.5(2)
C(34)-C(35)-C(36)	120.1(2)	C(35)-C(36)-C(37)	119.7(2)

Table 4-5. (cont'd)

C(32)-C(37)-C(36)	120.6(2)	N(2)-C(38)-P(2)	112.39(13)
C(40)-C(39)-N(2)	123.53(19)	C(44)-C(39)-C(40)	118.19(19)
C(44)-C(39)-N(2)	118.12(18)	C(41)-C(40)-C(39)	120.2(2)
C(42)-C(41)-C(40)	121.2(2)	C(41)-C(42)-C(43)	119.5(2)
C(41)-C(42)-O(2)	116.1(2)	C(43)-C(42)-O(2)	124.5(2)
C(42)-C(43)-C(44)	119.3(2)	C(39)-C(44)-C(43)	121.6(2)
N(2)-C(46)-P(1)	112.55(14)	C(48)-C(47)-C(52)	118.88(19)
C(48)-C(47)-P(1)	117.92(16)	C(52)-C(47)-P(1)	123.19(16)
C(49)-C(48)-C(47)	120.6(2)	C(50)-C(49)-C(48)	120.1(2)
C(51)-C(50)-C(49)	120.1(2)	C(50)-C(51)-C(52)	120.5(2)
C(51)-C(52)-C(47)	119.9(2)	N(1)-C(53)-P(1)	109.74(14)
C(55)-C(54)-N(1)	118.27(19)	C(59)-C(54)-C(55)	118.5(2)
C(59)-C(54)-N(1)	123.18(19)	C(56)-C(55)-C(54)	120.6(2)
C(55)-C(56)-C(57)	120.6(2)	C(56)-C(57)-C(58)	119.6(2)
O(1)-C(57)-C(56)	116.55(19)	O(1)-C(57)-C(58)	123.9(2)
C(57)-C(58)-C(59)	119.6(2)	C(54)-C(59)-C(58)	121.0(2)
C(31)-N(1)-C(53)	114.54(16)	C(54)-N(1)-C(31)	114.85(16)
C(54)-N(1)-C(53)	113.26(16)	C(38)-N(2)-C(46)	113.91(16)
C(39)-N(2)-C(38)	116.20(16)	C(39)-N(2)-C(46)	113.41(16)
C(23)-N(3)-C(1)	114.72(16)	C(24)-N(3)-C(1)	116.55(16)
C(24)-N(3)-C(23)	117.51(16)	C(8)-N(4)-C(16)	116.46(16)
C(9)-N(4)-C(8)	112.81(15)	C(9)-N(4)-C(16)	114.36(15)
C(57)-O(1)-C(60)	116.92(17)	C(42)-O(2)-C(45)	116.46(19)
C(27)-O(3)-C(30)	117.02(17)	C(12)-O(4)-C(15)	116.84(17)
C(46)-P(1)-C(53)	100.96(10)	C(46)-P(1)-Co(1)	116.06(7)
C(47)-P(1)-C(46)	101.44(9)	C(47)-P(1)-C(53)	103.37(10)
C(47)-P(1)-Co(1)	123.63(7)	C(53)-P(1)-Co(1)	108.50(7)
C(31)-P(2)-C(38)	102.95(10)	C(31)-P(2)-Co(1)	109.90(7)
C(32)-P(2)-C(31)	102.02(9)	C(32)-P(2)-C(38)	104.91(10)
C(32)-P(2)-Co(1)	118.77(7)	C(38)-P(2)-Co(1)	116.28(7)
C(1)-P(3)-Co(1)	109.70(7)	C(2)-P(3)-C(1)	102.23(9)
C(2)-P(3)-C(8)	102.21(9)	C(2)-P(3)-Co(1)	121.05(7)
C(8)-P(3)-C(1)	100.84(10)	C(8)-P(3)-Co(1)	117.99(7)
C(16)-P(4)-C(23)	99.67(10)	C(16)-P(4)-Co(1)	117.43(7)
C(17)-P(4)-C(16)	104.02(9)	C(17)-P(4)-C(23)	100.31(9)

Table 4-5. (cont'd)

C(17)-P(4)-Co(1)	123.13(7)	C(23)-P(4)-Co(1)	108.55(7)
P(1)-Co(1)-Cl(5)	118.96(2)	P(2)-Co(1)-P(1)	81.93(2)
P(2)-Co(1)-P(4)	96.96(2)	P(2)-Co(1)-Cl(5)	91.19(2)
P(3)-Co(1)-P(1)	99.00(2)	P(3)-Co(1)-P(2)	178.84(2)
P(3)-Co(1)-P(4)	81.98(2)	P(3)-Co(1)-Cl(5)	88.97(2)
P(4)-Co(1)-P(1)	119.74(2)	P(4)-Co(1)-Cl(5)	121.29(2)
F(1)-B(1)-F(3)	108.7(2)	F(1)-B(1)-F(4)	109.7(2)
F(2)-B(1)-F(1)	109.2(2)	F(2)-B(1)-F(3)	110.3(2)
F(2)-B(1)-F(4)	109.9(2)	F(3)-B(1)-F(4)	109.0(2)

Chapter 5

Hydricity trends, part two: CO_2 reduction by $[Pd(P_2N_2)_2]^{2+}$ catalysts

5.1 Introduction

Having learned that $[Co(P_2N_2)_2]^-$ complexes are energetic enough to react with CO_2, but too energetic to remain intact, we returned to the hydricity chart in **Figure 4-1** to look for a slightly more stable alternative. This time, we took care to look for complexes that would be just hydridic enough to reduce CO_2, but not much more, thereby decreasing the likelihood of stability problems as well as the catalyst overpotential. Based on comparisons with the series of $[HM(PNP)_2]^+$ (M = Ni, Pd, Pt) complexes, we anticipated that Pd bis-P_2N_2 complexes would be 15–20 kcal/mol more negative than the Ni complexes, placing some of them just over the HCOOH reduction line.[1]

Although several chiral and water-soluble Pd and $Pt(P_2N_2)Cl_2$ complexes have been studied by the Sinyashin group for information on ligand conformation and dynamics and for

ethylene/CO copolymerization,[2,3] few bis-P_2N_2 complexes of any metal other than Ni, and none of the heavier Group 10 metals, have been reported in the literature. In synthesizing and characterizing new $[Pd(P_2N_2)_2]^{2+}$ complexes, we hoped to further extend the rich chemistry of these proton relay-containing ligands. Furthermore, we hoped that comparing the structures and reactivity of the bis-P_2N_2 Pd and Ni complexes would provide insight into the chemistry of both.

In 1978, Inoue and Hashimoto described the use of $Pd(dppe)_2$ (dppe = diphenylphosphinoethane) as a catalyst for the production of HCOOH under 25 atm of CO_2 and H_2 in the presence of base.[4] In this report, they hypothesized that an intermediate $[HPd(dppe)_2]^+$ species formed via hydrogen splitting was the species that reacted with CO_2. The successful use of H_2 as a reducing agent by this thermal catalyst further suggested that a Pd bis-diphosphine electrocatalyst might be able to use protons and electrons to accomplish the same.

In this chapter, we discuss the synthesis, structures, and electrochemical characterization of a series of four new $[Pd(P^R{}_2N^{R'}{}_2)_2]^{2+}$ complexes ($P^R{}_2N^{R'}{}_2$ = $P^{Ph}{}_2N^{Ph}{}_2$ (**1**), $P^{Cy}{}_2N^{Ph}{}_2$ (**2**), $P^{Ph}{}_2N^{Bn}{}_2$(**3**), $P^{Me}{}_2N^{Ph}{}_2$ (**4**)), extending the chemistry of these P_2N_2 ligands to a new metal. We investigated the electrochemical reactivity of these complexes in the presence of $HCOO^-$ or CO_2 and H^+ and found that the complexes favor proton reduction, but are much poorer catalysts for this reaction than their $[Ni(P^R{}_2N^{R'}{}_2)_2]^{2+}$ counterparts. We discuss the implication of these results for the mechanism of proton reduction by $[Ni(P^R{}_2N^{R'}{}_2)_2]^{2+}$ catalysts and for the design of CO_2 to HCOOH reduction electrocatalysts.

5.2 Experimental Section

Materials and Methods

All chemicals were purchased from commercial sources and used as received unless otherwise specified. All manipulations were carried out using standard Schlenk and glove

box techniques under an atmosphere of nitrogen. Acetonitrile, tetrahydrofuran (THF), pentane, and diethyl ether (Et_2O) were sparged with argon and dried over basic alumina in a custom dry solvent system. Liquid aniline reagents were dried over CaH_2 and distilled under vacuum or nitrogen to yield clear, air-free reagents. Tetrabutylammonium hexafluorophosphate (NBu_4PF_6) was recrystallized from MeOH prior to use in electrochemical experiments. ^1H and $^{31}P\{^1H\}$ NMR spectra were recorded on a Varian 400 or a Jeol ECA-500 spectrometer. ^1H NMR spectra are referenced to residual solvent resonances and reported downfield of TMS (δ=0). ^{31}P NMR shifts are referenced to H_3PO_4 (δ=0). Combustion analysis was performed by Midwest MicroLab, LLC, Indianapolis, IN. $P^{Ph}{}_2N^{Ph}{}_2$,[5] $P^{Ph}{}_2N^{Bn}{}_2$,[6] $P^{Me}{}_2N^{Ph}{}_2$,[7] $P^{Cy}{}_2N^{Ph}{}_2$,[8] and $NBu_4HCO_2{\bullet}HCO_2H$[8] were prepared according to previously published procedures.

Electrochemical experiments

All electrochemical experiments were carried out under an atmosphere of nitrogen in a 0.1 M NBu_4PF_6 solution in benzonitrile or acetonitrile using a BAS Epsilon three electrode potentiostat. The working electrode was a glassy carbon disk (3 mm diameter), the counter electrode was a glassy carbon rod, and a silver wire in electrolyte solution separated from the working compartment by porous Vycor (4mm, BAS) was used as a pseudo-reference electrode. All potentials were measured using $[FeCp_2]PF_6$ as an internal reference, with all of the potentials reported vs. the $FeCp_2^{+/0}$ couple. For bulk electrolysis experiments, 20 equivalents of TFA were added to 10 mL of catalyst solution and the solution was purged with CO_2 for 10 min prior to electrolysis. Gas analyses were performed using 1 mL sample injection volumes on a HP 7890A gas chromatograph with a mol-sieve column (30 m x 0.53 mm ID x 25 μ m film).

Formate Oxidation Studies

1 M solution of $NBu_4HCO_2•HCO_2H$ was prepared by dissolving 0.334 g $NBu_4HCO_2•HCO_2H$ in 1 mL of electrolyte solution. 1 mM solutions of 1–4 were titrated with the 1 M HCOO– solution and followed via CV using the general procedure in a previous publication.[8]

Proton and CO_2 Reduction Studies

1 mL of 1 M trifluoroacetic acid (77 μL) and 1 M [(HDMF)(OTf)] (0.4460 g) were prepared volumetrically via dilution with electrolyte solution. 1 mM solutions of **1**–**4** were sparged with CO_2 or N_2 for one minute, then titrated with the 1 M acid solutions and followed via CV using the general procedure in a previous publication.[9]

Crystallography

Crystals of **1**–**4** suitable for X-ray structural determinations were mounted in polybutene oil on a glass fiber and transferred on the goniometer head to the precooled instrument. Crystallographic measurements were carried out on a Bruker P4 diffractometer using Mo Kα radiation (λ = 0.71073 Å) in conjunction with a Bruker APEX detector. All structures were solved by direct methods using OLEX2 and refined with full-matrix least-squares procedures using SHELXL-97.[10,11] All non-hydrogen atoms are anisotropically refined unless otherwise reported; the hydrogen atoms were included in calculated positions as riding models in the refinement. Crystallographic data collection and refinement information can be found in the supporting material.

Synthesis of $[Pd(P^{Ph}{}_2N^{Ph}{}_2)_2](BF_4)_2•(CH_3CN)$ (1)

$P^{Ph}{}_2N^{Ph}{}_2$ (348 mg, 0.86 mmol) and $[Pd(CH_3CN)_4](BF_4)_2$ (191.0 mg, 0.43 mmol) were placed in a 25 mL Schlenk flask and suspended in 15 mL of acetonitrile to yield in a slightly cloudy orange solution. The solution was stirred at room temperature overnight until the ligand dissolved. The solution was then dried under vacuum, resulting in a flakey orange

solid. The solid was further purified by recrystallization from CH_3CN/Et_2O. Crystals suitable for x-ray diffraction were obtained after cooling of a super-saturated CH_3CN/Et_2O solution to 0 °C. Yield = 395 mg (0.32 mmol, 75%). Elemental Analysis for $C_{58}H_{59}B_2F_8N_5P_4Pd$: C, 56.63%; H, 4.83%; N: 5.69%. Found: C, 56.79; H, 5.01%; N, 5.45%. $^{31}P\{^1H\}$ NMR (CD_3CN, 121 MHz, H_3PO_4) [ppm]: δ_P –7.67 (s).

Synthesis of $[Pd(P^{Cy}{}_2N^{Ph}{}_2)_2](BF_4)_2 \bullet (CH_3CN)$ (2)

$P^{Cy}{}_2N^{Ph}{}_2$ (372 mg, 0.80 mmol)) and $[Pd(CH_3CN)_4](BF_4)_2$ (177 mg, 0.40 mmol) were reacted using an analogous procedure. Crystals suitable for x-ray diffraction were obtained via CH_3CN/Et_2O vapor diffusion. Yield = 376 mg (0.30 mmol, 75%). Elemental Analysis for $C_{58}H_{83}B_2F_8N_5P_4Pd$: C, 55.54%; H, 6.67%; N: 5.58%. Found: C, 55.54; H, 6.74%; N, 5.30%. $^{31}P\{^1H\}$ NMR (CD_3CN, 121 MHz, triphenylphosphine oxide) [ppm]: δ_P 1.07 (s).

Synthesis of $[Pd(P^{Ph}{}_2N^{Bn}{}_2)_2](BF_4)_2 \bullet (CH_3CN)$ (3)

$P^{Ph}{}_2N^{Bn}{}_2$ (363 mg, 0.78 mmol) and $[Pd(CH_3CN)_4](BF_4)_2$ (173 mg, 0.39 mmol) were reacted using an analogous procedure to that described above. Crystals suitable for x-ray diffraction were obtained after cooling of a super-saturated CH_3CN/Et_2O solution to 0 °C. Yield = 329 mg (0.26 mmol, 66%). Elemental Analysis for $C_{62}H_{67}B_2F_8N_5P_4Pd$: C, 57.90%; H, 5.25%; N: 5.45%. Found: C, 57.77; H, 5.41%; N, 5.31%. $^{31}P\{^1H\}$ NMR (CD_3CN, 121 MHz, H_3PO_4) [ppm]: δ_P –2.24 (s).

Synthesis of $[Pd(P^{Me}{}_2N^{Ph}{}_2)_2](BF_4)_2$ (4)

$P^{Cy}{}_2N^{Ph}{}_2$ (135 mg, 0.41 mmol)) and $[Pd(CH_3CN)_4](BF_4)_2$ (91 mg, 0.20 mmol) were added to a 20 mL scintillation vial and dissolved in 15 mL of acetonitrile, resulting in an orange solution. The orange solution was stirred at room temperature overnight and turned dark green in color. The solution was filtered and a green precipitate was removed from the mixture, giving a yellow solution. The solution was then dried under vacuum, resulting in a

crystalline yellow solid. Crystals suitable for x-ray diffraction were obtained via CH_3CN/Et_2O vapor diffusion. Yield = 156 mg (0.17 mmol, 81%). Elemental Analysis for $C_{36}H_{48}B_2F_8N_4P_4Pd$: C, 45.96%; H, 5.14%; N: 5.96%. Found: C, 46.21%; H, 5.23%; N, 5.98%. $^{31}P\{^1H\}$ NMR (CD_3CN, 121 MHz, H_3PO_4) [ppm]: δ_P −11.38(s).

5.3 Results

5.3.1 Synthesis

The $P^R{}_2N^{R'}{}_2$ ligands used for this study were chosen to sample a variety of phosphorus (R) and nitrogen (R') substituents in hopes of defining the range of $[Pd(P^R{}_2N^{R'}{}_2)_2]^{2+}$ reduction potentials and hydricities. These included $P^{Ph}{}_2N^{Ph}{}_2$, $P^{Cy}{}_2N^{Ph}{}_2$, $P^{Ph}{}_2N^{Bn}{}_2$, and $P^{Me}{}_2N^{Ph}{}_2$. The ligands were synthesized according to literature procedures.[5–8] The bis-P_2N_2 palladium complexes were prepared by reacting $[Pd(CH_3CN)_4][BF_4]_2$ with each ligand in 1:2 ratios and isolating these under vacuum as yellow or orange powders. Purification was achieved by recrystallization from CH_3CN and Et_2O. The spectroscopic data are consistent with the data from reports of $[Ni(P^R{}_2N^{R'}{}_2)_2]^{2+}$ complexes and other Pd(II) bis-disphosphine complexes, and are provided in the Experimental Section. All four complexes **1**–**4** were characterized by X-ray diffraction studies, as discussed below.

We tried several routes to synthesize Pd(0) P_2N_2 complexes for structural studies and for preparation of the hydride complexes. Reduction of **2** with 2 equivalents of $CoCp_2$ resulted in poor yields of light yellow Pd(0). Attempts to synthesize $Pd(P^{Cy}{}_2N^{Ph}{}_2)_2$ in preparative yields from $Pd_2(dba)_3$ resulted in a product with a ^{31}P NMR containing a doublet of doublets AX pattern. These doublets were centered around the singlet (4.8 ppm) separately obtained via reduction of **2** with $CoCp_2$ (**Figure 5-1**). Prolonged heating (48 hrs) at 100 °C resulted in partial conversion of the doublet of doublets to the 4.8 ppm singlet, along with some compound degradation as evidenced by the appearance of free ligand in ^{31}P NMR

spectrum. Based on these results, we believe the product in this case may be a phosphine-bridged dimer, $Pd_2(P^{Cy}{}_2N^{Ph}{}_2)_4$.

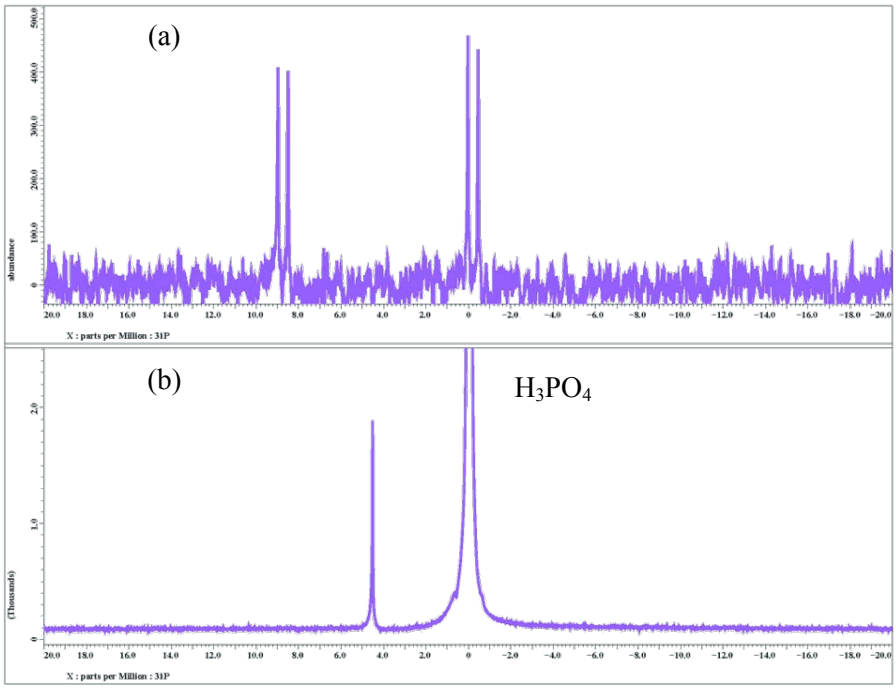

Figure 5-1. (**a**) ^{31}P NMR of the product obtained upon reaction of $Pd_2(dba)_3$ with 2 equivalents of $P^{Cy}{}_2N^{Ph}{}_2$. δ = 9.4, 8.7, 0.0, -0.5 ppm. J = 994 Hz, 7.8 Hz (**b**) ^{31}P NMR of the product obtained upon reaction of $[Pd(P^{Cy}{}_2N^{Ph}{}_2)_2]^{2+}$ with 2 equivalents $CoCp_2$. δ = 4.8 ppm. Data obtained in d^8-toluene, referenced to a capillary containing 85% H_3PO_4 at 0 ppm.

5.3.2 X-ray Diffraction Studies

Crystal structures of the four dicationic complexes $[Pd(P^{Ph}{}_2N^{Ph}{}_2)_2](BF_4)_2$•4($CH_3CN$) (**1cr**), $[Pd(P^{Cy}{}_2N^{Ph}{}_2)_2](BF_4)_2$•2($CH_3CN$) (**2cr**), $[Pd(P^{Ph}{}_2N^{Bn}{}_2)_2](BF_4)_2$•2($CH_3CN$) (**3cr**), and $[Pd(P^{Me}{}_2N^{Ph}{}_2)_2](BF_4)_2$•2($CH_3CN$) (**4cr**) were obtained, as shown in **Figure 2**. Crystals of **2cr** and **4cr** were grown from vapor diffusion of diethyl ether into acetonitrile solutions of the complexes at –35 °C. The crystals of **1cr** and **3cr** precipitated from supersaturated acetonitrile/diethyl ether solutions of the complexes at 0 °C. The Pd atoms of the former two complexes lie on crystallographic inversion centers such that Z'=0.5; they both exhibit a

diphosphine dihedral angle of 0° and are square planar. The latter two complexes exhibit dihedral angles of ca. 20° and are slightly distorted towards tetrahedral.

In contrast to all of the known $[Ni(P_2N_2)_2]^{2+}$ complexes besides $[Ni(P^{Me}{}_2N^{Ph}{}_2)_2]^{2+}$, none of the complexes **1–4** crystallize with acetonitrile as a bound fifth ligand. However, all were prone to rapid desolvation. The unit cells were found to contain multiple molecules of unbound acetonitrile, modeled as disordered solvent in complex **2cr** and as discrete molecules in the others. Elemental analyses of **1–3** dried for 24 hours under vacuum reveals the presence of 1 molecule of CH_3CN per dication in these dried samples. This suggests that acetonitrile may bind weakly to these complexes when they are not supported by an environment of bulk solvent, possibly due to slight differences in the energy of binding between complexes with different ligand conformations. The ligands of all four complexes consistently crystallize in alternating chair-boat-chair-boat conformations when considered going clockwise around the central Pd atom. The Pd–P bond lengths of all four structures are on the order of 2.35 Å, which is about 0.1 Å longer than those of the corresponding Ni complexes. The measured bite angles and phosphine cone angles are accordingly slightly smaller by an average of 1° and 3°, respectively.

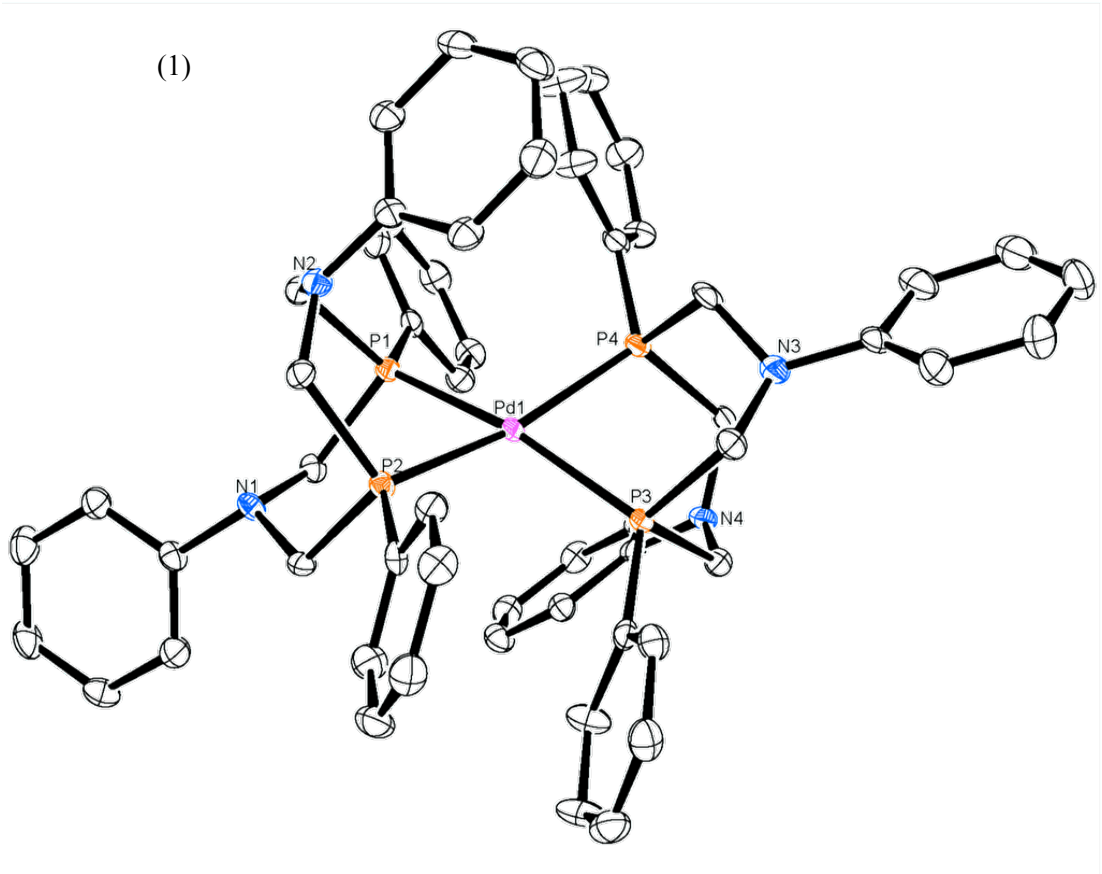

Figure 5-2. Thermal ellipsoid plots of (**1**) $[Pd(P^{Ph}{}_2N^{Ph}{}_2)_2]^{2+}$, (**2**) $[Pd(P^{Cy}{}_2N^{Ph}{}_2)_2]^{2+}$, (**3**) $[Pd(P^{Ph}{}_2N^{Bn}{}_2)_2]^{2+}$, and (**4**) $[Pd(P^{Me}{}_2N^{Ph}{}_2)_2]^{2+}$, shown at the 50% probability level. Hydrogen atoms, uncoordinated counterions, and solvent molecules omitted for clarity.

(2)

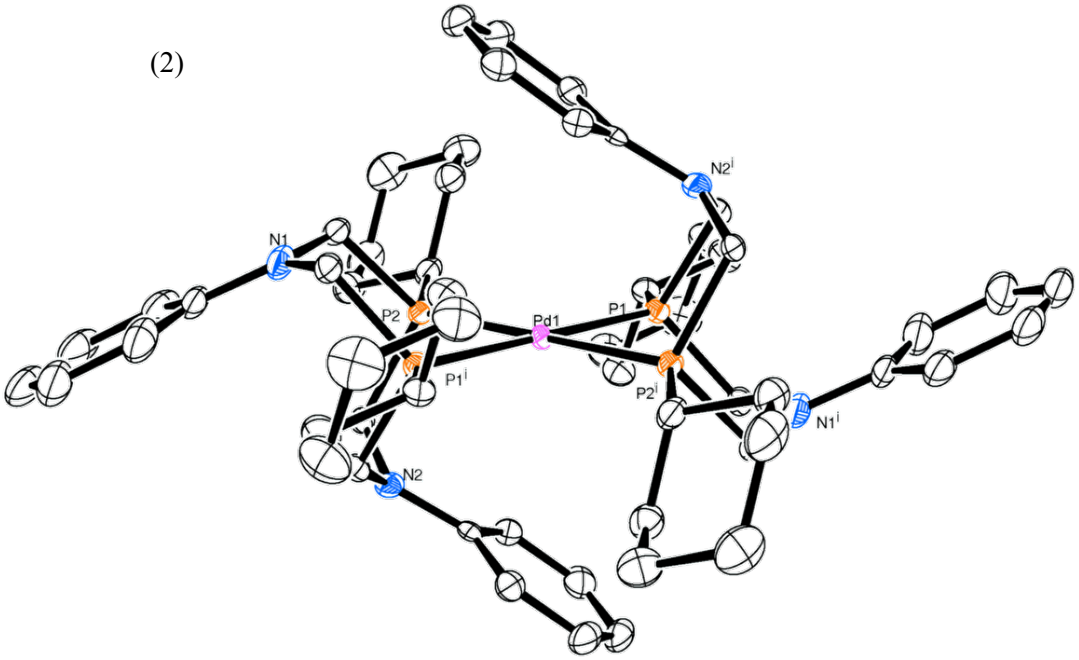

(3)

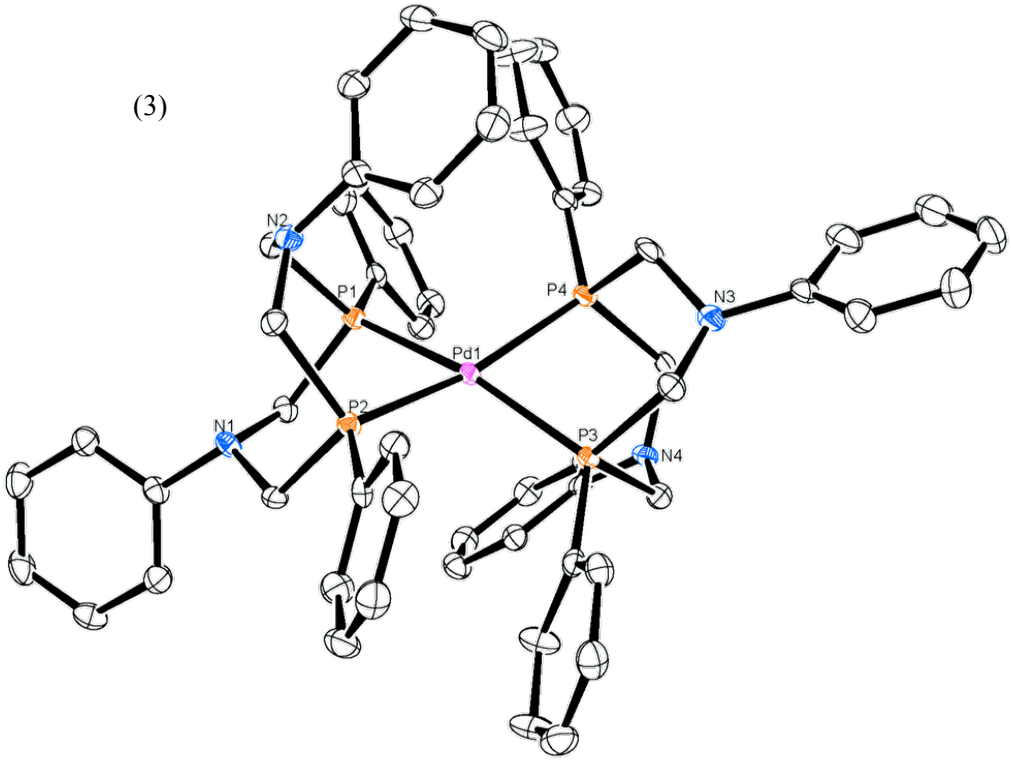

Figure 5-2. (Continued)

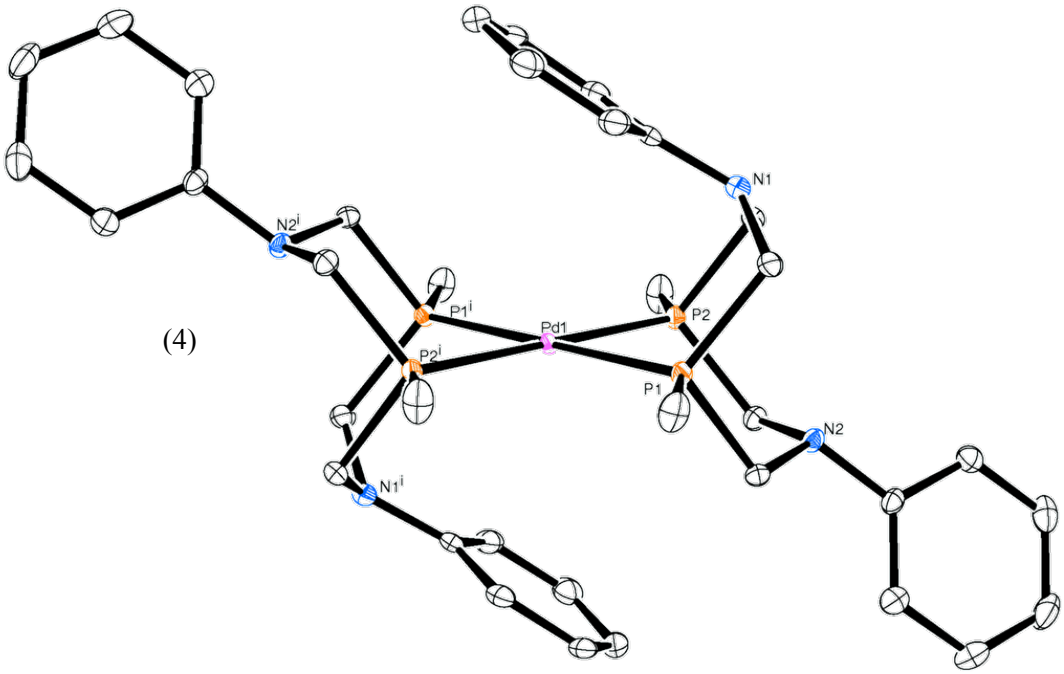

Figure 5-2. (Continued)

Although the structures of these compounds are expected to be dynamic and fluxional in solution, several different packing interactions can be observed in the solid state. Moreover, the type of interaction appears to correlate with the type of substituent at the phosphorus. The alkyl phosphine complexes **2** and **4** display pi-capping interactions between the phenyl amine rings and the metal center. The Pd–Ar distances of 3.87 and 3.73 Å suggest that bonding, if any, is very weak. Meanwhile, the phenyl phosphine complexes **1** and **3** display pi-stacking interactions between the phosphino phenyl rings, which sit in a parallel, stacked configuration at distances of 3.64 and 3.57 Å, respectively. Similar pi-stacked geometries can be seen in the phosphino phenyl rings of the corresponding Ni species.[8,9]

5.3.3 Attempted hydride syntheses and characterization

The hydricity of metal complexes can be measured and calculated using several different thermochemical schemes which rely on NMR measurement of various equilibria. These include hydrogen splitting by the complex in the presence of base (**Scheme 5-1**), hydride deprotonation by base (**Scheme 5-2**), and hydride transfer between metal complexes (**Scheme 5-3**), which have been described in detail in various DuBois publications.[8,12,13]

		ΔG° (kcal/mol)	
$[HM]^+ + HB^+ \rightleftharpoons H_2 + M^{2+} + B$		$-RT\ln K_{eq}$	(1)
$B + H^+ \rightleftharpoons HB^+$		$-1.364pK_a$	(2)
$H_2 \rightleftharpoons H^+ + H^-$		76.0	(3)
$[HM]^+ \rightleftharpoons M^{2+} + H^-$	$\Delta G°_{H^-} = -RT\ln K_{eq} - 1.364pK_a + 76.0$		(4)

Scheme 5-1. Thermochemical scheme for calculation of ΔG_{H^-} using the equilibrium between metal-activated hydrogen and hydrogen gas.

		ΔG° (kcal/mol)	
$[HM]^+ + B \rightleftharpoons M^0 + HB^+$		$-RT\ln K_{eq}$	(5)
$HB^+ \rightleftharpoons H^+ + B$		$1.364pK_a$	(6)
$M^0 \rightleftharpoons M^{2+} + 2e^-$		$-nF[E(II/0)]$	(7)
$H^+ + 2e^- \rightleftharpoons H^-$		79.6	(8)
$[HM]^+ \rightleftharpoons M^{2+} + H^-$	$\Delta G°_{H^-} = -RT\ln K_{eq} + 1.364pK_a - nF[E(II/0)] - 79.6$		(9)

Scheme 5-2. Thermochemical scheme for calculation of ΔG_{H^-} using the equilibrium between a metal hydride and its conjugate base.

		ΔG° (kcal/mol)	
$[HM_A]^+ + M_B^{2+} \rightleftharpoons M_A^{2+} + [HM_B]^+$		$-RT\ln K_{eq}$	(10)
$[HM_B]^+ \rightleftharpoons M_B^{2+} + H^-$		$\Delta G_{H^-}(M_B)$	(11)
$[HM_A]^+ \rightleftharpoons M_A^{2+} + H^-$	$\Delta G°_{H^-} = -RT\ln K_{eq} + \Delta G_{H^-}(M_B)$		(12)

Scheme 5-3. Thermochemical scheme for calculation of ΔG_{H^-} using the equilibrium between two metal hydrides.

It has been noted multiple times in the literature that palladium hydrides are very difficult to isolate.[1,12,14] They are simultaneously strongly acidic and hydridic, which makes them prone to producing H_2 by reaction with added hydride or proton sources, or sometimes by disproportionation. Nevertheless, we attempted to prepare these complexes by a variety of methods. Complexes **1–4** were found to be unreactive with $Na[HB(OMe)_3]$ and unstable to $NaBH_4$ and $LiAlH_4$; in these latter cases multiple ^{31}P peaks were observed, suggesting a variety of products. Attempts to produce a hydride complex by sparging solutions of $[Pd(P^{Ph}{}_2N^{Ph}{}_2)_2]^{2+}$ with H_2 in the presence of excess base showed no reaction with 20 equivalents of NEt_3. The complex is unstable in the presence of the same amount of 1,1,3,3-tetramethylguanidine (TMG), but reacts with 3 equivalents under an H_2 atmosphere to give two broad singlets at –8.0 and –10.1. A similar pattern was observed for the $[HPd(PNP)_2]^+$ hydride complex.[1] However, the low signal/noise ratio of this spectrum, even with a saturated solution of starting material, suggests that the complex partially degrades under these conditions, precluding isolation and further characterization. The fact that Pd(0) is not produced in both cases suggests that $[HPd(P^{Ph}{}_2N^{Ph}{}_2)_2]^+$ is several pK_a units more basic than TMG (pK_a > 23.3), consistent with the reported pK_as of Pd complexes with similar $E_{1/2}$(Pd(II/0)).[1,15]

An attempt to break apart and protonate the $Pd_2(P^{Cy}{}_2N^{Ph}{}_2)_4$ dimer using two equivalents of [(HDMF)(OTf)] (acetonitrile pK_a = 6) resulted in a ^{31}P NMR spectrum corresponding to $[Pd(P^{Cy}{}_2N^{Ph}{}_2)_2]^{2+}$, which suggests that the intermediate product $[HPd(P^{Cy}{}_2N^{Ph}{}_2)_2]^+$ is unstable to subsequent disproportionation. This is consistent with the ΔpK_a *vs.* dihedral angle correlation reported in Raebiger *et al.*, where ΔpK_a is the difference between the pK_a of the metal hydride and the pK_a of the metal-H_2 complex, in essence, the range over which the hydride is stable to deprotonation or second protonation.[15] In this report, a Pd bis-diphosphine with a natural bite angle of 80° and a dihedral angle of 0°

($[Pd(depe)_2]^{2+}$) had $\Delta pK_a = -0.7$. It appears that this rule may hold true for these nitrogen-containing bis-disphosphines as well.

5.3.4 Electrochemical studies

Cyclic voltammograms (CVs) for complexes **1**–**4** in benzonitrile are shown in **Figure 5-3**. Each consists of a single two-electron wave assigned to the Pd(II/0) couple. The $2e^-$ nature of this peak was confirmed using differential pulse voltammetry (DPV) on a sample containing equal amounts of $[FeCp_2]PF_6$ and **1**; the area of the oxidation peak for Pd was found to have twice the area of the peak for ferrocene (**Figure 5-4**). The potentials, peak-to-peak separations, and i_{pc}/i_{pa} ratios for these couples in acetonitrile and benzonitrile are listed in **Table 5-1**. The quasi-reversibility of the redox couple in both solvents likely reflects the kinetic difficulty of reorganizing the molecule from a square planar Pd(II) to tetrahedral Pd(0) geometry. A further increase in irreversibility in the acetonitrile case is attributed to Pd(0) precipitation, consistent with earlier work.[1] As a result, the majority of catalytic studies were carried out in benzonitrile. The linear dependence of the cathodic and anodic peak heights on the square root of scan rate in benzonitrile indicates that both the Pd(II) and Pd(0) species are freely diffusing in solution, and are not confined to the surface (**Figure 5-5**).

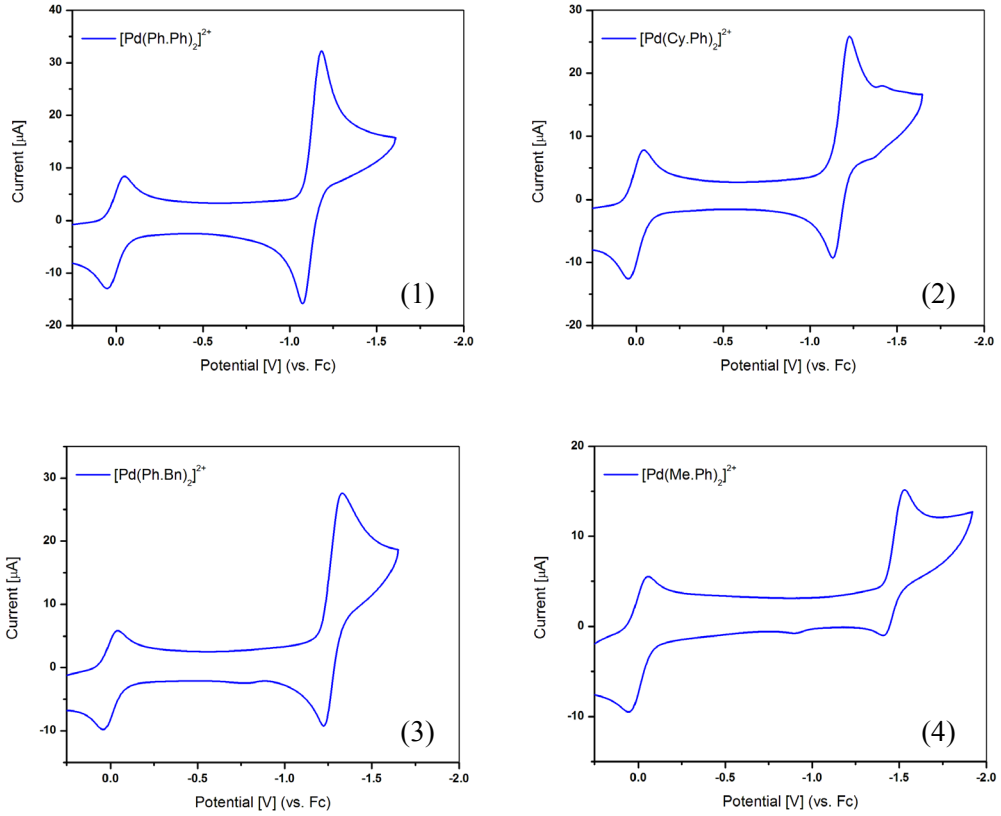

Figure 5-3. Cyclic voltammograms of (**1**) $[Pd(P^{Ph}{}_2N^{Ph}{}_2)_2]^{2+}$, (**2**) $[Pd(P^{Cy}{}_2N^{Ph}{}_2)_2]^{2+}$, (**3**) $[Pd(P^{Ph}{}_2N^{Bn}{}_2)_2]^{2+}$, and (**4**) $[Pd(P^{Me}{}_2N^{Ph}{}_2)_2]^{2+}$ with $FeCp_2^{+/0}$ as an internal standard in 0.1 M NBu_4PF_6/benzonitrile, glassy carbon working and counter electrodes, 100 mV/s.

The noticeably decreased anodic peak current in the benzonitrile CV of complex **4** suggests that $Pd(P^{Me}{}_2N^{Ph}{}_2)_2$ participates in some chemical reaction after being formed at the electrode. The product of this reaction is likely associated with the appearance of a second oxidation peak at –0.9 V. This peak quickly disappears at scan rates above 100 mV/s, suggesting that the chemical reaction is slow and can be outcompeted by reoxidation of Pd(0) at moderate scan rates.

Table 5-1. Reduction potentials and peak data for the series of $[Pd(P_2N_2)_2]^{2+}$ complexes.

Complex	$E_{1/2}(Pd^{II/0})$ (V *vs.* $FeCp_2^{+/0}$)		ΔE_p	i_{pc}/i_{pa}
1	-1.13	(-1.16)	109	1.1
2	-1.18	(-1.22)	97	1.1
3	-1.28	(-1.28)	105	1.4
4	-1.47	(-1.48)	112	1.5

Conditions: 1 mM complex in 0.1 M NBu_4PF_6 in benzonitrile or acetonitrile solution, 50 mV/s scan rate, 3 mM glassy carbon working electrode. Values for acetonitrile in parentheses.

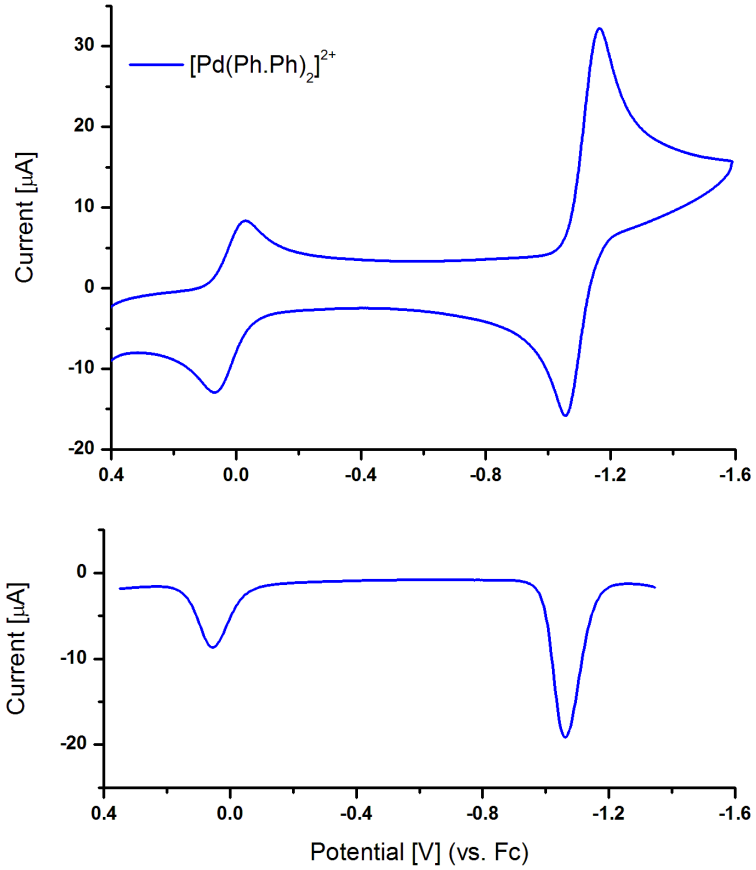

Figure 5-4. Cyclic voltammogram and differential pulse voltammogram of 1 mM $[FeCp_2]PF_6$ and $[Pd(P^{Ph}{}_2N^{Ph}{}_2)_2(CH_3CN)][BF_4]_2$. The areas of the DPV peaks for ferrocene and palladium are 45 and 94, respectively. Conditions: 0.1 M NBu_4PF_6 in benzonitrile, glassy carbon working and counter electrodes. 100 mV/s scan rate for CV; 4 mV step, 50 ms pulse width, 200 ms pulse period, 50 mV pulse amplitude for DPV.

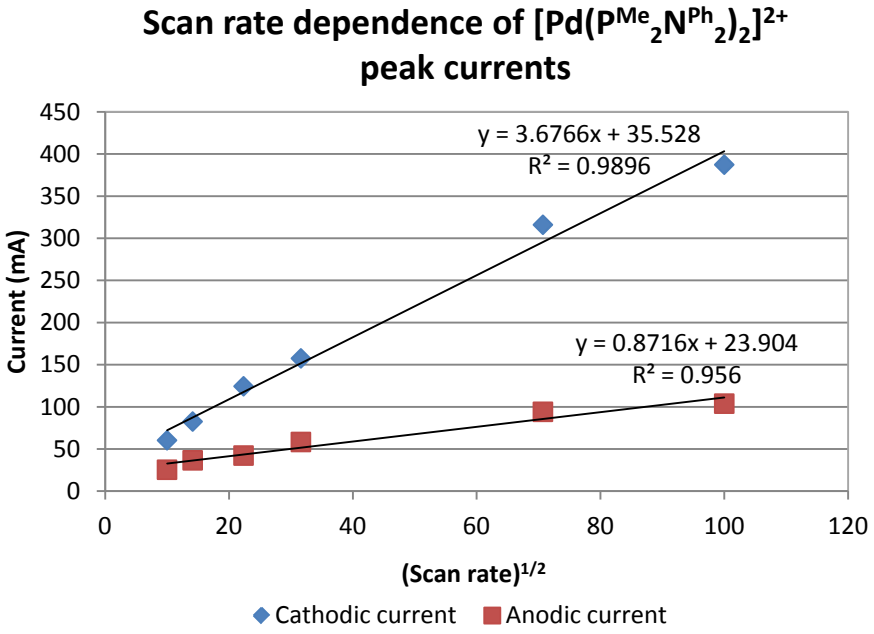

Figure 5-5. Scan rate dependence study carried out on 1 mM $[Pd(P^{Me}{}_2N^{Ph}{}_2)_2](BF_4)_2$. Conditions: 0.1 M NBu_4PF_6 in benzonitrile, glassy carbon working and counter electrodes.

It has been noted multiple times in the literature that although $P^{Cy}{}_2N^{R'}{}_2$ ligands are more donating than $P^{Ph}{}_2N^{R'}{}_2$ ligands, the much greater tetrahedral distortion in $[Ni(P^{Cy}{}_2N^{R'}{}_2)_2]^{2+}$ complexes results in an overall lowering of the $E_{1/2}$(II/I) couple.[8,15–17] This distortion effect is reversed in the Pd complexes, and it can be seen that the more donating and more planar $P^{Cy}{}_2N^{Ph}{}_2$ complex **1** exhibits a more negative reduction potential than the $P^{Ph}{}_2N^{Ph}{}_2$ complex **2**.

5.3.5 Reactivity with $HCOO^-$

The four Pd(II) complexes were tested for electrochemical oxidation of NBu_4HCO_2•HCO_2H and found to be unreactive. The anodic peak current of **1** was observed to decrease and approach an S-shaped plateau upon formate addition (**Figure 5-6**), suggesting that binding and/or an extremely slow but diffusion-controlled catalytic process might be occurring. ^{31}P NMR was used to test whether formate binding or decarboxylation

spontaneously occurs under stoichiometric conditions. No changes were observed in the ^{31}P NMR spectrum when 1 equivalent of $NBu_4HCO_2{\bullet}HCO_2H$ was added to **1** or **2**, other than partial ligand exchange to yield free ligand. This suggests that the Pd complexes do not oxidize formate, and prefer to form $Pd(O_2CH)_2$ rather than binding formate as a stable fifth ligand.

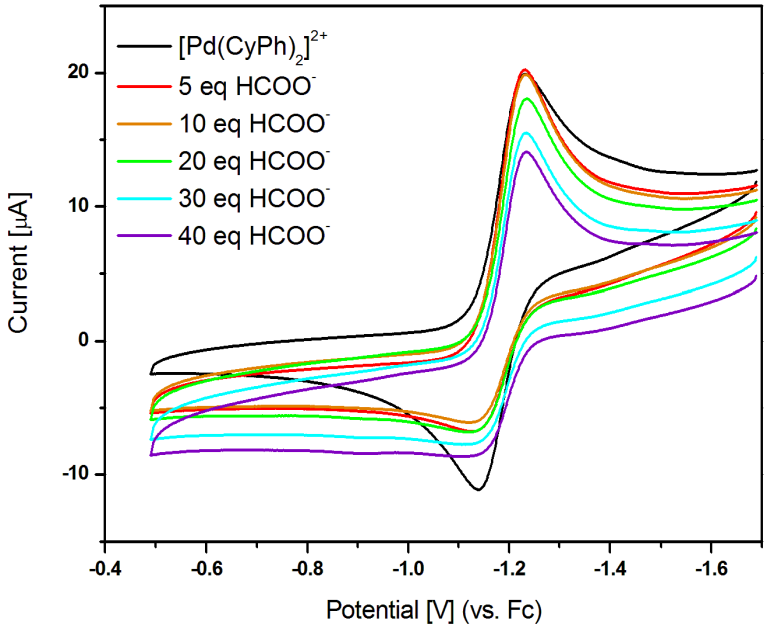

Figure 5-6. Cyclic voltammograms of 1 mM $[Pd(P^{Cy}{}_2N^{Ph}{}_2)_2(CH_3CN)](BF_4)_2$ (**1**) in the presence of increasing amounts of $NBu_4(HCOO)_2H$. Conditions: 0.1 M NBu_4PF_6 in benzonitrile, glassy carbon working and counter electrodes, 100 mV/s scan rate.

5.3.6 Reactivity with CO_2 and H^+

Hess's law was used to calculate the standard reduction potential for CO_2 to formate in neutral acetonitrile:

	$\Delta G°$ (kcal/mol)	
$CO_2 + H^- \rightleftharpoons HCOO^-$	–43	(13)
$H^+ + 2e^- \rightleftharpoons H^-$	+79.6	(14)
$CO_2 + H^+ + 2e^- \rightleftharpoons HCOO^-$	+36.6	(15)
$\Delta G = -nFE$	= –0.79 V vs NHE	
	= –1.42 V (vs $FeCp_2^{+/0}$)[18]	

Addition of H^+ would be expected to shift this potential more positive by 59 mV per pK_a unit. Based on this shift and the correlation between $E_{1/2}$(II/I) reduction potential and hydricity, we anticipated that the hydricities of **3** and **4** might be high enough to reduce CO_2 under certain conditions. Both complexes were tested for reaction with CO_2 in the presence of differing acid concentrations. 1,1,1-Trifluoroacetic acid (TFA) was chosen for these studies because it is sufficiently acidic to protonate the ligand[19] and displays less background proton reduction at the electrode than other acids, including protonated DMF. These experiments are complicated by the appearance of a reductive peak at –1.3 V possibly attributed to protonated benzonitrile (pK_a = 7.4),[20] as well as non-specific proton reduction at the glassy carbon electrode around –1.5 V (**Figure 5-7**). However, the larger current in the presence of Pd as well as the irreversible behavior of the Pd peak upon substrate addition confirms that Pd also reacts with protons, and the current from reduction at the electrode can be quantified and subtracted from the signal to yield Pd catalyst turnover frequencies.

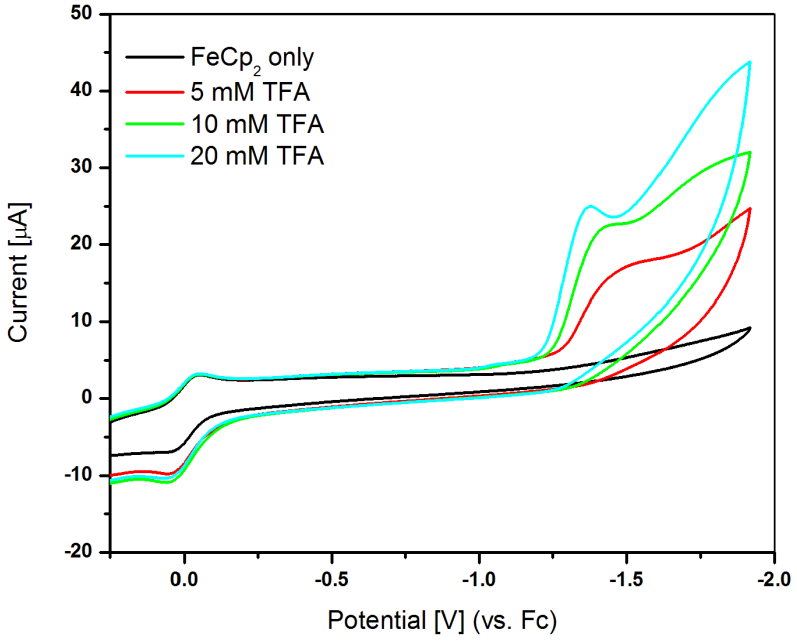

Figure 5-7. Cyclic voltammograms of increasing amounts of 1,1,1-trifluoroacetic acid in blank 0.1 M NBu_4PF_6/benzonitrile solution. Conditions: glassy carbon working and counter electrodes, 50 mV/s scan rate.

The CVs of complexes **3** and **4** remained unchanged after sparging with CO_2 in the absence of added excess protons. An increase in reductive current at the Pd(II/0) couple was observed upon addition of TFA (**Figure 5-8**). This increase reaches a plateau after approximately 30 equivalents of acid. An analogous set of CVs was taken under N_2 as a control (**Figure 5-9**). These showed approximately the same increase in current at the same acid concentrations (**Table 5-2**). Bulk electrolysis and gas chromatography of **4** in the presence of 20 equivalents trifluoroacetic acid under CO_2 showed a Faradaic efficiency of 81% for H_2 gas. The appearance of a yellow precipitate and a decrease in i_{cat} after electrolysis suggested that some of the electrons were lost via precipitation or side reactions of Pd(0), which could leave to species that are unable to reduce protons. The equation $i_{cat} = n_{cat}FA[catalyst](Dk[H^+]^2)^{1/2}$ can be used with the decrease in i_{cat} to estimate the decrease in [catalyst], given that $[H^+]$ was sufficiently high as to be unchanged during the course of the

electrolysis.[9] The Faradaic efficiency of Pd(0) side products was thus estimated to be 21%, accounting for the remaining electrons. The turnover frequency for proton reduction by **4** was calculated to be less than 1 s^{-1} using the i_{cat}/i_p ratio method described by previous DuBois publications, using the current in the plateau region at 30 equivalents H^+ and subtracting the background current from the H^+-only control.[9] Addition of up to 4 M H_2O did not change the amount of catalytic current.

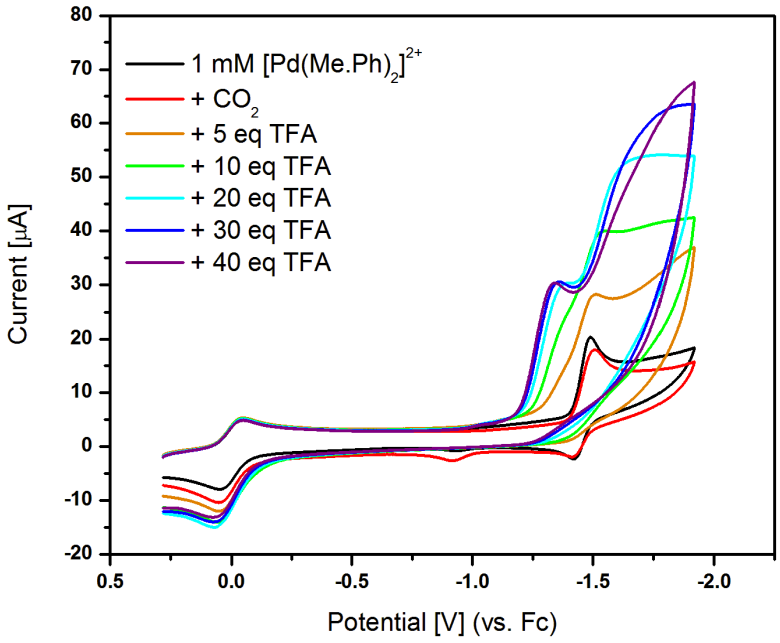

Figure 5-8. Cyclic voltammograms of 1 mM **4** in the presence of increasing amounts of 1,1,1-trifluoroacetic acid under an atmosphere of CO_2.

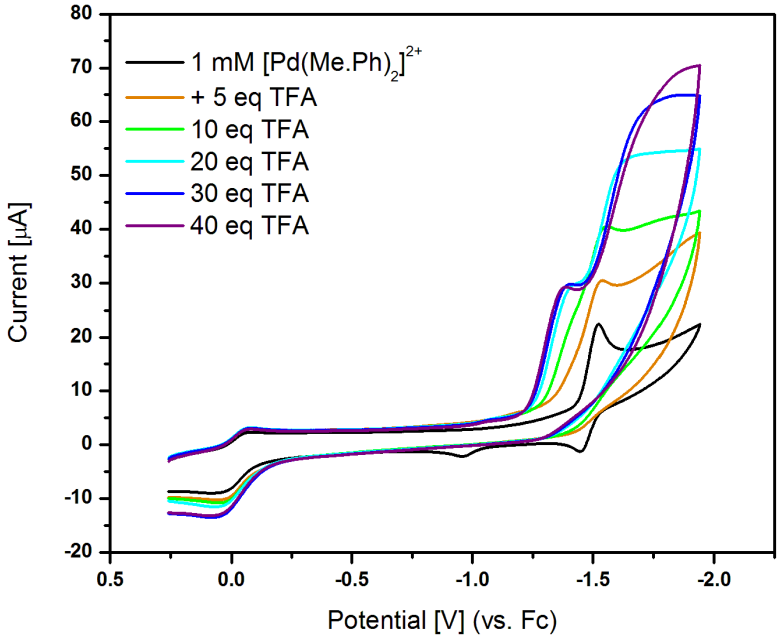

Figure 5-9. Cyclic voltammograms of 1 mM **4** in the presence of increasing amounts of 1,1,1-trifluoroacetic acid under an atmosphere of N_2.

Table 5-2. i_c/i_p for 1 mM **4** with 1,1,1-trifluoroacetic acid under CO_2 and N_2

[TFA]	CO_2	N_2
5 mM	1.53	1.52
10 mM	2.33	2.16
20 mM	3.04	2.95

5.4 Discussion

Comparative CV titrations and bulk electrolysis experiments indicated that production of hydrogen via protonation of a hydride intermediate is favored over CO_2 insertion into that hydride. We believe that this can be explained on two levels. First, the increased activity of pendant base-containing nickel complexes compared to regular bis-diphosphine complexes for H_2 production and formate oxidation,[8,9] the formation of H_2 well positive of the Ni(I/0) potential,[9,21] and the oxidation of $H[Ni(P_2N_2)_2]^+$ complexes at

unusually negative potentials[8] have demonstrated that many proton-dependent reactions of the metal center are significantly accelerated by the pendant base. It is thus unsurprising that the pendant base would indiscriminately accelerate not only hydride formation, but also protonation of the resulting hydride to produce H_2. It is conceivable that CO_2 might out-compete this second protonation if $[CO_2]$ is significantly higher than $[H^+]$. However, since reducing the concentration of $[H^+]$ would also negatively affect hydride formation, this would have to be achieved by CO_2 pressurization. A better strategy for developing catalysts that favor CO_2 insertion over protonation might entail careful tuning of the pK_as and electronic structures of the catalyst.

This brings us to the second explanation, by which the preferred reactivity for protons over CO_2 can be rationalized in terms of the electronic structure of the d^8 Pd hydride complex. A survey of the literature reveals that some of the best thermal and electrocatalysts for CO_2 reduction to formic acid include the Ir(III) pincer complexes studied by Nozaki,[22] Hazari,[23] and Meyer and Brookhart,[24] the Ru(II) bis-diphosphines studied by Jessop and co-workers,[25,26] and the Ir(III)/Ru(II)/Rh(III) bipy half-sandwiches studied by Himeda,[27,28] Fukuzumi,[29] and Deronzier.[30] The Meyer electrocatalyst is particularly relevant because it is run in the presence of excess protons, and yet does not produce H_2 gas. Li and Yoshizawa have calculated the structure of a related Ir(III) pincer complex and have suggested that reaction of the Ir–H with CO_2 is supported by a pi-symmetry interaction between the metal HOMO and CO_2 π^* LUMO.[31] Sakaki and coworkers obtained a similar result when they calculated the reaction of cis-$Ru(H_2)(PMe_3)_3(H_2O)$ with CO_2.[32] In both cases, the authors suggested that the bonding interaction served to stabilize negative charge on the O atoms, also making the central carbon more electrophilic.

Assuming that the structure of $[HPd(P^{Me}{}_2N^{Ph}{}_2)_2]^+$ is similar to that of the $[HPt(depe)_2]PF_6$ complex isolated by Miedaner *et al.*, the d^8 distorted trigonal bipyramidal

geometry results in an electronic structure where the HOMO has $d_{xy}/_{dx2-y2}$ character, and d_{xz}/d_{yz} are relatively buried.[33] In contrast, many of the CO_2 reduction catalysts have d^6 electron counts within an effectively octahedral ligand field, resulting in a pi symmetry d_{xz} or d_{yz} HOMO that can stabilize a pi-symmetry substrate. The thermal catalyst $[HPd(dppe)_2]^+$ may appear to be a counterexample to this idea; however, it should be remembered that this catalyst is run under high pressures of H_2 in the first place.

The mechanism of H_2 production by $[Ni(P_2N_2)_2]^{2+}$ complexes is the topic of a continually deepening discussion. At present, the combined experimental and theoretical data suggest that H_2 evolution proceeds through a number of energy-saving proton-coupled electron transfers and is enhanced in the presence of solvent molecules that speed up conversion between protonated isomers.[21,34–39] Previous work by Kilgore *et al.* showed that hydrogen evolution was faster for complexes with stronger hydrides and less basic amines, and suggested that a larger driving force for H_2 release (metal hydricity + pendant base acidity) correlated with faster rates.[19,40] The increased H_2 production rate later found for the $[Ni(P^{Me}{}_2N^{Ph}{}_2)_2]^{2+}$ complex is consistent with this correlation.[41] However, the much decreased H_2 production rates for the Pd complexes are not.

We hypothesize that the source of this discrepancy arises from a large increase in molecular and solvent reorganizational energy requirements. CVs of the hydrogen evolution reaction (HER) by $[Ni(P_2N_2)_2]^{2+}$ consistently show an increase in catalytic current at or before the Ni(II/I) potential; the increase in positive shift is dependent on acid strength and thought to be indicative of ligand protonation prior to reduction. In all cases, it is not necessary to hold the catalyst at a potential higher than the Ni(I/0) couple even though the reaction formally requires a $2e^-$ reduction of the metal. Calculations suggest that the electrochemistry reflects a hydride formation process that avoids a higher-energy Ni(0) species, specifically:[38,39]

1. Double protonation of the ligands, shifting the Ni(II/I) and Ni(I/0) potentials more positive.
2. $1e^-$ reduction of the metal center (ET) to make Ni(I).
3. Proton transfer (PT) from the ligand to metal to make a short-lived Ni(III)–H species, accompanied by a fast and possibly concerted second $1e^-$ reduction (ET).

In contrast to Ni, $[Pd(P_2N_2)_2]^{2+}$ complexes cannot access an intermediate redox state. The energies of the redox couples are such that the electron transfers occur together rather than being split by a protonation event, and Pd(0) is necessarily an intermediate. This process involves a geometry change from dicationic square planar Pd(II) to neutral tetrahedral Pd(0) and requires a larger amount of inner-sphere (complex) and outer-sphere (solvent) reorganization than the corresponding Ni(II/I) transition, as reflected in the peak-to-peak separations of analogous complexes (ΔE = 105 mV for $[Pd(P^{Ph}{}_2N^{Bn}{}_2)_2]^{2+/0}$ *vs*. ΔE = 85 mV for $[Ni(P^{Ph}{}_2N^{Bn}{}_2)_2]^{2/1+}$, ideal cases ΔE = 30 mV for $[Pd]^{2+/0}$ *vs*. ΔE = 59 mV for $[Ni]^{2/1+}$). Protonation of Pd(0) to make a hydride intermediate would again be hindered by a second reorganization that is comparatively minimized in the Ni case for hydrogen evolution. We note that the doubly exo-ligand-protonated Ni(0) species is an observable intermediate in NMR studies of hydrogen oxidation, and suggest that involvement of this intermediate in the catalytic cycle may play a part in the overall lower rates for H_2 oxidation as compared to H_2 production.[21,42]

If this analysis is correct, the $[Ni(P_2N_2)_2]^{2+}$ system is an elegant illustration of how a metal center and a ligand that enables proton-coupled electron transfer can be most effectively combined to achieve lower catalytic barriers. In this case, the judicious combination of Ni with P_2N_2 ligand enables access to multiple redox and protonation states, leveling the reorganizational energies involved in moving between reaction intermediates. Conscious minimization of the geometric and redox changes involved in formation of

reaction intermediates will guide our future work on the design of catalysts for CO_2 and H^+ reduction.

5.5 Conclusions

A series of four $[Pd(P_2N_2)_2]^{2+}$ complexes were synthesized and characterized for the first time, expanding our understanding of the structure and chemistry of these proton-relay containing ligands to a new metal. Cyclic voltammograms of these complexes showed a single quasi-reversible $2e^-$ wave in comparison to analogous Ni complexes, which show two $1e^-$ waves. $[Pd(P^{Ph}_2N^{Bn}_2)_2]^{2+}$ and $[Pd(P^{Me}_2N^{Ph}_2)_2]^{2+}$ were tested for catalysis of energy conversion reactions in the presence of excess protons and found to preferentially produce H_2. Furthermore, the Pd complexes were observed to be less efficient than their Ni counterparts for H_2 production despite the larger driving force of the Pd hydride. We attribute both of these observations to an electronic structure that does not actively favor CO_2 binding and predisposes the catalyst cycle towards several high-energy molecular and solvent reorganization barriers.

5.6 References

1. Curtis, C. J.; Miedaner, A.; Raebiger, J. W.; DuBois, D. L. *Organometallics*, **2004**, *23*, 511–516.

2. Karasik, A. A.; Naumov, R. N.; Balueva, A. S.; Spiridonova, Y. S.; Golodkov, O. N.; Novikova, H. V; Belov, G. P.; Katsyuba, S. A.; Vandyukova, E. E.; Peter, L.; Hey-Hawkins, E.; Sinyashin, O. G. *Heteroat. Chem.*, **2006**, *17*, 499–513.

3. Latypov, S. K.; Strelnik, A. G.; Ignatieva, S. N.; Hey-Hawkins, E.; Balueva, A. S.; Karasik, A. A.; Sinyashin, O. G. *J. Phys. Chem. A*, **2012**, *116*, 3182–93.

4. Inoue, Y.; Izumida, H.; Sasaki, Y.; Hashimoto, H. *Chem. Lett.*, **1976**, *5*, 863–864.

5. Markl, V. G.; Jin, G. Y.; Schoerner, C. *Tetrahedron Lett.*, **1982**, *21*, 1409–1412.

6. Fraze, K.; Wilson, A. D.; Appel, A. M.; DuBois, M. R.; DuBois, D. L. *Organometallics*, **2007**, *26*, 3918–3924.

7. Doud, M. D.; Grice, K.; Lilio, A.; Seu, C. S.; Kubiak, C. P. *Organometallics*, **2012**, *31*, 779–782.

8. Galan, B. R.; Schöffel, J.; Linehan, J. C.; Seu, C. S.; Appel, A. M.; Roberts, J. A. S.; Helm, M. L.; Kilgore, U. J.; Yang, J. Y.; DuBois, D. L.; Kubiak, C. P. *J. Am. Chem. Soc.*, **2011**, *133*, 12767–12779.

9. Wilson, A. D.; Newell, R.; McNevin, M. J.; Muckerman, J. T.; DuBois, M. R.; DuBois, D. L. *J. Am. Chem. Soc.*, **2006**, *128*, 358–366.

10. Sheldrick, G. M. *Acta Crystallogr., Sect. A: Found. Crystallogr.*, **2008**, *64*, 112–122.

11. Dolomanov, O. V.; Bourhis, L. J.; Gildea, R. J.; Howard, J. A. K.; Puschmann, H. *J. Appl. Crystallogr.*, **2009**, *42*, 339–341.

12. Berning, D. E.; Noll, B. C.; DuBois, D. L. *J. Am. Chem. Soc.*, **1999**, *121*, 11432–11447.

13. Curtis, C. J.; Miedaner, A.; Ellis, W. W.; DuBois, D. L. *J. Am. Chem. Soc.*, **2002**, *124*, 1918–25.

14. Grushin, V. V. *Chem. Rev.*, **1996**, *96*, 2011–2033.

15. Raebiger, J. W.; Miedaner, A.; Curtis, C. J.; Miller, S. M.; Anderson, O. P.; DuBois, D. L. *J. Am. Chem. Soc.*, **2004**, *126*, 5502–5514.

16. Miedaner, A.; Haltiwanger, R. C.; DuBois, D. L. *Inorg. Chem.*, **1991**, *30*, 417–427.

17. Nimlos, M. R.; Chang, C. H.; Curtis, C. J.; Miedaner, A.; Pilath, H. M.; DuBois, D. L. *Organometallics*, **2008**, *27*, 2715–2722.

18. Pavlishchuk, V. V; Addison, A. W. *Inorg. Chim. Acta*, **2000**, *298*, 97–102.

19. Kilgore, U. J.; Roberts, J. A. S.; Pool, D. H.; Appel, A. M.; Stewart, M. P.; DuBois, M. R.; Dougherty, W. G.; Kassel, W. S.; Bullock, R. M.; DuBois, D. L. *J. Am. Chem. Soc.*, **2011**, *133*, 5861–5872.

20. Holcman, J.; Sehested, K. *J. Chem. Soc., Faraday Trans.*, **1975**, *71*, 1211–1213.

21. O'Hagan, M. J.; Shaw, W. J.; Raugei, S.; Chen, S.; Yang, J. Y.; Kilgore, U. J.; DuBois, D. L.; Bullock, R. M. *J. Am. Chem. Soc.*, **2011**, *133*, 14301–14312.

22. Tanaka, R.; Yamashita, M.; Nozaki, K. *J. Am. Chem. Soc.*, **2009**, *131*, 14168–14169.

23. Schmeier, T. J.; Dobereiner, G. E.; Crabtree, R. H.; Hazari, N. *J. Am. Chem. Soc.*, **2011**, *133*, 9274–9277.

24. Kang, P.; Cheng, C.; Chen, Z.; Schauer, C.; Meyer, T. J.; Brookhart, M. *J. Am. Chem. Soc.*, **2012**, *134*, 5000–5003.

25. Tai, C.-C.; Pitts, J.; Linehan, J. C.; Main, D.; Munshi, P.; Jessop, P. G. *Inorg. Chem.*, **2002**, *41*, 1606–1614.

26. Jessop, P. G.; Joo, F.; Tai, C.-C. *Coord. Chem. Rev.*, **2004**, *248*, 2425–2442.

27. Himeda, Y. *Eur. J. Inorg. Chem.*, **2007**, 3927–3941.

28. Himeda, Y.; Miyazawa, S.; Hirose, T. *ChemSusChem*, **2011**, *4*, 487–493.

29. Ogo, S.; Kabe, R.; Hayashi, H.; Harada, R.; Fukuzumi, S. *Dalton Trans.*, **2006**, 4657–4663.

30. Caix, C.; Chardon-Noblat, S.; Deronzier, A. *J. Electroanal. Chem.*, **1997**, *434*, 163–170.

31. Li, J.; Yoshizawa, K. *Bull. Chem. Soc. Jpn.*, **2011**, *84*, 1039–1048.

32. Ohnishi, Y.; Nakao, Y.; Sato, H.; Sakaki, S. *Organometallics*, **2006**, 3352–3363.

33. Miedaner, A.; DuBois, D. L.; Curtis, C. J.; Haltiwanger, R. C. *Organometallics*, **1993**, 299–303.

34. Fernandez, L. E.; Horvath, S.; Hammes-Schiffer, S. *J. Phys. Chem. C*, **2012**, *116*, 3171–3180.

35. Appel, A. M.; Pool, D. H.; O'Hagan, M. J.; Shaw, W. J.; Yang, J. Y.; DuBois, M. R.; DuBois, D. L.; Bullock, R. M. *ACS Catal.*, **2011**, *2*, 777–785.

36. Yang, J. Y.; Bullock, R. M.; Shaw, W. J.; Twamley, B.; Fraze, K.; DuBois, M. R.; DuBois, D. L. *J. Am. Chem. Soc.*, **2009**, *131*, 5935–5945.

37. O'Hagan, M. J.; Ho, M.; Yang, J. Y. *J. Am. Chem. Soc.*, **2012**, *134*, 19409–19424.

38. Horvath, S.; Fernandez, L. E.; Appel, A. M.; Hammes-Schiffer, S. *Inorg. Chem.*, **2013**, *52*, 3643–3652.

39. Horvath, S.; Fernandez, L. E.; Soudackov, A. V; Hammes-Schiffer, S. *Proc. Natl. Acad. Sci. U. S. A.*, **2012**.

40. Kilgore, U. J.; Stewart, M. P.; Helm, M. L.; Dougherty, W. G.; Kassel, W. S.; DuBois, M. R.; DuBois, D. L.; Bullock, R. M. *Inorg. Chem.*, **2011**, *50*, 10908–10918.

41. Wiese, S.; Kilgore, U. J.; DuBois, D. L.; Bullock, R. M. *ACS Catal.*, **2012**, *2*, 720–727.

42. Smith, S. E.; Yang, J. Y.; DuBois, D. L.; Bullock, R. M. *Angew. Chem., Int. Ed.*, **2012**, *51*, 3152–3155.

5.7 Appendix

5.7.1 Crystal data for $[Pd(P^{Ph}_2N^{Ph}_2)_2](BF_4)_2 \bullet 2(CH_3CN)$ (1cr)

Crystals of $[Pd(P^{Ph}_2N^{Ph}_2)_2](BF_4)_2 \bullet 2(CH_3CN)$ were found to have crystallized in space group P2(1)/c with one molecule per asymmetric unit (Z'=1). The crystal data was modeled to 5.47% (using 2Θ). Two molecules of acetonitrile solvent per unit cell were modeled discretely. Positional disorder in of one of the acetonitrile molecules was modeled using partial occupancies and EADP constraints for equivalent atoms.

Table 5-3. Crystal data and structure refinement for $[Pd(P^{Ph}_2N^{Ph}_2)_2](BF_4)_2 \bullet 2(CH_3CN)$ (**1cr**)

Identification code	ckdu005_0m	
Empirical formula	C60 H62 B2 F8 N6 P4 Pd	
Formula weight	1271.06	
Temperature	100(2) K	
Wavelength	0.71073 Å	
Crystal system	Monoclinic	
Space group	P2(1)/c	
Unit cell dimensions	a = 10.2698(5) Å	α= 90°.
	b = 19.0572(11) Å	β= 95.0210(10)°.
	c = 29.2752(17) Å	γ = 90°.
Volume	5707.6(5) $Å^3$	
Z	4	
Density (calculated)	1.479 Mg/m^3	
Absorption coefficient	0.510 mm^{-1}	
F(000)	2608	
Crystal size	0.23 x 0.18 x 0.10 mm^3	
Theta range for data collection	2.26 to 27.23°.	
Index ranges	-12<=h<=13, -24<=k<=24, -37<=l<=37	
Reflections collected	63875	
Independent reflections	12716 [R(int) = 0.0730]	
Completeness to theta = 25.00°	99.9 %	
Absorption correction	Semi-empirical from equivalents	
Max. and min. transmission	0.9532 and 0.8914	
Refinement method	Full-matrix least-squares on F^2	
Data / restraints / parameters	12716 / 2 / 743	
Goodness-of-fit on F^2	1.068	
Final R indices [I>2sigma(I)]	R1 = 0.0547, wR2 = 0.1088	
R indices (all data)	R1 = 0.0834, wR2 = 0.1213	
Extinction coefficient	not measured	
Largest diff. peak and hole	1.201 and -1.009 $e.Å^{-3}$	

Table 5-4. Bond lengths [Å] and angles [°] for $[Pd(P^{Ph}{}_2N^{Ph}{}_2)_2](BF_4)_2 \bullet 2(CH_3CN)$ (**1cr**).

Pd(1)-P(2)	2.3237(9)	Pd(1)-P(1)	2.3239(9)
Pd(1)-P(3)	2.3332(9)	Pd(1)-P(4)	2.3401(9)
P(1)-C(23)	1.807(4)	P(1)-C(1)	1.849(4)
P(1)-C(22)	1.872(3)	P(2)-C(9)	1.814(4)
P(2)-C(8)	1.846(3)	P(2)-C(15)	1.891(3)
P(3)-C(51)	1.814(4)	P(3)-C(29)	1.854(4)
P(3)-C(50)	1.892(3)	P(4)-C(37)	1.808(4)
P(4)-C(36)	1.862(4)	P(4)-C(43)	1.867(3)
N(1)-C(2)	1.450(4)	N(1)-C(8)	1.463(4)
N(1)-C(1)	1.464(4)	N(2)-C(16)	1.418(4)
N(2)-C(15)	1.442(5)	N(2)-C(22)	1.446(4)
N(3)-C(30)	1.425(5)	N(3)-C(36)	1.450(5)
N(3)-C(29)	1.454(5)	N(4)-C(44)	1.414(4)
N(4)-C(50)	1.438(4)	N(4)-C(43)	1.457(4)
C(1)-H(1A)	0.9900	C(1)-H(1B)	0.9900
C(2)-C(7)	1.386(5)	C(2)-C(3)	1.388(5)
C(3)-C(4)	1.391(5)	C(3)-H(3)	0.9500
C(4)-C(5)	1.377(6)	C(4)-H(4)	0.9500
C(5)-C(6)	1.388(6)	C(5)-H(5)	0.9500
C(6)-C(7)	1.389(5)	C(6)-H(6)	0.9500
C(7)-H(7)	0.9500	C(8)-H(8A)	0.9900
C(8)-H(8B)	0.9900	C(9)-C(14)	1.390(5)
C(9)-C(10)	1.394(5)	C(10)-C(11)	1.381(5)
C(10)-H(10)	0.9500	C(11)-C(12)	1.384(5)
C(11)-H(11)	0.9500	C(12)-C(13)	1.373(6)
C(12)-H(12)	0.9500	C(13)-C(14)	1.394(5)
C(13)-H(13)	0.9500	C(14)-H(14)	0.9500
C(15)-H(15A)	0.9900	C(15)-H(15B)	0.9900
C(16)-C(17)	1.392(5)	C(16)-C(21)	1.412(5)
C(17)-C(18)	1.400(5)	C(17)-H(17)	0.9500
C(18)-C(19)	1.373(6)	C(18)-H(18)	0.9500
C(19)-C(20)	1.392(6)	C(19)-H(19)	0.9500
C(20)-C(21)	1.386(5)	C(20)-H(20)	0.9500
C(21)-H(21)	0.9500	C(22)-H(22A)	0.9900
C(22)-H(22B)	0.9900	C(23)-C(28)	1.380(5)

Table 5-4. (cont'd)

C(23)-C(24)	1.400(5)	C(24)-C(25)	1.384(5)
C(24)-H(24)	0.9500	C(25)-C(26)	1.382(5)
C(25)-H(25)	0.9500	C(26)-C(27)	1.383(6)
C(26)-H(26)	0.9500	C(27)-C(28)	1.395(6)
C(27)-H(27)	0.9500	C(28)-H(28)	0.9500
C(29)-H(29A)	0.9900	C(29)-H(29B)	0.9900
C(30)-C(31)	1.383(5)	C(30)-C(35)	1.398(5)
C(31)-C(32)	1.396(5)	C(31)-H(31)	0.9500
C(32)-C(33)	1.377(7)	C(32)-H(32)	0.9500
C(33)-C(34)	1.362(7)	C(33)-H(33)	0.9500
C(34)-C(35)	1.381(6)	C(34)-H(34)	0.9500
C(35)-H(35)	0.9500	C(36)-H(36A)	0.9900
C(36)-H(36B)	0.9900	C(37)-C(42)	1.391(5)
C(37)-C(38)	1.400(5)	C(38)-C(39)	1.386(6)
C(38)-H(38)	0.9500	C(39)-C(40)	1.382(6)
C(39)-H(39)	0.9500	C(40)-C(41)	1.378(6)
C(40)-H(40)	0.9500	C(41)-C(42)	1.392(5)
C(41)-H(41)	0.9500	C(42)-H(42)	0.9500
C(43)-H(43A)	0.9900	C(43)-H(43B)	0.9900
C(44)-C(45)	1.390(5)	C(44)-C(49)	1.406(5)
C(45)-C(46)	1.389(5)	C(45)-H(45)	0.9500
C(46)-C(47)	1.385(5)	C(46)-H(46)	0.9500
C(47)-C(48)	1.390(5)	C(47)-H(47)	0.9500
C(48)-C(49)	1.377(5)	C(48)-H(48)	0.9500
C(49)-H(49)	0.9500	C(50)-H(50A)	0.9900
C(50)-H(50B)	0.9900	C(51)-C(56)	1.395(5)
C(51)-C(52)	1.397(5)	C(52)-C(53)	1.391(5)
C(52)-H(52)	0.9500	C(53)-C(54)	1.389(6)
C(53)-H(53)	0.9500	C(54)-C(55)	1.380(6)
C(54)-H(54)	0.9500	C(55)-C(56)	1.383(5)
C(55)-H(55)	0.9500	C(56)-H(56)	0.9500
F(1)-B(4)	1.391(5)	F(2)-B(4)	1.390(5)
F(3)-B(4)	1.378(5)	F(4)-B(4)	1.387(5)
F(5)-B(5)	1.384(5)	F(6)-B(5)	1.404(5)
F(7)-B(5)	1.368(5)	F(8)-B(5)	1.380(5)

Table 5-4. (cont'd)

N(5)-C(57)	1.131(6)	C(57)-C(58)	1.470(7)
C(58)-H(58A)	0.9800	C(58)-H(58B)	0.9800
C(58)-H(58C)	0.9800	N(6)-C(59)	1.16(2)
C(59)-C(60)	1.48(3)	C(60)-H(60A)	0.9800
C(60)-H(60B)	0.9800	C(60)-H(60C)	0.9800
N(6A)-C(59A)	1.15(4)	C(59A)-C(61)	1.43(4)
C(61)-H(61A)	0.9800	C(61)-H(61B)	0.9800
C(61)-H(61C)	0.9800		
P(2)-Pd(1)-P(1)	81.15(3)	P(2)-Pd(1)-P(3)	99.84(3)
P(1)-Pd(1)-P(3)	168.08(3)	P(2)-Pd(1)-P(4)	165.72(3)
P(1)-Pd(1)-P(4)	99.92(3)	P(3)-Pd(1)-P(4)	82.08(3)
C(23)-P(1)-C(1)	98.65(16)	C(23)-P(1)-C(22)	110.06(16)
C(1)-P(1)-C(22)	101.57(16)	C(23)-P(1)-Pd(1)	120.14(11)
C(1)-P(1)-Pd(1)	108.08(12)	C(22)-P(1)-Pd(1)	115.20(11)
C(9)-P(2)-C(8)	103.25(16)	C(9)-P(2)-C(15)	103.71(16)
C(8)-P(2)-C(15)	105.06(16)	C(9)-P(2)-Pd(1)	123.16(11)
C(8)-P(2)-Pd(1)	111.00(12)	C(15)-P(2)-Pd(1)	109.10(12)
C(51)-P(3)-C(29)	103.85(16)	C(51)-P(3)-C(50)	103.22(16)
C(29)-P(3)-C(50)	102.61(16)	C(51)-P(3)-Pd(1)	123.12(11)
C(29)-P(3)-Pd(1)	112.90(12)	C(50)-P(3)-Pd(1)	108.95(11)
C(37)-P(4)-C(36)	102.21(16)	C(37)-P(4)-C(43)	109.11(17)
C(36)-P(4)-C(43)	103.82(17)	C(37)-P(4)-Pd(1)	121.60(12)
C(36)-P(4)-Pd(1)	101.84(13)	C(43)-P(4)-Pd(1)	115.36(11)
C(2)-N(1)-C(8)	113.8(3)	C(2)-N(1)-C(1)	109.8(3)
C(8)-N(1)-C(1)	114.4(3)	C(16)-N(2)-C(15)	120.1(3)
C(16)-N(2)-C(22)	117.1(3)	C(15)-N(2)-C(22)	115.4(3)
C(30)-N(3)-C(36)	116.9(3)	C(30)-N(3)-C(29)	119.3(3)
C(36)-N(3)-C(29)	115.9(3)	C(44)-N(4)-C(50)	120.7(3)
C(44)-N(4)-C(43)	117.3(3)	C(50)-N(4)-C(43)	114.2(3)
N(1)-C(1)-P(1)	113.0(2)	N(1)-C(1)-H(1A)	109.0
P(1)-C(1)-H(1A)	109.0	N(1)-C(1)-H(1B)	109.0
P(1)-C(1)-H(1B)	109.0	H(1A)-C(1)-H(1B)	107.8
C(7)-C(2)-C(3)	119.8(3)	C(7)-C(2)-N(1)	117.8(3)
C(3)-C(2)-N(1)	122.4(3)	C(2)-C(3)-C(4)	119.8(4)

Table 5-4. (cont'd)

C(2)-C(3)-H(3)	120.1	C(4)-C(3)-H(3)	120.1
C(5)-C(4)-C(3)	120.7(4)	C(5)-C(4)-H(4)	119.6
C(3)-C(4)-H(4)	119.6	C(4)-C(5)-C(6)	119.3(4)
C(4)-C(5)-H(5)	120.3	C(6)-C(5)-H(5)	120.3
C(5)-C(6)-C(7)	120.5(4)	C(5)-C(6)-H(6)	119.7
C(7)-C(6)-H(6)	119.7	C(2)-C(7)-C(6)	119.9(4)
C(2)-C(7)-H(7)	120.1	C(6)-C(7)-H(7)	120.1
N(1)-C(8)-P(2)	111.6(2)	N(1)-C(8)-H(8A)	109.3
P(2)-C(8)-H(8A)	109.3	N(1)-C(8)-H(8B)	109.3
P(2)-C(8)-H(8B)	109.3	H(8A)-C(8)-H(8B)	108.0
C(14)-C(9)-C(10)	119.2(3)	C(14)-C(9)-P(2)	120.9(3)
C(10)-C(9)-P(2)	119.8(3)	C(11)-C(10)-C(9)	120.2(3)
C(11)-C(10)-H(10)	119.9	C(9)-C(10)-H(10)	119.9
C(10)-C(11)-C(12)	120.2(4)	C(10)-C(11)-H(11)	119.9
C(12)-C(11)-H(11)	119.9	C(13)-C(12)-C(11)	120.2(4)
C(13)-C(12)-H(12)	119.9	C(11)-C(12)-H(12)	119.9
C(12)-C(13)-C(14)	120.0(4)	C(12)-C(13)-H(13)	120.0
C(14)-C(13)-H(13)	120.0	C(9)-C(14)-C(13)	120.2(4)
C(9)-C(14)-H(14)	119.9	C(13)-C(14)-H(14)	119.9
N(2)-C(15)-P(2)	118.2(2)	N(2)-C(15)-H(15A)	107.8
P(2)-C(15)-H(15A)	107.8	N(2)-C(15)-H(15B)	107.8
P(2)-C(15)-H(15B)	107.8	H(15A)-C(15)-H(15B)	107.1
C(17)-C(16)-C(21)	118.1(3)	C(17)-C(16)-N(2)	122.8(3)
C(21)-C(16)-N(2)	119.0(3)	C(16)-C(17)-C(18)	120.5(4)
C(16)-C(17)-H(17)	119.7	C(18)-C(17)-H(17)	119.7
C(19)-C(18)-C(17)	121.0(4)	C(19)-C(18)-H(18)	119.5
C(17)-C(18)-H(18)	119.5	C(18)-C(19)-C(20)	119.1(4)
C(18)-C(19)-H(19)	120.4	C(20)-C(19)-H(19)	120.4
C(21)-C(20)-C(19)	120.7(4)	C(21)-C(20)-H(20)	119.7
C(19)-C(20)-H(20)	119.7	C(20)-C(21)-C(16)	120.5(4)
C(20)-C(21)-H(21)	119.7	C(16)-C(21)-H(21)	119.7
N(2)-C(22)-P(1)	111.8(2)	N(2)-C(22)-H(22A)	109.2
P(1)-C(22)-H(22A)	109.2	N(2)-C(22)-H(22B)	109.2
P(1)-C(22)-H(22B)	109.2	H(22A)-C(22)-H(22B)	107.9
C(28)-C(23)-C(24)	119.5(3)	C(28)-C(23)-P(1)	123.6(3)

Table 5-4. (cont'd)

C(24)-C(23)-P(1)	116.6(3)	C(25)-C(24)-C(23)	120.3(3)
C(25)-C(24)-H(24)	119.8	C(23)-C(24)-H(24)	119.8
C(26)-C(25)-C(24)	120.2(3)	C(26)-C(25)-H(25)	119.9
C(24)-C(25)-H(25)	119.9	C(25)-C(26)-C(27)	119.5(4)
C(25)-C(26)-H(26)	120.2	C(27)-C(26)-H(26)	120.2
C(26)-C(27)-C(28)	120.8(4)	C(26)-C(27)-H(27)	119.6
C(28)-C(27)-H(27)	119.6	C(23)-C(28)-C(27)	119.7(4)
C(23)-C(28)-H(28)	120.2	C(27)-C(28)-H(28)	120.2
N(3)-C(29)-P(3)	110.0(2)	N(3)-C(29)-H(29A)	109.7
P(3)-C(29)-H(29A)	109.7	N(3)-C(29)-H(29B)	109.7
P(3)-C(29)-H(29B)	109.7	H(29A)-C(29)-H(29B)	108.2
C(31)-C(30)-C(35)	118.7(4)	C(31)-C(30)-N(3)	122.3(4)
C(35)-C(30)-N(3)	119.0(4)	C(30)-C(31)-C(32)	119.4(4)
C(30)-C(31)-H(31)	120.3	C(32)-C(31)-H(31)	120.3
C(33)-C(32)-C(31)	120.9(4)	C(33)-C(32)-H(32)	119.5
C(31)-C(32)-H(32)	119.5	C(34)-C(33)-C(32)	119.8(4)
C(34)-C(33)-H(33)	120.1	C(32)-C(33)-H(33)	120.1
C(33)-C(34)-C(35)	120.2(4)	C(33)-C(34)-H(34)	119.9
C(35)-C(34)-H(34)	119.9	C(34)-C(35)-C(30)	120.8(4)
C(34)-C(35)-H(35)	119.6	C(30)-C(35)-H(35)	119.6
N(3)-C(36)-P(4)	111.4(2)	N(3)-C(36)-H(36A)	109.4
P(4)-C(36)-H(36A)	109.4	N(3)-C(36)-H(36B)	109.4
P(4)-C(36)-H(36B)	109.4	H(36A)-C(36)-H(36B)	108.0
C(42)-C(37)-C(38)	119.6(3)	C(42)-C(37)-P(4)	124.0(3)
C(38)-C(37)-P(4)	116.3(3)	C(39)-C(38)-C(37)	120.0(4)
C(39)-C(38)-H(38)	120.0	C(37)-C(38)-H(38)	120.0
C(40)-C(39)-C(38)	120.0(4)	C(40)-C(39)-H(39)	120.0
C(38)-C(39)-H(39)	120.0	C(41)-C(40)-C(39)	120.2(4)
C(41)-C(40)-H(40)	119.9	C(39)-C(40)-H(40)	119.9
C(40)-C(41)-C(42)	120.6(4)	C(40)-C(41)-H(41)	119.7
C(42)-C(41)-H(41)	119.7	C(37)-C(42)-C(41)	119.5(4)
C(37)-C(42)-H(42)	120.2	C(41)-C(42)-H(42)	120.2
N(4)-C(43)-P(4)	112.0(2)	N(4)-C(43)-H(43A)	109.2
P(4)-C(43)-H(43A)	109.2	N(4)-C(43)-H(43B)	109.2
P(4)-C(43)-H(43B)	109.2	H(43A)-C(43)-H(43B)	107.9

Table 5-4. (cont'd)

C(45)-C(44)-C(49)	118.2(3)	C(45)-C(44)-N(4)	122.3(3)
C(49)-C(44)-N(4)	119.4(3)	C(46)-C(45)-C(44)	121.1(3)
C(46)-C(45)-H(45)	119.4	C(44)-C(45)-H(45)	119.4
C(47)-C(46)-C(45)	120.1(4)	C(47)-C(46)-H(46)	120.0
C(45)-C(46)-H(46)	120.0	C(46)-C(47)-C(48)	119.4(3)
C(46)-C(47)-H(47)	120.3	C(48)-C(47)-H(47)	120.3
C(49)-C(48)-C(47)	120.7(4)	C(49)-C(48)-H(48)	119.6
C(47)-C(48)-H(48)	119.6	C(48)-C(49)-C(44)	120.5(3)
C(48)-C(49)-H(49)	119.7	C(44)-C(49)-H(49)	119.7
N(4)-C(50)-P(3)	118.8(2)	N(4)-C(50)-H(50A)	107.6
P(3)-C(50)-H(50A)	107.6	N(4)-C(50)-H(50B)	107.6
P(3)-C(50)-H(50B)	107.6	H(50A)-C(50)-H(50B)	107.0
C(56)-C(51)-C(52)	118.9(3)	C(56)-C(51)-P(3)	119.6(3)
C(52)-C(51)-P(3)	121.5(3)	C(53)-C(52)-C(51)	119.8(3)
C(53)-C(52)-H(52)	120.1	C(51)-C(52)-H(52)	120.1
C(54)-C(53)-C(52)	120.8(4)	C(54)-C(53)-H(53)	119.6
C(52)-C(53)-H(53)	119.6	C(55)-C(54)-C(53)	119.2(4)
C(55)-C(54)-H(54)	120.4	C(53)-C(54)-H(54)	120.4
C(54)-C(55)-C(56)	120.5(4)	C(54)-C(55)-H(55)	119.7
C(56)-C(55)-H(55)	119.7	C(55)-C(56)-C(51)	120.7(4)
C(55)-C(56)-H(56)	119.6	C(51)-C(56)-H(56)	119.6
F(3)-B(4)-F(4)	110.3(4)	F(3)-B(4)-F(2)	109.9(3)
F(4)-B(4)-F(2)	107.9(4)	F(3)-B(4)-F(1)	110.9(4)
F(4)-B(4)-F(1)	108.6(3)	F(2)-B(4)-F(1)	109.1(4)
F(7)-B(5)-F(8)	110.6(4)	F(7)-B(5)-F(5)	109.1(4)
F(8)-B(5)-F(5)	111.0(4)	F(7)-B(5)-F(6)	109.1(4)
F(8)-B(5)-F(6)	107.7(4)	F(5)-B(5)-F(6)	109.2(3)
N(5)-C(57)-C(58)	179.8(6)	C(57)-C(58)-H(58A)	109.5
C(57)-C(58)-H(58B)	109.5	H(58A)-C(58)-H(58B)	109.5
C(57)-C(58)-H(58C)	109.5	H(58A)-C(58)-H(58C)	109.5
H(58B)-C(58)-H(58C)	109.5	N(6)-C(59)-C(60)	178(2)
N(6A)-C(59A)-C(61)	174(6)	C(59A)-C(61)-H(61A)	109.5
C(59A)-C(61)-H(61B)	109.5	H(61A)-C(61)-H(61B)	109.5
C(59A)-C(61)-H(61C)	109.5	H(61A)-C(61)-H(61C)	109.5
H(61B)-C(61)-H(61C)	109.5		

5.7.2 Crystal data for $[Pd(P^{Cy}{}_2N^{Ph}{}_2)_2](BF_4)_2 \bullet 2(CH_3CN)$ (2cr)

Crystals of $[Pd(P^{Cy}{}_2N^{Ph}{}_2)_2](BF_4)_2 \bullet 2(CH_3CN)$ were found to have crystallized in space group P–1 with half a molecule per asymmetric unit (Z'=0.5). The crystal data was modeled to 5.58% (using 2Θ). The unit cell contains one void (485 $Å^3$) containing 4 molecules of acetonitrile that were modeled using SQUEEZE.

Table 5-5. Crystal data and structure refinement for $[Pd(P^{Cy}{}_2N^{Ph}{}_2)_2](BF_4)_2 \bullet 2(CH_3CN)$ (**2cr**)

Identification code	du002	
Empirical formula	C64 H92 B2 F8 N8 P4 Pd	
Formula weight	1377.39	
Temperature	100(2) K	
Wavelength	0.71073 Å	
Crystal system	Triclinic	
Space group	P-1	
Unit cell dimensions	a = 9.5588(7) Å	α= 94.027(3)°.
	b = 12.4960(9) Å	β= 99.551(2)°.
	c = 14.8568(11) Å	γ = 97.422(2)°.
Volume	1727.7(2) $Å^3$	
Z	1	
Density (calculated)	1.323 Mg/m^3	
Absorption coefficient	0.427 mm^{-1}	
F(000)	720	
Crystal size	0.25 x 0.17 x 0.11 mm^3	
Theta range for data collection	2.37 to 26.56°.	
Index ranges	-11<=h<=11, -15<=k<=15, 0<=l<=18	
Reflections collected	6719	
Independent reflections	6719 [R(int) = 0.0000]	
Completeness to theta = 25.00°	96.0 %	
Absorption correction	Semi-empirical from equivalents	
Max. and min. transmission	0.7454 and 0.6389	
Refinement method	Full-matrix least-squares on F^2	
Data / restraints / parameters	6719 / 0 / 340	
Goodness-of-fit on F^2	1.064	
Final R indices [I>2sigma(I)]	R1 = 0.0558, wR2 = 0.1437	
R indices (all data)	R1 = 0.0706, wR2 = 0.1514	
Extinction coefficient	not measured	
Largest diff. peak and hole	1.378 and -1.364 $e.Å^{-3}$	

Table 5-6. Bond lengths [Å] and angles [°] for $[Pd(P^{Cy}{}_2N^{Ph}{}_2)_2](BF_4)_2 \bullet 2(CH_3CN)$ (**2cr**).

Pd(1)-P(1)	2.3776(11)	Pd(1)-P(1)#1	2.3776(11)
Pd(1)-P(2)#1	2.3878(9)	Pd(1)-P(2)	2.3879(9)
P(1)-C(1)	1.872(4)	P(1)-C(7)	1.878(4)
P(1)-C(22)	1.883(4)	P(2)-C(9)	1.844(5)
P(2)-C(8)	1.867(4)	P(2)-C(15)	1.883(4)
F(1)-B(1)	1.389(7)	F(2)-B(1)	1.407(8)
F(3)-B(1)	1.388(6)	F(4)-B(1)	1.365(7)
N(1)-C(23)	1.405(5)	N(1)-C(8)	1.428(6)
N(1)-C(7)#1	1.436(5)	N(2)-C(16)	1.410(5)
N(2)-C(22)#1	1.436(5)	N(2)-C(15)	1.447(5)
C(30)-C(23)	1.386(7)	C(30)-C(24)	1.399(7)
C(30)-H(30)	0.9300	C(1)-C(6)	1.524(6)
C(1)-C(2)	1.551(5)	C(1)-H(1)	0.9800
C(2)-C(3)	1.522(6)	C(2)-H(2A)	0.9700
C(2)-H(2B)	0.9700	C(3)-C(4)	1.496(8)
C(3)-H(3A)	0.9700	C(3)-H(3B)	0.9700
C(4)-C(5)	1.536(7)	C(4)-H(4A)	0.9700
C(4)-H(4B)	0.9700	C(5)-C(6)	1.524(7)
C(5)-H(5A)	0.9700	C(5)-H(5B)	0.9700
C(6)-H(6A)	0.9700	C(6)-H(6B)	0.9700
C(7)-N(1)#1	1.436(5)	C(7)-H(7A)	0.9700
C(7)-H(7B)	0.9700	C(8)-H(8A)	0.9700
C(8)-H(8B)	0.9700	C(9)-C(10)	1.525(6)
C(9)-C(14)	1.540(5)	C(9)-H(9)	0.9800
C(10)-C(11)	1.534(7)	C(10)-H(10A)	0.9700
C(10)-H(10B)	0.9700	C(11)-C(12)	1.532(7)
C(11)-H(11A)	0.9700	C(11)-H(11B)	0.9700
C(12)-C(13)	1.514(7)	C(12)-H(12A)	0.9700
C(12)-H(12B)	0.9700	C(13)-C(14)	1.534(7)
C(13)-H(13A)	0.9700	C(13)-H(13B)	0.9700
C(14)-H(14A)	0.9700	C(14)-H(14B)	0.9700
C(15)-H(15A)	0.9700	C(15)-H(15B)	0.9700
C(16)-C(17)	1.395(6)	C(16)-C(21)	1.409(6)
C(17)-C(18)	1.394(6)	C(17)-H(17)	0.9300
C(18)-C(19)	1.385(7)	C(18)-H(18)	0.9300

Table 5-6. (cont'd)

C(19)-C(20)	1.387(7)	C(19)-H(19)	0.9300
C(20)-C(21)	1.386(6)	C(20)-H(20)	0.9300
C(21)-H(21)	0.9300	C(22)-N(2)#1	1.436(5)
C(22)-H(22A)	0.9700	C(22)-H(22B)	0.9700
C(23)-C(27)	1.416(6)	C(24)-C(25)	1.396(8)
C(24)-H(24)	0.9300	C(25)-C(26)	1.373(9)
C(25)-H(25)	0.9300	C(26)-C(27)	1.403(7)
C(26)-H(26)	0.9300	C(27)-H(27)	0.9300
P(1)-Pd(1)-P(1)#1	180.00(6)	P(1)-Pd(1)-P(2)#1	81.33(4)
P(1)#1-Pd(1)-P(2)#1	98.67(4)	P(1)-Pd(1)-P(2)	98.67(4)
P(1)#1-Pd(1)-P(2)	81.33(4)	P(2)#1-Pd(1)-P(2)	180.0
C(1)-P(1)-C(7)	99.05(18)	C(1)-P(1)-C(22)	105.90(19)
C(7)-P(1)-C(22)	105.78(17)	C(1)-P(1)-Pd(1)	128.13(13)
C(7)-P(1)-Pd(1)	112.21(15)	C(22)-P(1)-Pd(1)	104.00(13)
C(9)-P(2)-C(8)	98.15(18)	C(9)-P(2)-C(15)	107.10(18)
C(8)-P(2)-C(15)	105.45(18)	C(9)-P(2)-Pd(1)	127.71(13)
C(8)-P(2)-Pd(1)	112.26(12)	C(15)-P(2)-Pd(1)	104.41(12)
C(23)-N(1)-C(8)	123.4(3)	C(23)-N(1)-C(7)#1	122.1(4)
C(8)-N(1)-C(7)#1	113.1(3)	C(16)-N(2)-C(22)#1	120.1(3)
C(16)-N(2)-C(15)	119.2(4)	C(22)#1-N(2)-C(15)	114.3(3)
C(23)-C(30)-C(24)	121.5(5)	C(23)-C(30)-H(30)	119.3
C(24)-C(30)-H(30)	119.3	C(6)-C(1)-C(2)	110.6(3)
C(6)-C(1)-P(1)	112.3(3)	C(2)-C(1)-P(1)	111.0(3)
C(6)-C(1)-H(1)	107.6	C(2)-C(1)-H(1)	107.6
P(1)-C(1)-H(1)	107.6	C(3)-C(2)-C(1)	109.7(4)
C(3)-C(2)-H(2A)	109.7	C(1)-C(2)-H(2A)	109.7
C(3)-C(2)-H(2B)	109.7	C(1)-C(2)-H(2B)	109.7
H(2A)-C(2)-H(2B)	108.2	C(4)-C(3)-C(2)	111.3(4)
C(4)-C(3)-H(3A)	109.4	C(2)-C(3)-H(3A)	109.4
C(4)-C(3)-H(3B)	109.4	C(2)-C(3)-H(3B)	109.4
H(3A)-C(3)-H(3B)	108.0	C(3)-C(4)-C(5)	110.9(4)
C(3)-C(4)-H(4A)	109.5	C(5)-C(4)-H(4A)	109.5
C(3)-C(4)-H(4B)	109.5	C(5)-C(4)-H(4B)	109.5
H(4A)-C(4)-H(4B)	108.0	C(6)-C(5)-C(4)	112.1(4)

Table 5-6. (cont'd)

C(6)-C(5)-H(5A)	109.2	C(4)-C(5)-H(5A)	109.2
C(6)-C(5)-H(5B)	109.2	C(4)-C(5)-H(5B)	109.2
H(5A)-C(5)-H(5B)	107.9	C(5)-C(6)-C(1)	109.8(4)
C(5)-C(6)-H(6A)	109.7	C(1)-C(6)-H(6A)	109.7
C(5)-C(6)-H(6B)	109.7	C(1)-C(6)-H(6B)	109.7
H(6A)-C(6)-H(6B)	108.2	N(1)#1-C(7)-P(1)	114.5(3)
N(1)#1-C(7)-H(7A)	108.6	P(1)-C(7)-H(7A)	108.6
N(1)#1-C(7)-H(7B)	108.6	P(1)-C(7)-H(7B)	108.6
H(7A)-C(7)-H(7B)	107.6	N(1)-C(8)-P(2)	114.8(3)
N(1)-C(8)-H(8A)	108.6	P(2)-C(8)-H(8A)	108.6
N(1)-C(8)-H(8B)	108.6	P(2)-C(8)-H(8B)	108.6
H(8A)-C(8)-H(8B)	107.5	C(10)-C(9)-C(14)	109.7(3)
C(10)-C(9)-P(2)	111.7(3)	C(14)-C(9)-P(2)	113.1(3)
C(10)-C(9)-H(9)	107.3	C(14)-C(9)-H(9)	107.3
P(2)-C(9)-H(9)	107.3	C(9)-C(10)-C(11)	111.0(3)
C(9)-C(10)-H(10A)	109.4	C(11)-C(10)-H(10A)	109.4
C(9)-C(10)-H(10B)	109.4	C(11)-C(10)-H(10B)	109.4
H(10A)-C(10)-H(10B)	108.0	C(12)-C(11)-C(10)	111.6(4)
C(12)-C(11)-H(11A)	109.3	C(10)-C(11)-H(11A)	109.3
C(12)-C(11)-H(11B)	109.3	C(10)-C(11)-H(11B)	109.3
H(11A)-C(11)-H(11B)	108.0	C(13)-C(12)-C(11)	110.7(4)
C(13)-C(12)-H(12A)	109.5	C(11)-C(12)-H(12A)	109.5
C(13)-C(12)-H(12B)	109.5	C(11)-C(12)-H(12B)	109.5
H(12A)-C(12)-H(12B)	108.1	C(12)-C(13)-C(14)	111.7(4)
C(12)-C(13)-H(13A)	109.3	C(14)-C(13)-H(13A)	109.3
C(12)-C(13)-H(13B)	109.3	C(14)-C(13)-H(13B)	109.3
H(13A)-C(13)-H(13B)	108.0	C(13)-C(14)-C(9)	109.3(4)
C(13)-C(14)-H(14A)	109.8	C(9)-C(14)-H(14A)	109.8
C(13)-C(14)-H(14B)	109.8	C(9)-C(14)-H(14B)	109.8
H(14A)-C(14)-H(14B)	108.3	N(2)-C(15)-P(2)	113.0(2)
N(2)-C(15)-H(15A)	109.0	P(2)-C(15)-H(15A)	109.0
N(2)-C(15)-H(15B)	109.0	P(2)-C(15)-H(15B)	109.0
H(15A)-C(15)-H(15B)	107.8	C(17)-C(16)-C(21)	117.7(4)
C(17)-C(16)-N(2)	121.4(4)	C(21)-C(16)-N(2)	120.7(4)
C(18)-C(17)-C(16)	121.4(4)	C(18)-C(17)-H(17)	119.3

Table 5-6. (cont'd)

C(16)-C(17)-H(17)	119.3	C(19)-C(18)-C(17)	120.2(5)
C(19)-C(18)-H(18)	119.9	C(17)-C(18)-H(18)	119.9
C(18)-C(19)-C(20)	119.0(4)	C(18)-C(19)-H(19)	120.5
C(20)-C(19)-H(19)	120.5	C(21)-C(20)-C(19)	121.2(4)
C(21)-C(20)-H(20)	119.4	C(19)-C(20)-H(20)	119.4
C(20)-C(21)-C(16)	120.5(4)	C(20)-C(21)-H(21)	119.8
C(16)-C(21)-H(21)	119.8	N(2)#1-C(22)-P(1)	113.7(3)
N(2)#1-C(22)-H(22A)	108.8	P(1)-C(22)-H(22A)	108.8
N(2)#1-C(22)-H(22B)	108.8	P(1)-C(22)-H(22B)	108.8
H(22A)-C(22)-H(22B)	107.7	C(30)-C(23)-N(1)	121.8(4)
C(30)-C(23)-C(27)	117.5(4)	N(1)-C(23)-C(27)	120.7(5)
C(25)-C(24)-C(30)	120.5(6)	C(25)-C(24)-H(24)	119.7
C(30)-C(24)-H(24)	119.7	C(26)-C(25)-C(24)	118.8(5)
C(26)-C(25)-H(25)	120.6	C(24)-C(25)-H(25)	120.6
C(25)-C(26)-C(27)	121.2(5)	C(25)-C(26)-H(26)	119.4
C(27)-C(26)-H(26)	119.4	C(26)-C(27)-C(23)	120.5(6)
C(26)-C(27)-H(27)	119.8	C(23)-C(27)-H(27)	119.8
F(4)-B(1)-F(3)	111.0(4)	F(4)-B(1)-F(1)	110.1(5)
F(3)-B(1)-F(1)	110.3(5)	F(4)-B(1)-F(2)	109.6(5)
F(3)-B(1)-F(2)	107.5(5)	F(1)-B(1)-F(2)	108.1(4)

Symmetry transformations used to generate equivalent atoms:
#1 -x+1,-y,-z+1

5.7.3 Crystal data for $[Pd(P^{Ph}{}_2N^{Bn}{}_2)_2](BF_4)_2 \bullet 2(CH_3CN)$ (3cr)

Crystals of $[Pd(P^{Ph}{}_2N^{Bn}{}_2)_2](BF_4)_2 \bullet 2(CH_3CN)$ were found to have crystallized in space group P2(1)/n with one molecule per asymmetric unit (Z'=1). The crystal data was modeled to 4.32% (using 2Θ). Two molecules of acetonitrile solvent per unit cell were modeled discretely.

Table 5-7. Crystal data and structure refinement for $[Pd(P^{Ph}_2N^{Bn}_2)_2](BF_4)_2 \bullet 2(CH_3CN)$ (**3cr**)

Identification code	ck_du004_0m	
Empirical formula	C64 H74 B2 F8 N6 P4 Pd	
Formula weight	1331.19	
Temperature	100(2) K	
Wavelength	0.71073 Å	
Crystal system	Monoclinic	
Space group	P2(1)/n	
Unit cell dimensions	a = 10.5769(5) Å	α= 90°.
	b = 24.5160(8) Å	β= 99.188(2)°.
	c = 24.1638(9) Å	γ = 90°.
Volume	6185.4(4) $Å^3$	
Z	4	
Density (calculated)	1.430 Mg/m^3	
Absorption coefficient	0.474 mm^{-1}	
F(000)	2752	
Crystal size	0.29 x 0.08 x 0.06 mm^3	
Theta range for data collection	1.66 to 26.48°.	
Index ranges	-13<=h<=13, -30<=k<=29, -30<=l<=30	
Reflections collected	77773	
Independent reflections	12691 [R(int) = 0.0694]	
Completeness to theta = 25.00°	100.0 %	
Absorption correction	Semi-empirical from equivalents	
Max. and min. transmission	0.9721 and 0.8749	
Refinement method	Full-matrix least-squares on F^2	
Data / restraints / parameters	12691 / 0 / 768	
Goodness-of-fit on F^2	1.078	
Final R indices [I>2sigma(I)]	R1 = 0.0432, wR2 = 0.0778	
R indices (all data)	R1 = 0.0677, wR2 = 0.0866	
Extinction coefficient	not measured	
Largest diff. peak and hole	0.771 and -0.808 $e.Å^{-3}$	

Table 5-8. Bond lengths [Å] and angles [°] for $[Pd(P^{Ph}{}_2N^{Bn}{}_2)_2](BF_4)_2 \bullet 2(CH_3CN)$ (**3cr**).

B(1)-F(2)	1.378(4)	B(1)-F(1)	1.387(4)
B(1)-F(3)	1.392(4)	B(1)-F(4)	1.398(4)
B(2)-F(7)	1.375(4)	B(2)-F(6)	1.382(4)
B(2)-F(5)	1.395(4)	B(2)-F(8)	1.402(4)
C(1)-C(2)	1.387(4)	C(1)-C(6)	1.391(4)
C(1)-P(1)	1.811(3)	C(2)-C(3)	1.388(4)
C(2)-H(2A)	0.9500	C(3)-C(4)	1.388(4)
C(3)-H(3A)	0.9500	C(4)-C(5)	1.375(4)
C(4)-H(4A)	0.9500	C(5)-C(6)	1.395(4)
C(5)-H(5)	0.9500	C(6)-H(6)	0.9500
C(7)-N(1)	1.462(3)	C(7)-P(1)	1.847(3)
C(7)-H(7A)	0.9900	C(7)-H(7B)	0.9900
C(8)-N(1)	1.479(4)	C(8)-C(9)	1.505(4)
C(8)-H(8A)	0.9900	C(8)-H(8B)	0.9900
C(9)-C(10)	1.390(4)	C(9)-C(14)	1.390(4)
C(10)-C(11)	1.385(4)	C(10)-H(10)	0.9500
C(11)-C(12)	1.380(5)	C(11)-H(11)	0.9500
C(12)-C(13)	1.388(5)	C(12)-H(12)	0.9500
C(13)-C(14)	1.381(4)	C(13)-H(13)	0.9500
C(14)-H(14)	0.9500	C(15)-N(1)	1.465(3)
C(15)-P(2)	1.822(3)	C(15)-H(15A)	0.9900
C(15)-H(15B)	0.9900	C(16)-C(17)	1.386(4)
C(16)-C(21)	1.396(4)	C(16)-P(2)	1.799(3)
C(17)-C(18)	1.389(4)	C(17)-H(17)	0.9500
C(18)-C(19)	1.378(4)	C(18)-H(18)	0.9500
C(19)-C(20)	1.380(4)	C(19)-H(19)	0.9500
C(20)-C(21)	1.389(4)	C(20)-H(20)	0.9500
C(21)-H(21)	0.9500	C(22)-N(2)	1.453(3)
C(22)-P(2)	1.846(3)	C(22)-H(22A)	0.9900
C(22)-H(22B)	0.9900	C(23)-N(2)	1.470(4)
C(23)-C(24)	1.511(4)	C(23)-H(23A)	0.9900
C(23)-H(23B)	0.9900	C(24)-C(29)	1.387(4)
C(24)-C(25)	1.394(4)	C(25)-C(26)	1.384(4)
C(25)-H(25)	0.9500	C(26)-C(27)	1.387(5)
C(26)-H(26)	0.9500	C(27)-C(28)	1.374(5)

Table 5-8. (cont'd)

C(27)-H(27)	0.9500	C(28)-C(29)	1.393(4)
C(28)-H(28)	0.9500	C(29)-H(29)	0.9500
C(30)-N(2)	1.459(3)	C(30)-P(1)	1.831(3)
C(30)-H(30A)	0.9900	C(30)-H(30B)	0.9900
C(31)-C(36)	1.392(4)	C(31)-C(32)	1.395(4)
C(31)-P(3)	1.808(3)	C(32)-C(33)	1.383(4)
C(32)-H(32)	0.9500	C(33)-C(34)	1.388(4)
C(33)-H(33)	0.9500	C(34)-C(35)	1.379(4)
C(34)-H(34)	0.9500	C(35)-C(36)	1.392(4)
C(35)-H(35)	0.9500	C(36)-H(36)	0.9500
C(37)-N(3)	1.460(3)	C(37)-P(3)	1.825(3)
C(37)-H(37A)	0.9900	C(37)-H(37B)	0.9900
C(38)-N(3)	1.483(3)	C(38)-C(39)	1.507(4)
C(38)-H(38A)	0.9900	C(38)-H(38B)	0.9900
C(39)-C(40)	1.388(4)	C(39)-C(44)	1.391(4)
C(40)-C(41)	1.391(4)	C(40)-H(40)	0.9500
C(41)-C(42)	1.378(4)	C(41)-H(41)	0.9500
C(42)-C(43)	1.382(4)	C(42)-H(42)	0.9500
C(43)-C(44)	1.382(4)	C(43)-H(43)	0.9500
C(44)-H(44)	0.9500	C(45)-N(3)	1.462(3)
C(45)-P(4)	1.849(3)	C(45)-H(45A)	0.9900
C(45)-H(45B)	0.9900	C(46)-C(51)	1.394(4)
C(46)-C(47)	1.396(4)	C(46)-P(4)	1.802(3)
C(47)-C(48)	1.388(4)	C(47)-H(47)	0.9500
C(48)-C(49)	1.381(5)	C(48)-H(48)	0.9500
C(49)-C(50)	1.388(4)	C(49)-H(49)	0.9500
C(50)-C(51)	1.378(4)	C(50)-H(50)	0.9500
C(51)-H(51)	0.9500	C(52)-N(4)	1.462(3)
C(52)-P(4)	1.819(3)	C(52)-H(52A)	0.9900
C(52)-H(52B)	0.9900	C(53)-N(4)	1.475(4)
C(53)-C(54)	1.506(4)	C(53)-H(53A)	0.9900
C(53)-H(53B)	0.9900	C(54)-C(55)	1.382(4)
C(54)-C(59)	1.392(4)	C(55)-C(56)	1.385(4)
C(55)-H(55)	0.9500	C(56)-C(57)	1.381(4)
C(56)-H(56)	0.9500	C(57)-C(58)	1.383(4)

Table 5-8. (cont'd)

C(57)-H(57)	0.9500	C(58)-C(59)	1.382(4)
C(58)-H(58)	0.9500	C(59)-H(59)	0.9500
C(60)-N(4)	1.464(3)	C(60)-P(3)	1.848(3)
C(60)-H(60A)	0.9900	C(60)-H(60B)	0.9900
N(1)-H(1)	0.9300	N(2)-H(2)	0.9300
N(3)-H(3)	0.9300	N(4)-H(4)	0.9300
P(1)-Pd(1)	2.3117(7)	P(2)-Pd(1)	2.2870(7)
P(3)-Pd(1)	2.3023(7)	P(4)-Pd(1)	2.2950(7)
C(61)-N(5)	1.133(4)	C(61)-C(62)	1.462(5)
C(62)-H(62A)	0.9800	C(62)-H(62B)	0.9800
C(62)-H(62C)	0.9800	C(63)-N(6)	1.144(4)
C(63)-C(64)	1.446(5)	C(64)-H(64A)	0.9800
C(64)-H(64B)	0.9800	C(64)-H(64C)	0.9800
F(2)-B(1)-F(1)	109.9(3)	F(2)-B(1)-F(3)	110.4(3)
F(1)-B(1)-F(3)	108.9(3)	F(2)-B(1)-F(4)	110.0(2)
F(1)-B(1)-F(4)	108.9(3)	F(3)-B(1)-F(4)	108.8(3)
F(7)-B(2)-F(6)	110.7(3)	F(7)-B(2)-F(5)	110.5(3)
F(6)-B(2)-F(5)	109.8(3)	F(7)-B(2)-F(8)	109.0(3)
F(6)-B(2)-F(8)	108.1(3)	F(5)-B(2)-F(8)	108.7(3)
C(2)-C(1)-C(6)	120.3(3)	C(2)-C(1)-P(1)	116.0(2)
C(6)-C(1)-P(1)	123.7(2)	C(1)-C(2)-C(3)	120.0(3)
C(1)-C(2)-H(2A)	120.0	C(3)-C(2)-H(2A)	120.0
C(4)-C(3)-C(2)	119.9(3)	C(4)-C(3)-H(3A)	120.0
C(2)-C(3)-H(3A)	120.0	C(5)-C(4)-C(3)	120.0(3)
C(5)-C(4)-H(4A)	120.0	C(3)-C(4)-H(4A)	120.0
C(4)-C(5)-C(6)	120.8(3)	C(4)-C(5)-H(5)	119.6
C(6)-C(5)-H(5)	119.6	C(1)-C(6)-C(5)	119.0(3)
C(1)-C(6)-H(6)	120.5	C(5)-C(6)-H(6)	120.5
N(1)-C(7)-P(1)	116.27(19)	N(1)-C(7)-H(7A)	108.2
P(1)-C(7)-H(7A)	108.2	N(1)-C(7)-H(7B)	108.2
P(1)-C(7)-H(7B)	108.2	H(7A)-C(7)-H(7B)	107.4
N(1)-C(8)-C(9)	112.6(2)	N(1)-C(8)-H(8A)	109.1
C(9)-C(8)-H(8A)	109.1	N(1)-C(8)-H(8B)	109.1
C(9)-C(8)-H(8B)	109.1	H(8A)-C(8)-H(8B)	107.8

Table 5-8. (cont'd)

C(10)-C(9)-C(14)	119.0(3)	C(10)-C(9)-C(8)	121.3(3)
C(14)-C(9)-C(8)	119.7(3)	C(11)-C(10)-C(9)	120.5(3)
C(11)-C(10)-H(10)	119.8	C(9)-C(10)-H(10)	119.8
C(12)-C(11)-C(10)	120.3(3)	C(12)-C(11)-H(11)	119.9
C(10)-C(11)-H(11)	119.9	C(11)-C(12)-C(13)	119.4(3)
C(11)-C(12)-H(12)	120.3	C(13)-C(12)-H(12)	120.3
C(14)-C(13)-C(12)	120.5(3)	C(14)-C(13)-H(13)	119.8
C(12)-C(13)-H(13)	119.8	C(13)-C(14)-C(9)	120.4(3)
C(13)-C(14)-H(14)	119.8	C(9)-C(14)-H(14)	119.8
N(1)-C(15)-P(2)	111.61(19)	N(1)-C(15)-H(15A)	109.3
P(2)-C(15)-H(15A)	109.3	N(1)-C(15)-H(15B)	109.3
P(2)-C(15)-H(15B)	109.3	H(15A)-C(15)-H(15B)	108.0
C(17)-C(16)-C(21)	120.0(3)	C(17)-C(16)-P(2)	123.4(2)
C(21)-C(16)-P(2)	116.1(2)	C(16)-C(17)-C(18)	119.6(3)
C(16)-C(17)-H(17)	120.2	C(18)-C(17)-H(17)	120.2
C(19)-C(18)-C(17)	120.6(3)	C(19)-C(18)-H(18)	119.7
C(17)-C(18)-H(18)	119.7	C(18)-C(19)-C(20)	119.8(3)
C(18)-C(19)-H(19)	120.1	C(20)-C(19)-H(19)	120.1
C(19)-C(20)-C(21)	120.5(3)	C(19)-C(20)-H(20)	119.7
C(21)-C(20)-H(20)	119.7	C(20)-C(21)-C(16)	119.4(3)
C(20)-C(21)-H(21)	120.3	C(16)-C(21)-H(21)	120.3
N(2)-C(22)-P(2)	112.98(19)	N(2)-C(22)-H(22A)	109.0
P(2)-C(22)-H(22A)	109.0	N(2)-C(22)-H(22B)	109.0
P(2)-C(22)-H(22B)	109.0	H(22A)-C(22)-H(22B)	107.8
N(2)-C(23)-C(24)	109.9(2)	N(2)-C(23)-H(23A)	109.7
C(24)-C(23)-H(23A)	109.7	N(2)-C(23)-H(23B)	109.7
C(24)-C(23)-H(23B)	109.7	H(23A)-C(23)-H(23B)	108.2
C(29)-C(24)-C(25)	118.5(3)	C(29)-C(24)-C(23)	121.9(3)
C(25)-C(24)-C(23)	119.5(3)	C(26)-C(25)-C(24)	120.6(3)
C(26)-C(25)-H(25)	119.7	C(24)-C(25)-H(25)	119.7
C(25)-C(26)-C(27)	120.0(3)	C(25)-C(26)-H(26)	120.0
C(27)-C(26)-H(26)	120.0	C(28)-C(27)-C(26)	120.0(3)
C(28)-C(27)-H(27)	120.0	C(26)-C(27)-H(27)	120.0
C(27)-C(28)-C(29)	119.9(3)	C(27)-C(28)-H(28)	120.1
C(29)-C(28)-H(28)	120.1	C(24)-C(29)-C(28)	120.9(3)

Table 5-8. (cont'd)

C(24)-C(29)-H(29)	119.6	C(28)-C(29)-H(29)	119.6
N(2)-C(30)-P(1)	107.26(19)	N(2)-C(30)-H(30A)	110.3
P(1)-C(30)-H(30A)	110.3	N(2)-C(30)-H(30B)	110.3
P(1)-C(30)-H(30B)	110.3	H(30A)-C(30)-H(30B)	108.5
C(36)-C(31)-C(32)	119.5(3)	C(36)-C(31)-P(3)	123.0(2)
C(32)-C(31)-P(3)	117.5(2)	C(33)-C(32)-C(31)	120.4(3)
C(33)-C(32)-H(32)	119.8	C(31)-C(32)-H(32)	119.8
C(32)-C(33)-C(34)	119.9(3)	C(32)-C(33)-H(33)	120.1
C(34)-C(33)-H(33)	120.1	C(35)-C(34)-C(33)	120.1(3)
C(35)-C(34)-H(34)	119.9	C(33)-C(34)-H(34)	119.9
C(34)-C(35)-C(36)	120.3(3)	C(34)-C(35)-H(35)	119.8
C(36)-C(35)-H(35)	119.8	C(31)-C(36)-C(35)	119.8(3)
C(31)-C(36)-H(36)	120.1	C(35)-C(36)-H(36)	120.1
N(3)-C(37)-P(3)	110.58(18)	N(3)-C(37)-H(37A)	109.5
P(3)-C(37)-H(37A)	109.5	N(3)-C(37)-H(37B)	109.5
P(3)-C(37)-H(37B)	109.5	H(37A)-C(37)-H(37B)	108.1
N(3)-C(38)-C(39)	113.2(2)	N(3)-C(38)-H(38A)	108.9
C(39)-C(38)-H(38A)	108.9	N(3)-C(38)-H(38B)	108.9
C(39)-C(38)-H(38B)	108.9	H(38A)-C(38)-H(38B)	107.7
C(40)-C(39)-C(44)	119.0(3)	C(40)-C(39)-C(38)	122.0(3)
C(44)-C(39)-C(38)	118.8(3)	C(39)-C(40)-C(41)	120.5(3)
C(39)-C(40)-H(40)	119.8	C(41)-C(40)-H(40)	119.8
C(42)-C(41)-C(40)	120.1(3)	C(42)-C(41)-H(41)	120.0
C(40)-C(41)-H(41)	120.0	C(41)-C(42)-C(43)	119.6(3)
C(41)-C(42)-H(42)	120.2	C(43)-C(42)-H(42)	120.2
C(42)-C(43)-C(44)	120.7(3)	C(42)-C(43)-H(43)	119.6
C(44)-C(43)-H(43)	119.6	C(43)-C(44)-C(39)	120.1(3)
C(43)-C(44)-H(44)	120.0	C(39)-C(44)-H(44)	120.0
N(3)-C(45)-P(4)	114.69(19)	N(3)-C(45)-H(45A)	108.6
P(4)-C(45)-H(45A)	108.6	N(3)-C(45)-H(45B)	108.6
P(4)-C(45)-H(45B)	108.6	H(45A)-C(45)-H(45B)	107.6
C(51)-C(46)-C(47)	119.6(3)	C(51)-C(46)-P(4)	115.8(2)
C(47)-C(46)-P(4)	124.6(2)	C(48)-C(47)-C(46)	119.1(3)
C(48)-C(47)-H(47)	120.4	C(46)-C(47)-H(47)	120.4
C(49)-C(48)-C(47)	120.9(3)	C(49)-C(48)-H(48)	119.6

Table 5-8. (cont'd)

C(47)-C(48)-H(48)	119.6	C(48)-C(49)-C(50)	120.0(3)
C(48)-C(49)-H(49)	120.0	C(50)-C(49)-H(49)	120.0
C(51)-C(50)-C(49)	119.6(3)	C(51)-C(50)-H(50)	120.2
C(49)-C(50)-H(50)	120.2	C(50)-C(51)-C(46)	120.7(3)
C(50)-C(51)-H(51)	119.7	C(46)-C(51)-H(51)	119.7
N(4)-C(52)-P(4)	109.59(18)	N(4)-C(52)-H(52A)	109.8
P(4)-C(52)-H(52A)	109.8	N(4)-C(52)-H(52B)	109.8
P(4)-C(52)-H(52B)	109.8	H(52A)-C(52)-H(52B)	108.2
N(4)-C(53)-C(54)	112.9(2)	N(4)-C(53)-H(53A)	109.0
C(54)-C(53)-H(53A)	109.0	N(4)-C(53)-H(53B)	109.0
C(54)-C(53)-H(53B)	109.0	H(53A)-C(53)-H(53B)	107.8
C(55)-C(54)-C(59)	118.8(3)	C(55)-C(54)-C(53)	120.5(3)
C(59)-C(54)-C(53)	120.6(3)	C(54)-C(55)-C(56)	120.7(3)
C(54)-C(55)-H(55)	119.6	C(56)-C(55)-H(55)	119.6
C(57)-C(56)-C(55)	119.9(3)	C(57)-C(56)-H(56)	120.1
C(55)-C(56)-H(56)	120.1	C(56)-C(57)-C(58)	120.1(3)
C(56)-C(57)-H(57)	120.0	C(58)-C(57)-H(57)	120.0
C(59)-C(58)-C(57)	119.8(3)	C(59)-C(58)-H(58)	120.1
C(57)-C(58)-H(58)	120.1	C(58)-C(59)-C(54)	120.7(3)
C(58)-C(59)-H(59)	119.7	C(54)-C(59)-H(59)	119.7
N(4)-C(60)-P(3)	114.74(19)	N(4)-C(60)-H(60A)	108.6
P(3)-C(60)-H(60A)	108.6	N(4)-C(60)-H(60B)	108.6
P(3)-C(60)-H(60B)	108.6	H(60A)-C(60)-H(60B)	107.6
C(7)-N(1)-C(15)	115.1(2)	C(7)-N(1)-C(8)	108.9(2)
C(15)-N(1)-C(8)	110.0(2)	C(7)-N(1)-H(1)	107.5
C(15)-N(1)-H(1)	107.5	C(8)-N(1)-H(1)	107.5
C(22)-N(2)-C(30)	114.6(2)	C(22)-N(2)-C(23)	112.1(2)
C(30)-N(2)-C(23)	114.0(2)	C(22)-N(2)-H(2)	105.0
C(30)-N(2)-H(2)	105.0	C(23)-N(2)-H(2)	105.0
C(37)-N(3)-C(45)	113.7(2)	C(37)-N(3)-C(38)	109.8(2)
C(45)-N(3)-C(38)	109.8(2)	C(37)-N(3)-H(3)	107.8
C(45)-N(3)-H(3)	107.8	C(38)-N(3)-H(3)	107.8
C(52)-N(4)-C(60)	115.4(2)	C(52)-N(4)-C(53)	110.0(2)
C(60)-N(4)-C(53)	110.6(2)	C(52)-N(4)-H(4)	106.8
C(60)-N(4)-H(4)	106.8	C(53)-N(4)-H(4)	106.8

Table 5-8. (cont'd)

C(1)-P(1)-C(30)	109.75(13)	C(1)-P(1)-C(7)	102.76(13)
C(30)-P(1)-C(7)	103.06(13)	C(1)-P(1)-Pd(1)	116.69(9)
C(30)-P(1)-Pd(1)	113.90(9)	C(7)-P(1)-Pd(1)	109.19(9)
C(16)-P(2)-C(15)	110.09(13)	C(16)-P(2)-C(22)	99.07(12)
C(15)-P(2)-C(22)	105.83(13)	C(16)-P(2)-Pd(1)	118.90(9)
C(15)-P(2)-Pd(1)	113.35(9)	C(22)-P(2)-Pd(1)	107.78(9)
C(31)-P(3)-C(37)	108.89(13)	C(31)-P(3)-C(60)	102.16(13)
C(37)-P(3)-C(60)	107.00(13)	C(31)-P(3)-Pd(1)	117.15(9)
C(37)-P(3)-Pd(1)	112.91(9)	C(60)-P(3)-Pd(1)	107.73(9)
C(46)-P(4)-C(52)	109.80(13)	C(46)-P(4)-C(45)	102.38(13)
C(52)-P(4)-C(45)	104.04(13)	C(46)-P(4)-Pd(1)	116.91(9)
C(52)-P(4)-Pd(1)	112.61(10)	C(45)-P(4)-Pd(1)	109.85(9)
P(2)-Pd(1)-P(4)	164.70(3)	P(2)-Pd(1)-P(3)	101.00(3)
P(4)-Pd(1)-P(3)	80.94(3)	P(2)-Pd(1)-P(1)	81.09(3)
P(4)-Pd(1)-P(1)	100.91(3)	P(3)-Pd(1)-P(1)	165.37(3)
N(5)-C(61)-C(62)	178.6(4)	C(61)-C(62)-H(62A)	109.5
C(61)-C(62)-H(62B)	109.5	H(62A)-C(62)-H(62B)	109.5
C(61)-C(62)-H(62C)	109.5	H(62A)-C(62)-H(62C)	109.5
H(62B)-C(62)-H(62C)	109.5	N(6)-C(63)-C(64)	179.7(4)
C(63)-C(64)-H(64A)	109.5	C(63)-C(64)-H(64B)	109.5
H(64A)-C(64)-H(64B)	109.5	C(63)-C(64)-H(64C)	109.5
H(64A)-C(64)-H(64C)	109.5	H(64B)-C(64)-H(64C)	109.5

5.7.4 Crystal data for $[Pd(P^{Me}{}_2N^{Ph}{}_2)_2](BF_4)_2 \bullet 2(CH_3CN)$ (4)

Crystals of $[Pd(P^{Me}{}_2N^{Ph}{}_2)_2](BF_4)_2 \bullet 2(CH_3CN)$ were found to have crystallized in space group P–1 with half a molecule per asymmetric unit (Z'=0.5). The crystal data was modeled to 2.14% (using 2Θ). Two molecules of acetonitrile solvent per unit cell were modeled discretely.

Table 5-9. Crystal data and structure refinement for $[Pd(P^{Me}{}_2N^{Ph}{}_2)_2](BF_4)_2 \bullet 2(CH_3CN)$ (**4cr**).

Identification code	du003_0m	
Empirical formula	C44 H60 B2 F8 N8 P4 Pd	
Formula weight	1104.90	
Temperature	100(2) K	
Wavelength	0.71073 Å	
Crystal system	Monoclinic	
Space group	P2(1)/c	
Unit cell dimensions	a = 14.0539(7) Å	α= 90°.
	b = 10.0080(5) Å	β= 108.980(2)°.
	c = 18.7335(10) Å	γ = 90°.
Volume	2491.6(2) $Å^3$	
Z	2	
Density (calculated)	1.473 Mg/m^3	
Absorption coefficient	0.572 mm^{-1}	
F(000)	1136	
Crystal size	0.20 x 0.11 x 0.09 mm^3	
Theta range for data collection	2.30 to 26.42°.	
Index ranges	-17<=h<=17, -12<=k<=12, -23<=l<=23	
Reflections collected	21606	
Independent reflections	5130 [R(int) = 0.0219]	
Completeness to theta = 25.00°	99.9 %	
Absorption correction	Semi-empirical from equivalents	
Max. and min. transmission	0.9503 and 0.8942	
Refinement method	Full-matrix least-squares on F^2	
Data / restraints / parameters	5130 / 0 / 319	
Goodness-of-fit on F^2	1.047	
Final R indices [I>2sigma(I)]	R1 = 0.0214, wR2 = 0.0513	
R indices (all data)	R1 = 0.0258, wR2 = 0.0535	
Extinction coefficient	not measured	
Largest diff. peak and hole	0.436 and -0.338 $e.Å^{-3}$	

Table 5-10. Bond lengths [Å] and angles [°] for $[Pd(P^{Me}{}_2N^{Ph}{}_2)_2](BF_4)_2 \bullet 2(CH_3CN)$ (**4cr**) .

Pd(1)-P(2)	2.3254(4)	Pd(1)-P(2)#1	2.3254(4)
Pd(1)-P(1)#1	2.3396(4)	Pd(1)-P(1)	2.3396(4)
P(1)-C(8)	1.8090(16)	P(1)-C(9)	1.8381(15)
P(1)-C(7)	1.8606(15)	P(2)-C(17)	1.8081(16)
P(2)-C(16)	1.8408(15)	P(2)-C(18)	1.8615(16)
N(1)-C(1)	1.4131(19)	N(1)-C(18)	1.452(2)
N(1)-C(7)	1.456(2)	N(2)-C(10)	1.4379(18)
N(2)-C(9)	1.4562(19)	N(2)-C(16)	1.4660(19)
C(1)-C(6)	1.401(2)	C(1)-C(2)	1.404(2)
C(2)-C(3)	1.387(2)	C(2)-H(2)	0.9500
C(3)-C(4)	1.385(2)	C(3)-H(3)	0.9500
C(4)-C(5)	1.383(2)	C(4)-H(4)	0.9500
C(5)-C(6)	1.391(2)	C(5)-H(5)	0.9500
C(6)-H(6)	0.9500	C(7)-H(7A)	0.9900
C(7)-H(7B)	0.9900	C(8)-H(8A)	0.9800
C(8)-H(8B)	0.9800	C(8)-H(8C)	0.9800
C(9)-H(9A)	0.9900	C(9)-H(9B)	0.9900
C(10)-C(11)	1.388(2)	C(10)-C(15)	1.390(2)
C(11)-C(12)	1.391(2)	C(11)-H(11)	0.9500
C(12)-C(13)	1.379(3)	C(12)-H(12)	0.9500
C(13)-C(14)	1.382(3)	C(13)-H(13)	0.9500
C(14)-C(15)	1.387(2)	C(14)-H(14)	0.9500
C(15)-H(15)	0.9500	C(16)-H(16A)	0.9900
C(16)-H(16B)	0.9900	C(17)-H(17A)	0.9800
C(17)-H(17B)	0.9800	C(17)-H(17C)	0.9800
C(18)-H(18A)	0.9900	C(18)-H(18B)	0.9900
F(1)-B(1)	1.394(2)	F(2)-B(1)	1.374(2)
F(3)-B(1)	1.388(2)	F(4)-B(1)	1.381(2)
N(3)-C(19)	1.140(3)	C(19)-C(20)	1.453(3)
C(20)-H(20A)	0.97(3)	C(20)-H(20B)	0.92(3)
C(20)-H(20C)	0.94(3)	N(4)-C(21)	1.112(3)
C(21)-C(22)	1.432(3)	C(22)-H(22A)	0.9800
C(22)-H(22B)	0.9800	C(22)-H(22C)	0.9800
P(2)-Pd(1)-P(2)#1	179.999(16)	P(2)-Pd(1)-P(1)#1	99.777(14)

Table 5-10. (cont'd)

P(2)#1-Pd(1)-P(1)#1	80.222(14)	P(2)-Pd(1)-P(1)	80.225(14)
P(2)#1-Pd(1)-P(1)	99.776(14)	P(1)#1-Pd(1)-P(1)	180.0
C(8)-P(1)-C(9)	101.10(7)	C(8)-P(1)-C(7)	103.44(8)
C(9)-P(1)-C(7)	103.35(7)	C(8)-P(1)-Pd(1)	125.51(6)
C(9)-P(1)-Pd(1)	109.99(5)	C(7)-P(1)-Pd(1)	111.03(5)
C(17)-P(2)-C(16)	99.61(8)	C(17)-P(2)-C(18)	104.26(8)
C(16)-P(2)-C(18)	103.97(7)	C(17)-P(2)-Pd(1)	124.24(6)
C(16)-P(2)-Pd(1)	112.45(5)	C(18)-P(2)-Pd(1)	110.16(5)
C(1)-N(1)-C(18)	118.24(13)	C(1)-N(1)-C(7)	116.74(13)
C(18)-N(1)-C(7)	111.65(12)	C(10)-N(2)-C(9)	113.82(12)
C(10)-N(2)-C(16)	110.85(11)	C(9)-N(2)-C(16)	114.71(12)
C(6)-C(1)-C(2)	117.93(14)	C(6)-C(1)-N(1)	121.66(14)
C(2)-C(1)-N(1)	120.35(14)	C(3)-C(2)-C(1)	120.69(16)
C(3)-C(2)-H(2)	119.7	C(1)-C(2)-H(2)	119.7
C(4)-C(3)-C(2)	121.01(16)	C(4)-C(3)-H(3)	119.5
C(2)-C(3)-H(3)	119.5	C(5)-C(4)-C(3)	118.73(15)
C(5)-C(4)-H(4)	120.6	C(3)-C(4)-H(4)	120.6
C(4)-C(5)-C(6)	121.19(16)	C(4)-C(5)-H(5)	119.4
C(6)-C(5)-H(5)	119.4	C(5)-C(6)-C(1)	120.43(15)
C(5)-C(6)-H(6)	119.8	C(1)-C(6)-H(6)	119.8
N(1)-C(7)-P(1)	113.05(10)	N(1)-C(7)-H(7A)	109.0
P(1)-C(7)-H(7A)	109.0	N(1)-C(7)-H(7B)	109.0
P(1)-C(7)-H(7B)	109.0	H(7A)-C(7)-H(7B)	107.8
P(1)-C(8)-H(8A)	109.5	P(1)-C(8)-H(8B)	109.5
H(8A)-C(8)-H(8B)	109.5	P(1)-C(8)-H(8C)	109.5
H(8A)-C(8)-H(8C)	109.5	H(8B)-C(8)-H(8C)	109.5
N(2)-C(9)-P(1)	111.69(10)	N(2)-C(9)-H(9A)	109.3
P(1)-C(9)-H(9A)	109.3	N(2)-C(9)-H(9B)	109.3
P(1)-C(9)-H(9B)	109.3	H(9A)-C(9)-H(9B)	107.9
C(11)-C(10)-C(15)	119.43(14)	C(11)-C(10)-N(2)	122.43(14)
C(15)-C(10)-N(2)	118.14(13)	C(10)-C(11)-C(12)	119.97(16)
C(10)-C(11)-H(11)	120.0	C(12)-C(11)-H(11)	120.0
C(13)-C(12)-C(11)	120.50(16)	C(13)-C(12)-H(12)	119.7
C(11)-C(12)-H(12)	119.7	C(12)-C(13)-C(14)	119.51(16)
C(12)-C(13)-H(13)	120.2	C(14)-C(13)-H(13)	120.2

Table 5-10. (cont'd)

C(13)-C(14)-C(15)	120.54(16)	C(13)-C(14)-H(14)	119.7
C(15)-C(14)-H(14)	119.7	C(14)-C(15)-C(10)	120.01(15)
C(14)-C(15)-H(15)	120.0	C(10)-C(15)-H(15)	120.0
N(2)-C(16)-P(2)	114.25(10)	N(2)-C(16)-H(16A)	108.7
P(2)-C(16)-H(16A)	108.7	N(2)-C(16)-H(16B)	108.7
P(2)-C(16)-H(16B)	108.7	H(16A)-C(16)-H(16B)	107.6
P(2)-C(17)-H(17A)	109.5	P(2)-C(17)-H(17B)	109.5
H(17A)-C(17)-H(17B)	109.5	P(2)-C(17)-H(17C)	109.5
H(17A)-C(17)-H(17C)	109.5	H(17B)-C(17)-H(17C)	109.5
N(1)-C(18)-P(2)	113.63(10)	N(1)-C(18)-H(18A)	108.8
P(2)-C(18)-H(18A)	108.8	N(1)-C(18)-H(18B)	108.8
P(2)-C(18)-H(18B)	108.8	H(18A)-C(18)-H(18B)	107.7
F(2)-B(1)-F(4)	109.94(15)	F(2)-B(1)-F(3)	110.07(15)
F(4)-B(1)-F(3)	109.67(15)	F(2)-B(1)-F(1)	109.84(15)
F(4)-B(1)-F(1)	108.74(15)	F(3)-B(1)-F(1)	108.55(15)
N(3)-C(19)-C(20)	179.3(2)	C(19)-C(20)-H(20A)	109.4(14)
C(19)-C(20)-H(20B)	109.2(16)	H(20A)-C(20)-H(20B)	109(2)
C(19)-C(20)-H(20C)	108.3(16)	H(20A)-C(20)-H(20C)	112(2)
H(20B)-C(20)-H(20C)	109(2)	N(4)-C(21)-C(22)	178.7(3)
C(21)-C(22)-H(22A)	109.5	C(21)-C(22)-H(22B)	109.5
H(22A)-C(22)-H(22B)	109.5	C(21)-C(22)-H(22C)	109.5
H(22A)-C(22)-H(22C)	109.5	H(22B)-C(22)-H(22C)	109.5

Symmetry transformations used to generate equivalent atoms:
#1 -x,-y,-z

5.7.5 Copyright Note

Much of the material for this chapter comes directly from a manuscript entitled "Synthesis, structural, and electrocatalytic reduction studies of $[Pd(P_2N_2)_2]^{2+}$ complexes," by Candace S. Seu, David Ung, Michael D. Doud, Curtis E. Moore, Arnold L. Rheingold, and Clifford P. Kubiak. This manuscript is currently in preparation. The dissertation author is the primary author of this manuscript.

Chapter 6

Recommendations for future work

6.1 Introduction

One of the few downsides to graduating that I have found is that leaving a lab also entails leaving behind an abundance of unanswered questions and unfinished ideas. My goals in this chapter are to 1) illustrate how the studies described in this thesis might guide future work on catalyst design for CO_2-based solar fuel reactions, and 2) briefly describe some projects that future Kubiak lab researchers may find worthwhile.

6.2 Developing $[Ni(P_2N_2)_2]^{2+}$ systems for electro-oxidation

In Chapter 2 we showed that formate oxidation by $[Ni(P_2N_2)_2]^{2+}$ proceeds through a separated transfer of two electrons and one proton instead of a hydride transfer. The advantage of this mechanism is that it avoids the formation of a metal hydride thermodynamic sink. Our attempts to extend this oxidation chemistry to other substrates and

solvents were mostly unsuccessful, but revealed several details about the reactivity of these complexes.

First, we discovered that the $[Ni(P_2N_2)_2]^{2+}$ complexes do not oxidize hydrazine, formic acid, methylene glycol, or methanol on an electrochemical timescale, even at elevated temperatures and high concentrations (60 °C in pure methanol in the last case). All reactions are known to be thermodynamically favorable on the basis of their hydricities or reduction potentials;[1,2] the lack of oxidation is thus a kinetic problem. We believe that the formic acid case in particular shows that substrate binding to the metal center is highly favorable for anionic species and less favorable for neutral species, and that metal-substrate binding is a prerequisite for oxidation. This limits the scope of substrates that can be electrochemically oxidized.

Second, we made several attempts to produce water-soluble P_2N_2s in hopes of exploring how the change to a fuel cell-compatible solvent environment might affect the rate and mechanism of formic acid, methylene glycol, and methanol oxidation.[3] In these studies, we explored the effects of placing sulfonates and carboxylic acid groups on the amine substituent (**Figure 6-1**). We found that these functional groups were very effective in enhancing the water solubility of the molecules. However, we found it difficult to purify and isolate the resulting Ni complexes, as addition of any non-polar solvent tended to precipitate the ligand separately from the complex.

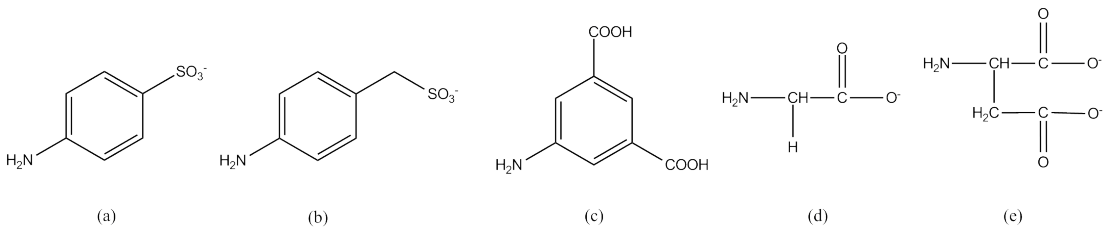

Figure 6-1. Primary amines used to synthesize water-soluble P_2N_2 ligands: (a) 4-sulfanilic acid, (b) 4-aminobenzylsulfonic acid, (c) 5-amino isophthalic acid, (d) glycine, (e) aspartic acid.

The carboxylic acid ligands were more stable than the sulfonate ligands, and we were able to synthesize the red $[Ni(P_2N_2)_2]^{2+}$ complexes after deprotonating the ligands with multiple equivalents of Na_2CO_3. Cyclic voltammograms of complexes **c** and **d**, however, showed no electrochemical features between a potential range of +1.5 to –1.3 V vs. SCE. We believe this is due to folding of the amine substituents over the Ni such that the carboxylic acid groups bond to the metal center and displace the second P_2N_2 ligand. This ion-paired bonding interaction is stabilized by the multi-dentate nature of the ligand, and the resulting high kinetic barriers to ligand dissociation drives the Ni reduction potentials very far negative, past the solvent window.

The high binding affinity of anionic groups for the metal center places limitations on their use as solubilizing agents, and one possible project would deal with finding an alternative. One strategy is to place the carboxylic acid groups at the meta- or para-positions of the phosphino phenyl. This would prevent them from folding up and chelating to the metal. However, it is unclear whether these groups might then intermolecularly bind to other Ni centers. An alternate strategy would be to employ cationic groups such as methylated pyridine as the solubilizing agent.

A second, more ambitious project deals with probing the PCET transfer nature of the formate oxidation mechanism. The oxidation proceeds only as fast at the proton can be transferred, and we have seen that increasing the strength of the acceptor amine increases the rate of proton transfer. It follows that increasing the strength of the carbon donor—that is, making it more acidic—should also increase the rate of proton transfer. We attempted to achieve this by employing phosphines containing electron-withdrawing substituents, reasoning that this would favor delocalization of the formate electrons onto the metal, weakening the C–H bond. The relative strengths of the phosphine ligands were estimated by comparing the pK_as of analogous alcohols (**Figure 6-2**).

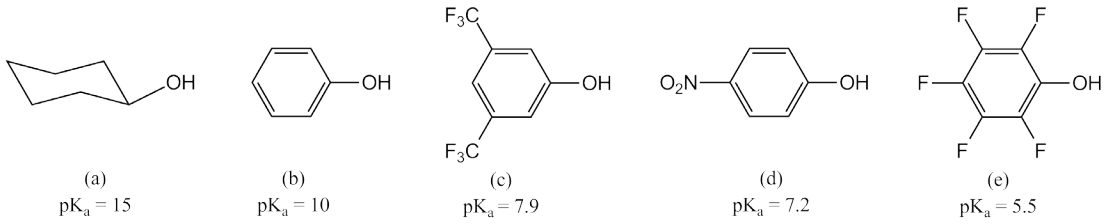

Figure 6-2. pK_as of alcohols used to estimate the relative donating abilities of various primary phosphines to be used in the synthesis of P_2N_2 ligands, (a) cyclohexanol, (b) phenol, (c) 3,5-bis(trifluoromethyl)phenol, (d) 4-nitrophenol, (e) 2,3,4,5,6-pentafluorophenol.

The electron-withdrawing primary phosphines required to make such ligands are not commercially available, and we attempted to synthesize these phosphines using two different approaches. Pd-mediated cross-coupling of fluorinated aryl iodides and diethylphosphite followed by $LiAlH_4$ reduction gave just enough of the primary phosphine to make us grateful for the fume hood,[4] but was ultimately unsuccessful due to the stability of the P=O bond against reduction. Similar reductions had been previously demonstrated with other phosphine oxides,[5–7] and we hypothesize that the electron withdrawing groups on the aryl substituent lower the energy of the phosphorus orbitals, increasing their overlap with oxygen and strengthening the double bond.

The second approach involved nucleophilic aromatic substitution of $KP(TMS)_2$ phosphide onto a fluorinated aromatic ring,[8] followed by hydrolysis of the TMS groups.[9] The advantage of this preparation is that it allows inclusion of functional groups that are sensitive to reduction, such as $-NO_2$. Although the substitution at low temperature produced an observable color change, we were unable to isolate and observe any product by ^{31}P NMR. It is highly possible that trace water in the THF solvent resulted in hydrolysis of the most of the phosphide to PH_3; however, we did not have time to test these reaction conditions.

An alternate, third approach to synthesizing these primary phosphines involved nucleophilic attack of a Grignard reagent on PCl_3[10,11] or $P(OR)_3$,[12,13] followed by $LiAlH_4$ reduction.[14,15] The disadvantage of this reaction is that it has the ability to form secondary and

tertiary phosphines, hence our attempts to synthesize the phosphine using the first two methods.[16] That said, it should be possible to disfavor these other products by carefully controlling the reaction temperature, concentration, and order of addition, or possibly (it seems) by using the less reactive $P(OPh)_3$ as the phosphorus source. Had I been a wiser phosphine chemist, I probably would have opted to start with this method from the beginning. I am ambivalent about the fact that I am not, and I wish the best of luck to those brave students who set out on this path. I will also add one warning to this project: we know that some P_2N_2 ligands are prone to dissociation in the presence of formate, and there is a possibility that these more weakly donating ligands may not form stable complexes.

6.3 Developing new CO_2/HCOOH reduction electrocatalysts

Professor Josh Figueroa was not the first person to come up with the idea or present it in my class lectures, but he is the person I will forever think of when I say to myself: electronic structure determines reactivity. If we are to synthesize effective catalysts for the reduction of CO_2 to formic acid, we will need to become much more sophisticated in our understanding and design of catalyst electronic structure. The first step towards this is to identify which aspects of reactivity need to improved. The second step is to then determine how the electronic structure can be tuned or optimized to provide this reactivity.

As before, the thermodynamic feasibility of hydride (or proton and electron) transfer from the metal to CO_2, as predicted by hydricity, remains our first concern. I would add several kinetic considerations to the wish list for an effective CO_2 reduction catalyst:

1. The rate of CO_2 insertion into the hydride should be much larger than the rate of hydride protonation.

2. The catalyst should be able to access multiple redox and protonation states in order to reduce the energy requirements of storing and supplying multiple protons and electrons to the substrate.
3. Conversion between intermediates in the catalytic cycle should occur with minimal changes in ligand geometry and polarity.
4. The rate of ligand dissociation should be low under a variety of conditions.

Without ruling out any particular metal, ligand, or metal-ligand combination, I would like to suggest that these requirements can be met by applying the following design principles, in order of importance:

1. The catalyst should be composed of a metal which is capable of assuming two or more consecutive redox states (n, n-1), and should avoid a mechanism which requires cycling between charged and neutral states. As we saw in Chapter 5, it is energetically more costly to cycle between Pd(II), Pd(0), and Pd(II)–H (n, n-2, n) than it is to cycle between Ni(II), Ni(I), Ni(II)–H (n, n-1, n) in order to make a metal hydride, both in terms of reduction potentials and in reorganizational barriers. Such redox flexibility might also be achieved by participation of a non-innocent ligand as an electron reservoir.
2. The metal should be more electropositive than Ni, and/or the hydride complex of the metal should be in a relatively high oxidation state. The increased ion pairing between the negatively charged hydride and the positively charged metal should reduce ion pairing between the hydride and surrounding protons, disfavoring hydride protonation relative to CO_2 insertion. Moreover, electrostatic attraction between the positively charged metal and $HCOO^-$ product should also make CO_2 insertion more favorable by pulling the transition state energy down from the product side.

3. It is preferable that the ligands be anionic and multi-dentate in order to stabilize binding of the ligand to the metal. The increased donating ability of anionic ligands as compared to neutral ligands is also necessary to raise the energy of the metal orbitals and compensate for the lower metal energy HOMO that would result from suggestion #2.[17] Furthermore, the geometric constraints afforded by multi-dentate ligands may minimize inner-sphere reorganization between reaction intermediates, although this will have to be carefully considered in the context of the specific metal and its redox states. Carbonyls and other highly pi-accepting ligands appear to significantly decrease hydricity, and should probably be avoided.[18]
4. The ligand-metal combination should result in a pi-symmetry metal HOMO that is able to bind to the π^* LUMO of CO_2, thereby favoring CO_2 binding and reaction with the metal hydride.
5. The inclusion of proton relays near the active site may not be necessary to speed up proton transfer if such transfers are not rate-determining, but may be important for stabilizing the buildup of negative charge on oxygen.

The validities of these principles, of course, remain to be borne out by experiment. Some of the best results published thus far, however, have involved CO_2 insertion into d^6 octahedral Ir(III)–H complexes supported by anionic PCP and Cp^- ligands.[19–21]

6.4 Conclusions

In this chapter I have described two possible projects concerned with developing the formate oxidation activity of $[Ni(P_2N_2)_2]^{2+}$ complexes, as well as some ideas about developing future catalysts for reduction of CO_2 to HCOOH. There is ample room for work

on CO_2 reduction electrocatalysis, particularly as it relates to developing a mechanistic understanding of how this can be achieved.

6.5 References

1. Zhu, X.-Q.; Chen, X.; Mei, L.-R. Org. Lett., 2011, 13, 2456–2459.
2. Connelly, N. G.; Geiger, W. E. Chem. Rev., 1996, 96, 877–910.
3. Shaughnessy, K. H. Chem. Rev., 2009, 109, 643–710.
4. Gooßen, L. J.; Dezfuli, M. K. Synlett, 2005, 445–448.
5. Mallion, K. B.; Mann, F. G. J. Chem. Soc., 1964, 6121–6130.
6. Kyba, E. P.; Liu, S. T. Inorg. Chem., 1985, 24, 1613–1616.
7. Kyba, E. P.; Liu, S. T.; Harris, R. L. Organometallics, 1983, 2, 1877–1879.
8. Reis, A.; Dehe, D.; Farsadpour, S.; Munstein, I.; Sun, Y.; Thiel, W. R. New J. Chem., 2011, 35, 2488.
9. Englich, U.; Hassler, K.; Ruhlandt-Senge, K.; Uhlig, F. Inorg. Chem., 1998, 37, 3532–3537.
10. Hosein, A. I.; Le Goff, X. F.; Ricard, L.; Caffyn, A. J. M. Inorg. Chem., 2011, 50, 1484–1490.
11. Fild, M.; Glemser, O.; Hollenberg, I. Z. Naturforsch, 1966, 21, 920–923.
12. Keller, J.; Schlierf, C.; Nolte, C.; Mayer, P.; Straub, B. F. Synthesis, 2006, 2, 354–365.
13. Luetkens, M. . J.; Sattelberger, A. .; Murray, H. H.; Basil, J. D.; Fackler, J. P. J. Inorg. Synth., 1990, 28, 305–310.
14. Zhang, W.; Zhu, S.-F.; Qiao, X.-C.; Zhou, Q.-L. Chem. Asian J., 2008, 3, 2105–2111.
15. Moser, C.; Orthaber, A.; Nieger, M.; Belaj, F.; Pietschnig, R. Dalton Trans., 2006, 3879–3885.
16. Evans, S. J. Sterically hindered and unsymmetrical phosphines: synthetic and catalytic aspects. Ph.D. Dissertation, University of Johannesburg, South Africa, 2006.

17. Kim, K.; Kishima, T.; Matsumoto, T.; Nakai, H.; Ogo, S. Organometallics, 2012, 32, 79–87.

18. DuBois, D. L.; Berning, D. E. Appl. Organomet. Chem., 2000, 14, 860–862.

19. Hull, J. F.; Himeda, Y.; Wang, W.-H.; Hashiguchi, B.; Periana, R.; Szalda, D. J.; Muckerman, J. T.; Fujita, E. Nature Chem., 2012, 4, 383–388.

20. Kang, P.; Cheng, C.; Chen, Z.; Schauer, C.; Meyer, T. J.; Brookhart, M. J. Am. Chem. Soc., 2012, 134, 5000–5003.

21. Tanaka, R.; Yamashita, M.; Nozaki, K. J. Am. Chem. Soc., 2009, 131, 14168–14169.